MASS SPECTROMETRIC PROFILING AND LOCALIZATION OF METABOLITES IN BIOLOGICAL SAMPLES

By

CHAO LI

A DISSERTATION

Submitted to
Michigan State University
in partial fulfillment of the requirements
for the degree of

DOCTOR OF PHILOSOPHY

Chemistry

2011

ABSTRACT

MASS SPECTROMETRIC PROFILING AND LOCALIZATION OF METABOLITES IN BIOLOGICAL SAMPLES

By

CHAO LI

Metabolomics is a rapidly growing approach based on global analysis of all metabolites in a tissue, fluid or organism. This approach is based on the assumption that the metabolome serves as a holistic measure of metabolic status. Most metabolomic analyses have been based on bulk sample analyses, which do not differentiate metabolites from specific tissues or cells. Since metabolic activity is organized in complex networks, bulk analyses involve a loss of potentially important chemical information. This dissertation presents development of analytical methods to profile localized metabolites in biological tissues, and applies these to investigations of glandular trichomes, which are epidermal plant cells that are prolific at chemical synthesis. Microsampling of individual trichomes from wild tomato relatives of the genus *Solanum* was achieved using micropipettes, and blasting of tissue from surfaces of corals was performed using a waterpik. Metabolite detection, identification, and quantification were performed using liquid chromatography/mass spectrometry (LC/MS). Through accurate mass measurements and chromatographic peak alignments, 109 metabolite signals were annotated from extracts of single trichome types. Methylated flavonoids represented one class of trichome metabolites, but mass spectra alone were not adequate to distinguish isomers. Complete assignment of isomeric methylated myricetins was achieved by employing two recombinant O-methyltransferase

enzymes from *Solanum habrochaites* LA1777 for selective semisynthesis of methylated myricetins. Tandem mass spectrometric analysis and chromatographic retention times provided evidence needed for structure annotation, aided by selective enzymatic incorporation of deuterium labeled methyl groups. These structural assignments aided demonstration of substrate selectivity of the two methyltransferases.

To accelerate profiling of individual trichomes, a contact printing approach was developed to transfer cells from across an entire leaf to a carbon substrate while preserving spatial information during the transfer. Direct and matrix-free laser desorption ionization from the printed cells allowed chemical imaging of trichomes across an entire leaflet. Individual trichome resolution was achieved using smaller steps of stage position, yielding about 50 μm resolution. Using this scheme, the first spatially-resolve profiling of trichome metabolites across the *Solanum* leaflet was achieved, and demonstrated chemical heterogeneity among trichomes within a single type.

Localized metabolite profiling was also performed for reef coral tissues collected from a field location near Curacao. A stable isotope dilution method was developed for quantifying seven betaine metabolites, which may serve as photosystem stabilizing substances, and dimethylsulfoniopropionate (DMSP) in extracts of coral tissues. The LC-MS protocol employed a pentafluorophenylpropyl (PFPP) column and time-of-flight mass spectrometry. The results demonstrate that corals accumulate multiple betaines, that betaine profiles vary widely among different coral species, and that betaine levels are correlated with ambient light levels.

ACKNOWLEDGEMENTS

This dissertation would be impossible without the contribution from many others. It is difficult to mention them all. I will first express my sincere thanks to Dr. A. Daniel Jones, my advisor, for his guidance, influence and support. He has guided me through the ups and downs of my graduate career and personal life. I am so lucky to have such a wonderful mentor who I will continue to benefit from for the rest of my career.

I would also like to thank my collaborators Dr. Robert Last's group from Michigan State University, Dr. Eran Pichersky's group from the University of Michigan and Dr. David Gang's group from the University of Arizona. It is honor to learn from them and work with them.

I am also grateful to my committee members, Dr. Gavin Reid, Dr. Merlin Bruening, and Dr. Marcos Dantus for their constructive comments and insightful suggestion on my work.

I would like to extend my appreciation to many past and present members of Jones's group for their engaging discussion and their friendship, which bring joy and happiness to my life at Michigan State University.

Completion of this dissertation would have been difficult without the moral and financial support from my family, my parents, my parents-in-law, and my sister. I'd like to give special thanks to my wife Jiamin, who has tolerated the long distance separation for years but been standing by me throughout my graduate career and has been a constant source of encouragement and support.

TABLE OF CONTENTS

LIST OF TABLES

LIST OF FIGURES

LIST OF SCHEMES

CHAPTER ONE

INTRODUCTION

1.1 Metabolite profiles and the quest to understand biological functions

For centuries, the mysteries of living organisms have fascinated people, and a great deal of research effort has been invested to improve our understanding about how living things function. The discoveries of chromosomes, genes, and DNA focused much of this research over the past few decades upon the influence of specific genetic contributions to biological functions [1]. In the 1980s, several teams of researchers set about to sequence entire genomes, including those of bacteria [2], yeast [3], the model plant *Arabidopsis thaliana* [4], rice [5], and ultimately, humans, in 2003 [6]. In the early 21st century, numerous whole genomes have been sequenced, and the number of sequenced genomes is expected to undergo explosive growth during the next decade owing to improvements in the cost and speed of DNA sequencing. However, genome sequences only provide a starting point for understanding gene functions, because these functions are usually inferred by comparing sequences with genes of similar sequence for which the functions are already known. However, small differences in DNA and protein sequences, even single mutations can have dramatic effects on protein functions. A new area of research called “functional genomics”, which tries to understand the functions of unknown genes, has emerged as genomic information and genetic technologies including expressed

sequence tag (EST) sequencing, microarrays, or sequencing based analysis of gene expression (RNA-Seq) for large-scale transcriptome profiling [7].

Unlike the genome, transcriptomes, which are global profiles of mRNA levels, are dynamic, varying with external environmental conditions. Transcriptomes provide measures and identities of which genes are actively expressed. It was initially thought that transcriptome profiling could answer most questions about gene functions. However it was soon realized that transcriptomes do not always correlate to the content and level of proteins in specific tissues for several reasons [8-11]. First, the rapid degradation of mRNA and also degradation of proteins contribute to poor correlations between levels of specific mRNAs and the proteins for which they encode. Second, many proteins must undergo post-translational modification to convert to their functional forms. This information cannot be captured from analysis of transcriptomes. In addition, due to alternative splicing of transcripts, a single mRNA may yield proteins with more than one amino acid sequence, which also leads to further discrepancies between transcriptome and proteome. Last, but not least, many proteins become active only when they interact with other protein or mRNA molecules. All of these complexities give birth to another research area, “proteomics”, which is large scale study of all proteins in a biological system.

Despite the progress made in genomics, transcriptomics and proteomics, there are still knowledge gaps regarding cell functions. The “omics” data mentioned above provide information about the potential functions of cells, and many of these functions

involve the synthesis, degradation, transport, and sensing of the most downstream products of the biological cascade, which are metabolites. Metabolites are the end products of cellular regulatory processes and their levels reflect the combination of genetic and environmental influences, which give a close reflection of biochemical activity. Analysis of metabolic snapshots serves as a valid approach for quantitative rather than qualitative description of cellular regulation and control. Thus the metabolome can be regarded as the unbiased chemical phenotype of a cell or tissue and can be used to establish effects of genes and/or environment influence cellular chemistry [12]. This is summarized in a comment attributed to Dr. Bill Lasley of UC Davis: "Genomics and proteomics tell you what might happen, but metabolomics tells you what actually did happen!" [13]

Another relatively new research area called "metabolic genomics" is based on the combination of genomics and metabolomics [14, 15]. Metabolic genomics research aims to extend and refine our understanding of relationships between genes and cellular biochemistry by creating more detailed functional genomics maps connecting biosynthetic pathways, regulation of metabolite levels, with the genetic components involved. The ultimate goal is to reveal regulatory mechanisms of the complex interacting networks underlying functions in whole biological systems.

Together with proteomics and transcriptomics, integration of profiling of transcripts, proteins, and metabolites provides a more complete picture of biological functions and dynamics. By taking account of the metabolome, researchers have more opportunities to

discover the links between macromolecules, identify functional linkages between phenotypes, and also construct dynamic networks for predicting biological behavior.

Although metabolomics alone cannot answer all questions about biological functions, there are special merits of metabolome analysis compared to other "-omics" approaches. Annotations of gene functions must have a definitive phenotype to differentiate function from absence of function. One advantage of metabolomics derives from the smaller number of metabolites relative to the number of genes and proteins in a cell. This decrease in experimental complexity is exploited when the metabolome is used as a proxy to represent phenotypes. Second, the metabolome can often magnify changes in activity of low abundance proteins, particularly when the protein acts as a catalyst or transporter. In such cases, metabolites can be far more abundant than the proteins involved in their synthesis, and this feature makes phenotypes more readily detected and distinguished. In many cases, levels of individual or groups of metabolites are indicators of altered biological functions. Third, the expense of metabolite analysis is estimated to be two to three orders of magnitude lower than global transcriptomics or proteomics [16]. In certain scenarios, the metabolome provides a shortcut to recognize outlier phenotypes, and metabolome data can direct other analyses, including proteome and transcript analyses, toward those samples that exhibit phenotypes of interest. For example, the forward genetics approach of random mutation is one popular way to discover gene functions. However, the vast majority of mutations do not lead to obvious morphological phenotypes, a phenomenon called silent mutation. In this case, metabolite screening as the starting

point provides a more efficient and cost-effective way to identify biochemical phenotypes that otherwise might be missed [17].

1.2 The Application of Metabolomics in Plant Research

Plants are sessile organisms that are not capable of moving to avoid environmental stresses such as temperature or water stress, predation by animals, or diseases caused by pathogens. As a result, plants largely respond to stress by changing their cellular chemistry. Because of this evolved behavior, plants accumulate an extensive and diverse group of metabolites, estimated to be around 10^5 to 10^6 distinct chemicals across the plant kingdom [18]. This huge diversity of phytochemicals indicates diversified gene functions in plants, and these functions are often specialized in individual plant species or lines based on the environmental stresses that specific plants encounter in their natural habitats. For example, there are 272 and 303 cytochrome P450 enzymes, which catalyze metabolite oxidations, discovered in *Arabidopsis* and rice, respectively, compared to only 57 in humans [19, 20].

Modern research is only beginning to explore the composition of the metabolome in individual plant species. Despite longstanding knowledge that certain plants make compounds of economic interest to humans, remarkably little is known about the biosynthetic pathways leading to even those compounds of greatest interest. The metabolome of *Arabidopsis thaliana*, a model plant for which the genome has been

sequenced, is probably the most extensively studied metabolome among all plants. Metabolite profiles have been generated for well-defined libraries of *Arabidopsis* mutants [21], but much of the chemical information gathered to date has focused on abundant "primary" metabolites including sugars, organic acids, and amino acids that are essential for plant survival. Many of these mutants showed metabolic differences compared to wild type plants, and research is heading toward discoveries of how single point mutations change metabolite profiles even though no visible phenotypic change occurs. Using metabolite information as the bridge, the prediction of the functions of unknown genes could be made by monitoring the metabolic changes caused by deletion/insertion of unknown genes. This approach could become more effective if supplementary analyses such as large scale enzyme analysis [22] were combined with metabolite profiling and gene mapping to build an unprecedented overview of plant metabolism.

Another practical application of metabolomics is for population screening and plant breeding. To humans, the intrinsic interest to understand plants derives from a desire to improve food products, medical therapies, and other valuable feedstocks including biofuels. For the applied scientist, e.g. in the plant breeding industry, the metabolomics approaches have already gained a great deal of attention recently [23] owing to their potential to help define better phenotypes and assist breeding of plants for desirable traits. Economically valuable traits of the plants such as disease resistance, nutrient content and quality, flavor, and fragrance are based on metabolite composition, and these are traits breeders value. Using metabolite information to regularly select plants having better

disease resistance, greater nutrient content and desirable appearance (pigments) have substantial economic value for breeders. Some plants even contain metabolites which have potentially health-promoting properties, e.g. Chinese herbal medicines.

The interest in linking food composition and human health has grown rapidly in recent years. People are paying more attention to purchasing healthier food products, leading to introduction of the term “nutraceuticals” to describe food products that offer potential therapeutic benefits. Food producers and supply companies also want to advertise their products with scientific support of claims that consuming certain foods, such as those rich in antioxidant plant metabolites, leads to better health. Considering that metabolite profiling is a relatively inexpensive analytical procedure, metabolomic analyses are finding increased use for screening natural or induced mutant plants or, to demonstrate that genetically modified foods are functionally equivalent to “natural” foods. One good example is the mutant or modified tomatoes [24-26]. Davuluri reported using targeted genetic modification for generating lines of tomato accumulating more health related carotenoid and flavonoid antioxidants. He also used metabolite analysis to identify novel antioxidants in transgenic tomatoes transfected with a stilbene synthase gene from grape.

Aside from developing more nutritious foods, metabolomics can help plant industry to engineer stronger plants that can better resist disease and predation. Plants have sophisticated chemical defense mechanisms that are triggered when they are subjected to biotic or abiotic stresses. It has suggested that a coordinated ‘metabolic reprogramming’

occurs in plants subjected to sudden environmental changes including both biotic and abiotic stresses [27]. An example of where this may play important roles in the future lies in the development of more energy-rich biofuel crops. Such plants, which accumulate large stores of metabolites designed as fuel precursors, are likely to be attractive foods for animals and microbes. Successful development of biofuel crops will require metabolic engineering of pathogen and herbivore defenses. In this context, it is important to understand stress responses fully from their molecular basis, and design crops with better stress resistance. Metabolomics will play major a role in guiding these research efforts.

1.3 Analytical platforms for metabolomics

A metabolite may come from more than one metabolic pathway. Researchers can best identify which pathways are involved in its metabolism when they assess the metabolome as a whole. There are several challenges to metabolome analysis that pose greater barriers relative to genomics, transcriptomics or proteomics. DNA and RNA are each constructed as linear polymers from four nucleotides, so the structural diversity is somewhat limited. Furthermore, many oligonucleotides participate in predictable molecular recognition events. This selective binding, coupled with modern capabilities to amplify DNA, makes it easy to implement high throughput platforms for analyzing DNA or RNA. Similarly, proteins are linear combinations of twenty amino acids, and an

assortment of methods has been developed to assess their primary structures and quantify proteins. In comparison, metabolites exhibit structural diversity that is vast relative to oligonucleotides or proteins because there are virtually no limits on the structural features that make up the metabolome. Wide variations of physicochemical properties across the metabolome make any global analysis challenging, especially with regard to structure annotation. Furthermore, the large range of metabolite concentrations (can differ over several orders of magnitude) challenges even the most powerful analytical technologies.

The current state of global metabolite analysis is based on three types of platforms, gas chromatography-mass spectrometry (GC/MS), nuclear magnetic resonance spectroscopy (NMR), and liquid chromatography-mass spectrometry (LC/MS) [28-31]. NMR finds widespread use for medical metabolomics but has found limited application for profiling of specialized plant metabolites. NMR has the advantage of uniform detection of hydrogen-containing metabolites without substantial artificial matrix effects, so the magnitude of each observed signal provides an accurate measure of the true metabolite level. The weakness of NMR lies in the need to analyze milligram quantities of each detected metabolite. Therefore, NMR is a powerful approach for profiling metabolites of high abundance [32], but lacks the capability to measure the numerous metabolites that are orders of magnitude less abundant than the major constituents. Quick annotation of metabolites can be achieved by comparing spectra to NMR spectra of authentic standards. However for previously undiscovered metabolites for which standards are not available, explicit structure elucidation often requires purified materials

and multidimensional NMR, and these techniques require yet more metabolite.

GC-MS is one widely used method for metabolomics, and its use for global metabolite profiling predates the word ‘metabolomics’. Its popularity comes from its remarkably high separation efficiency, and its coupling with electron ionization which provides near-universal detection. Since electron ionization employs a standard fixed ionization condition (70 eV electron energy), mass spectra for the same analyte are similar across instruments and laboratories. The availability of libraries of mass spectra and metabolite identification software facilitates metabolite annotation. However, the technique is only applicable to separation and detection of volatile and chemically stable metabolites at temperatures up to about 300℃ (e.g. alcohols, monoterpenes and esters). Therefore chemical derivatization needs to be employed for analysis of nonvolatile or polar metabolites, including amino acids, sugars and organic acids [33]. Derivatization involves drying and conversion of polar functional groups to nonpolar substructures. These processing steps can introduce variability and losses during the process of drying and derivatization. Even with derivatization, many metabolites including glycoconjugates may still not be detected using GC/MS owing to their decomposition during heating and evaporation in the GC injector, and such reactions can generate new compounds that were not in the original metabolite extracts.

Application of liquid chromatography-mass spectrometry (LC/MS) for global metabolic profiling has increased in recent years [34]. The greatest advantage of LC/MS is that it is usually coupled with soft ionization, e.g. electrospray ionization (ESI), which

can preserve fragile molecules such as glycosylated flavonoids intact. Analyses that employ LC/MS often involve minimal sample preparation, as derivatization is usually not necessary. Furthermore, LC column efficiencies have improved dramatically in recent years [35], leading to coining of the term ultrahigh performance liquid chromatography (UHPLC). These efficient columns have stimulated renewed interest in moderate to high throughput LC/MS methods, and these are emerging as the preferred approach for many metabolome analyses. Advances in novel column chemistries (e.g. hydrophilic interaction chromatography (HILIC) and long monolithic columns) offer the potential for greater coverage of the metabolome over a wider range of properties. Although electrospray ionization (ESI) is not as universal as electron ionization (EI), a range of alternative ionizations techniques is available to ensure ionization of a broad range of metabolites. These methods include atmospheric pressure chemical ionization (APCI) and atmospheric pressure photoionization (APPI). The greatest challenge for LC/MS based metabolite analysis comes from two points. Unlike GC-MS, libraries of mass spectra, particularly tandem mass spectra, for LC-MS are limited. Because experimental parameters differ across laboratories, standard libraries of spectra have been slow to develop. How to annotate metabolite structures without standard spectra for comparison remains a challenge. This topic has been the subject of continuing discussion [36-41]. A second challenge that confronts LC/MS-based metabolome analysis arises from the phenomenon called “matrix effects”. A coeluting compound(s) often changes the extent of ionization of another analyte, and causes its signal to be reduced (or in some cases,

increased). This problem is especially severe for analyses of extracts having complex and unknown composition, because it is virtually impossible to resolve all metabolites in a single LC separation.

1.4 Spatially resolved metabolite profiling, and the emerging interest in micrometabolomics

Since shortly after the invention of the microscope, researchers have suspected, and later confirmed, that biological functions are organized at the level of cells and subcellular domains such as organelles. During the intervening years between then and now, the functions of these small domains have largely remained a mystery, in part because analytical tools lacked the sensitivity, speed, and resolution needed to probe how chemistry is organized at these levels. Recent and dramatic technological improvements in all of these areas have opened doors to profiling of metabolites in specific organs, tissues, and even single cells.

Plants are considered to have about 40 different cell types [42]. Extracting and analyzing an entire tissue of organ as a whole generates a mixture of metabolites that are derived from multiple cell types, and is not the optimal way to study complex biological systems. There are important questions that still remain unanswered, such as how different cells differentiate and communicate with each other; how cells with different ages or developmental stages within a tissue are different in their chemistry; how

metabolites or enzyme substrate are transported from one tissue location to another; and how signaling molecules trigger metabolic cascade responses throughout the whole organism. These questions are best answered by investigating biochemical behavior of individual organs, tissues, and cells. As the resolution and content of information increases, the knowledge gained reaches closer proximity to the truth [43, 44]. So far, metabolomics analyses have been mainly conducted on whole plants, or on whole organs such as leaves or roots. Only a few examples of metabolite analyses have been reported for specific tissues [45, 46] or on specific plant cells, most notably lignified cells in spruce bark [47, 48], level have been reported.

Analyses of a single tissue or individual cells pose daunting challenges, particularly with regard to sample preparation. Microsampling of individual cells is complicated by the potential for contamination, whether the contaminants are derived from adjacent cells of a different type, or simply because the small quantities of metabolite may be obscured by contaminants derived from other sources. Two major sampling methods have been developed for microanalyses, with most focusing on collection of nucleic acids [43, 44, 49, 50]. The first involves usage of microcapillaries or micropipettes to extract cells or their contents from tissues [49-52]. A typical experimental setup employs a microcapillary or micropipette mounted on a microscope. The targeted tissue or cell can be visualized using a CCD camera, and sampling is controlled using a micromanipulator. The second method involves microdissection, and is sometimes referred to as Laser-Assisted Microdissection (LAM) [53]. LAM uses focused light from a laser to cut a selected area

of tissue, including single cells, and the materials are collected from the sample either by contact sampling e.g., attachment to a sticky surface or non-contact sampling, e.g. gravity deposition, ejection by photon pressure. LAM was initially developed for RNA isolation [43] to measure gene expression in individual cell types. Most recently, it has been applied to small molecule analysis in specific plant tissues and cells [47, 48, 54, 55]. For metabolite analysis, it is important to avoid sources of contamination from the material used in LAM such as paraffin, plastics, adhesives, dehydrating agents, and staining tinctures, as these contain low-molecular-weight contaminants that may interfere with metabolite profiling [56].

Two additional complications arise from microsampling, namely preservation of unstable metabolites during the long sampling process, and the limited amount of material present in tiny samples such as individual cells. Many metabolites have short lifetimes and are converted to other products by the action of various enzymes. Halting these enzymatic transformations often requires quick freezing of tissues. Unfortunately, most microsampling methods depend on the cytoplasm being in a liquid state, and when this is the case, enzymes may be active, transforming the metabolite pool. For this reason, microsampling has been most successful for analyses of substances such as lipids that undergo slow turnover. The issue of analyte quantity has been challenging to address, as single cells may contain only a picoliters to nanoliters of material. Only the most abundant metabolites, those present at low millimolar concentrations, are easily detected because the amounts of metabolites of interest are present at attomole to femtomole

quantities which are below the routine capabilities of most instruments.

In terms of detection, many detection schemes have been used for analysis of single tissues or cells, including fluorescence [57-61], electrochemical detection [62-65] and mass spectrometry [66-86]. These are among the most sensitive analytical tools. Single tissue or cell metabolome analysis requires technologies that offer low limits of detection, high throughput, and also the capability to detect a wide range of analytes. Although fluorescence and electrochemical analysis offer remarkably low detection limits, these techniques are not universal for a wide range of metabolites, and fail to give information that can distinguish a large number of substances from one another, as analytes need to be fluorescent or electrochemically active to be detected. Chemical derivatization could be performed to introduce labels to facilitate detection, but this rarely has provided adequate selectivity relative to background signal. In view of these considerations, mass spectrometry has emerged as the predominant technique for single tissue or cell metabolome analysis owing to its near universal detection.

Mass spectrometric schemes for single cell analysis can be grouped into four categories. The first scheme is sampling the cell using a capillary probe, followed introduction into the mass spectrometer using nanoelectrospray [80]. The greatest drawback of this technique is that it is difficult to make it to be a high throughput platform owing to the need to analyze numerous cells of a given type and because coordination of nL/min flows from large numbers of cells is inherently slow. The second scheme employs microfluidic chips coupled with mass spectrometry. At the front

end, the microchip sorts cells and can also quench, lyse and separate the metabolites using electrophoretic or nanochromatographic methods. The chip can be coupled to a variety of ion interfaces, such as electrospray (online detection) or matrix-assisted laser desorption/ionization (MALDI) (off-line detection). The complete setup has not yet been realized as a routine practice, but advances promise to introduce more robotic operation, which is promising in terms of throughput [87-90]. A third scheme is called sample arrays [91]. A MALDI sample plate was first coated with a solvent-repelling coating, patterned in a checkerboard array format. Cell suspensions were then sprayed on the array. An appropriate cell suspension density will yield only one to two cells in each well. Such samples can be analyzed using MALDI afterward [91]. This technique could have broad application on certain types of cells such as microbes grown in liquid culture, but it is difficult to envision how this might be implemented for other types of cells in complex eukaryotes such as plant epidermal cells without compromising the integrity of the metabolome. The fourth scheme, which is believed to be most promising, is imaging mass spectrometry [68, 69, 92-94], which can use any one of several ionization methods including desorption electrospray, secondary ion mass spectrometry (SIMS), or MALDI. The biggest advantage of MALDI imaging is it requires minimal sample preparation aside from introduction of an absorbing matrix that can convert laser light into energy for ion formation and evaporation. Another merit of imaging mass spectrometry is that each pixel yields a mass spectrum, generating spatially resolved chemical profiles. A growing wave of interest is pushing improvements in

spatial resolution of imaging mass spectrometry over the past few years. For example, a spatial resolution of 10 μm was reached with state-of-the-art LDI instrumentation based on a near-infrared femtosecond laser [95], which offers potential for single cell metabolite profiling. With advances in laser technologies and sample preparation methods, imaging mass spectrometry is expected to have great impact on single cell metabolite analysis that will improve our understanding of cellular chemical heterogeneity and cell-cell communication.

1.5 Summary of Research

As mentioned above, metabolomics is an important component of the growing interest in systems biology, which often requires multidisciplinary collaborations encompassing genetics, bioinformatics, molecular biology, and bioanalytical chemistry. This dissertation presents results, in Chapters II-IV, of my role in developing and applying analytical methods for metabolite profiling in a multidisciplinary team. The scope of this work has covered almost all aspects of metabolite analysis discussed above including microsampling, high throughput screening, imaging mass spectrometry, detailed structural elucidation, separation method development and quantitative analysis. The various chapters of this dissertation are derived from two projects. One is the National Science Foundation funded *Solanum* trichome project, which has involved plant geneticist, biochemist, biologist, chemical ecologist, and bioinformaticist team members from

Michigan State University, the University of Michigan, and the University of Arizona. The goals of this effort have been focused on identifying the genes and proteins involved in the synthesis of specialized metabolites stored and excreted by *Solanum* trichomes. Since the genus *Solanum* includes many important crop species including tomato, potato, pepper, and eggplant, discoveries of these gene functions can open the door to molecular level understanding of the factors that regulate metabolite synthesis, and form the foundation for future efforts at metabolic engineering of plants and other organisms. The second project, a collaboration with Professor Richard Hill and his group from the Michigan State University Department of Zoology, is described in Chapter V. This work focused on developing and applying metabolite profiling approaches to understand the dynamics of the coral reef metabolome under different environmental stress conditions. My role in all of these projects has been to develop and apply sampling and analytical methods for metabolite profiling. Aspects of the research that are based on field collection of coral samples and expression and assay of recombinant enzymes were performed by collaborators identified in the individual chapters.

In Chapter II of this dissertation, the development of methodology for sampling individual trichomes from five *Solanum* species is described. The application of a high throughput LC/MS platform, called multiplexed collision induced dissociation (multiplexed CID) for profiling metabolites in individual trichome types is reported. The cell-specific chemical information discussed in Chapter II paved the way for our collaborators to construct a network of genes expressed in trichomes that can be

associated with specific biochemical traits. Chapter III illustrates a new technique for matrix-free imaging mass spectrometric profiling of metabolites for *Solanum* trichomes. This technique conquers several sample preparation challenges for imaging of trichome by mass spectrometry. In addition to showing different metabolites in different plant species and genotypes, it is illustrated that the spatial distribution of trichome chemistry is heterogeneous across a single tissue. This information provides clear evidence of the importance of incorporating spatial information into metabolite profiling. In Chapter IV, analytical strategies were developed and applied to demonstrate the specificity of two trichome-containing methyltransferase enzymes through MS/MS-based structure elucidation of regioisomeric enzyme products. These unknown enzyme products do not have authentic standards available for spectra comparisons, and the mass spectrometric data provide convincing evidence for individual structure assignments. The approach used in this effort employed semisynthetic preparation of products through use of the recombinant enzymes coupled with isotopic labeling. In Chapter V, the development of a stable isotope dilution LC/MS method demonstrated, for the first time, the extraordinary abundance of betaine metabolites in coral tissues, and the variation in betaine composition across multiple species of field-collected corals. Betaines are believed to be protective metabolites that confer resistance to environmental stresses. The results of this investigation demonstrate that betaine content is regulated by environmental factors in a way consistent with being a plastic metabolic response.

Some of the research described in this dissertation has already been published in

modified form. Metabolite profiles from individual trichome types that are described in Chapter II have appeared in a manuscript in Plant Physiology (E. T. McDowell, J. Kapteyn, A. Schmidt, C. Li, J.-H. Kang, A. Descour, F. Shi, M. Larson, A. Schilmiller, L. An, G. A. Howe, A. D. Jones, E. Pichersky, C. A. Soderlund, and D. R. Gang, Comparative functional genomic analysis of *Solanum* glandular trichome types, *Plant Physiology*, ***2011***, **155**: 524-539). Some of the principles of metabolite localization, established in Chapter III, have been discussed in a recent book chapter (L. W. Sumner, D. S. Yang, B. J. Bench, B. S. Watson, C. Li, and A. D. Jones. 'Spatially resolved plant metabolomics' in *Biology of Plant Metabolomics, Annual Plant Reviews*, Volume 43, R. Hall, Ed., Chapter 11, pp. 344-366, 2011). Discoveries of O-methyltransferase functions, described in part in Chapter IV, were included in another paper (A. Schmidt, C. Li, F. Shi, A. D. Jones, and E. Pichersky, Polymethylated myricetin in trichomes of the wild tomato species *Solanum habrochaites* and characterization of trichome-specific 3′/5′ and 7/4′ myricetin *O*- methyltransferases, *Plant Physiology*, ***2011***, **155**: 1999-2009). The methods for quantifying betaines in coral tissues described in Chapter V have appeared in two papers (C. Li, R. W. Hill, and A. D. Jones, Determination of betaine metabolites and dimethylsulfoniopropionate in coral tissues using liquid chromatography/time-of-flight mass spectrometry and stable isotope-labeled internal standards, *Journal of Chromatography B*, ***2010***, **878**: 1809-1816; and R. W. Hill, C. Li, A. D. Jones, J. P. Gunn, and P. R. Frade. Abundant betaines in reef-building corals and ecological indicators of a photoprotective role. *Coral Reefs*, ***2010***, **29**: 869-880).

CHAPTER TWO

ANNOTATION OF SPECIALIZED METABOLITES ACCUMULATING IN INDIVIDUAL TYPES OF GLANDULAR TRICHOMES OF THE GENUS *SOLANUM*

2.1 Specialized Metabolites in Plants

The plant kingdom has been estimated to synthesize more than 100,000 different natural product metabolites, but the genetic basis for production of these compounds remains largely unexplored. The majority of these substances are considered specialized, or secondary metabolites, that are not essential to plant survival, yet confer beneficial traits that have evolved over long time scales as responses to evolutionary pressures. Researchers are driving renewed efforts to understand the basis of interspecies and intraspecies genetic variations responsible for biosynthesis of such a diversified suite of metabolites. The key approach used in these efforts involves correlating the genotype with chemical phenotype, or composition. In addition, it is typical for a metabolite to be synthesized in a specialized tissue. For plants, the most prolific tissue involved in metabolite accumulation is the glandular trichome, which is a specialized epidermal cell type that occurs on the surfaces of leaves, stems, and other tissues. Trichomes provide a near-ideal model for investigations of plant metabolism. Multiple trichome types are known for a variety of plant species, and trichomes may be collected using a variety of microsampling methods that facilitate cell type-specific investigations of metabolism and

gene expression.

The common approach for studies of plant specialized metabolism has relied on chemical profiling of bulk tissue extracts and interpretation of this chemistry in the context of plant genetics, perhaps involving measures of gene expression in the extracted tissue. However, this strategy suffers when metabolite biosynthesis is largely confined to a specific cell type, because genes expressed in tissues not involved in biosynthesis may obscure the roles of the key biosynthetic genes. Because it is not feasible to study every individual type of tissue or cell within a plant, researchers should aim to select a model plant system with sufficient allelic diversity, genomic tools, and distinct metabolic phenotypes to investigate genotype and phenotype correlations. Furthermore, accessibility of specialized cell types provides a valuable handle for investigating cell-specific biochemical behavior. Based on those requirements, the genus *Solanum*, which includes tomato, potato, and other crops and is known to produce an assortment of trichome morphological types, serves as a great system to be the model for research on specialized metabolite biosynthesis.

2.2 Glandular Trichomes in the Genus *Solanum*

Trichomes are epidermal cells on plant surfaces which are easy to isolate compared to tissues on which the trichomes are attached. As a result, it is possible to collect and analyze RNAs, proteins, and metabolites from trichomes with minimal contamination from other

cells. Tomato has recently been reassigned to the genus *Solanum*, and an extensive collection of wild relatives of tomato are available. Also, many *Solanum* species (tomato, eggplant, potato) can inter-cross with each other and produce a diverse group of genetic variant hybrids (~1500-2000 so far). Those genetic variants offer a large number of allelic variants that can facilitate elucidation of biosynthetic pathways. Sequencing of the tomato genome is nearly complete, and this information can be taken advantage of to facilitate the recognition of candidate genes. Finally, besides the advantages of using *Solanum* species for research, tomato and its relatives are grown internationally and have important economic value that might be improved by metabolic engineering.

Many plant trichomes store or secrete a complex array of metabolites. It was proposed that trichomes have many attributes important to the success of the plant [96]. The well-accepted theory is that trichomes accumulate metabolites that protect plants against insect herbivory. For example, the model plant *Arabidopsis* produces more methyl salicylate in trichomes after wounding and insect attack [97]. The glandular trichomes in tobacco secrete nicotine, which is toxic to insects [98]. Trichomes of *Aristolochia elegans* decrease insect herbivory [99]. Removal of trichomes from leaf surfaces makes the plant more vulnerable to insect herbivory [100]. Ecological studies show that *Arabidopsis* increases trichome density under pressure from insect herbivore attack [101]. All of the evidence above shows that trichome provide an important protective layer of cells and metabolites. In addition to these defensive functions, trichomes play roles in plant responses to changes in temperature, water loss, and gas exchange regulation [102, 103].

Trichomes are described as belonging to one of two categories: nonglandular and glandular trichomes. Since nonglandular trichomes are not known to accumulate substantial amounts of specialized metabolites, this discussion will focus on glandular trichomes which accumulate a diverse collection of metabolites in large quantities. Based on Luckwill's definition (Figure II-1) [104], there are four types of glandular trichomes in the genus Solanum. Type I trichomes are defined as having a long multicellular stalk and a small glandular head; type IV trichomes have a similar appearance, but a shorter multicellular stalk and a small glandular head; type VI trichomes are composed of a short stalk with a larger mushroom-shaped glandular head made up of a cluster of four cells; type VII trichomes consist of a short stalk and also a mushroom-shaped small glandular head, but are smaller than type VI. The feature of multiple gland types often forms the basis for difference phenotypes between individual plants that can facilitate our understanding of trichome functions and biosynthetic pathways in different trichomes.

The comparison between cultivated tomato and wild types indicates that many important metabolites synthesized by the trichome have been lost during tomato domestication [105-109]. Conventional cultivated tomato crops are more susceptible to insects than are wild tomato relatives [105, 110-112], and this has been attributed largely to differences in trichome chemistry. One long-term goal of current studies of tomato trichomes is to discover genes responsible for chemical defenses against insects, and this information offers the potential to reintroduce key genes into tomato to improve insect resistance.

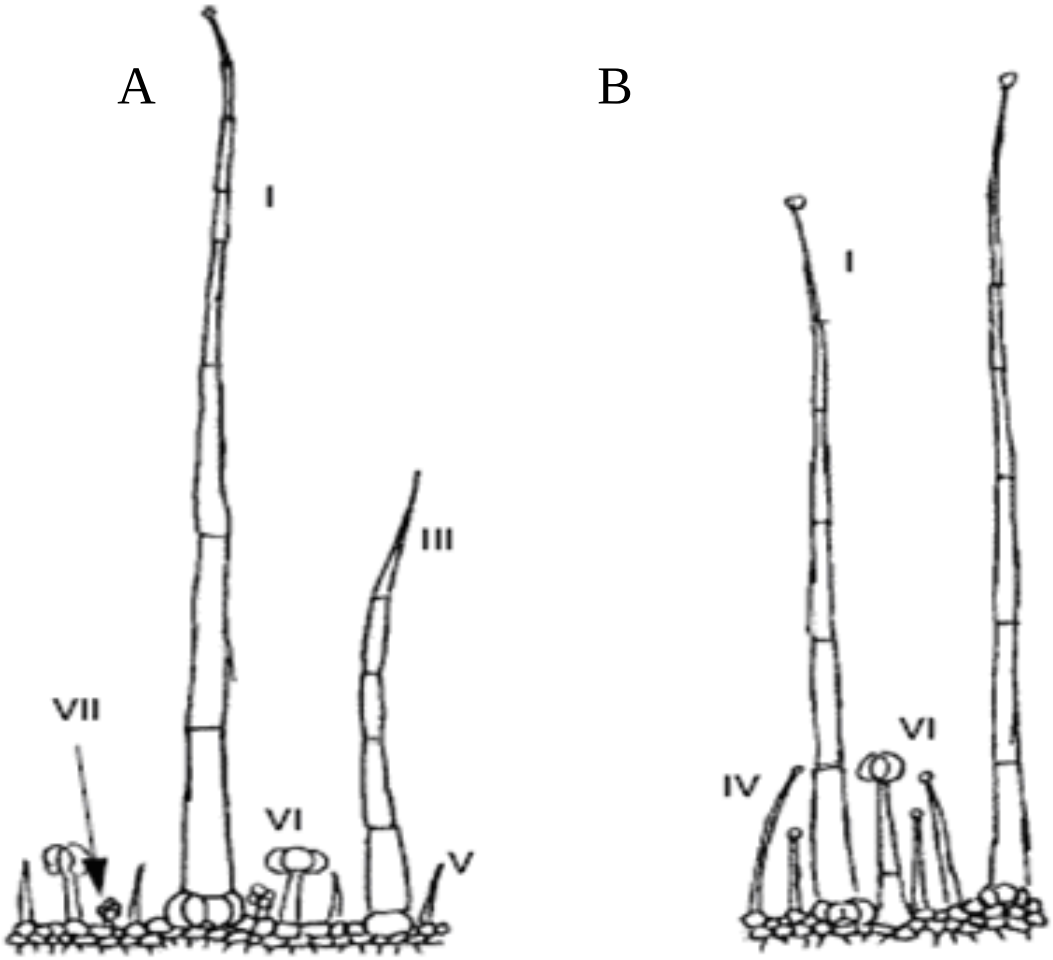

Figure II-1 Trichomes on *L. esculentum* (A) and *L. hirsutum* (B). Roman numerals indicate trichome type. Adapted from Reference [104].

2.3 Challenges of Analysis of Trichome Specialized Metabolites

Discoveries of the genetic basis of trichome functions and biosynthetic pathways ultimately rely on DNA sequencing and biochemical characterization of enzyme functions involved in the metabolite biosynthesis. However, understanding of the chemistry in different trichome types

is central to these research efforts, because the chemistry defines the phenotype. Since different cell types exhibit different chemical phenotypes, microsampling of individual trichome types must be performed, and the chemical composition of individual trichome types must be defined and interpreted in the context of genes expressed in each cell type. The volume of the largest glandular trichome (type VI) of tomato is about 100 picoliter. Although trichomes are surface tissues and are relatively easy to isolate, each individual trichome contains a tiny amount of metabolites owing to its small size. Isolation of large numbers of trichomes for chemical analysis is labor intensive, tedious, and time-consuming. To achieve the goal of profiling numerous trichome types from different plants, a more rapid approach was called for.

Our efforts have aimed to gather deep metabolome information for individual trichomes. To date, the most popular analytical method for metabolite profiling has been mass spectrometry. The advantage of mass spectrometry is that it serves as a near-universal detection technology that is useful for detecting a wide range of chemicals and providing information helpful for compound identification. In terms of structure elucidation capability, it is only second to NMR among routinely used analytical techniques. However, the detection limit of mass spectrometry is several orders of magnitude lower compared to NMR, which often requires milligram quantities of purified compound. For nontargeted structure elucidation of metabolites by mass spectrometry, the initial step involves determining the molecular mass and formula. High resolution mass spectrometers (e.g. time-of-flight, Orbitrap, Fourier Transform-Ion Cyclotron Resonance) provide mass measurements with errors of less than 5 ppm, and are employed to limit the range of molecular formulas consistent with a measured ion mass. More detailed

structure information can be deduced from the masses of fragment ions generated from MS/MS experiments.

A big challenge for metabolome analysis is encountered because a single analysis (e.g. of a trichome extract), yields more than one thousand detectable ion masses based on the current technologies. To generate MS/MS spectra for individual metabolites to gain structure information, large number, perhaps thousands, of MS/MS experiments need to be conducted. Performing traditional MS/MS scans for all of the metabolite molecular masses is not feasible due to enormous number of peaks detected. For trichome microsampling, the quantity of metabolite in each sample is severely limited. Tandem mass spectrometric analyses of complex mixtures has been advanced by the advent of data dependent MS/MS, which involves real-time spectrum evaluation, selection of an ion for further MS/MS analysis, and generation of a product ion MS/MS spectrum for the computer-selected ion. This approach increases the throughput of MS/MS experiments. However, the drawback of data dependent MS/MS is that it can only fragment a few (e.g. up to five) of the most abundant ions within a certain time window that is largely defined by chromatographic peak widths. This makes it likely that low abundance metabolites that coelute with more abundant compounds will not be selected for MS/MS analysis, and structural information for the less abundant compounds will be lacking. This issue can be addressed by repeated analyses, but such an approach is not feasible when extracts are limited in sample size. Defining a trichome's metabolic phenotype requires deep and comprehensive profiling of as many metabolites as can be measured. Generation of fragment mass information for both high- and low-abundance metabolites is not feasible for small sample sizes owing to the

limitations described above. To overcome those technical limitations and improve analytical throughput, the Jones laboratory developed a time-of-flight mass spectrometry (TOF-MS) method called multiplexed collision induced dissociation (multiplexed CID), which provides quasi-simultaneous molecular mass information for metabolites and also nonselectively fragments all of the ions in a single mass spectrometry analysis. Its nonselective nature avoids the limitations of data dependent MS/MS, and generate fragment ion information for low abundance metabolites. This analytical approach was applied for metabolite profiling of individual trichomes as described in more detail below. Even when we have limited volume of trichome extracts, extensive and comprehensive generation of molecular and fragment ions can be achieved in a single analysis.

2.4 Experimental Section

2.4.1 Materials

Seeds for *Solanum lycopersicum* M82**,** *S. habrochaites* LA1777, *S. pennellii* LA0716**,** *S. arcanum* LA1708**,** and *S. pimpinellifolium* LA1589 were purchased from the C.M. Rick Tomato Genetics Resource Center at the University of California-Davis. The seeds were grown in a growth chamber for 3 to 4 weeks, depending on the species, then seedlings were transferred to pots and grown in the same growth chamber until analysis. Plant growth was distributed among multiple locations (East Lansing, MI, Ann Arbor, MI, and Tucson, AZ).

2.4.2 Chemicals

Acetonitrile (HPLC grade), 2-propanol (HPLC grade), methanol (HPLC grade), and formic acid (88% aqueous solution) were purchased from VWR Scientific.

2.4.3 Trichome Collection

A summary of the trichome types collected from each plant species is presented in Table II-1.

Table II-1 List of wild tomato species and trichome types subjected to metabolite profiling.

Species	Trichome Types
S. pennellii (LA0716)	leaf type IV (L4), leaf type VI (L6)
S. lycopersicum (M82)	leaf I (L1), leaf VI (L6)
S. habrochaites (LA1777)	leaf I (L1), leaf IV (L4), leaf VI (L6), leaf VII (L7) stem I (S1), stem IV (S4), stem VI (S6)
S. arcanum (LA1708)	leaf VI (L6)
S. pimpinellifolium (LA1589)	leaf VI (L6)

To collect the type I and IV glands from the various *Solanum* species, microscissors were used to cut the gland off from the stalk. Type VI gland heads were collected using the stretched glass pipettes [113, 114]. Type VII trichome glands were collected by agitating with glass beads in buffer to abrasively remove trichomes from the leaf surface [115, 116].

S. habrochaites type VII trichomes were first transferred to a microcentrifuge tube and centrifuge at 3,000g for 30 s and the pellet was extracted with extraction solvent (2-propanol:CH_3CN:water 3:3:2, v/v/v). For the remaining trichome types, 50 picked trichomes were immediately transferred to 50 μL ice-cold extraction solvent. The gland/solvent mixture was then sonicated for 5 min followed by vortexing for 30 s and centrifugation at 5,000g for 10 min. The supernatant was then transferred to a glass autosampler vial equipped with a 100-μL glass insert.

2.4.4 LC-MS Analysis

LC-MS analyses of isolated gland metabolites were performed using a model LCT Premier mass spectrometer (Waters) coupled to an LC-20AD pump and SIL-5000 autosampler (Shimadzu). All analyses utilized electrospray ionization in negative ion mode and employed a custom-packed Supelco Discovery Bio C18 column (1 × 150 mm, 3-μm particles; 300 Å). Mobile phase gradients were based on solvent A (0.15% aqueous formic acid) and solvent B (methanol), with a total flow rate of 0.05 mL min^{-1}. The gradient consisted of initial condition 95% A, a linear gradient to 50% A at 5 min, a linear gradient to 5% A at 33 min, and then to 0% A at 35 min. The mobile phase was held constant until 38 min, when the composition returned to the original composition. Spectra were acquired using three quasi-simultaneous conditions: high energy (aperture 1, 75 V), medium energy (aperture 1, 45V), and low energy (aperture 1, 10 V) in the instrument transit lens.

2.4.5 Data Processing

Processing of mass spectra for elemental composition analysis was performed using MassLynx v 4.1 software (Waters). For nontargeted metabolite profiling, Waters MarkerLynx software was employed for peak detection, integration, retention time alignment, and export of peak areas organized by mass-retention time pairs. Principal component analysis was performed using the online resource at http://www.metaboanalyst.ca/.

2.5 Results and Discussion

Details of the multiplexed CID technique have been discussed in the Ph.D. dissertation of Feng Shi from our lab before [117]. The technique is explained briefly here. The ion optics element aperture 1, located behind the orifice of the ion source has relatively high pressure (~ 10^{-3} mbar) owing to gas leaking from the ion source (Figure II-2). The voltage applied on the aperture 1 can be manipulated by the instrument control software, and this potential controls the ion kinetic energies as they pass through this region of the mass spectrometer. Low aperture 1 potentials will deposit low energies per ion-molecule collision, and will preserve most of the pseudomolecular ion signals. Elevated aperture 1 voltages raise the ion kinetic energies, and subsequent ion-molecule collisions deposit sufficient internal energy to cause fragmentation. The comparison of the multiplexed CID spectra with MS/MS product ion spectra and the similarity of the CID spectra got from those two approaches has been established [117]. Due to

the fast spectrum acquisition rate of the TOF instrument (20000 transients/sec), the optics can switch between multiple voltage values in a single analysis, and spectra acquired under each condition are stored as separate functions. This approach enables the molecular ion and fragment ions to be obtained in separate data acquisition functions in a single analysis. The more important feature of this multiplexed CID technique is that it does not rely on a single set of CID parameters to yield fragment ion spectra across a diverse range of metabolites. Instead, multiple conditions are employed with the intent that one set of parameters will generate useful CID spectra without need for an additional analysis. The most basic MS/MS scan uses a fixed collision energy (although some instruments offers ramping energy scan option), which may be not optimal without the pre-examination of the energy dependence of fragmentation. The multiplexed CID technique can easily generate as many as 5 mass spectra in parallel with different collision energies (CE), and this approach does not require any compound-dependent optimization. Furthermore, endogenous metabolites often present across wide concentration ranges within and between samples, and the multiplexed CID approach reduces signals from high-abundance metabolites into the linear dynamic range of the instrument.

An additional advantage of the multiplexed CID technique is an improvement in dynamic quantitative range. Functions with high CE can knock down saturated signals to within the linear dynamic range of the instrument. At the same time, low CE scan will still keep the low abundant metabolites detectable.

Although mass spectrometry often fails to yield all the information needed for unambiguous structure assignment of novel metabolites, annotation of detected metabolites can be made based

upon combinations of accurate measurements of molecular and fragment ions. When combined with known reactions involved in specialized metabolism, this information can lead to assignments of candidate structures, even though isomeric metabolites may not be distinguishable by traditional mass spectrometric methods alone. An example of annotation of a metabolite detected as a negative ion at *m/z* 609 in a leaf dip extract of *S. habrochaites* LA1777 is presented here.

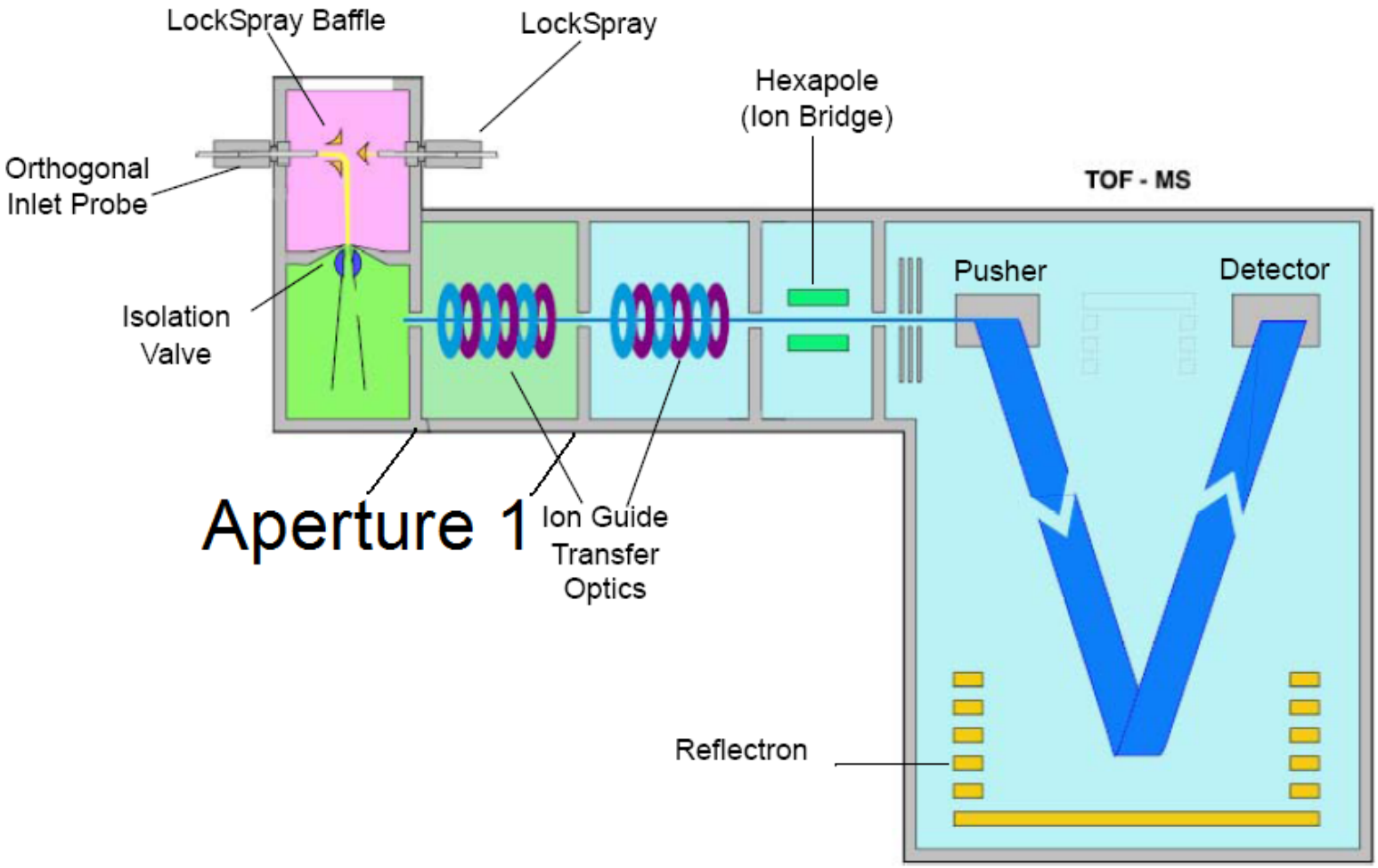

Figure II-2 Schematic Diagram of the Waters LCT Premier time-of-flight mass spectrometer. The region indicated in the diagram is where the ion kinetic energies are influenced by the potential applied to aperture 1. Adapted from Waters Micromass LCT Premier Mass Spectrometer Operator's Guide. For interpretation of the references to color in this and all other figures, the reader is referred to the electronic version of this or dissertation.

The TOF mass spectrometer determined the ion at *m/z* 609.1414 in the lowest Aperture 1 potential data acquisition function. The assignment of the molecular ion was confirmed by the appearance of peaks assigned as $[M+formate]^-$ and $[M+chloride]^-$ at m/z 655.15 and 645.12 respectively. In the spectrum generated using an intermediate CID voltage function (45 V), the formate and chloride adducts did not survive, and are presumed to eliminate formic acid and HCl respectively. The combination of this information confirmed the molecular ion assignment. A list of possible molecular formulas was generated using Waters MassLynx software using: 1) a conservative ± 20 ppm mass window; 2) assuming the ion is an even electron ion, which is most common with electrospray ionization; 3) limiting elemental composition to include only C, H, N, O, P, S. For this m/z 609 ion, the range of atoms allowed for each element were set as follows: C 1-50; H 1-100; N 0-4 (it is rare to find more than 4 N in a hydrophobic metabolite); O 0-20; P 0-2 (more than 1 P usually means a polyphosphate, and most of these are polar and not expected to be retained on reverse phase chromatography except the lipophilic prenyl pyrophosphates); S 0 (the isotope pattern did not indicate presence of sulfur). The software evaluated 1801 possible molecular formula based on the criteria 2), 3) and returned a list of 49 molecular formulas that satisfied ± 20 ppm mass window. Formulas were then ranked according to goodness of fit of the abundances of isotopolog ions using the MassLynx iFIT score, and the 10 formulas with the highest scores were selected (Figure II-3) and searched against the online database ChemSpider (http://www.chemspider.org) to generate a list of potential structures. Two of the ten formulas gave hits in ChemSpider. The formula $C_{27}H_{30}O_{16}$ yielded 20 possible isomers (total 193 hits), all of which were glycosylated flavonoids (Figure II-4). The other

formula giving matches was $C_{28}H_{26}N_4O_{12}$ with 4 hits (Figure II-5). Since mass spectrum exhibited an abundant $[M-H]^-$ ion, it was concluded that the molecule is likely to have one or more acidic functional groups. Three of the ChemSpider structures for $C_{28}H_{26}N_4O_{12}$ lacked acidic functional group, so only hit number 2, which has a carboxylic acid group, was considered a possible candidate.

Single Mass Analysis

Tolerance = 20.0 PPM / DBE: min = -1.5, max = 50.0

Selected filters: None

Monoisotopic Mass, Even Electron Ions

1801 formula(e) evaluated with 49 results within limits (up to 10 best isotopic matches for each mass)

Mass	Calc. Mass	mDa	PPM	DBE	Formula	i-FIT	C	H	N	O	P
609.1414	609.1456	-4.2	-6.9	13.5	C27 H29 O16	21.0	27	29		16	
	609.1373	4.1	6.7	13.5	C27 H30 O14 P	29.6	27	30		14	1
	609.1486	-7.2	-11.8	13.5	C26 H30 N2 O13 P	48.1	26	30	2	13	1
	609.1316	9.8	16.1	14.5	C24 H25 N4 O15	51.4	24	25	4	15	
	609.1403	1.1	1.8	13.5	C26 H31 N2 O11 P2	52.7	26	31	2	11	2
	609.1415	-0.1	-0.2	9.5	C22 H29 N2 O18	63.5	22	29	2	18	
	609.1469	-5.5	-9.0	18.5	C28 H25 N4 O12	69.8	28	25	4	12	
	609.1357	5.7	9.4	18.5	C29 H25 N2 O13	72.9	29	25	2	13	
	609.1387	2.7	4.4	18.5	C28 H26 N4 O10 P	74.5	28	26	4	10	1
	609.1303	11.1	18.2	9.5	C23 H29 O19	74.6	23	29		19	

Figure II-3 The top 10 possible molecular formula for m/z 609.1414, a metabolite ion from *S. habrochaites* LA1777, generated by Masslynx software (Waters). DBE (double bond equivalent), i-Fit is expressed in arbitrary units, and measures the goodness of fit to the isotopic pattern calculated for each elemental composition. Lower i-Fit values reflect a superior fit.

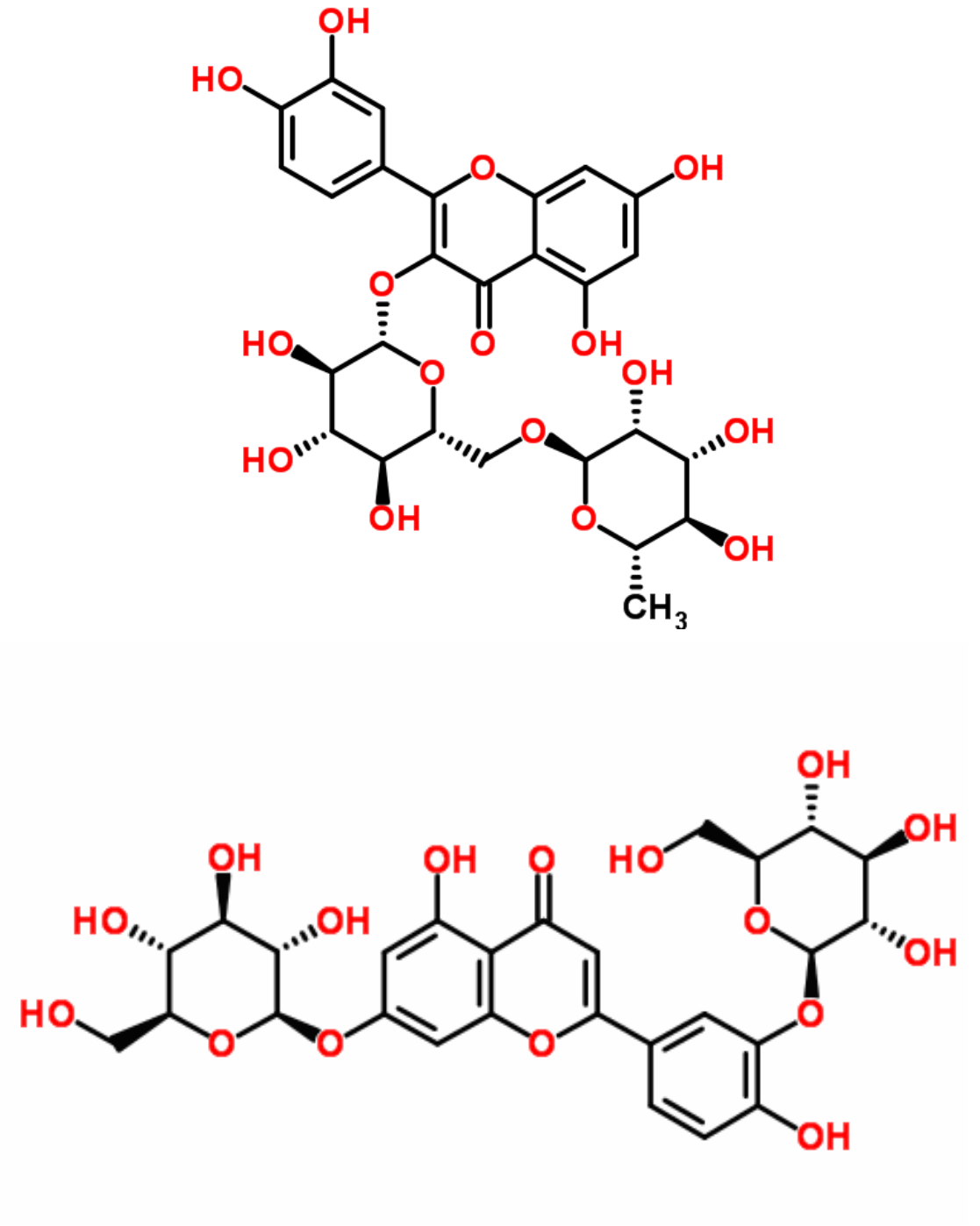

Figure II-4 The 2 examples of 20 matching structures found on the ChemSpider database for formula $C_{27}H_{30}O_{16}$.

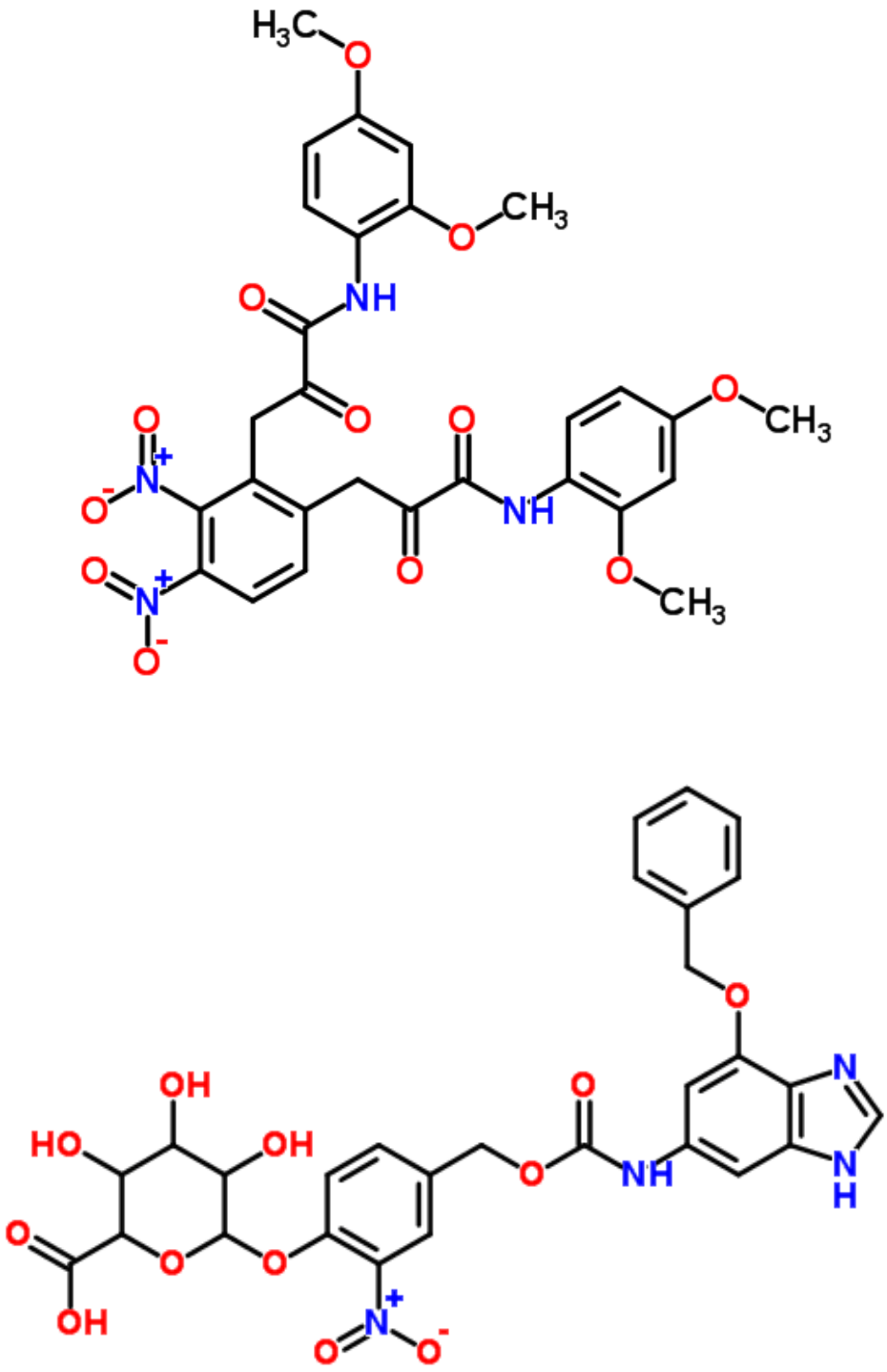

Figure II-5 The 4 matching structures found on the ChemSpider database for formula $C_{28}H_{26}N_4O_{12}$.

Figure II-5 (cont'd)

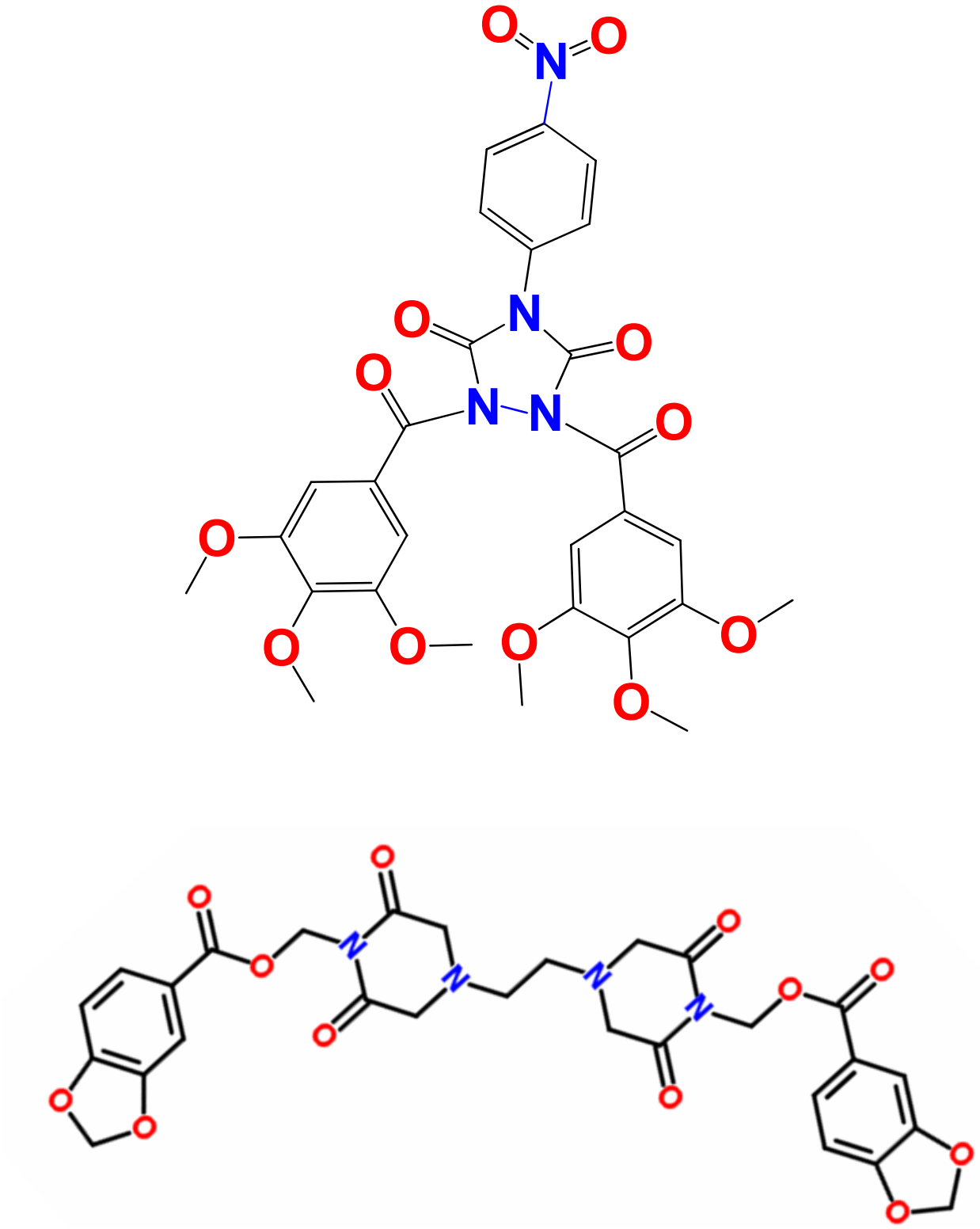

At this stage, information about masses of fragment ions, generated using the higher Aperture 1 voltage, was incorporated into the metabolite annotation process. The averaged mass spectrum across the entire elution profile for m/z 609 (using Aperture 1=75 V) showed the presence of two fragment ions at m/z 284 and 300. By aligning the extracted ion chromatogram of fragment ions with pseudomolecular ion m/z 609, the m/z 284 fragment was assigned to the same compound as m/z 609 owing to matching chromatographic elution profiles for these two masses (Figure II-6). Two partially resolved peaks in the XIC for m/z 609 are apparent, with retention times of 7.56 and 7.89 min. Mass measurements for these two peaks showed values of m/z 609 that only differ by 0.8 milliDaltons. Both peaks displayed a dominant fragment ion of m/z 284 at elevated Aperture 1 potential, which suggests they are isomers. The accurate mass for this fragment ion is m/z 284.0340 for the later eluting peak (theoretical m/z = 284.0326 for $C_{15}H_8O_6^-$, discussed in detail below). Within the spectra of these peaks, an additional fragment ion at m/z 300 was observed, but its elution profile did not match the elution for m/z 609. Instead, the retention time profile of this m/z 300 fragment ion reached a maximum at 7.67 min, and matches the profile of m/z 625. Both pseudomolecular and fragment ion masses are 16 Da heavier than the m/z 609 and 284 pair, suggesting an additional oxygen atom in the former.

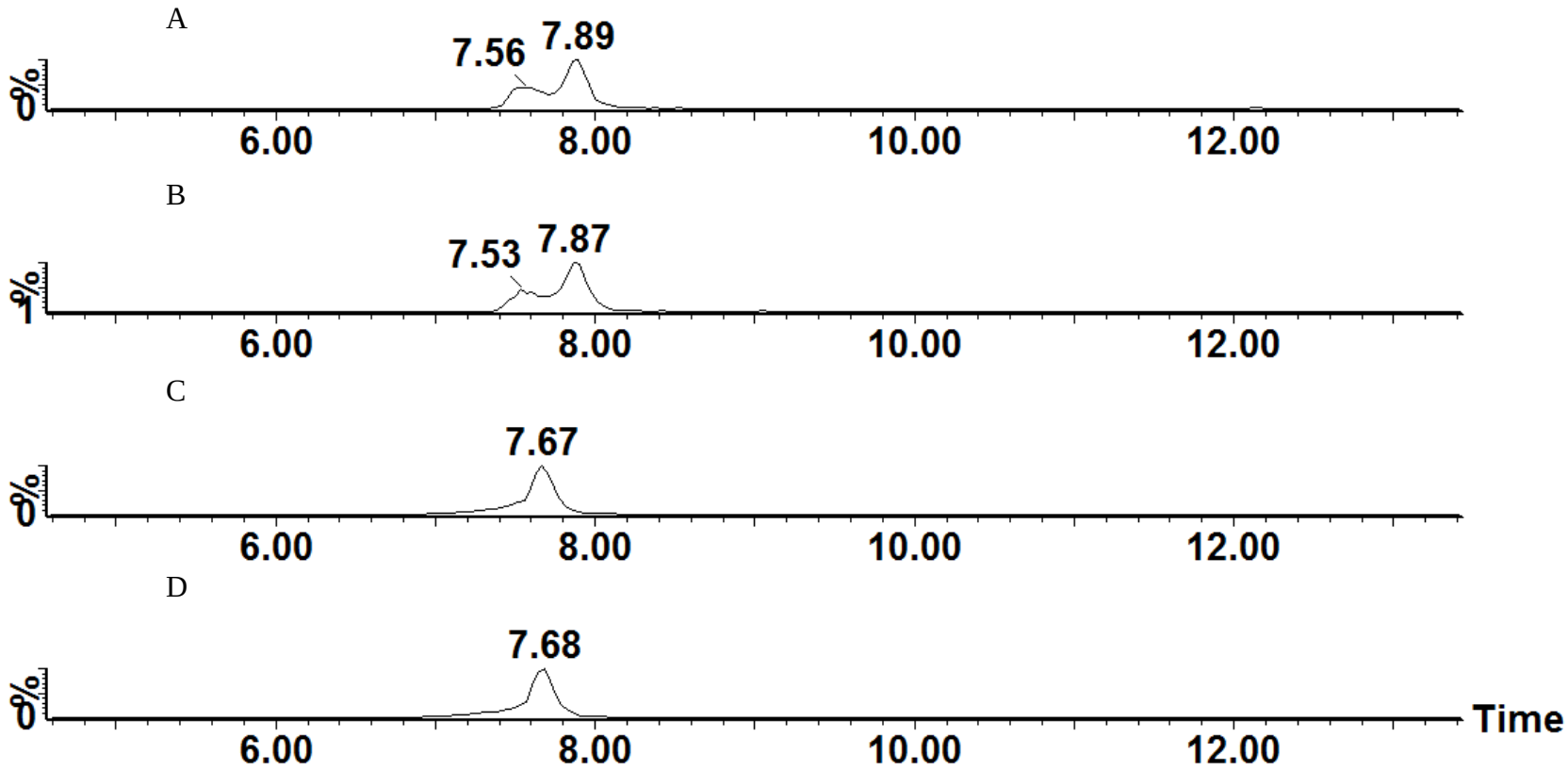

Figure II-6 Extracted ion LC/TOF MS chromatograms (XIC) for an extract of *S. habrochaites* LA1777 leaf type VI trichomes (electrospray, negative): A) m/z 609 at low CID potential (aperture 1 = 10 V); B) m/z 284 at high CID (aperture 1= 75 V); C) m/z 625 at low CID (aperture 1 = 10 V); D) m/z 300 at high CID (aperture 1=75 V).

To identify possible elemental formulas for the m/z 284 fragment ion, criteria 1) and 3) mentioned above (mass match window and elemental composition limits) were applied within MassLynx software to generate a list of candidate formulas for the fragment ion. Limitation of ion type was extended to include both odd- and even-electron ions because some metabolites, particularly those that can stabilize a radical by delocalization, fragment under CID conditions to generate odd-electron fragments. The elemental composition calculator generated 530 potential formulas within the elemental formula constraints, but only 25 results lay within 20 ppm of the measured mass. Ten elemental formulas with the highest scores of isotopolog pattern fitting were considered and these are displayed in Figure II-7. This list was filtered further by not allowing any increases in the number of an element during fragmentation, and limiting the increase in DBE upon fragmentation to no more than +2. For pseudomolecular ion $C_{27}H_{29}O_{16}^-$, the radical anion fragment $C_{15}H_8O_6^-$ (radical ion) is the only formula that meets these criteria. This formula also has the lowest DBE per carbon atom, with a value of 0.8. Formulas with DBE/#C much greater than this are unlikely because such formulas leave limited opportunities to accommodate hydrogens and other elements, and metabolites with such low hydrogen counts are rare in nature.

The two molecular ions proposed above were subjected to a search of the ChemSpider database, which returned numerous structures matching the candidate formulas. For the $C_{28}H_{26}N_4O_{12}$ options, no simple fragmentation scheme can account for the fragment ions observed under any CID conditions. In contrast, all 20 structures reported for $C_{27}H_{30}O$ are glycosylated flavonoids with a variety of aglycone and sugar moieties. Plants in the genus

Solanum are already known to make a range of flavonoid aglycones, including kaempferol, quercetin, and myricetin [118, 119], which only differ in the number of hydroxyl groups. These findings point to the likelihood that these isomeric metabolites are glycosylated flavonoids.

Single Mass Analysis

Tolerance = 20.0 PPM / DBE: min = -1.5, max = 50.0

Selected filters: None

Monoisotopic Mass, Odd and Even Electron Ions

530 formula(e) evaluated with 25 results within limits (up to 10 best isotopic matches for each mass)

Mass	Calc. Mass	mDa	PPM	DBE	Formula	i-FIT	C	H	N	O	P
284.0340	284.0374	-3.4	-12.0	21.0	C21 H4 N2	428.5	21	4	2		
	284.0391	-5.1	-18.0	16.0	C19 H9 O P	571.3	19	9		1	1
	284.0348	-0.8	-2.8	16.5	C18 H6 N O3	579.2	18	6	1	3	
	284.0378	-3.8	-13.4	16.5	C17 H7 N3 P	648.9	17	7	3		1
	284.0334	0.6	2.1	17.0	C16 H4 N4 O2	662.9	16	4	4	2	
	284.0321	1.9	6.7	12.0	C15 H8 O6	760.8	15	8		6	
	284.0394	-5.4	-19.0	11.5	C15 H12 N O P2	817.7	15	12	1	1	2
	284.0351	-1.1	-3.9	12.0	C14 H9 N2 O3 P	827.0	14	9	2	3	1
	284.0307	3.3	11.6	12.5	C13 H6 N3 O5	856.0	13	6	3	5	
	284.0381	-4.1	-14.4	12.0	C13 H10 N4 P2	907.5	13	10	4		2

Figure II-7 The top 10 possible elemental formulas for fragment ion m/z 284.0340 obtained by averaging spectra (7.5-7.9 min; aperture 1= 75 V) from LC/TOF MS analysis of an extract of leaf type VI trichomes from *S. habrochaites* LA1777 (electrospray, negative mode).

The fragment ion of m/z 284 matches the mass of kaempferol anion radical. For kaempferol glycosides, the observed fragment ion mass can be explained by homolytic cleavage of the glycosidic bond to give the kaempferol anion radical with m/z 284 (Figure II-8). The formation of a single aglycone radical anion fragment suggests that a diglycoside is attached to a single position, probably at the 3-position. However, kaempferol-3,7-di-O-glucoside has been annotated in tomato species before [120, 121], and in the absence of an authentic standard, should be considered as a possibility. The positive mode spectra shows two sequential losses of 162 Da, indicating two hexoses attached to the aglycone (Figure II-8), and would be consistent with kaempferol-3-7-di-O-glucoside. The minor and earlier eluting isomer was putatively annotated as kaempferol-3-sophoroside, which has a diglycoside on the 3-position, based on previous publication [122].

Annotations of other metabolites were performed following similar procedures. It is worth emphasizing that, unlike DNA or protein sequencing, putative annotation of metabolites involves many manual steps that are not easily automated because the chemical diversity of metabolites is far greater than the diversity in building blocks of proteins and oligonucleotides. As a result, metabolite identification remains one of greatest bottlenecks studying the development of metabolomics. Fortunately, mass spectrometric methods that provide rapid determination of pseudomolecular and fragment ion masses provide the most powerful information for aiding metabolite identification.

There are four major classes of metabolites annotated from LC/MS analyses performed of individual trichomes types, with 109 peaks analyzed. These metabolites can be divided into

four different groups: a) flavonoids, b) acylsugars, c) terpenoids, and d) glycoalkaloids. The occurrence of these metabolites is described in more detail below.

A variety of flavonoids were detected in the extracts of individual trichome types. The flavonoids are polyphenolic compounds found in plants, with more than 4000 diversified structures having been catalogued. Most are conjugated to sugar molecules. The roles that flavonoids play in plants remain uncertain. Some proposed mechanisms include protection against UV-B radiation and defense against pathogen attack [123, 124]. Based on the LC/MS analyses, two subclasses of flavonoids were annotated.

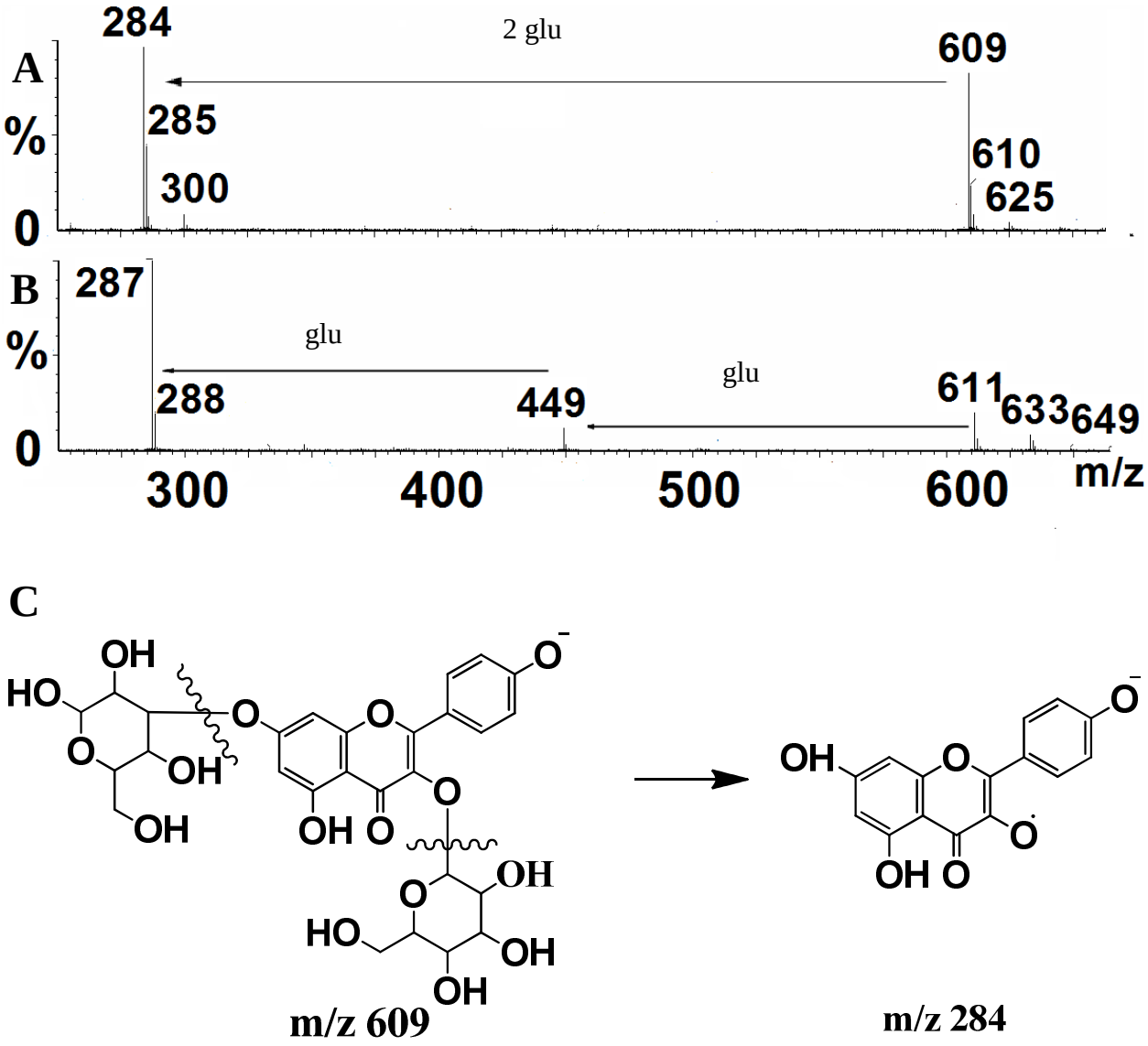

Figure II-8 A) Collision induced dissociation (CID) spectra of *S. habrochaites* LA1777 leaf type VI trichome extract (retention time 7.89 min) using aperture 1= 75 V in negative mode; B) Collision induced dissociation (CID) spectra of the same retention time using aperture 1=75 V in positive mode; C) Proposed fragmentation for kaempferol-3,7-O-diglucoside detected from LA1777 type VI trichome extracts in ESI negative mode.

The first group consists of flavonoid glycosides. The characteristic fragment ion observed for all flavonoid glycosides is derived from cleavage at the glycosidic bond as shown in Figure II-8. The aglycones for flavonoid glycosides were either kaempferol or quercetin, as established using accurate fragment mass measurements as described above. The second subclass of flavonoids consists of methylated flavonoid aglycones which will be discussed in chapter IV in detail. The methylated flavonoids were O-methylated aglycones of myricetin and kaempferol but methylated quercetins were not found in this investigation. The flavonoids detected in individual trichome types are presented in (Table II-2).

Acylsugars comprise the most abundant and diverse group of specialized metabolites detected in trichomes. Acylsugars are viscous lipids with various acyl chains attached on the sugar core. It constitutes a significant portion of leaf biomass in the wild type tomatoes [125]. Due to the potent anti-insects activity of acylsugars, increasing acylsugar production has long been a major target of tomato breeding [126-129]. Acylsugars have also been recognized as potential feedstocks for food and some cosmetic applications [130, 131]. So far, the mechanism of acylsugar biosynthesis and factors that regulate this biochemistry are not completely understood yet.

Table II-2 List of glycosylated flavonoids and methylated flavonoids detected in all trichome extracts using LC/MS in negative ion mode. Listed fragment ions were generated using aperture 1= 75 V aperture 1.

Glycosylated flavonoid annotation	$[M-H]^-$	$[M+formate]^-$	Major fragment ions (m/z)	Observed species and types
Quercetin-3-rutinoside	609	655	300	M82 (type VI), LA0716 (type VI)
Kaempferol-hexosides	609	655	284	LA1777 (both leaf and stem type I, IV, VI) LA1589 (type VI) LA1708 (type VI)
Quercetin-dihexoside	625	671	300	LA1777 (both leaf and stem type I, IV, VI), M82 (type VI)

Methyl flavonoid annotation	$[M-H]^-$	Major fragment ions (m/z)	Observed species and types
monomethyl myricetin	331	316	M82 (type I, type VI)
dimethyl myricetin	345	330, 315	LA1777 (both leaf and stem type I, IV, VI, VII)
trimethyl myricetin	359	344, 329, 314	LA1777 (both leaf and stem type I, IV, VI, VII)
tetramethyl myricetin	373	358, 343, 328, 313	LA1777 (both leaf and stem type I, IV, VI, VII)
monomethyl kaempferol	299	284	LA0716 (type IV, VI)
dimethyl kaempferol	313	298, 283	LA0716 (type IV, VI),

A large number of acylsugars were detected in extracts of individual trichome types. Under energetic CID conditions, the characteristic fragmentation of acylsugars involves sequential losses of acyl chains from the sugar core as illustrated in Figure II-9. Since acylsugars lack functional groups that readily gain or lose protons, acylsugars are predominantly

observed as $[M+HCOO]^-$ in negative mode electrospray ionization mass spectra. Upon CID, such acylsugar ions generate a series of fatty acid anion fragments that are observed at the low mass end of the CID spectra. From their masses, it is possible to establish which acyl chains were attached to the sugar core. In Figure II-9, m/z 87, 101 and 171 indicates C_4, C_5, and C_{10} acyl chains. The presence of acetate ester groups is not apparent owing to the low ion transmission of the mass spectrometer at low masses, but can be established from mass differences between the deprotonated acylsugars (which form under slightly elevated CID energies) and fragment ions in the high mass region, e.g. from the 42 Da difference between m/z 691→ 649. The exact positions of acyl chain substitutions cannot be assigned explicitly from mass spectra because cleavage of sugar carbon-carbon bonds, which would help indicate positions of esters, have not been observed under any CID conditions.

To simplify naming of acylsugar metabolites, we developed a nomenclature as follows: a single letter corresponding to the base sugar (G = glucose; S = sucrose) followed by the designation of number of fatty acyl groups and total number of acyl carbon atoms. For example, a sucrose tetraester acylated with C_2, C_4, C_5, C_{10} fatty acids as mentioned above would be designated as $S4:21^{(2,4,5,10)}$. A compilation of acylsugars detected in individual trichome types is presented in Table II-3, and the differences between trichomes are discussed in more detail below.

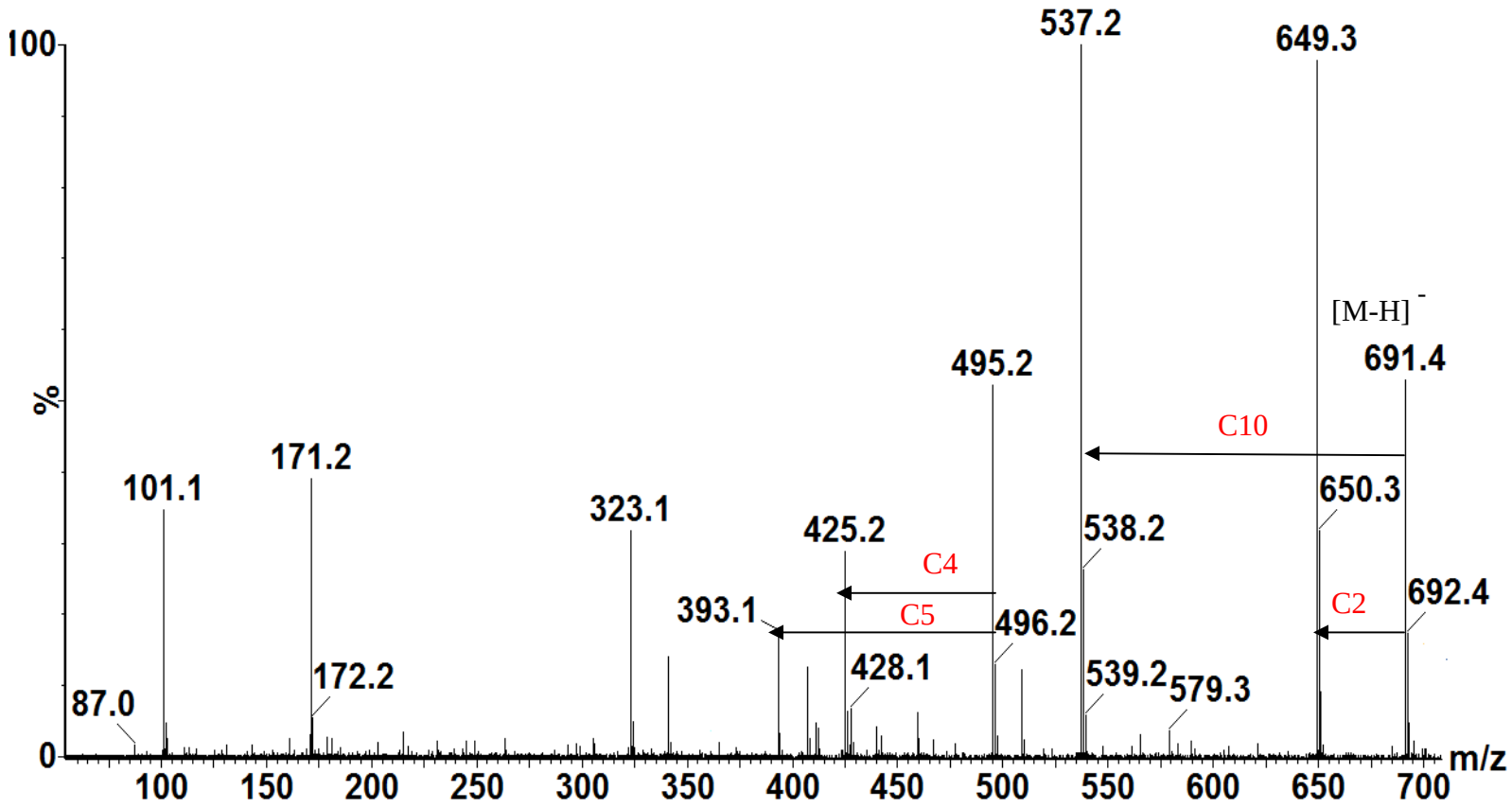

Figure II-9 Top panel: CID spectra of acylsugar S4:21 (75V aperture 1 voltage) from extract of *S. habrochaites* LA1777 type I trichomes in ESI negative mode; bottom panel: proposed fragment ions observed for S4:21$^{(2,4,5,10)}$.

Figure II-9 (cont'd)

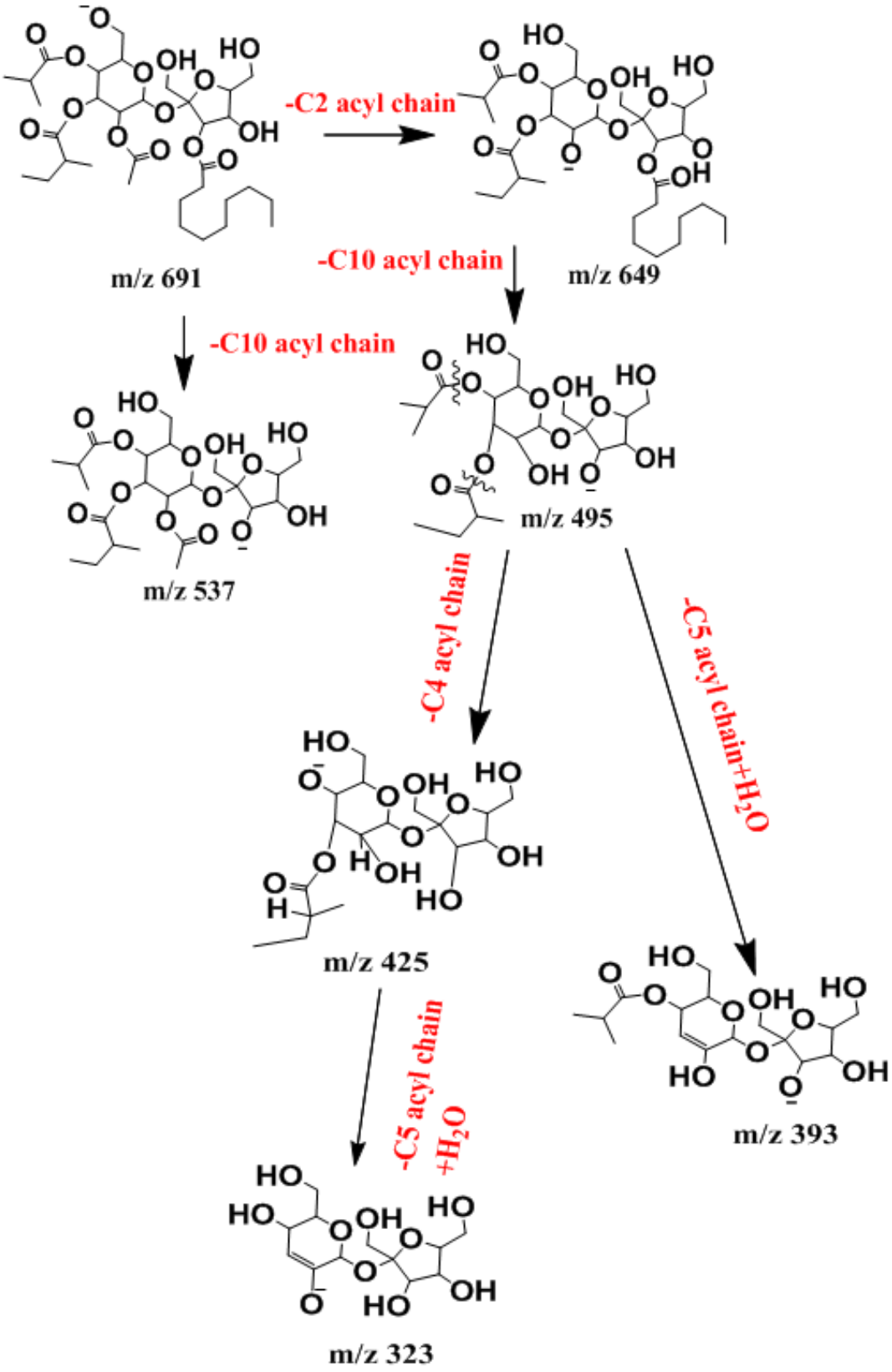

Table II-3 List of acylsugar metabolites detected in trichome extracts using LC/MS in negative ion mode. Fragment ions were generated using aperture 1= 45 V.

Acylsugar	Fatty acid ester groups	$[M+formate]^-$ (m/z)	Major fragment ions (m/z)	Observed species and types
G 3:12	C4, C4, C4	435	347, 213,143, 125, 87	LA 0716 (type IV, VI)
G 3:13	C4, C4, C5	449	361, 315, 227, 143, 125, 101, 87	
G 3:14	C4, C5, C5	463	375, 329, 227, 143, 125, 101, 87	
G 3:15	C5, C5, C5	477	375, 329, 227, 143, 125, 101	
G 3:16	C4, C4, C8	491	347, 301, 213, 125, 143, 87	
G 3:17	C4, C5, C8 C4, C4, C9	505	361, 315, 227, 125, 143, 101, 87 347, 301, 213, 125, 143,157, 87	
G 3:18	C4, C4, C10	519	347, 301, 213, 143, 125, 171, 87	
G 3:19	C4, C5, C10	533	361, 315, 227, 143, 171, 101, 87	
G 3:20	C5, C5, C10 C4, C4, C12	547	347, 301, 213, 143,125, 171, 101 375, 329, 227, 143,125, 199, 87	
G 3:21	C4, C5, C12	561	361, 315, 227, 143, 199, 101, 87	
G 3:22	C5, C5, C12	575	375, 329, 227, 143, 199, 101	

Table II-3 (cont'd)

S 3:12	C4, C4, C4	597	551, 481, 411, 341, 87	LA1777 (both leaf and stem type I, IV, VI, VII)
S 3:13	C4, C4, C5	611	565, 495, 411, 341, 101, 87	
S 3:14	C4, C5, C5	625	579, 495, 411, 341, 101, 87	
S 3:15	C5, C5, C5	639	593, 425, 407, 341, 323,101	LA1777 (both leaf and stem type I, IV, VI, VII) M82 (type I, type VI)
S 3:18	C4, C4, C10	681	635, 565, 481, 411, 341, 171, 87	LA1777 (both leaf and stem type I, IV, VI, VII)
S 3:19	C4, C5, C10	695	565,495,425,407,341,171, 101	
S 3:20	C5, C5, C10 C4, C4, C12	709	663, 579, 509, 425, 407, 341, 323, 171, 101 663, 593, 481, 397, 341, 199, 87	LA1777 (both leaf and stem type I, IV, VI, VII) M82 (type I, type VI)
S 3:21	C4,C5,C12	723	677, 593, 495, 425, 341, 199, 101, 87	LA1777 (both leaf and stem type I, IV, VI, VII)
S 3:22	C5,C5,C12	737	691, 607, 509, 425, 341, 199, 101	LA1777 (both leaf and stem type I, IV, VI, VII) M82 (type I, type VI)
S 3:24	C4, C10, C10	765	719, 649, 565, 395, 411, 341, 171, 87	LA1777 (both leaf and stem type I, IV, VI, VII)
S 3:25	C5, C10, C10	779	733, 629, 579, 425, 341, 171, 101	
S 4:14	C2,C4,C4,C4	639	593, 551, 87	
S 4:15	C2,C4,C4,C5	653	607, 565, 101, 87	

Table II-3 (cont'd)

S 4:16	C2,C4,C5,C5	667	621, 579, 537, 495, 393, 341, 323, 101, 87	LA1777 (both leaf and stem type I, IV, VI, VII)
S 4:17	C2,C5,C5,C5	681	635, 551, 509, 425, 407, 341, 323, 101	LA1777 (both leaf and stem type I, IV, VI, VII) M82 (type I, type VI)
S 4:20	C2,C4,C4,C10	723	677, 635, 481, 411, 393, 341, 323, 101, 87	LA1777 (both leaf and stem type I, IV, VI, VII)
S 4:21	C2,C4,C5,C10	737	691, 649, 495, 393, 341, 323, 171, 101, 87	
S 4:22	C2,C4,C4,C12	751	709, 663, 481, 393, 341, 323, 305, 199, 87	LA1777 (both leaf and stem type I, IV, VI, VII) M82 (type I, type VI)
S 4:23	C2,C4,C5,C12	765	719, 677, 495, 411, 341, 323, 199, 101, 87	LA1777 (both leaf and stem type I, IV, VI, VII)
S 4:24	C2,C5,C5,C12	779	733, 691, 509, 425, 407, 341, 323, 199, 101	LA1777 (both leaf and stem type I, IV, VI, VII) M82 (type I, type VI)

Trichomes also accumulate significant quantities of terpenoid metabolites. Terpenoids are derived from the five carbon isoprene substructural unit. The terpene biosynthesis pathways are important to plant growth because some plant growth regulators such as gibberellins are terpenoid metabolites. Structures of numerous other important metabolites also incorporate intermediates of the terpene biosynthesis such as the phytol tail group in chlorophylls. A large

proportion of interest in terpenes has focused on volatile terpenes, primarily the mono- and sesquiterpenes [113]. A variety of sesquiterpenes accumulating in *S. habrochaites* LA1777 were reported before [132-134], including carboxylic acid derivatives of α-santalenoic and bergamotenoic acids. Analyses of extracts of this accession using LC/MS in negative ion mode revealed three major isomers having m/z 233.15, consistent with these acids. Their putative assignment was based on exact mass and fragments (Figure II-10). Most notable is the formation of fragment ions at m/z 98 and 99, which are consistent with fragmentation at the allylic carbon-carbon bond. The former fragment ion is an unusual odd-electron fragment derived from an even-electron precursor. Its formation is attributed to stabilization of the allylic radical by delocalization. Several additional terpenoid acids from *S. habrochaites* LA1777 were also annotated based on accurate mass measurements and the calculated relative mass defect [135].

Despite the importance of terpenoid metabolites across plant, animal, and microbe species, tools for recognizing terpenoids based on negative ion mass spectra have been slow to develop. Terpenoid core structures are largely based on alkane and alkene moieties that are resistant to charge-directed fragmentation in negative ion mass spectra. It is proposed that a strong indicator that a metabolite is terpenoid is that these metabolites have moderately high hydrogen content. Owing to the positive mass defect of the hydrogen atom, such molecules have high positive “relative mass defects”. A brief discussion of the importance of mass defects is in order. Mass defect is defined as the difference between true mass and the integer, or nominal mass.

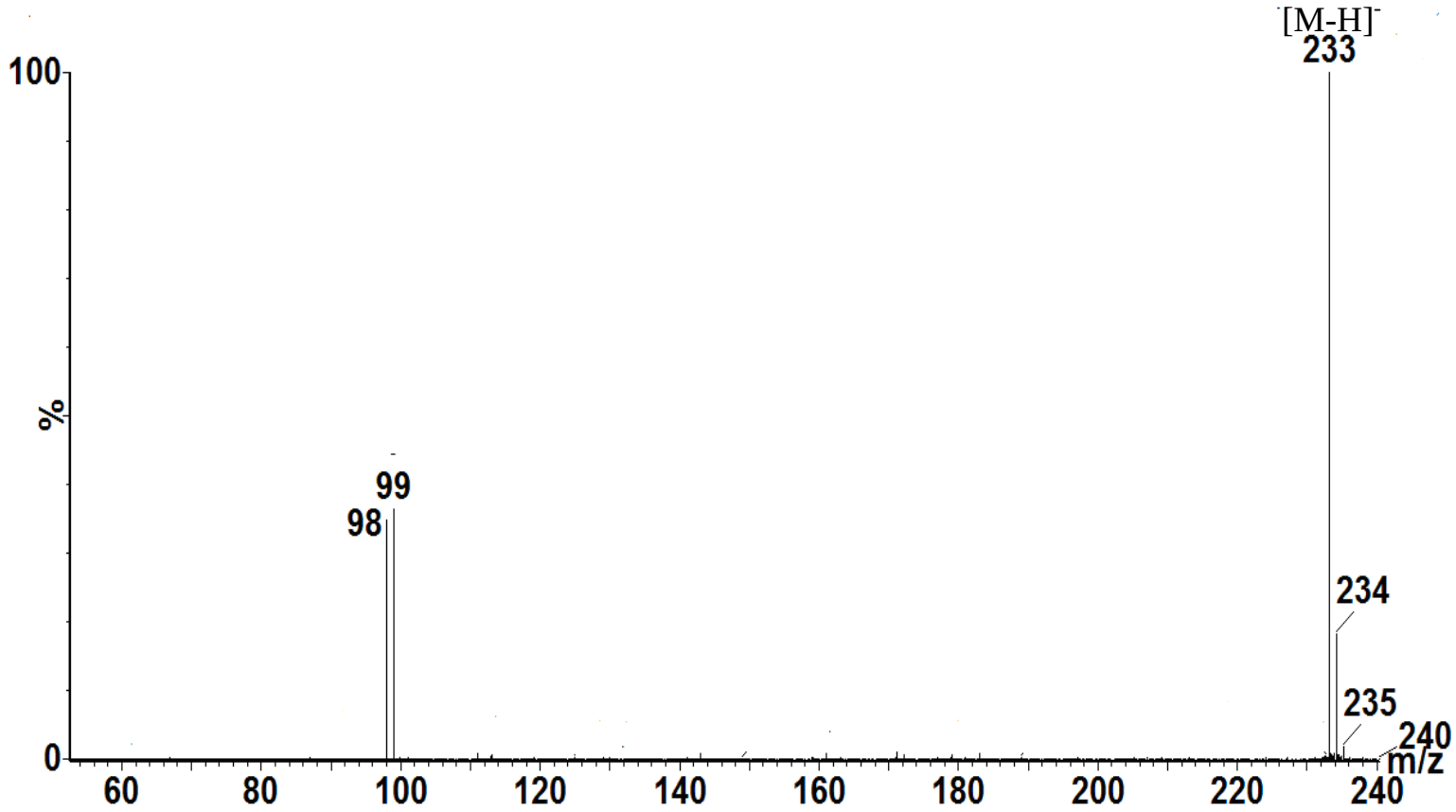

Figure II-10 Top panel: LC/MS product ion spectrum of m/z 233 with retention time 30.77 min from *S. habrochaites* LA1777 type VI trichome extract (ESI, negative) generated on a QTof mass spectrometer (45 V collision voltage); middle panel: LC/MS XIC of m/z 233 (aperture 1= 10 V) from LA1777 type VI trichome extracts in ESI negative mode, full scan MS analysis; bottom panel: proposed fragmentation for α-santalenoic acid.

Figure II-10 (cont'd)

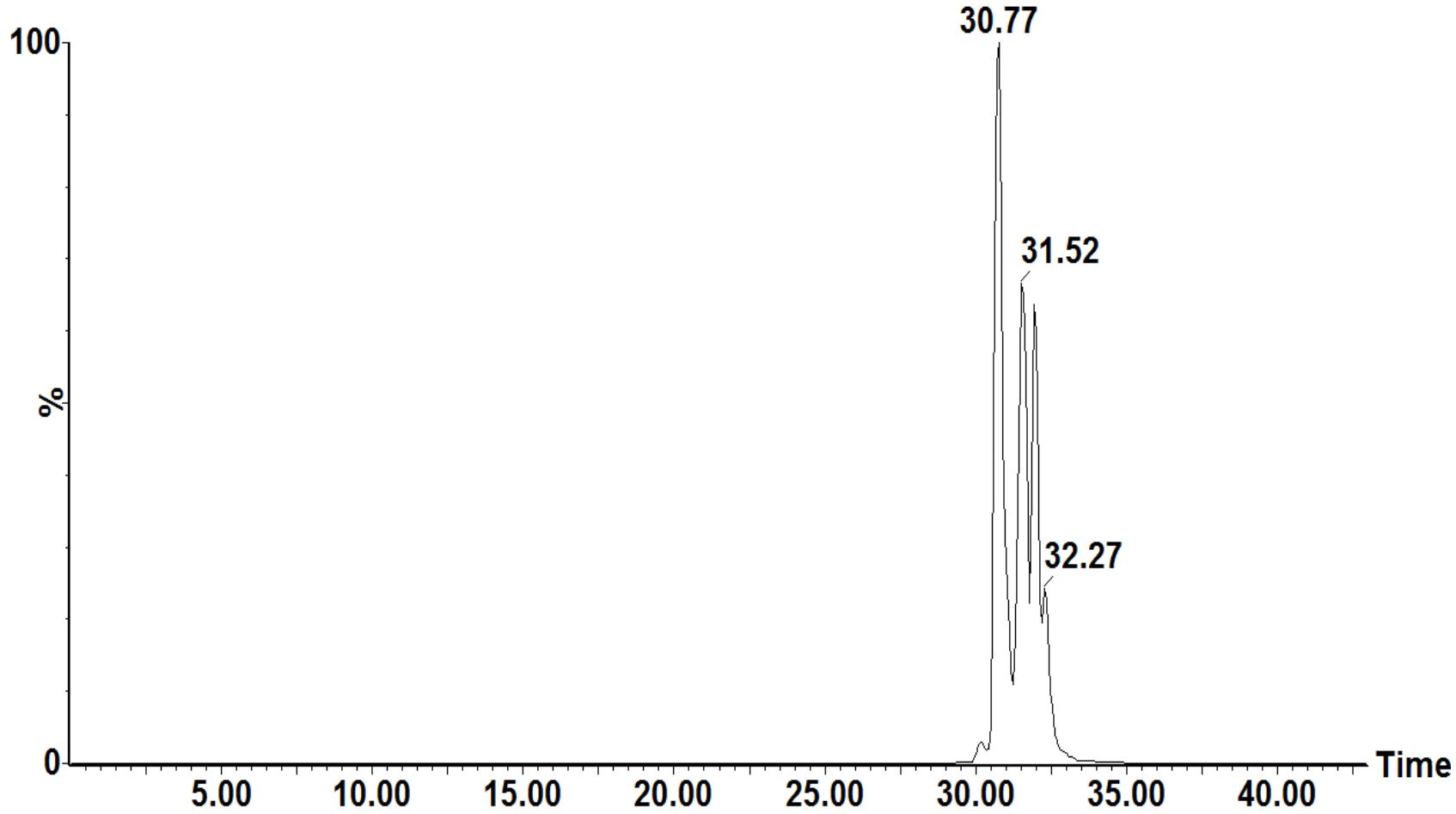

Figure II-10 (cont'd)

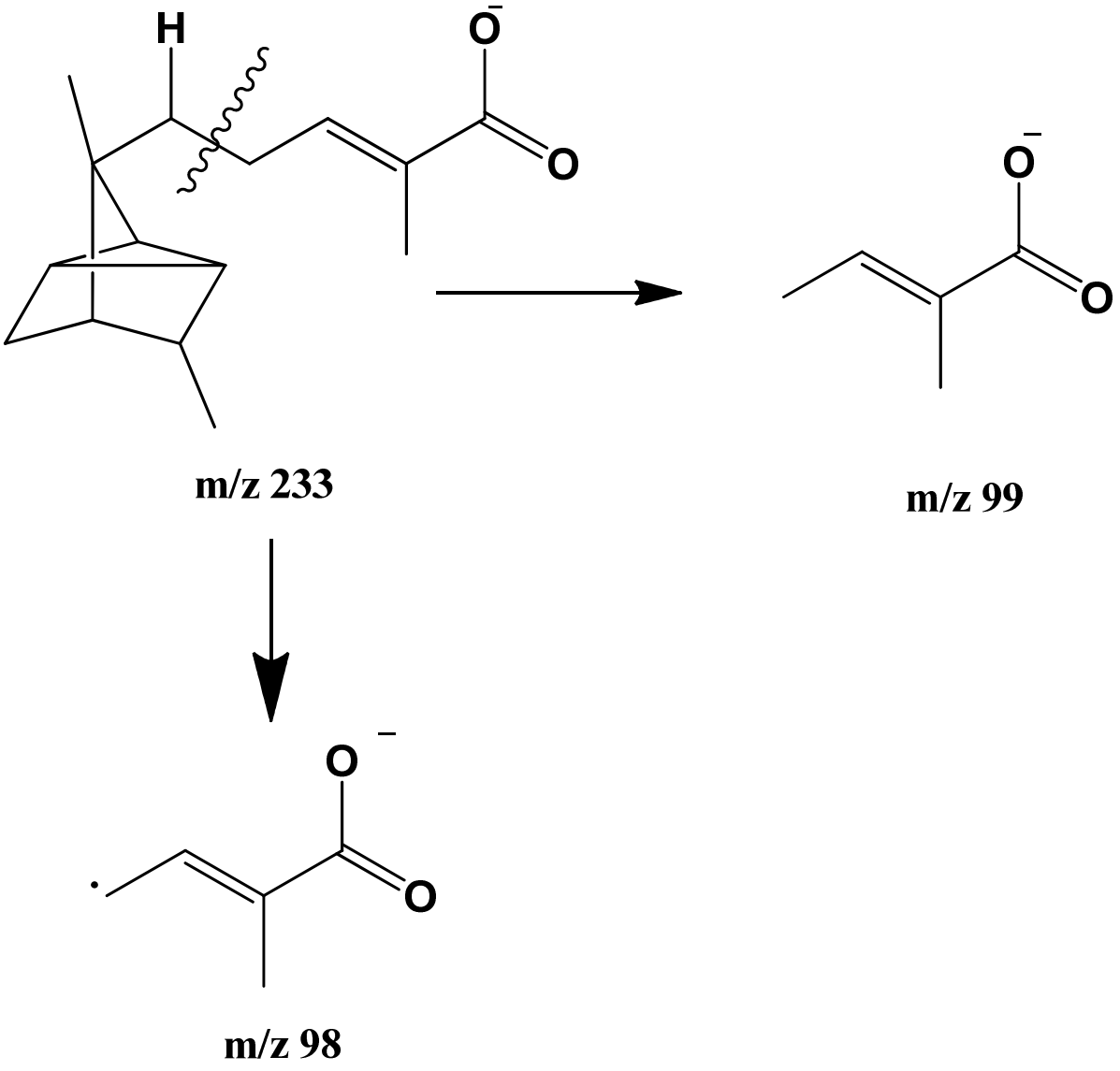

For example, the hydrogen atom (accurate mass: 1.00794 u) has positive mass defect of 0.00794 u. The mass of ^{12}C defines the mass scale at exactly the integer mass, therefore carbon atoms do not contribute to mass defect. Most elements heavier than carbon such as oxygen (accurate mass: 15.9994 u) have masses slightly less than their nominal masses owing to their

nuclear binding energies. Hydrogen atoms (^{1}H) have the highest positive mass defect because there is no nuclear binding energy. Furthermore, the number of hydrogen atoms in many metabolites exceeds the number of atoms of any other type (excluding carbon), and therefore the mass defect largely reflects the number of hydrogen atoms in a molecule. The elemental compositions of metabolites derived from specific biochemical pathways largely reflect their precursors, particularly with regard to hydrogen content. The notion of a relative mass defect, which is calculated by dividing the total mass defect of the molecule by its molecular mass, provides a measure that is strongly correlated with the %H by weight for that molecule. Since terpenes are synthesized from C_5H_8 building blocks, they have higher positive relative mass defect than metabolites such as flavonoids which are derived from precursors of lower hydrogen content. For example, the flavonoid kaempferol ($C_{15}H_{10}O_6$; 3.52% H), has molecular mass of 286.0477 u, and the sesquiterpene acid α-santalenoic acid ($C_{15}H_{22}O_2$, 9.46% H) has molecular mass of 234.1625 u. The relative mass defect for the former is 0.0477/286.0477=166 ppm, whereas the more hydrogen-rich santalenoic acid has a relative mass defect of 693 ppm. In extracts of *S. habrochaites* LA1777, an unknown metabolite with nominal m/z 319 in negative ion mode was annotated as a diterpenoid based on the following factors. a) its relative mass defect of 765 ppm suggested a hydrogen content similar to the sesquiterpene acids. b) the deprotonated ion underwent loss of water upon CID, but further fragmentation was not observed, as is typical for terpenoids c) the accurate mass measurement (m/z 319.2441) suggests it has one more isoprene unit C_5H_8 and addition of H_2O relative to the LA1777 sesquiterpene acids. There are also several sesquiterpene metabolites decorated with sugars and malonate esters as

listed in Table II-4.

Table II-4 List of terpenoid metabolites detected in extracts of individual trichome types using LC/MS in negative ion mode. Fragment ions were generated using aperture 1= 75 V except for the sesquiterpene acids, which were analyzed as product ion spectra using a QTof mass spectrometer with collision potential of 45 V.

Terpenoid metabolites	$[M-H]^-$ (m/z)	Major fragment ions (m/z)	Observed species and types
Sesquiterpene acids (α-santalenoic, bergamotenoic acids)	233	99, 98	LA1777 (both leaf and stem type I, IV, VI, VII)
Sesquiterpene diglycoside, malonate ester	649	605, 563, 401	LA1777 (both leaf and stem type I, IV, VI, VII)
Sesquiterpene diglycoside, malonate diester	717	629, 587, 545, 383	LA1777 (both leaf and stem type I, IV, VI, VII)
Sesquiterpene diglycoside, malonate ester, acetate ester	691	647, 605, 443, 401	LA1777 (both leaf and stem type I, IV, VI, VII)
Sesquiterpene monoglycoside, malonate ester	487	443, 401	LA1777 (both leaf and stem type I, IV, VI, VII)
diterpene acid	319	301	LA1777 (both leaf and stem type I, IV, VI, VII)

Trichomes of wild tomatoes also accumulate two glycoalkaloids. Tomatine, which is the most well known alkaloid in tomato was detected in LA1777 type VII leaf trichome extracts but trace amounts in other trichome types. Annotation was based on the accurate mass measurements, the fragmentation which largely occurs at the glycosidic bonds (Figure II-11), and comparisons to authentic standards. A related compound which has similar retention time and neutral losses as tomatine but is 2 Da lighter than tomatine is annotated as dehydrotomatine. Glycoalkaloids detected in various trichome types are presented in Table II-5.

Table II-5 List of glycoalkaloid metabolites detected in extracts of individual trichome types using LC/MS in positive ion mode. Fragment ions were generated using aperture 1 = 45 V.

Alkaloid glucoside	$[M+H]^-$ (m/z)	Major fragment ions (m/z)	Observed species and types
tomatine	1034.5	903, 740, 578, 560, 416, 398, 273, 255	LA1777 (leaf VII)
dehydrotomatine	1032.5	901. 738, 576, 558, 396, 271	LA1777 (leaf VII)

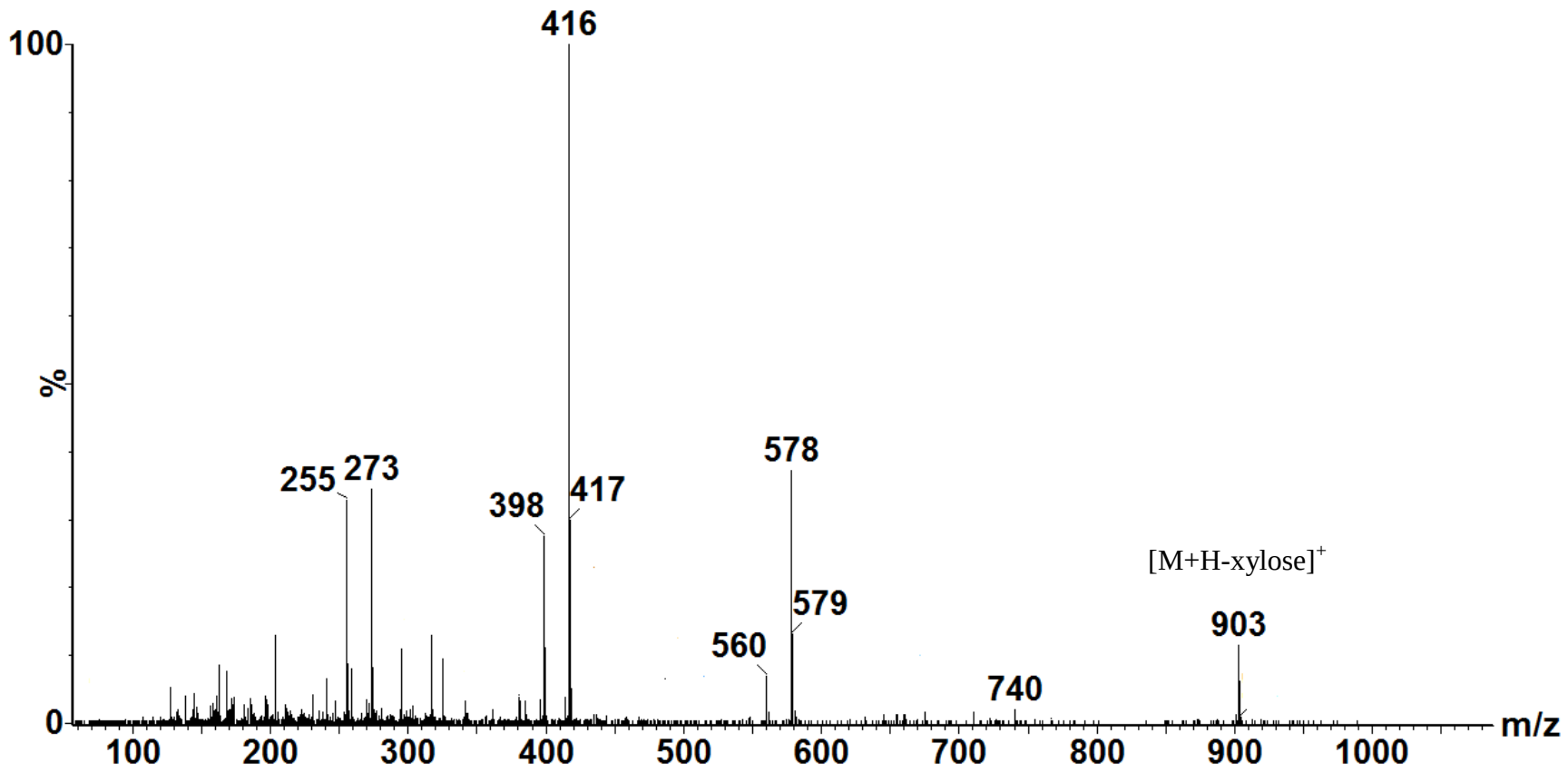

Figure II-11 Top panel: CID spectra of (tomatine) in ESI positive mode (aperture 1= 75 V) from *S. habrochaites* LA1777 type VII trichome extract; bottom panel: proposed fragmentation of protonated tomatine.

Figure II-11 (cont'd)

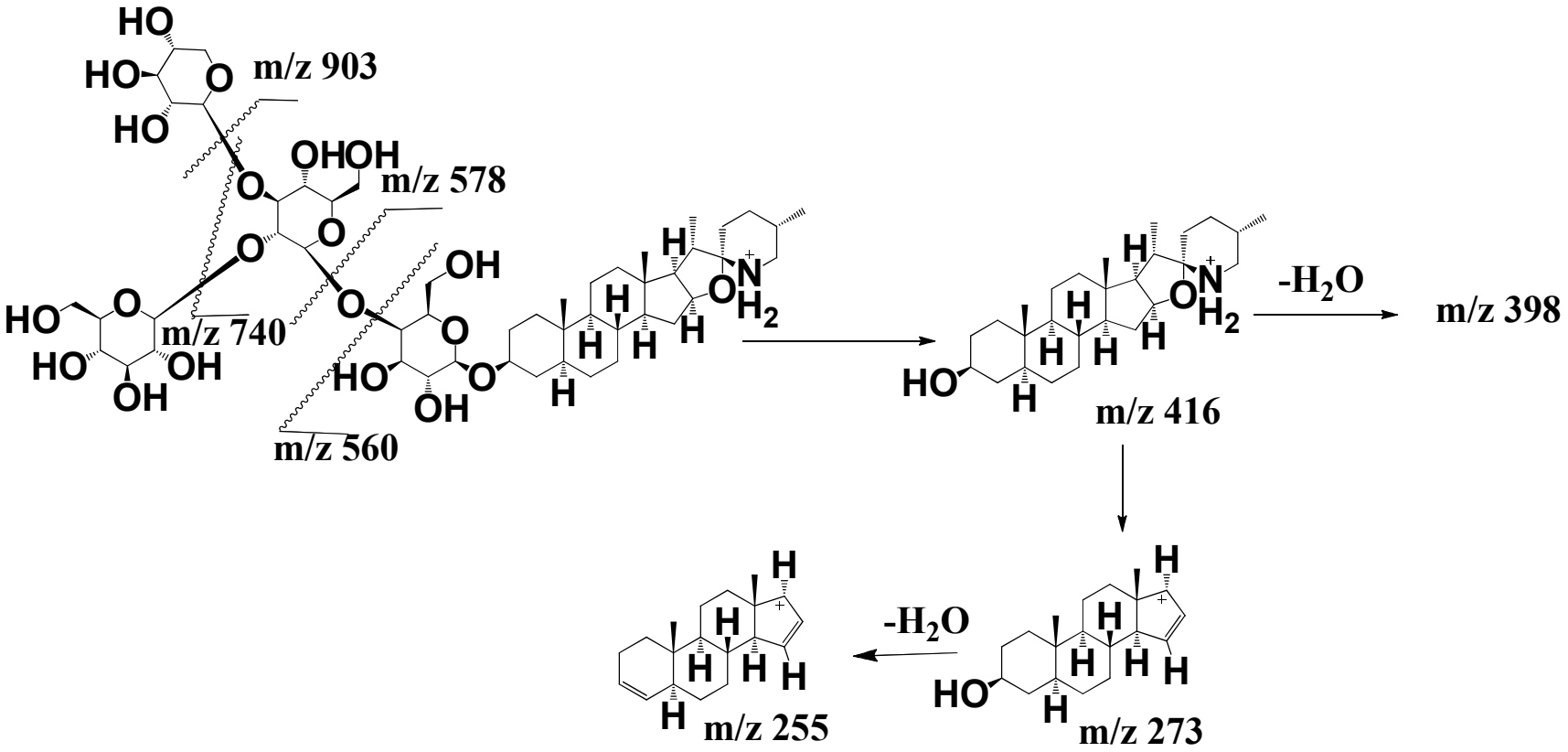

Since *S. arcanum* (LA1708) and *S. pimpinellifolium* (LA1589) have only one trichome type that was collected, and minimal levels of metabolites were detected in those two species, except for glycosylated flavonoids. As a result, the discussion below focuses on the conventional tomato *S. lycopersicum* (M82) and its wild relatives *S. habrochaites* LA1777 and *S. pennellii* LA0716.

An intraspecies comparison of trichome composition was first conducted using LC/MS profiling. For *S. habrochaites* LA1777, we both stem and leaf trichomes were collected, extracted, and analyzed using LC/TOF MS. From Figure II-12 to Figure II-16, metabolite profiles of stem and leaf trichomes of the same morphological types are almost indistiguishable. Type VI trichomes accumulate abundant glycosylated flavonoids (Figure II-12). However, methylated flavonoid aglycones, are predominantly found in type I and IV trichomes (Figure II-13). None of these extracts revealed the presence of flavonoids modified by both methylation and glycosylation, and it is hypothesized that each of these modification reactions precludes the other. These biochemical phenotypes suggest the possibility that glycosyltransferases are highly expressed in type VI glands, whereas O-methyltransferases are abundant in types I and IV.

Terpenoid metabolites exhibit a strong selectivity of accumulation in type VI trichomes (Figure II-14). LA1777 is the only accession studied that accumulates substantial amount of terpenoids. For this reason, the catalog of genes expressed selectively in type VI glands presents a promising source of information regarding candidates for terpenoid biosynthesis genes. For acylsugars the selectivity is reversed. Type I and IV glands accumulate at least 3-fold more

acylsugar per trichome than types VI and VII (Figure II-15). Type VII trichomes comprise the only type among all plant species and gland types that accumulates substantial amounts of glycoalkaloid (Figure II-16). The type VII trichome in LA1777 grows closest to the epidermal pavement cells, which also store tomatine. The possibility that sampling of type VII glands also sampled the pavement cells cannot be excluded.

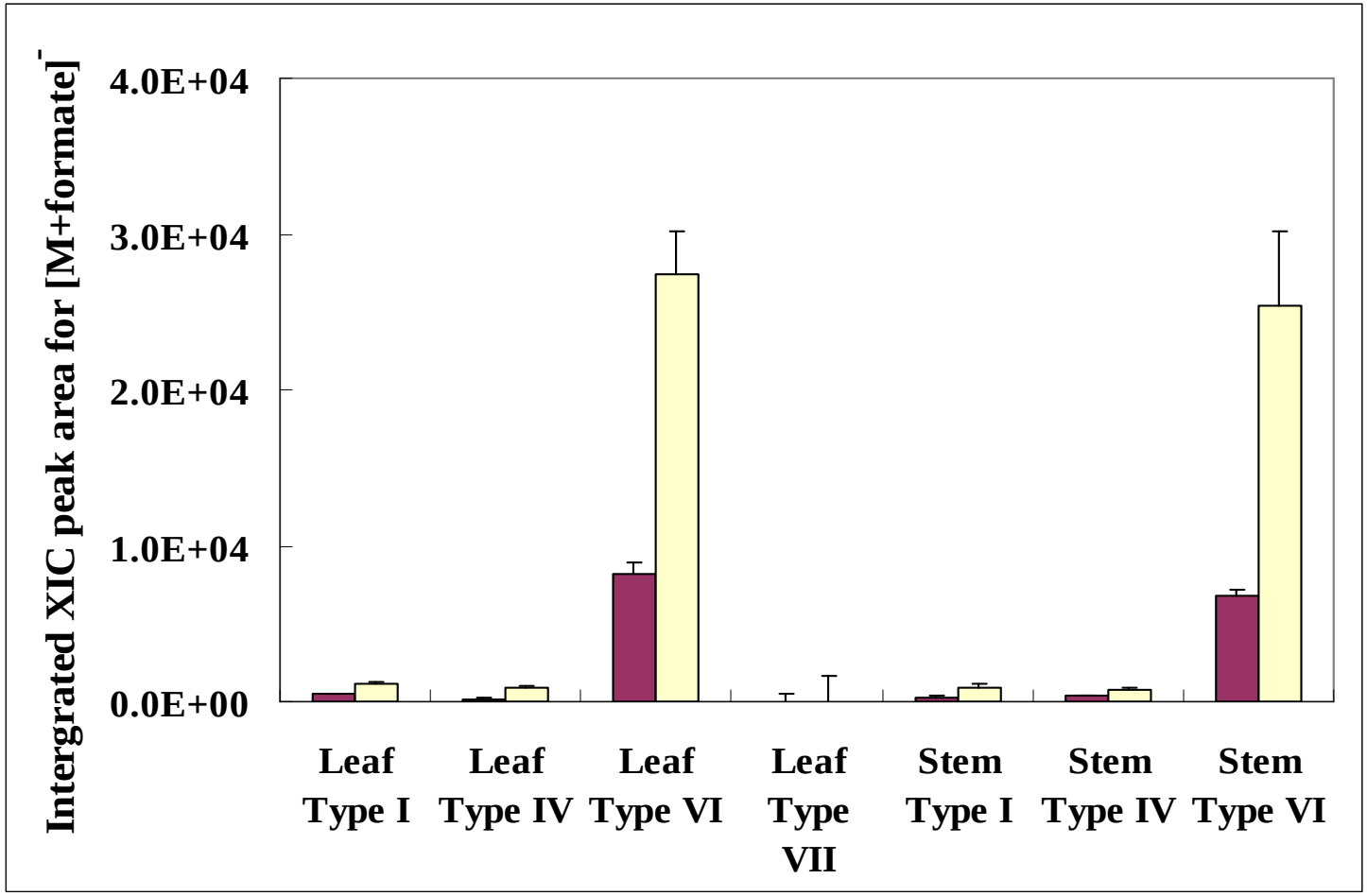

Figure II-12 Quantitative distribution of glycosylated flavonoids in extracts of each type of trichome (50 trichomes extracted in 50 µl solvent) from leaf and stem tissues of *S. habrochaites* (LA1777) measured using negative mode LC/MS. Key: Kaempferol-dihexosides (red) and quercetin –dihexoside (yellow). Error bars indicate standard error with n=3.

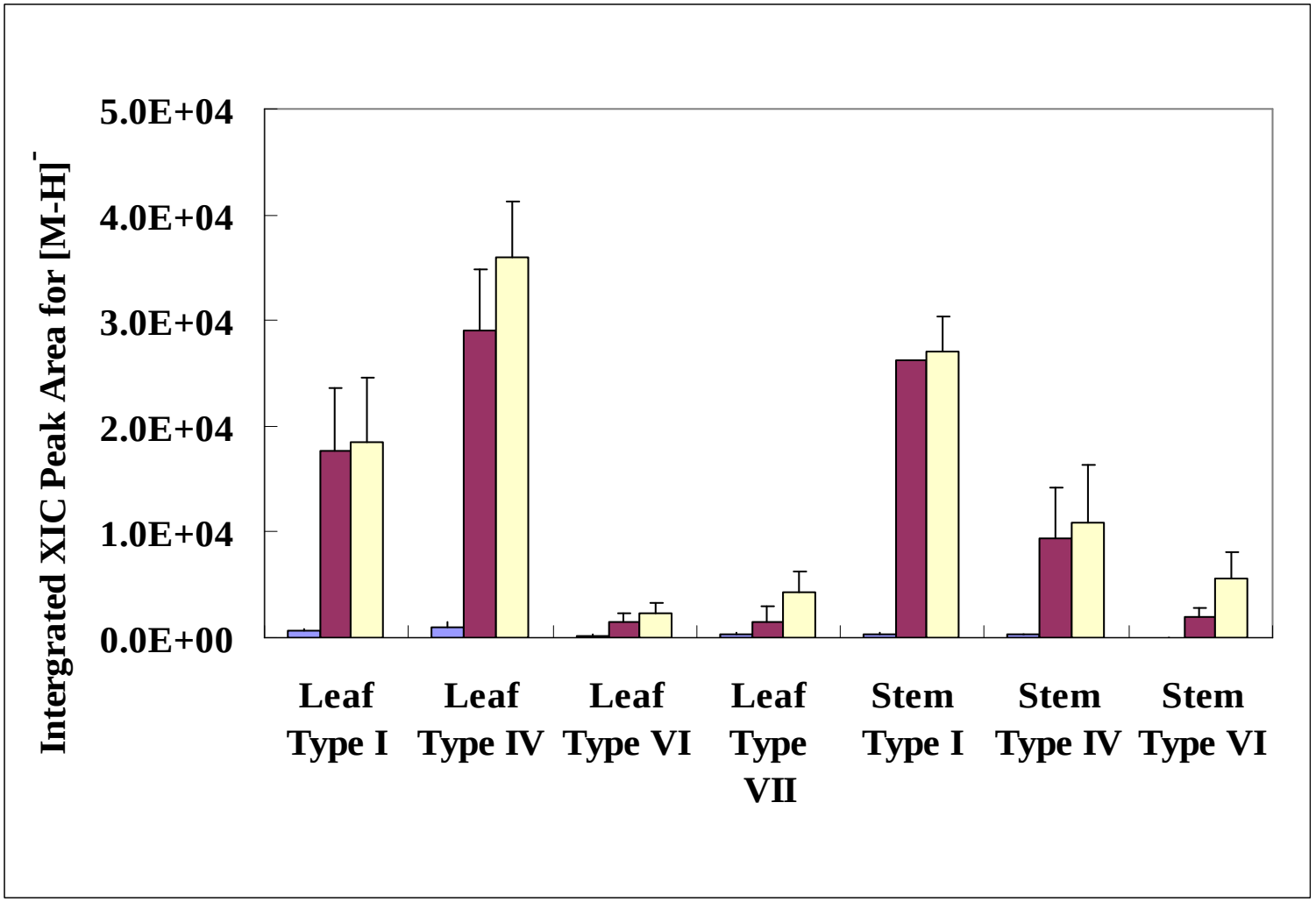

Figure II-13 Quantitative distribution of methylated flavonoids in each types of trichome (from 50 trichomes extracted in 50 µl solvent) from *S. habrochaites* (LA1777) measured using negative mode LC/MS. Key: Dimethyl myricetin (blue) trimethyl myricetin (red) tetramethyl myricetin (yellow). Error bars indicate standard error with n=3.

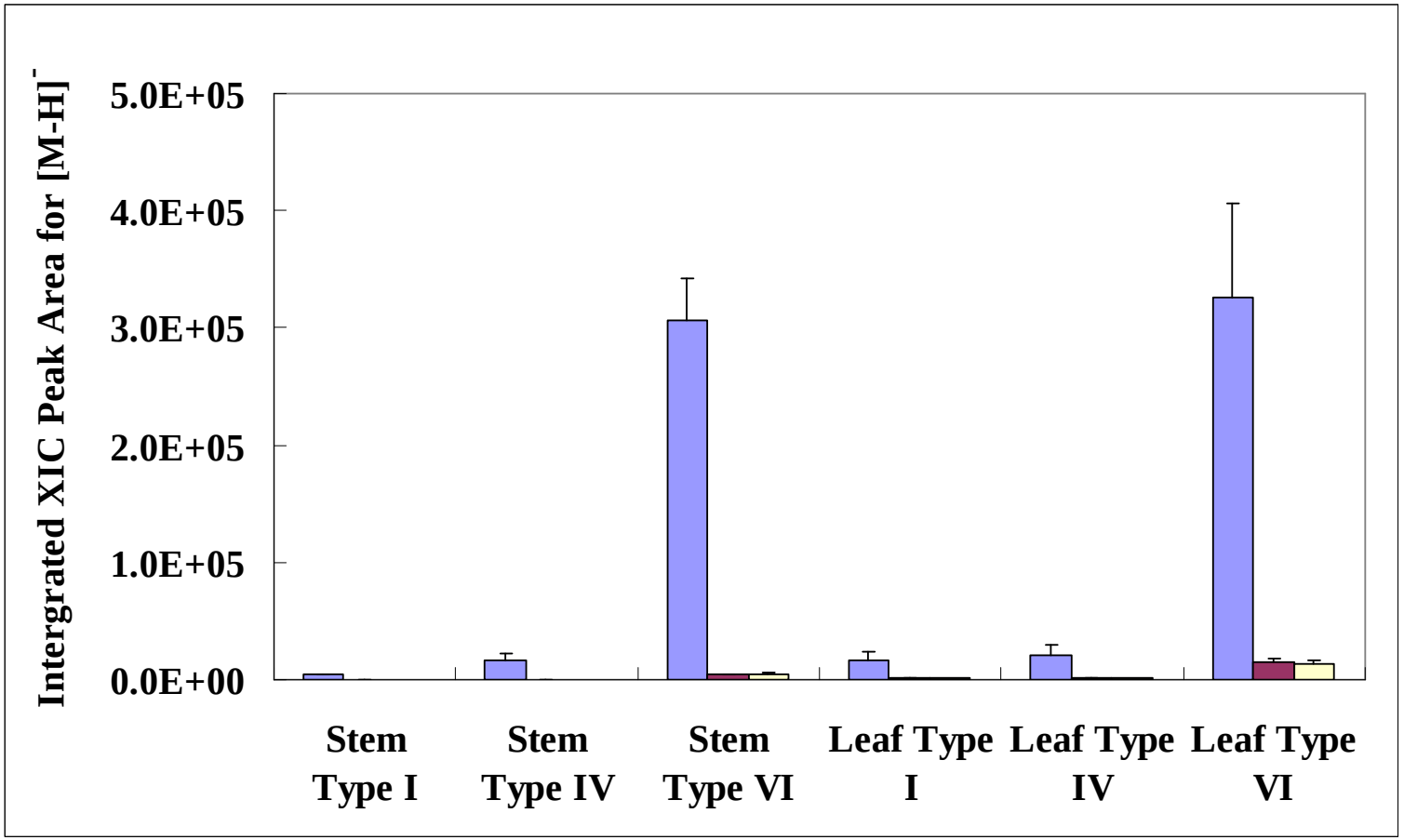

Figure II-14 Quantitative distribution of terpenoid metabolites in each types of trichome (from 50 trichomes extracted in 50 µl solvent) from *S. habrochaites* (LA1777) measured using negative mode LC/MS. Key: sesquiterpene acids (blue), sesquiterpene diglucoside, malonate ester (red), diterpene acid (yellow). Error bars indicate standard error with n=3.

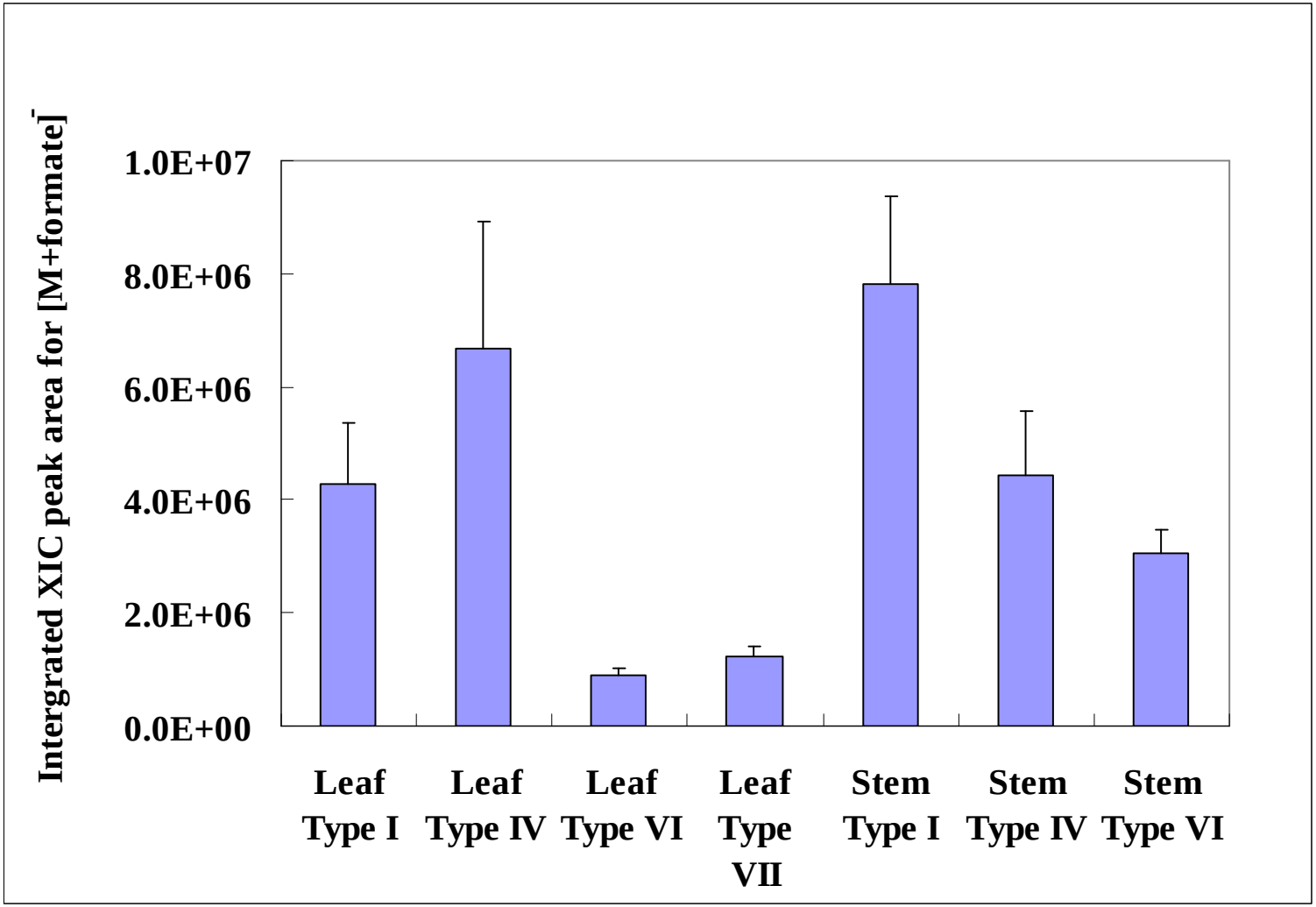

Figure II-15 Quantitative distribution of total acylsucroses in each types of trichome (from 50 trichomes extracted in 50 µl solvent) from *S. habrochaites* (LA1777) measured using negative mode LC/MS. Error bars indicate standard error with n=3.

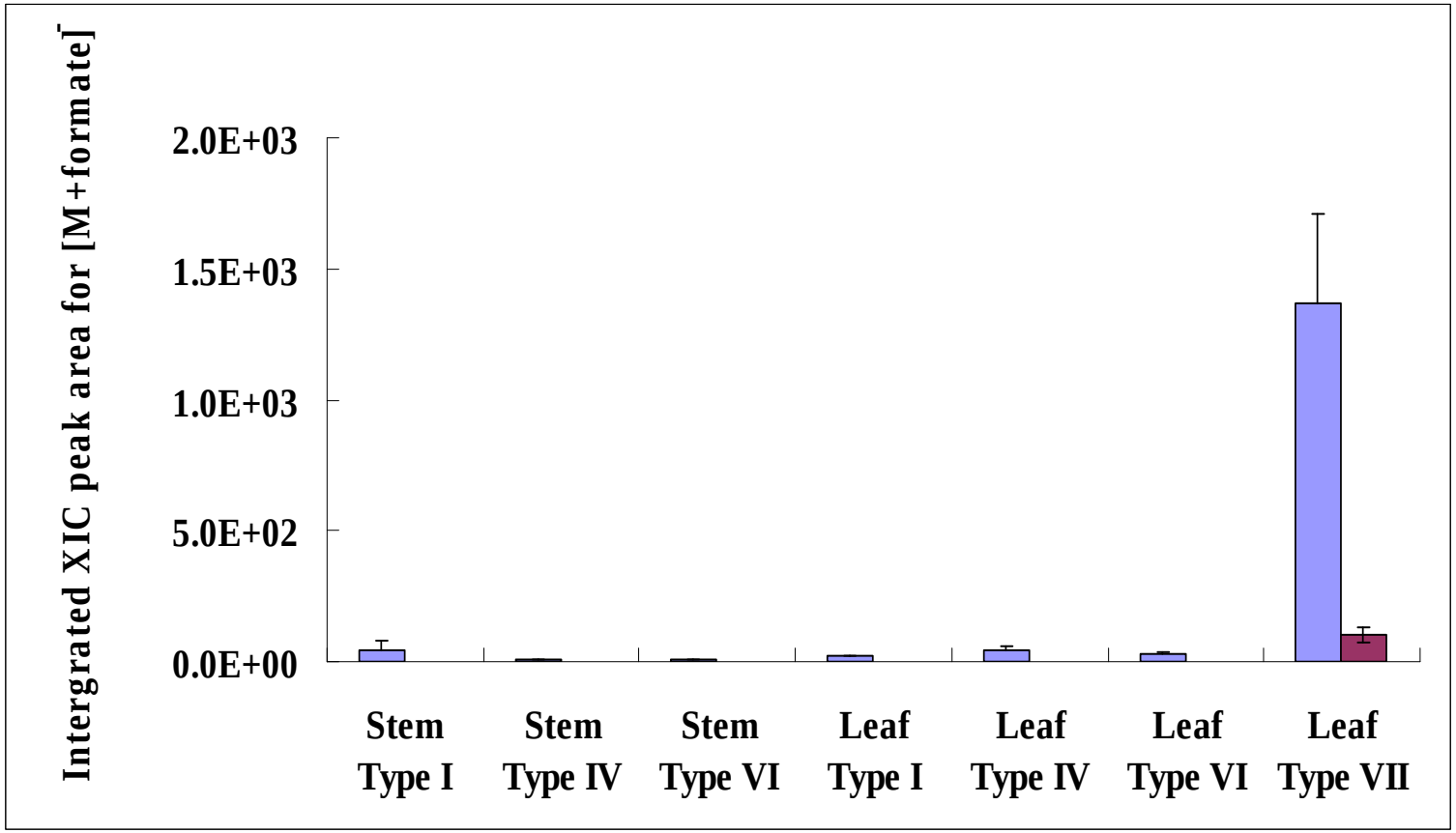

Figure II-16 Quantitative distribution of glycoalkaloids in each types of trichome (from 50 trichomes extracted in 50 µl solvent) from *S. habrochaites* (LA1777) measured using negative mode LC/MS. Key: tomatine (blue), dehydrotomatine (red). Error bars indicate standard error with n=3.

For *S. pennellii* LA0716, metabolites are less diversified compared to *S. habrochaites* LA1777, as the former did not accumulate terpenoids or alkaloids detected by LC/MS. In contrast to LA1777, LA0716 stored higher levels of methyl flavonoids in type VI glands with lesser amounts in type IV (Figure II-17). Type VI glands in the latter accession also contain more acylsugars, predominantly acylglucoses, and glycosylated flavonoids (Figure II-18, Figure II-19). In virtually all aspects, type VI glands in LA0716 are more biosynthetically prolific than type IV trichomes in the same species.

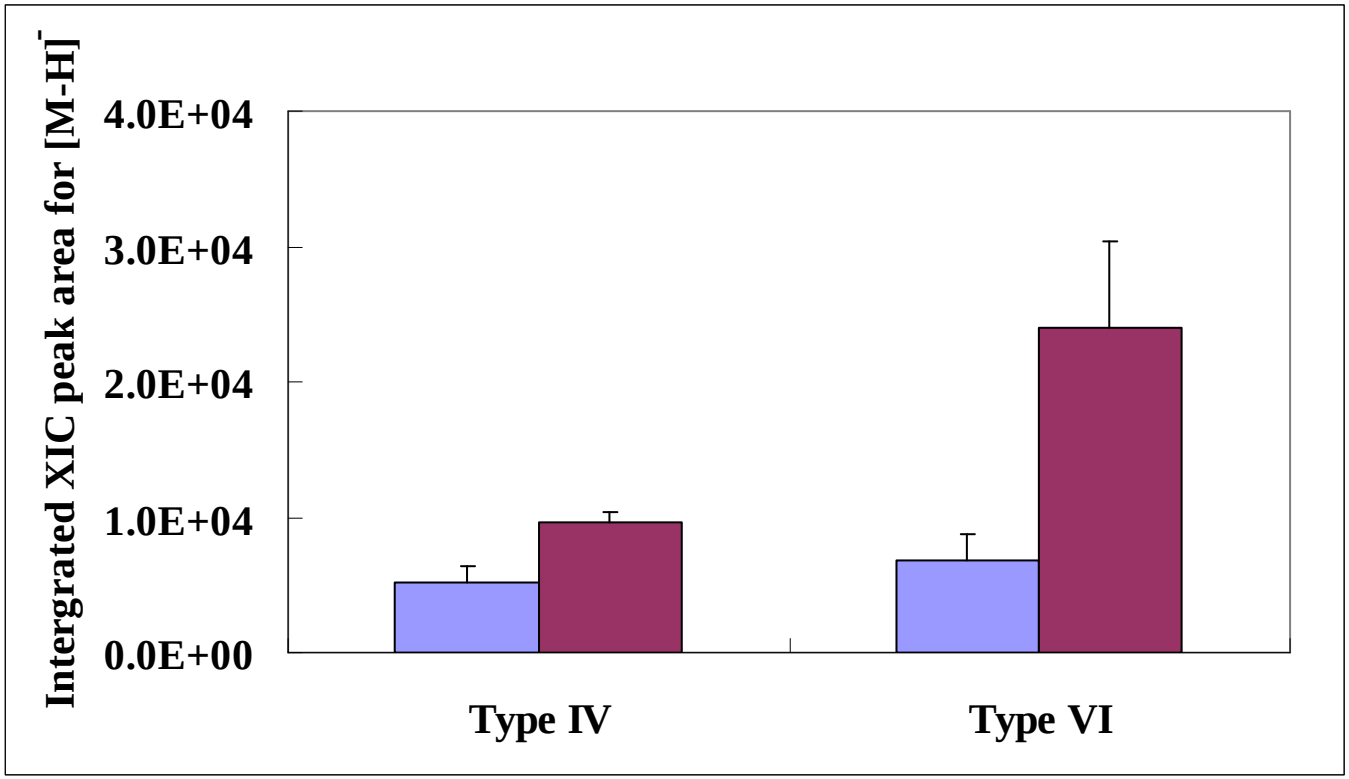

Figure II-17 Quantitative distribution of methylated flavonoids in each types of trichome (from 50 trichomes extracted in 50 µl solvent) from *S. pennellii* (LA0716) measured using negative mode LC/MS. Key: monomethyl kaempferol (blue), dimethyl kaempferol (red). Error bars indicate standard error with n=3.

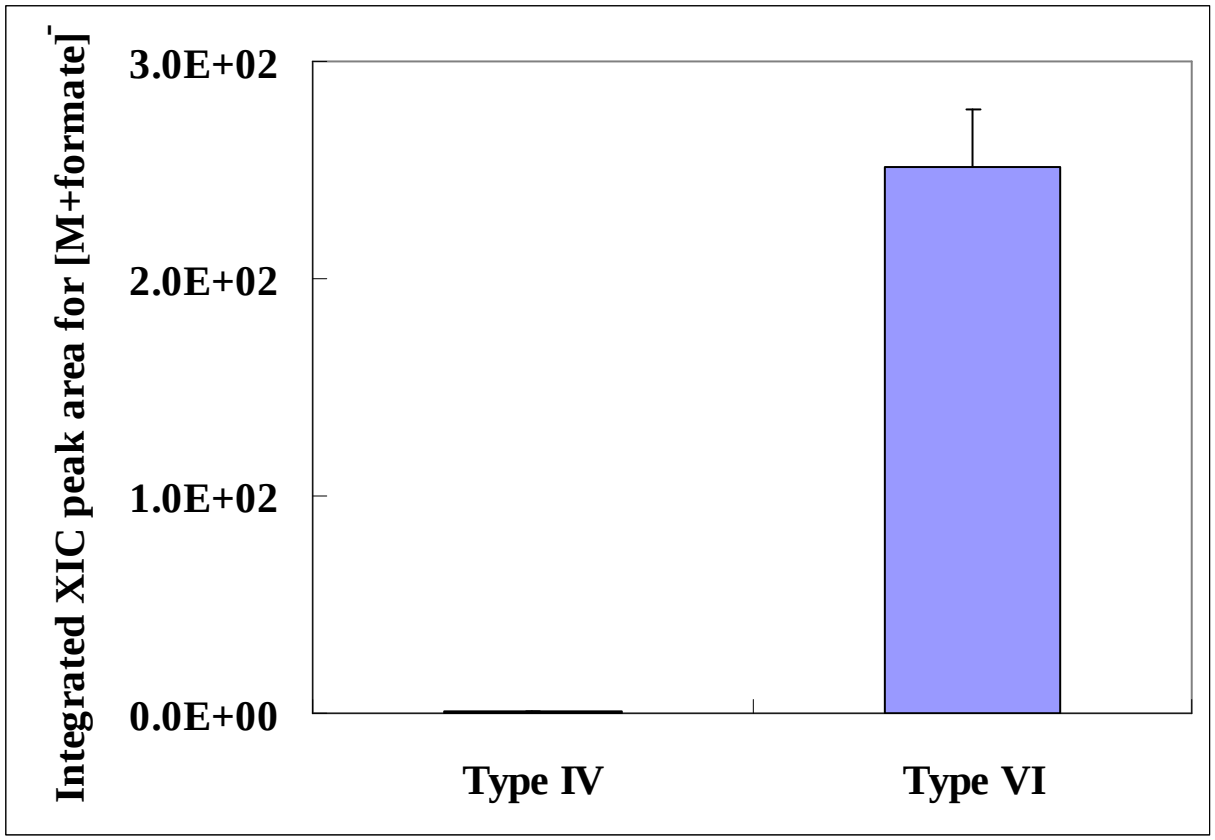

Figure II-18 Quantitative distribution of glycosylated flavonoid (rutin) in each types of trichome (from 50 trichomes extracted in 50 µl solvent) from *S. pennellii* (LA0716) measured using negative mode LC/MS. Error bars indicate standard error with n=3.

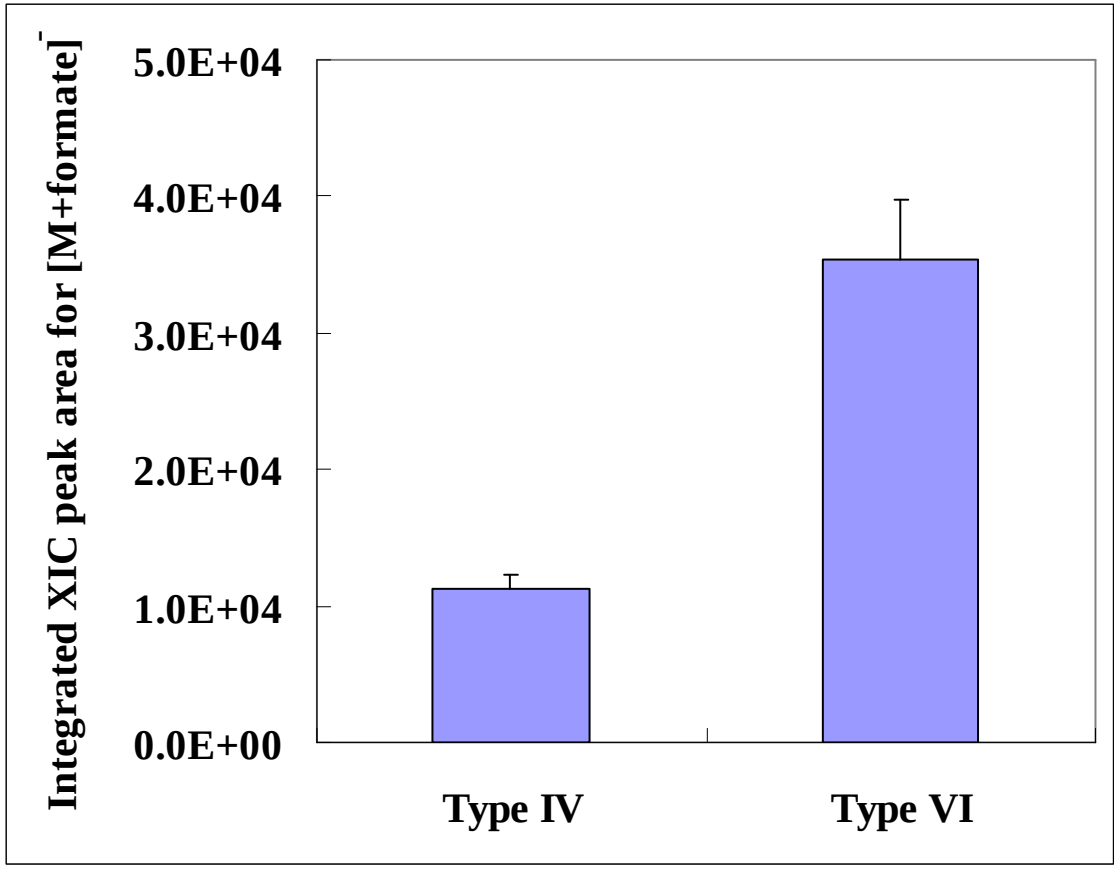

Figure II-19 Quantitative distribution of total acylsugar metabolites in each types of trichome (from 50 trichomes extracted in 50 µl solvent) from *S. pennellii* (LA0716) measured using negative mode LC/MS. Error bars indicate standard error with n=3.

Levels of specialized metabolites in trichomes from the conventional tomato *S. lycopersicum* (M82) were substantially less than the other accessions with a few exceptions. However, the distribution of specific metabolites classes is similar to *S. habrochaites* LA1777. Type VI glands accrue more glycosylated flavonoids than type I trichomes (Figure II-20), however type I accumulates more methylated flavonoids and acylsugars than type VI trichome (Figure II-21, 22).

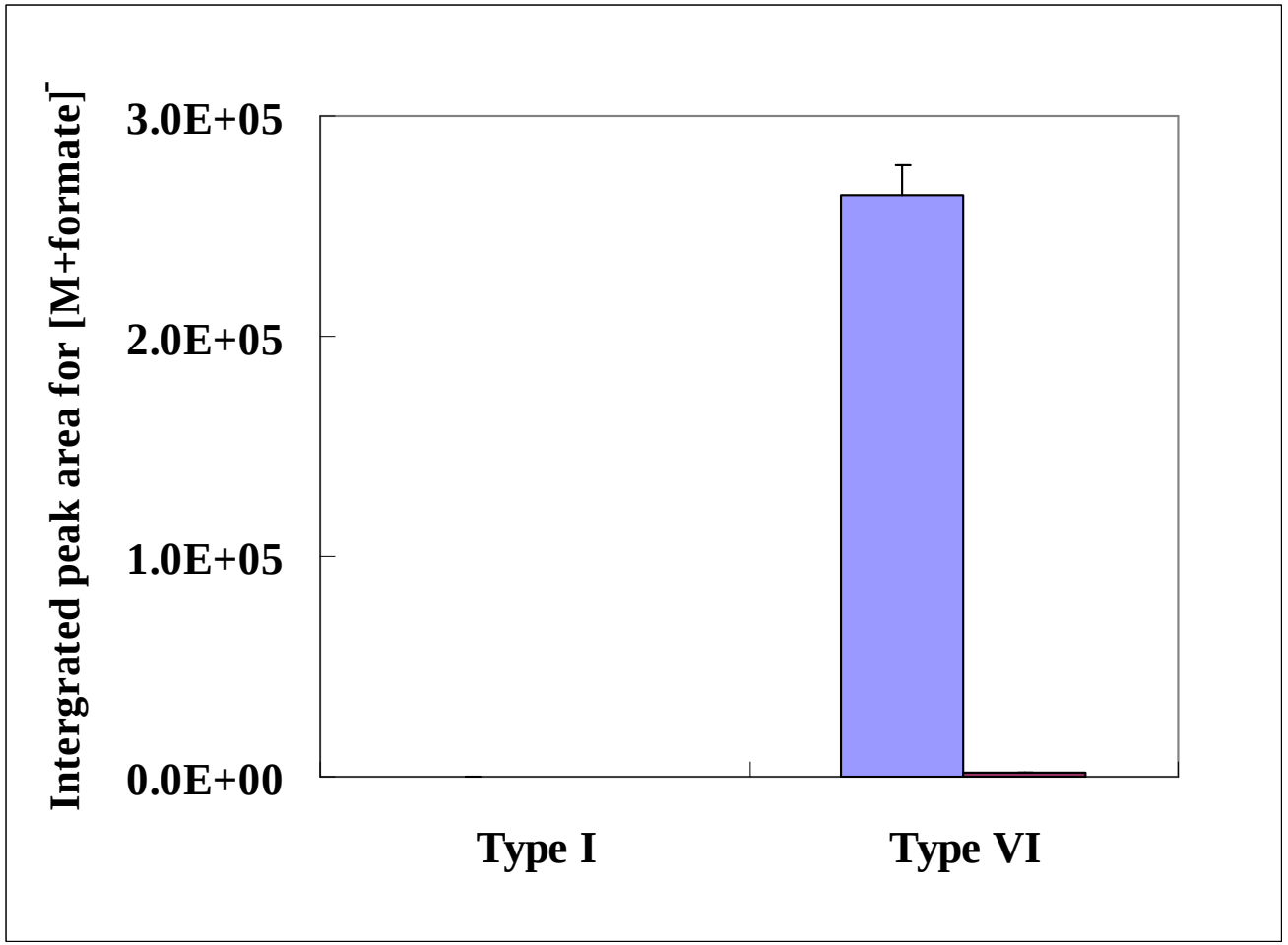

Figure II-20 Quantitative distribution of glycosylated flavonoids in each types of trichome (from 50 trichomes extracted in 50 µl solvent) from *S. lycopersicum* (M82) measured using negative mode LC/MS. Key: Rutin (blue) and quercetin-diglucoside (red). Error bars indicate standard error with n=3.

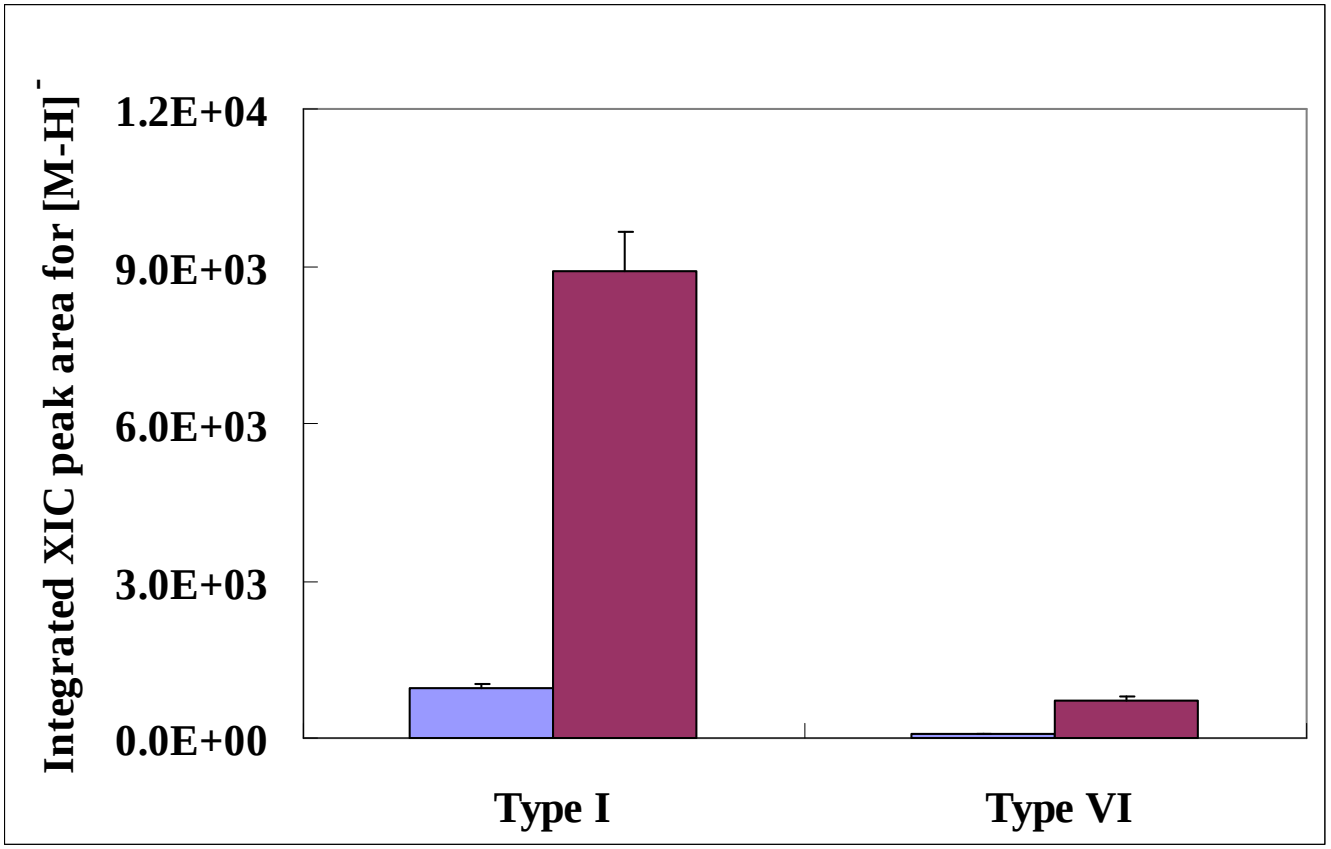

Figure II-21 Quantitative distribution of methylated flavonoids in each types of trichome (from 50 trichomes extracted in 50 µl solvent) from *S. lycopersicum* (M82) measured using negative mode LC/MS. Key: monomethyl myricetin (blue), dimethyl myricetin (red). Error bars indicate standard error with n=3.

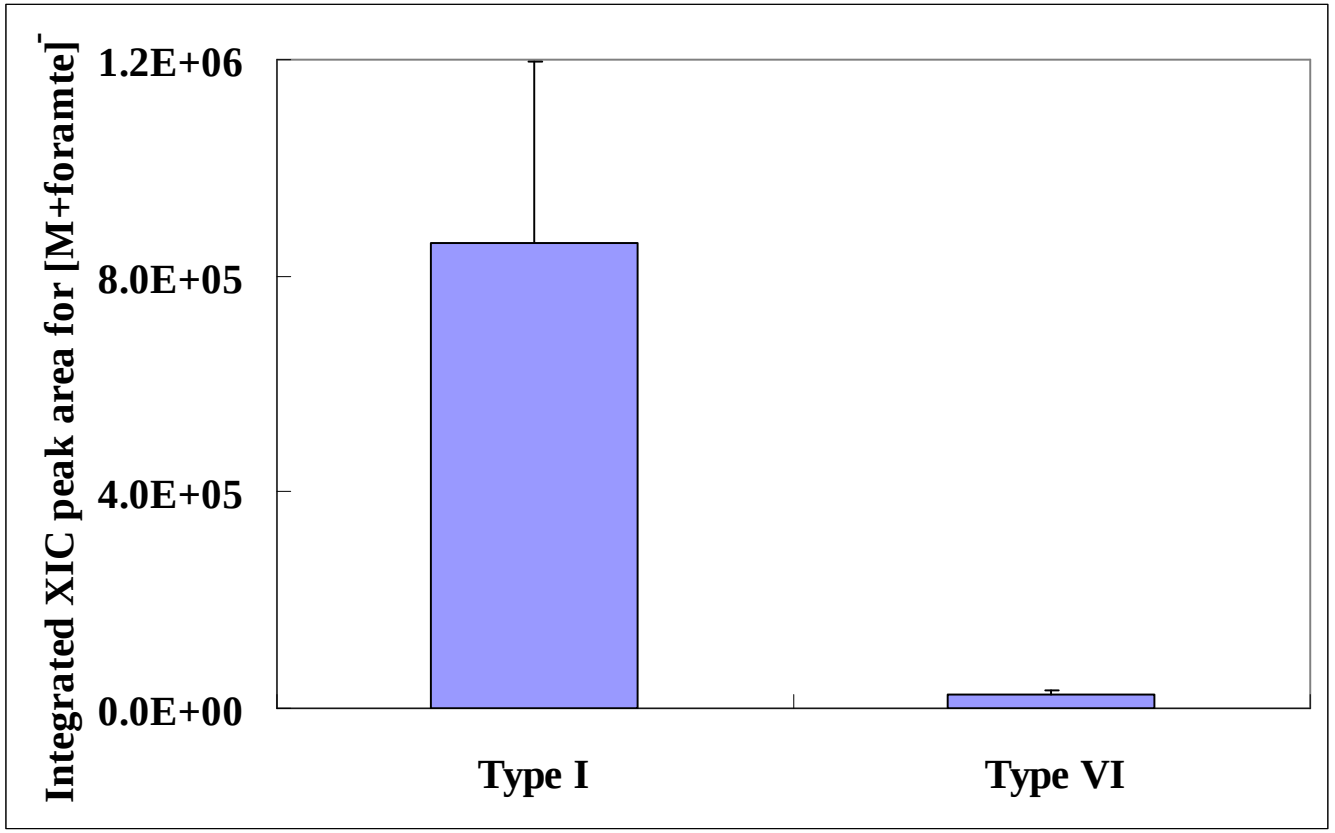

Figure II-22 Quantitative distribution of total acylsugar metabolites in each types of trichome (from 50 trichomes extracted in 50 µl solvent) from *S. lycopersicum* (M82) measured using negative mode LC/MS. Error bars indicate standard error with n=3.

The systematic comparative analysis of different species and types of trichome for *Solanum* species has not been reported before. The research described in this Chapter reports determination of metabolite identities and quantities for individual types of trichomes in several *Solanum* accessions. Integration of this information with genomic sequence information and assessment of mRNA transcript levels provides a foundation for determining where specific specialized metabolic processes occur. Comparisons of metabolite profiles in five accessions were made based on annotations of 109 mass spectral features that were extracted from these profiles using the automated peak detection, integration, and alignment capabilities of MarkerLynx software, which reports each feature as a mass-retention time pair for which a peak area is tabulated. This database of metabolite levels was exported and organized further as a text file. Despite this leap in our understanding of trichome chemistry, there are still thousands of unidentified peaks for which it is not feasible to make manual comparisons. One useful tool for visualizing data of such complexity employs principal component analysis (PCA), which is an unsupervised linear technique for reduction of dimensionality. The central idea is to reduce large dimensional data to a few principal components that represent a large proportion of the data variance. Graphic representation of much of the variance can be accomplished by generating two- or three-dimensional plots of the scores and loadings of the various measurements onto the principal components. The data were first scaled by dividing each peak area by the standard deviation of that peak area calculated across the entire data set. After scaling, all metabolites have a standard deviation normalized to one, and therefore further processing is based on correlations instead of covariances. In another word, all metabolites become equally weighted

without bias to metabolites based on their abundances. In the PCA scores plot derived from the scaled peak areas for metabolites from individual trichome types (Figure II-23A), it is evident that the species differences are more apparent than trichome type differences. The different types of trichomes cluster together, however, the different accessions are well separated. Figure II-23B presents the PCA loadings plot including all of the metabolites. The loadings plot displays each metabolite as a single data point with the position corresponding to the loadings on each principal component. For the scores plot, each data point represents an individual sample, and the scores are calculated by summing the loadings for all of the individual metabolites on the respective principal components. For example, the left upper corner in the loadings plot contains those metabolites that are more abundant in M82, *S. Arcanum,* and *S. pimpinellifolium* compared to other species because M82, *S. arcanum,* and *S. pimpinellifolium* samples are situated on the upper left corner of the corresponding scores plot. The right side of the loadings plot is dominated by those metabolites that are abundant in LA1777, and in turn, LA1777 samples are situated on the right side of the scores plot. Since representing thousands of metabolites on the loadings plot would compromise labeling of all individual metabolites with their names, metabolites were labeled as M (number) to display all of the metabolites.

The loadings plot of trichome metabolite data indicates that only a small set of metabolites (those located in the upper left corner) are distinguishing features of cultivated tomato (M82), *S. arcanum* LA1708, and *S. pimpinellifolium* LA1589, regardless of trichome types. The similarity of M82 to *S. arcanum* and *S. pimpinellifolium* is consistent with a previous report [136], which also recognized that specialized metabolites are less abundant in these accessions

than in the high acylsugar lines *S. pennellii* LA0716 and *S. habrochaites* LA1777. The differences in metabolite profiles may explain the lower resistance of the cultivated tomato to herbivores compared to wild type [137-139].

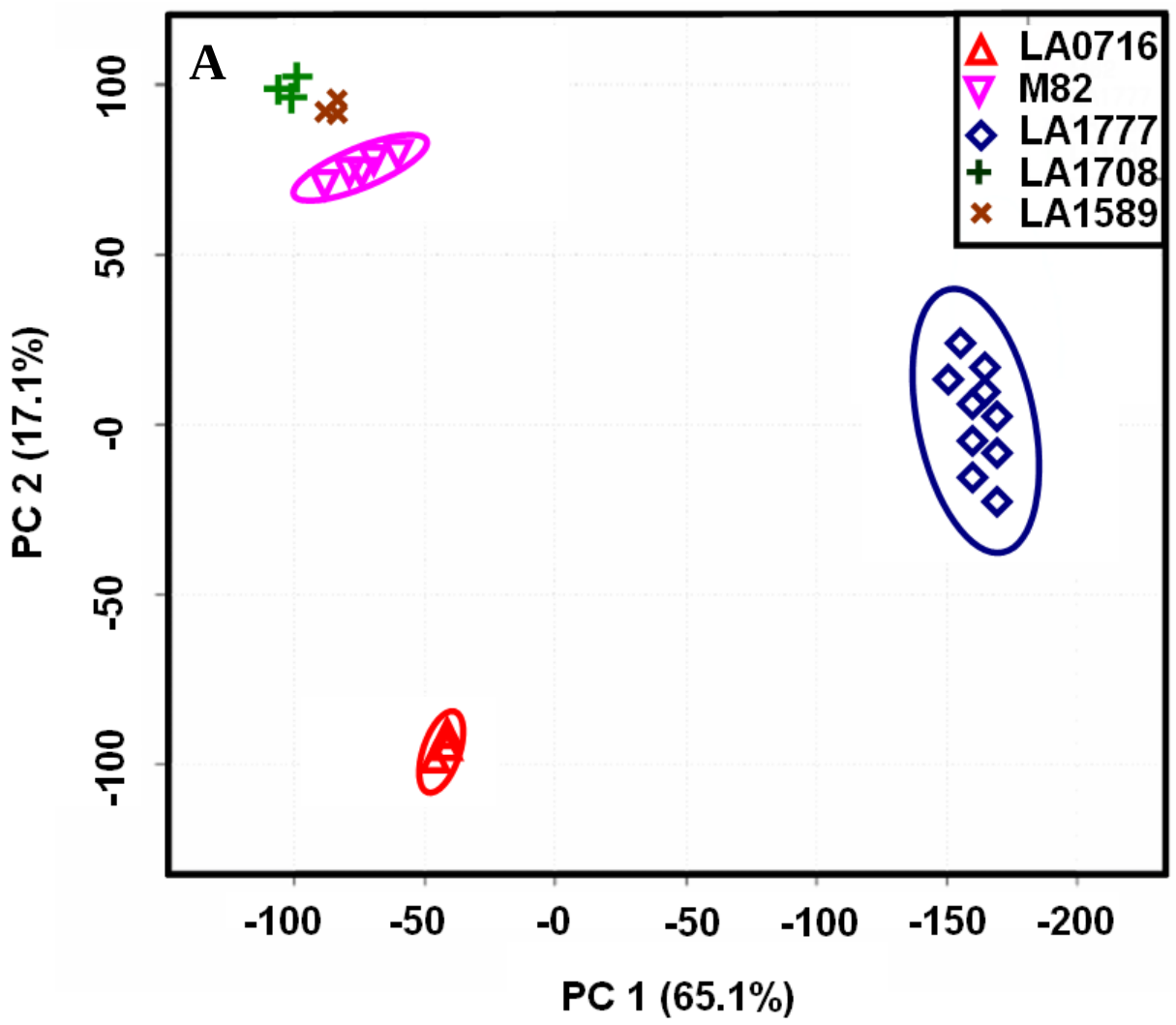

Figure II-23 Principal component analysis (PCA) of individual trichome metabolite A) score plot for first and second principal. B) loadings plot including all of the detected metabolites ("M" represents metabolites). L means leaf and S means stem.

Figure II-23 (cont'd)

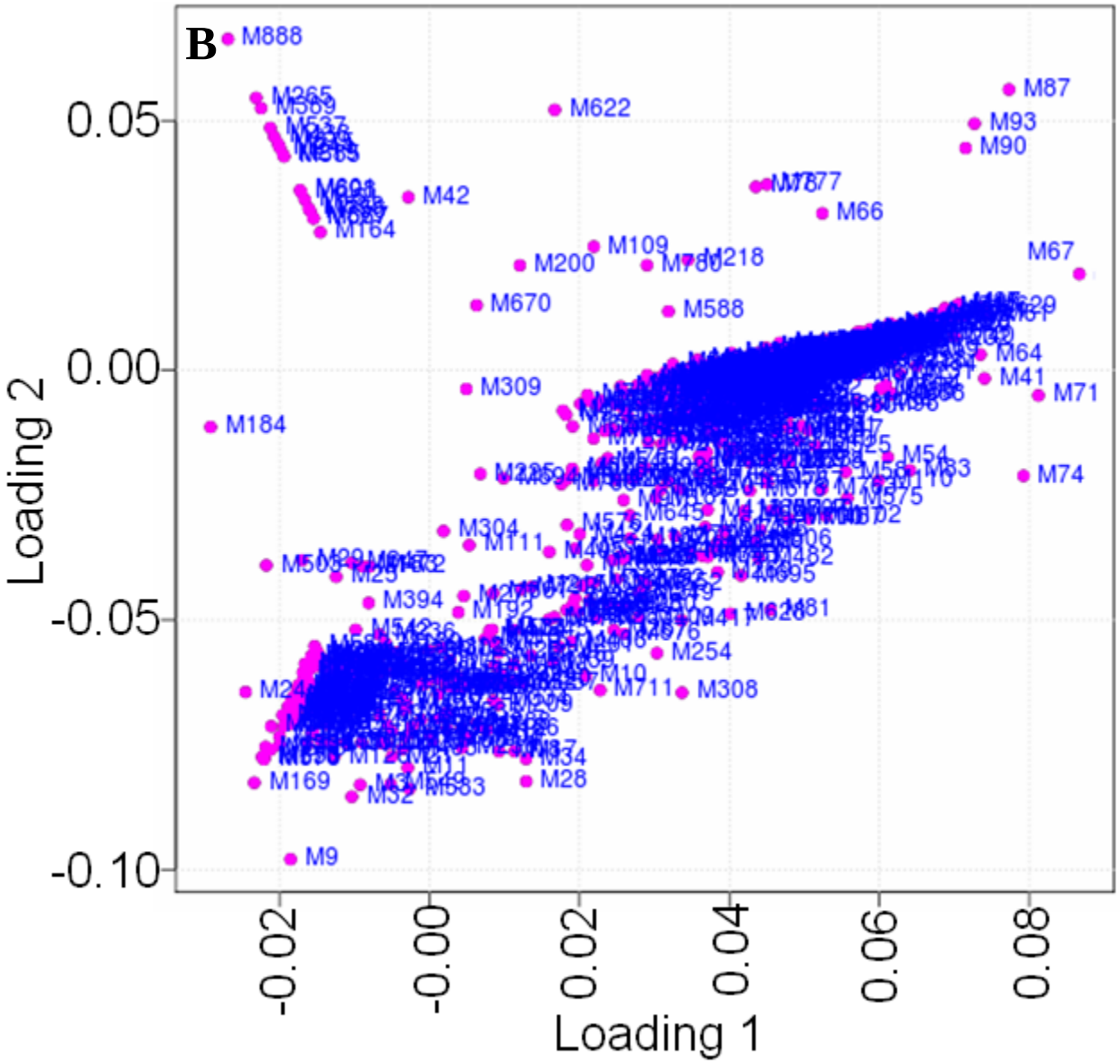

Metabolite profiles for *S. habrochaites* LA1777, the only accession that has all types of glandular trichomes (type I, IV, VI, VII), was analyzed by PCA separately from other accessions to highlight differences between trichome types (Figure II-24). It is evident from the PCA scores plot that type I and type IV cluster together regardless of whether the trichomes were

collected from stem or leaf tissues. However, type VI profiles are well separated from types I and IV. Again, differences between stem and leaf trichomes profiles are small, as leaf and stem profiles cluster together on the PCA scores plot. The morphologies of type I and type IV glands are similar, with both having a small gland tip and a long multicellular stalk. Results from this metabolite profiling show for the first time that the chemical content of these two trichome types is remarkably similar. Transcript analyses also failed to find significant differences between these two types [140]. It should be considered that type I and type IV may be different developmental stages of the same trichome type with one more developed than the other. Another finding from the PCA scores plot is the location of type VII trichome profiles between types I/IV and type VI (Figure II-24). Since most of the metabolites observed in type VII trichomes were also detected in other types of trichome which lie at greater heights above the leaf surface, it is suspected that exudates from the other types may have contaminated type VII trichomes before or during sampling. Two exceptions are the glycoalkaloids tomatine and dehydrotomatine, which exclusively present in the type VII trichomes. Except for these two metabolites, other annotated substances do not exclusively present in only one type of trichome. Metabolites profiles indicate that levels of terpenoid metabolites are present at ~100-fold greater levels per trichome than types I and IV (Figure II-14). Cross-contamination alone cannot account for such differences. It is proposed that the transcripts of type VI trichomes ought to be valuable for identifying candidate genes for terpenoid metabolite biosynthesis.

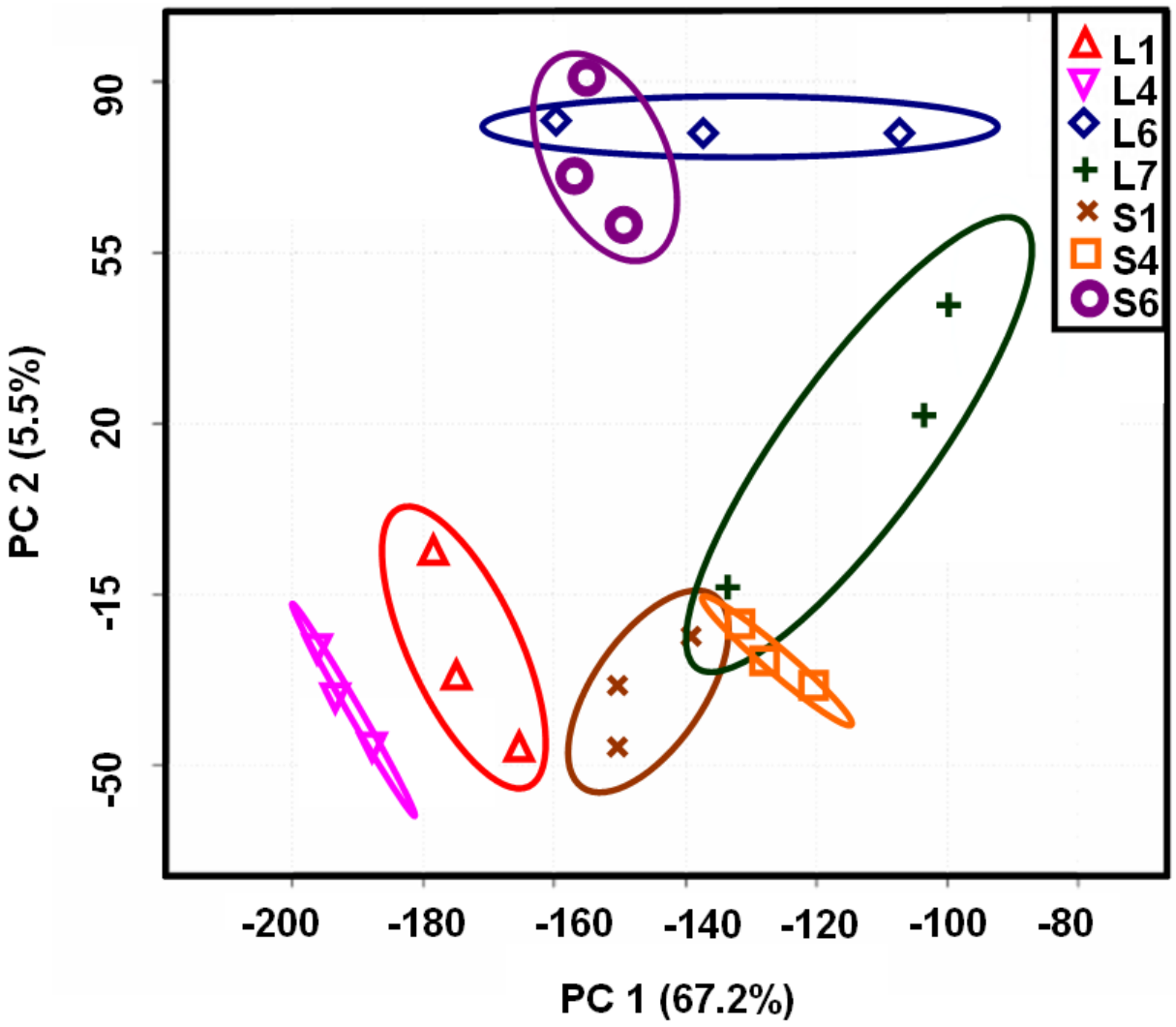

Figure II-24 Principal component analysis (PCA) of individual trichome metabolite from LA1777, displaying the scores plot for the first and third principal components. L means leaf and S means stem. The number after the underscore means biological replicate number.

The integration of metabolomic and transcriptomic data is ongoing at this point, and an initial report has been published [140]. At this stage, elucidation of metabolic pathways is incomplete and this may be attributed to one or more of the following:

a) the RNA profiling is not deep enough to cover low abundant transcripts;

b) some metabolites of interest may not be synthesized in their entirety within trichome, and import of key precursors into the trichome may be important;

c) the metabolite is synthesized by trichome, but may only be synthesized at a developmental stage earlier than mRNA collection; key transcripts involved in metabolite biosynthesis may no longer be present when trichomes were collected.

To answer questions b) and c), future investigations should collect trichomes at multiple developmental stages for both RNA and metabolite profiling. Awareness of this important aspect of experimental design represents a new challenge to the field of metabolomics, but is consistent with the dynamic nature of metabolite biosynthesis.

However, sampling of multiple cell types at different stages of development and different time points will cause a dramatic increase in the workload of tissue collection and metabolite analysis. In addition, for trichome analysis, when plant tissues are young and trichomes are at an early stage of development, the high density of trichomes prohibits manual collection of individual trichome types. Therefore, a different and high-throughput scheme is needed to achieve the goal of dynamic metabolite analysis which includes localization of metabolite profiles at locations across plant tissues. In Chapter III, a high throughput imaging mass spectrometry scheme for profiling leaf trichomes without manual microsampling is presented, and this approach could provide an appealing alternative that can address these scientific issues.

CHAPTER THREE

CHEMICAL IMAGING OF TRICHOME SPECIALIZED METABOLITES USING CONTACT PRINTING AND LASER DESORPTION/IONIZATION MASS SPECTROMETRY

3.1 Introduction

Biological functions are organized at molecular, subcellular organelle, cellular, tissue, and organismal levels, but the low levels of cellular constituents have provided a barrier to understanding and exploiting genomic information for control of biological functions. Measurements of the entire suite of metabolites, known as metabolomics, has emerged as a growing research area which is trying to answer how living systems respond to environmental stimuli or genetic modifications [141-143]. Most investigations of metabolite profiles have focused on whole tissue or whole organism levels, and for these studies, metabolite information represents averages over many cells and tissues and is dominated by contributions from the most abundant cell types [44]. However, as documented in Chapter II, metabolite accumulation is often organized in specialized cell types, such as glandular trichomes in plants. To investigate the functional roles of specialized cells and address the important questions such as the mechanism of cell differentiation and cell-cell signaling, studying individual cells is necessary. Several recent reports suggest chemical heterogeneity of cells, and it is likely that even cells of the same cell type may differ in metabolic functions depending on cell environments and stages

of development. These findings point to the necessity of individual cell analysis if research is to fully understand mechanisms that regulate metabolic dynamics [144-146].

A variety of approaches have been explored to address the challenges of sampling and detecting metabolites in single cells. For sampling, microcapillaries or micropipettes coupled with micromanipulation under a dissecting microscope [50, 147, 148] and laser-capture microdissection (LCM) [149] are successfully used for single cell isolation. However these sampling methods offer low throughput if many cells need to be isolated, as is desirable because metabolite profiles change with organism growth and development. For individual cell analysis, flow cytometry [150], microfluidics [151], capillary electrophoresis (CE) [152] coupled with electrochemical (ECD) [153], laser-induced fluorescence (LIF) detection [154] or mass spectrometry have been widely used because the detection schemes offer low levels of detection necessary for single cell analysis. Of these analytical methods, mass spectrometry offers near-universal detection of an assortment of metabolites, and is most appropriate for nontargeted metabolite profiling. Mass spectrometry based single cell analysis was pioneered in the late 1990s with peptide and biomarker analysis, as described by the Sweedler group at the University of Illinois [155]. More recently, the laboratory of Renato Zenobi demonstrated metabolite profiling of yeast with single cell sensitivity [156]. A new nanostructure-initiator mass spectrometry having the capability to analyze metabolites from single cells has also been reported by the Siuzdak laboratory at Scripps [71].

To develop a comprehensive understanding of cell metabolic heterogeneity, metabolite profiles need to be measured for many individual cells. Mass spectrometry imaging (MSI)

provides an approach for multiplexing cellular profiling by fast scanning through an area containing multiple cells, acquiring chemical information for individual pixels across the entire area. Several MSI approaches have been demonstrated in recent years, with matrix assisted laser desorption/ionization (MALDI) imaging finding extensive use in profiling proteins, lipids, and other metabolites in animal tissues. More recently, a few examples have been reported for localization of natural products in biological tissues from a range of organisms [157-159]. However, the MALDI imaging scheme has a few limitations, 1) sophisticated sample preparation is often required, 2) signals from the MALDI matrix often interfere with detection of low molecular mass (< 500 Da) metabolites, and 3) application of the laser-absorbing matrix to tissues has suffered from lack of uniformity, and the matrix deposition process may compromise localization of some metabolites.

The mechanisms of desorption and ionization for MALDI are complex and continue to be subjects of discussion and debate. The most accepted theory proposes a two step process: desorption/ablation and ionization [160]. During cocrystallization with matrix, the analyte molecules are surrounded and isolated by the excess matrix molecules, which have strong absorption at the laser wavelength. Upon laser irradiation, the matrix absorbs energy which is rapidly converted into internal and translational energy, i.e. heating. This heating leads to explosive evaporation and ejection of the matrix and analyte molecules into gas phase. The ejected materials consist of a combination of desorbed molecules, condensed clusters, droplets or chunks. The phase explosion has been successfully simulated by hydrodynamic models [161] and molecular dynamic calculation [162]. Ionization that results from this process is even less

understood than the desorption process. Two major models have been purposed. One model assumes that the matrix molecules were first ionized by direct photoionization, usually through a multiphoton process [163]. Although the ionization potential is somewhat lower in solid crystal compared to gas phase and the energy gap can be compensated by thermal energy, at least two laser photons (3.68 eV for 337 nm laser) are required for the direct photoionization of matrix molecules (> 7 eV) [164]. The flux of laser photon during a typical MALDI experiment is too low for resonant two-photon absorption to be efficient. Instead, it has been proposed that the interaction of Π electrons between aromatic molecules in condensed phases leads to energy pooling, which involves combining energy from two electronically excited molecules into a single molecule [165]. After primary ionization of the matrix molecules, transfer of charged groups such as protons takes place as a result of collisions between two matrix molecules. Subsequent collisions between ionized matrix and analyte in the high density plume lead to a secondary proton transfer reaction and protonation of the analyte [166]. This second model was purposed by Karas and coworkers, and is referred to as the “lucky survivor” model [167]. It has also been proposed that some analytes exist in ionized forms in the matrix as they are in solution. The model assumes the desorption process breaks the lattice into small clusters. Some clusters can have excess positive charge or negative charge. Most of the ionized analytes are subsequently reneutralized by collisions with counterions within the plume and only the lucky survivor can be detected by mass spectrometry.

Analytes can also be desorbed/ionized from many semiconductor materials surfaces including silicon and graphite. Proposed mechanisms of analyte desorption and ionization

under matrix free laser desorption ionization (LDI) conditions are largely speculative, with limited experimental evidence. In such experiments, ion signal was found to be independent of laser wavelength [168]. It was explained that only absorption of a photon that exceeds the band gap energy of the semiconductor materials is required. A thermal desorption process has been proposed to be involved in desorption ionization of analytes under these experimental conditions [169, 170]. Rapid heating can cause fluctuation in electron densities, and the region of intrinsic instability that results may lead to redistribution of energy into translational energies, leading to evaporation of analytes. Subsequent ionization could involve various ion-molecule reactions including proton transfer, disproportionation reactions, and cation or anion attachment. Such rapid heating will increase bond distances and facilitate charge separation from interfacial water or the acid –OH group on the semiconductor surfaces [171-173]. Gas phase ion-molecule reactions between proton or cation donors and analytes can form ions by attachment of protons or cations such as alkali metal ions.

Water has been developed as alternative option as an endogenous matrix for mass spectrometry imaging [83, 174]. However the atmospheric pressure matrix assisted laser desorption/ionization (AP-MALDI) system, which is necessary to prevent water evaporation during plant tissue imaging, normally has lower ion transmission efficiency than vacuum MALDI, and may be limited to detection of abundant metabolites. Recently, an infrared laser ablation electrospray ionization (LAESI) system was developed that employs a fiber tip to focus radiation onto a small (~ 30 μm) spot followed by electrospray assisted ionization of desorbed neutrals, and this approach has been applied for profiling of constituents in single cells [74, 175],

however the instrument design and parameter optimization required special expertise, and this report did not demonstrate formation of mass spectrometry images. Desorption Electrospray Ionization (DESI) has been used as a new alternative approach for imaging mass spectrometry. The resolution is generally around few hundred µm owing to dispersion of the primary ion beam at atmospheric pressure, and this approach has yet to demonstrate resolution of single cells [176]. Although 40 µm resolution has been achieved more recently, such performance places restrictions on the geometry of the surface, and uniform surface texture is required which is not always feasible for some tissues [177]. It has been reported that great effort was required to adjust instrument parameters to achieve optimal signal [178]. Secondary ion mass spectrometry (SIMS) imaging provides another alternative ionization method, and can give superior spatial resolution at 50 nm which is adequate for profiling individual cells [179, 180]. However SIMS requires ultrahigh vacuum, and special sample preparation for fresh tissues is needed that may involve freezing and water evaporation. SIMS deposits much higher energy per unit area than MALDI or DESI, and leads to extensive formation of fragment ions. In addition, the ions ejected by SIMS are formed only from a small area, and the abundances of metabolites in such small areas may preclude measurements except for the most abundant surface species. Although much effort has been devoted to method development for imaging mass spectrometry, most successful examples have employed sectioned animal tissue or tissues with flat surfaces. Examples of MS imaging of tissues having irregular shapes are scarce.

Plant trichomes (Figure III-1) are specialized epidermal cells that protrude from surfaces of plant tissues such as stems and leaves, and they are found on approximately one third of all

vascular plant species. In earlier reports, trichomes from the model plant *Arabidopsis thaliana* were chosen as a representative model for investigating cell differentiation [181, 182]. Trichomes are also prolific accumulators of specialized metabolites used by plants as chemical defenses. They are considered as one of the most effective "chemical factories" in the plant kingdom [183].

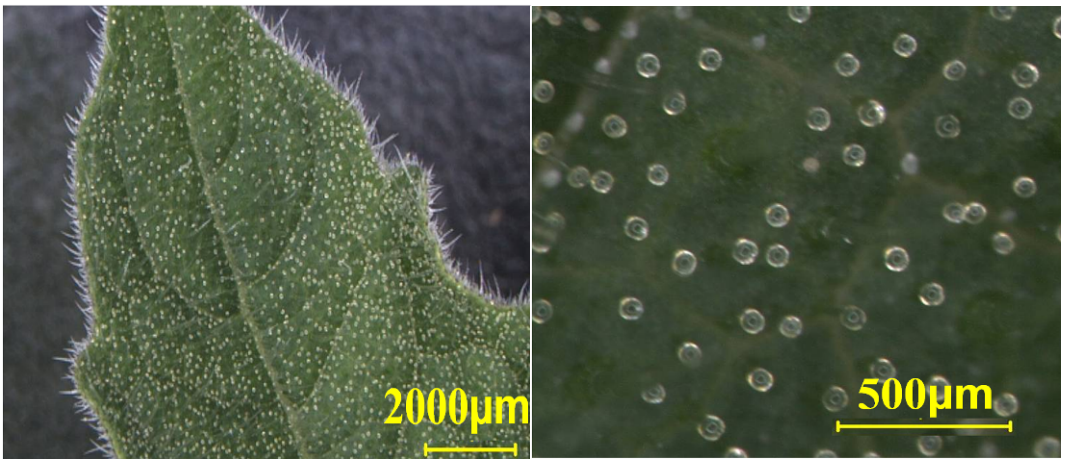

Figure III-1 Optical image of *S. habrochaites* LA1777 leaf (left) showing trichomes on the adaxial (upper) leaf surface including type VI glands (right). Adapted from Reference [140].

Current research focuses on understanding the mechanisms that govern metabolite accumulation in tomato trichomes because trichome chemicals serve as the first layer of protection against insects and other herbivores. Agricultural crop losses to insect damage represent a large economic loss to the worldwide economy, and the selective breeding of crops that are resistant to insects has great potential impact on yields of numerous crops.

One fascinating feature of tomato trichomes is that they occur, in the genus Solanum, with four distinct morphological types [184]. These specialized cell types provide a useful and

accessible model system in which different cell types are expected to accumulate different metabolites, and these differences promote discoveries of gene functions relevant to trichome biochemistry.

Most analytical methods developed for profiling of metabolites in individual cell types are laborious because of the need to selectively sample specific cell types. This can be accomplished by microcollection of individual cells under a microscope. However, the number of cells that can be collected in a short time is limited, perhaps to a few hundred cells per day. Before this work was initiated, most knowledge of trichome chemistry had come from nonselective mechanical removal of multiple trichome types, often following freezing of the plant tissue. The resulting chemical profiles have represented mixtures of trichome types, and have not exploited the diversity in cell types [185-187]. Furthermore, these efforts have pooled trichomes from multiple locations across plant tissues, so no spatial information about metabolite abundances could be obtained. Imaging mass spectrometry offers great potential for high throughput metabolomic analysis [83]. Therefore, we explored the application of imaging mass spectrometry for localizing trichome metabolite profiles across plant tissues. Herein, we present a carbon material based printing method for high spatial resolution imaging mass spectrometry profiling of tomato trichome metabolites without the need for tedious microsampling. This sensitive scheme is capable of profiling specialized metabolites of thousands of individual trichomes level on a single tomato leaf surface. The high spatial resolution capability offers the potential to explore chemical heterogeneity across a population of individual trichomes within a plant tissue. To our knowledge, this is the first report of mass

spectrometry imaging on irregular shaped tissues.

3.2 Materials and Methods

3.2.1 Chemicals

Acetonitrile, 2-propanol, methanol, dichloromethane, formic acid (88% aqueous solution) were purchased from VWR Scientific. α-Cyano-4-hydroxycinnamic acid (CHCA) and 2,5-dihydroxybenzoic acid (DHB) and tomatine were obtained from (Sigma-Aldrich, St. Louis, MO, USA).

3.2.2 Plants

Seeds for plants were obtained from the Tomato Genetics Resource Center at the University of California-Davis. Plants used for this study were grown in a greenhouse at Michigan State University.

3.2.3 Sample Preparation

A dissecting glass microscope slide was etched using HF or mechanically ground with rotating grinding by the Glass Shop of the Michigan State University Department of Chemistry.

A 2B pencil purchased from the Spartan Bookstore at Michigan State University was used to draw a layer of graphite on one side of the glass slide. The coverage of surface by the graphite was checked by examining the glass slide using transmitted light under a microscope. The glass slide was placed in a drying oven at 80˚C overnight, as removal of moisture strengthened the interaction of graphite with the glass surface. The slide was then immersed in Milli-Q water, dichloromethane and methanol for 1 hr each, and dried under a gentle stream of nitrogen. The slide was placed on a block of dry ice to chill the surface as a prelude to transfer of trichomes. Such cooling helps quench enzyme activity in the trichome and preserves the chemical composition during sample processing.

A fresh leaflet from *S. habrochaites* LA1777 was cut by razor blade from the base of the leaflet (petiolule). Since the analysis time for an imaging experiment increases with the square of the sample linear dimension, leaflets were chosen smaller than 3x3 cm to limit the time needed for analysis. The symmetric leaflet on the other side of the petiole which was not used for imaging was collected as well, and used to estimate leaflet thickness for construction of a parafilm mask. A mask was constructed by either stretching or folding a sheet of parafilm until the film thickness matched the thickness of the second leaflet. A rectangular region was removed from the middle of the parafilm mask, and the leaflet was positioned in the center of this recessed area. A graphite-coated glass slide was gently placed above the leaflet, and a 500 ml Pyrex beaker containing 200 ml water was placed on top of the slide to provide a reproducible amount of pressure for the contact transfer of trichomes from tissue to slide. Mass calibrant reference solutions were spotted onto the corners of the slides for calibrating the TOF

mass axis before each analysis. The glass slides, containing trichomes, were attached to the MALDI sample stage using adhesive tape. The procedures are illustrated in Scheme III-1. Some conductive material (e.g. aluminum foil) was used to ensure electrical contact between the coated slide surface and the metallic sample stage. For imaging of single trichomes, the trichomes were transferred onto the surface of a glassy carbon plate or a bare glass slide. Use of an uncoated glass slide aids visualization of trichomes under optical microscopes using transmitted or reflected light or fluorescent imaging. A target imaging area was marked with liquid paper beforehand to provide position references, and reflected light optical images were collected by a CCD camera mounted on the microscope. Before laser desorption ionization (LDI) imaging of trichomes on glass slides was performed, the slide was subjected to carbon coating under vacuum at the Michigan State University Center for Advanced Microscopy.

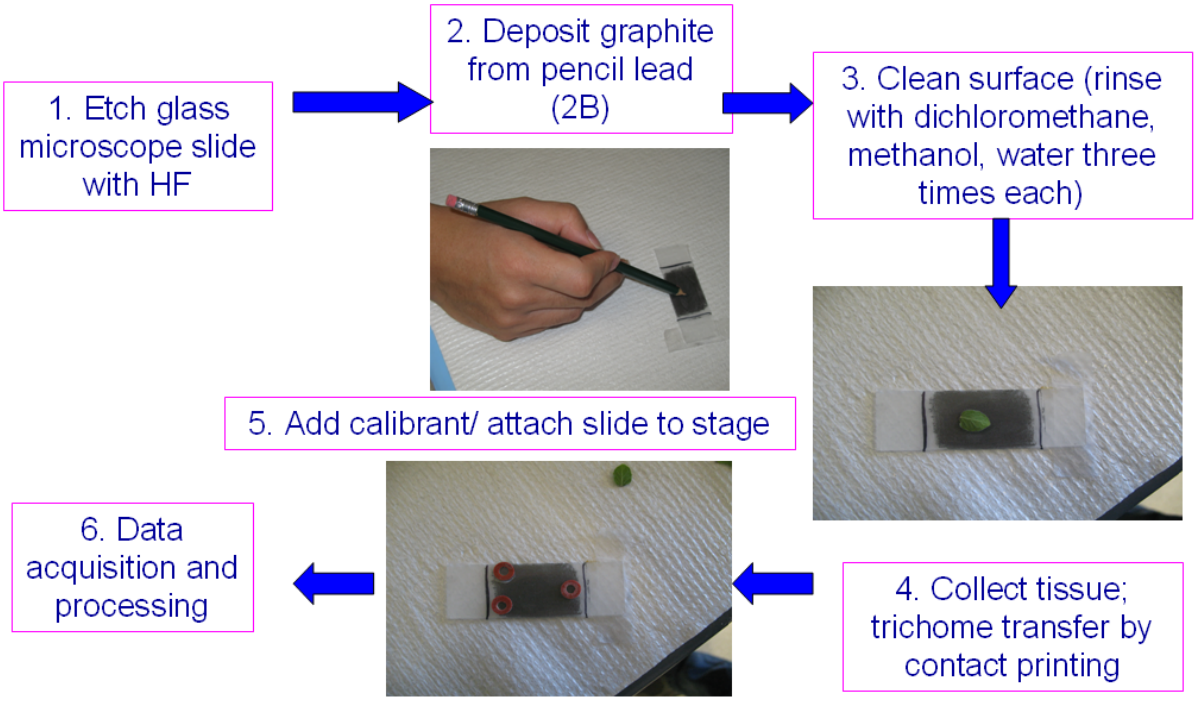

Scheme III-1 Sample preparation procedure for trichome contact printing.

3.2.4 Laser Desorption Ionization Imaging

A MALDI-TOF mass spectrometer (AXIMA cfr-plus, Shimadzu, Columbia, MD) used was equipped with a 337 nm N_2 laser delivering 3 ns pulses. In the MSI experiment, data were acquired in either positive or negative ionization mode using the linear time of flight detector. In some cases, the same sample was analyzed twice using different polarity of ion detection without further sample preparation. The slide surface was first interrogated using 20 laser shots per pixel. For whole leaflet imaging, the stage step size was set to 125 µm. For single trichome analysis, the laser step size was set to 25 µm, and signals from 200 laser shots

per pixel were combined and stored for each pixel. Ion signals between m/z 50 and 1500 were collected. Metabolites were identified by first matching spectra with those obtained for leaf dip extracts using liquid chromatography/mass spectrometry (LC/MS). The LC/MS analyses provided mass measurements with about 5 ppm accuracy. Annotation of metabolites was performed through searching of molecular masses against an assortment of public metabolite databases (ChemSpider, eMolecules, CSLS), and promising candidates were screened further by interpreting masses from nonselective CID spectra. Post-source decay (PSD) LDI mass spectra were acquired for further confirmation of metabolite structures. All LDI imaging data acquisition and processing was performed using Launchpad software (version 2.8.1, Kratos Analytical). The raw mass spectrometry imaging (MSI) data were exported to Biomap (Novartis) software for further processing.

3.2.5 LC/MS analysis

Leaflet metabolites were extracted by dipping the leaflets in 2 ml isopropanol: CH_3CN: H_2O (3:3:2 *v*/*v*/*v*) for 1 min. Extracts were centrifuged at 10000*g* for 10 min at 4 °C, and the supernatants were analyzed without further processing. Separations were performed on a Supelco Bio-C18 column (1 × 150 mm, 3 μm particles) held at 30 °C that was interfaced to an LCT Premier mass spectrometer (Waters, Milford, MA). A solvent gradient was executed based on 0.15% aqueous formic acid (A) and methanol (B) as follows: initial condition 5% B; linear gradient to 50% B (5 min); 95% B (33 min); 100% B (35 min); hold at 100% B until 38

min; return to 5% B (43 min). The flow rate was 0.1 ml·min^{-1}, and the injection volume was 10 µL. The LCT Premier mass spectrometer was operated using electrospray ionization (ESI) and under the control of MassLynx version 4.1 software. The ESI conditions were as follows: capillary voltage, 3200 V; cone voltage, 10 V; source temperature 90 ºC; desolvation gas flow, 300 L/h; desolvation gas temperature, 200 ºC; cone gas flow, 20 L/h. Detection was performed in both positive and negative ion modes over *m/z* 50-1500 using centroided peak acquisition and dynamic range enhancement. Aperture 1 voltages were 10, 45, 75 V for three functions to generate molecular ion and fragment ions at the same run. The fragment ions were aligned to the pseudomolecular ions by matching of retention time. .

3.3 Results and Discussion

The diversity of epidermal cell types on leaves and stems of tomato and its wild relatives presents challenges for research that aims to understand the mechanisms governing trichome chemistry. Complicating matters further are trichome fragility and the morphological differences between trichome types. In the wild tomato *S. habrochaites* (formerly known as *Lycopersicon hirsutum*), examination of the leaf surface quickly reveals the long hair-like type I and IV trichomes (Figure III-1). Closer examination at higher magnification reveals the type VI glands, which consist of bundles of four cells on a short stalk. To obtain a clear view of the type VI glands, one must adjust the microscope focus to a level below the tops of the longer type I and IV glands, which are less obvious in the microscope image owing to the limited depth of

focus. Probing of these different glands with optical or ion beams must account for this height heterogeneity. Furthermore, due to the variation of the stalk height of trichome, laser or ion beams might be easy to reach taller trichome but not the short one because of the potential block from the taller trichome. And also ions ejected from shorter trichome can also be blocked by adjacent taller trichome to prevent it for detection.

A recent review presented a critical evaluation of various sample preparation techniques used for mass spectrometry imaging [188]. Much of the discussion centered on tissue fixation, sectioning, and deposition of MALDI matrix materials as preludes to mass spectrometry imaging analyses. All of the matrix deposition approaches suffer from disadvantages of varying severity, particularly with regard to even deposition of matrix across a tissue surface. Furthermore, the approaches that have been used for MALDI imaging have largely focused on detection of proteins or lipids [189, 190] rather than soluble metabolites that more easily diffuse during sample preparation. Such concerns are particularly important for imaging of trichomes, which are fragile structures that secrete viscous mixtures of metabolites, and are easily broken from tissues during handling.

When imaging of trichomes is conducted using a laser for metabolite ionization and volatilization, no single laser focal plane will be optimal for all trichomes on a tissue surface. One promising approach to address this problem involves physical transfer of trichomes onto a single horizontal plane, presented in the form of a substrate that absorbs the laser radiation. A similar strategy for “tissue printing” of cells from various plant and animal tissues onto polymer surfaces was reviewed in 1994, and included microscopic, biochemical, and immunochemical

detection methods [191]. Even subcellular printing resolution has been achieved [192]. Tissue printing has also been successfully applied to live neuronal cells for investigation of synaptic communication [193] and human surgical specimens for tumor marker profiling [194]. A few chemical printing methods have been reported for MALDI imaging including localization of proteins, lipids, and agrochemicals in biological materials [195-200]. To my knowledge, these analyses have all involved transfer of tissue sections to solid substrates. Trichome fragility often makes sectioning of tissues impractical. Instead, the experiments described in this Chapter employed contacting printing, and successfully and selectively transferred trichomes onto a solid substrate, e.g. glass slide (Figure III-2). The optical image reveals the type VI trichome structure has been retained after the transfer. Type I/IV trichomes lack external cell walls, yet the transfer has retained the visible outline of the boundaries of the gland.

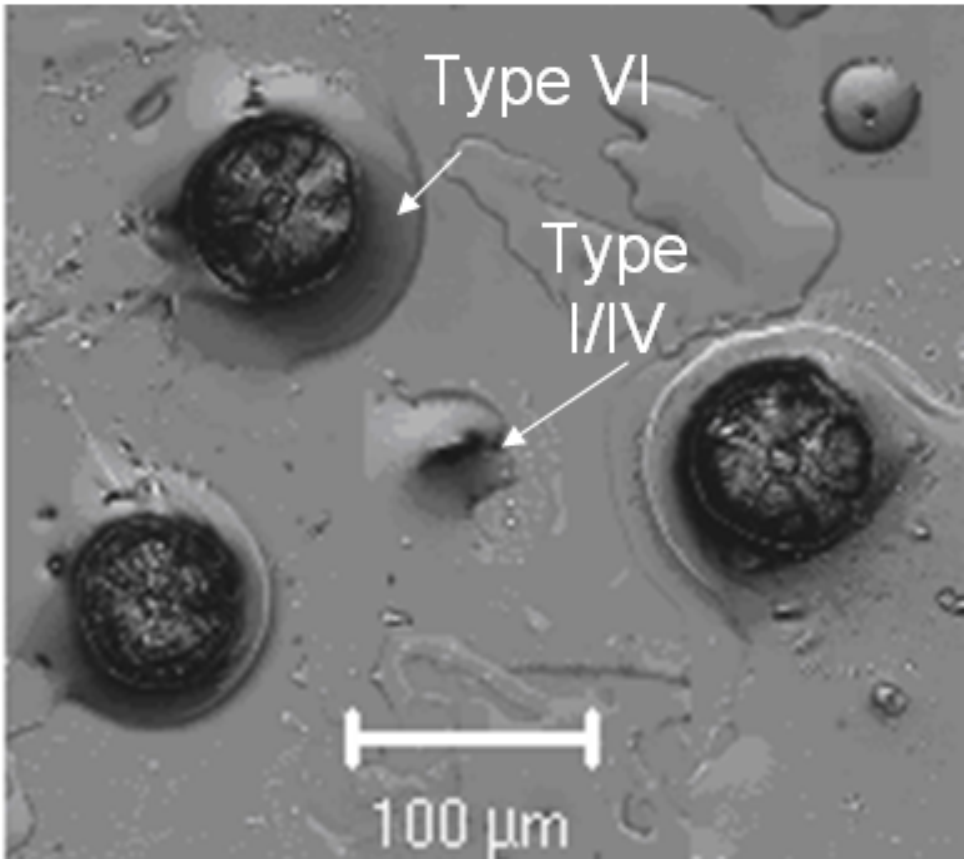

Figure III-2 Transmitted light optical image of trichomes from the adaxial (upper) leaf surface of *S. habrochaites* LA1777 transferred to a glass microscope slide.

In the course of this study, some concerns were expressed that epidermal cells other than trichomes might also be transferred during the contact printing process, and that printing force might break trichomes and spread metabolites over a large area. To achieve greater reproducibility, a 500 ml glass beaker containing 200 ml of water was placed on top of the glass slide to provide a consistent force (~ 500 N/m^2) for the printing. The optimal force was determined by visual inspection of the transferred trichomes on the glass slide under the dissecting microscope. No evidence of transfer of type VII trichomes was found. These glands have much shorter stalks and are of lower abundance, and may be protected from transfer

by the taller type I, IV, and VI glands.

We used detection of cell-specific metabolite markers to determine whether the transferred trichomes were contaminated by metabolites that leaked from epidermal pavement cells. Based on the LC/MS profiling of metabolites from pooled trichomes of a single gland type, the glycoalkaloid dehydrotomatine was not found in type I, IV, or VI trichomes, but was present in type VII trichome and was abundant in extracts of the entire leaf. It is proposed that this metabolite can serve as a marker of pavement epidermal cells and type VII glands. In order to make a more quantitative evaluation of the efficiency of transfer of trichomes from leaf surfaces to the bare glass slide substrate, trichomes on the glass slide were extracted using 3:3:2 (v:v:v) acetonitrile: isopropanol: water solvent with ultrasonication. This extract was analyzed using LC/MS, and the results were compared to analysis of extracts of the leaf tissue after trichome printing. Consistent with the result presented above, dehydrotomatine was not present at detectable levels in the slide surface extract, but was abundant in the leaf dip extracts for three replicate tissue samples (Figure III-3). This finding suggests that transfer of pavement epidermal cells to the glass slide was negligible.

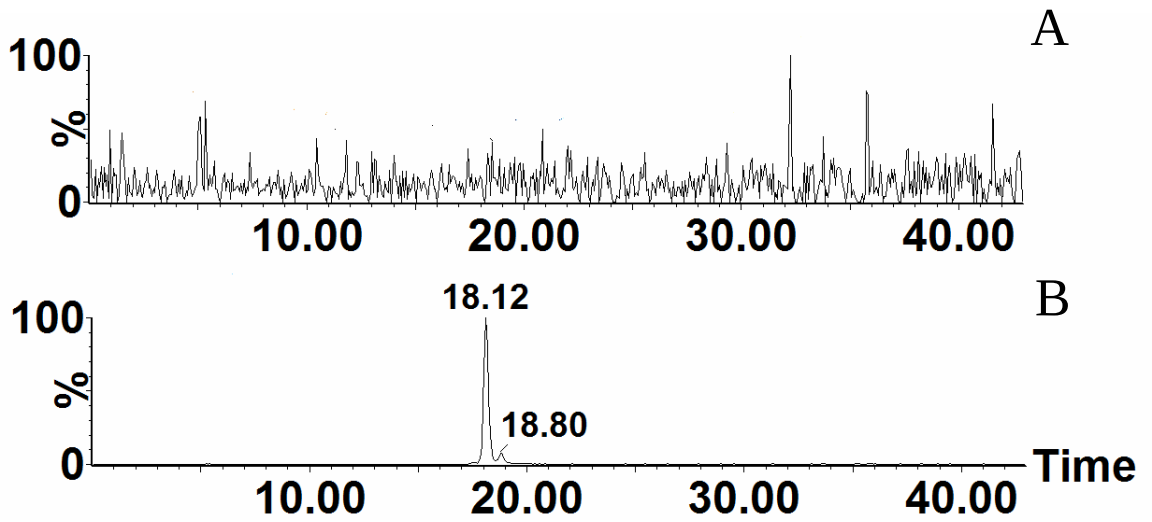

Figure III-3 Negative ion mode extracted ion LC/MS chromatogram of m/z 1076.5 showing dehydrotomatine for (A) metabolites washed off from the *S. habrochaites* LA1777 trichome printed glass substrate analyzed by LC/MS. (B) Metabolites remaining on the *S. habrochaites* LA1777 leaf surface after printing and flushing with extraction solvent and analyzed by LC/MS.

The selection of graphitic carbon for the substrate surface was made based on its ease of manipulation, efficient absorbance of laser light, inertness and ease of cleaning, and availability in numerous forms including pencil lead, graphite paint, and graphite plates. These materials often contain impurities that contribute background peaks in LDI mass spectra. To minimize these, the pencil lead coated slide was rinsed with multiple organic solvents and water before trichome transfer. After substrate cleaning, background ions are fewer in number and lower in abundance than in spectra obtained using the traditional MALDI matrix compounds α-Cyano-4-hydroxycinnamic acid (CHCA) and 2, 5-dihydroxybenzoic acid (DHB), between m/z 100 to 1500 (Figure III-4). For comparisons across these matrices, different laser powers were employed for the various matrices to achieve approximately the same total ion current for each

matrix. These laser power settings were; DHB = 105; CHCA = 85; pencil lead = 90. These laser power values are in arbitrary units, with the full range of 0-180 corresponding to laser output of 0-6 mW. When spectra were generated using negative ion mode, the pencil lead background showed carbon cluster peaks with m/z= 12n (n = an integer; up to m/z 180). In our study, most specialized metabolites in tomato trichomes have molecular masses greater than 200 Da, so the carbon cluster signals did not interfere with peak detection. The low mass carbon cluster peaks in negative mode can also be used to calibrate the instrument mass axis at low masses.

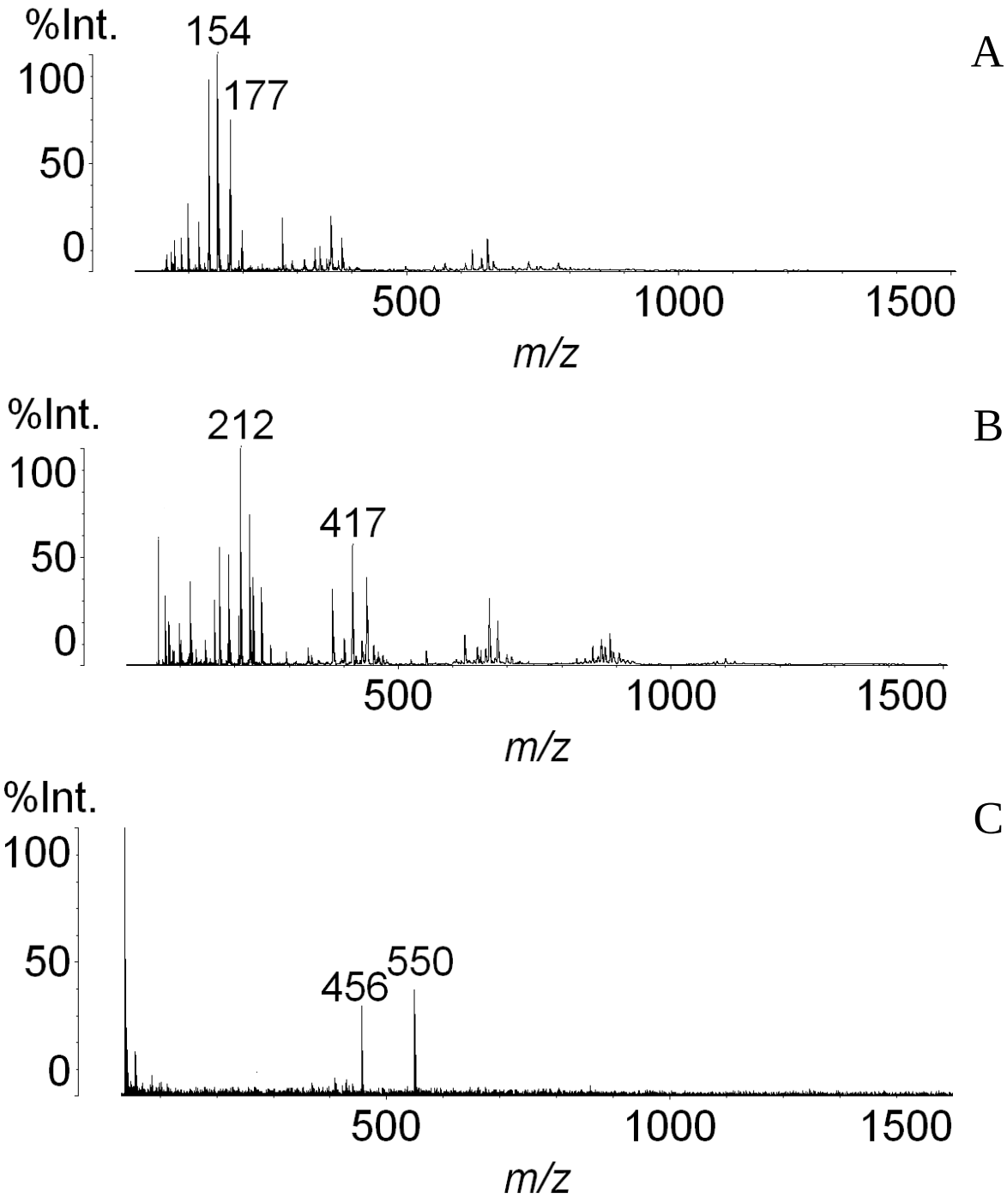

Figure III-4 The background MALDI and LDI mass spectra of DHB (A), CHCA (B), Pencil lead (C) over m/z 50~1500 in the positive mode. The spectra were scaled to the same absolute y-axis scale.

Pencil lead is manufactured in different grades that vary in the ratio of graphite to clay binders. One may anticipate that composition will influence the dynamics of the laser desorption ionization process. To investigate the effect of pencil lead composition, the analytical performance was evaluated using several different pencil types (H, 2H, 4H, B, 2B, 3B, 4B, 6B, and 8B). Aliquots (~ 1 µl) of trichome extracts from *S. habrochaites* LA1777 were applied to pencil lead coated slides for comparison. With increasing graphite content from H to 8B, the laser power required to achieve a base peak of 50 mV decreased. Comparisons of signal-noise-ratio and mass resolution under laser power yielding the same base peak signal abundance were made, using several different acyl sugar metabolites (in positive mode) and sesquiterpene acids (m/z 233 in negative mode) were evaluated. In a typical experiment, spectra generated from 50 laser shots were summed over multiple locations on the target, and the mass resolution and signal-to-noise ratio were calculated by the instrument software. Pencil leads B, 2B and 3B (low graphite content) gave the best mass resolution among the tested pencil leads when laser power was adjusted to yield approximately the same ion abundances. 2B pencil lead yielded the greatest signal-to-noise ratios (Table III-1). As a result of these findings, pencil lead 2B (74% graphite; http://www.blurtit.com/q9883867.html) was chosen for all subsequent analyses.

Table III-1 Mass spectra resolution (±SD, n=3) and S/N ratio (±SD, n=3) calculated by averaging the resolution and S/N ratio of five most abundant acylsugar peaks from *S. habrochaites* LA1777 extracts in positive mode and sesquiterpene acids (m/z 233) peak in negative mode. Resolution and S/N for individual peak is taken from peak lists generated using Launchpad software (version 2.8.1, Kratos Analytical).

Pencil types	Resolution (FWHM) (positive mode/negative mode)	S/N ratio (positive mode/negative)
H	982±131/1475±287	1593±576/2305±384
2H	531±273/1943±213	2207±711/2645±469
4H	1223±253/2912±432	2010±785/2216±453
B	2038±445/2653±372	2900±862/2357±432
2B	2164±387/2830±311	2875±693/4103±326
3B	2295±541/3013±306	2268±782/2177±333
4B	1338±379/2173±448	2362±847/2983±355
6B	1607±314/2150±337	2126±1020/2468±594
8B	1635±445/2089±356	1590±899/2298±513

The observed peaks in LDI mass spectra of trichome extracts spotted onto the pencil lead-coated slide were first compared to spectra obtained using LC/MS analysis of the same extracts. Putative annotation of metabolites was performed by the following: accurate LC-TOF MS measurements of pseudomolecular ions generated a list of candidate molecular formulas, which were searched against several chemical and natural products databases (ChemSpider, eMolecules, CSLS). Masses of fragment ions had also been generated using multiplexed CID on the LC-TOF spectrometer or as product ion spectra on the Q-Tof spectrometer. Putative structures were proposed based on the goodness of matching of predicted fragment ion masses with experimental MS/MS spectra and also prior knowledge of plant metabolites in the genus *Solanum* [117]. Ions observed in LDI mass spectra were assigned by comparing their m/z values with ions observed in LC/MS analysis.

In some cases, product ion MS/MS spectra were generated using post-source decay (PSD) to confirm assignment to structural classes (Figure III-5C and 5D). In the former case, the prominent ion at m/z 715 generated in positive ion mode for an extract of *S. habrochaites* LA1777 trichomes was selected for transmission by the ion gate of the Axima TOF mass spectrometer, and ions reaching the reflectron detector appear in the spectrum. Based on comparisons to the LC-TOF MS data, this was tentatively annotated as $[M+Na]^+$ of acylsugar S4:21. In the PSD spectrum (Figure III-5C), in addition to the precursor ion (m/z 715) that has not fragmented, an additional product ion is evident at m/z 399, corresponding to a loss of a neutral fragment of 316 Da. This ion corresponds to the sodiated triacylglucose fragment that contains C2, C4, and C5 ester groups. Complementary fragment information was obtained from the LC-TOF CID spectrum (Figure III-5E) which shows a major fragment at m/z 317, corresponding to the fructose moiety with a C10 ester group attached. The combined results point to S4:21 being a sucrose with C2, C4, and C5 groups on the glucose ring, and C10 on the fructose ring. The differences in information arise from different precursor ions. For the LC-TOF MS analysis, the CID process is non-selective, so all ions are activated by collision, with most fragment ions being generated from $[M+NH_4]^+$ ions (m/z 710), whereas the protons in the sodium adduct have limited mobility. Its fragmentation is inefficient under the LDI conditions, and is largely confined to formation of the sodiated triacylglucose ion. One important finding from this experiment is the localization of the long chain fatty acid on the fructose ring, which has not been reported in published descriptions of Solanum acylsugars.

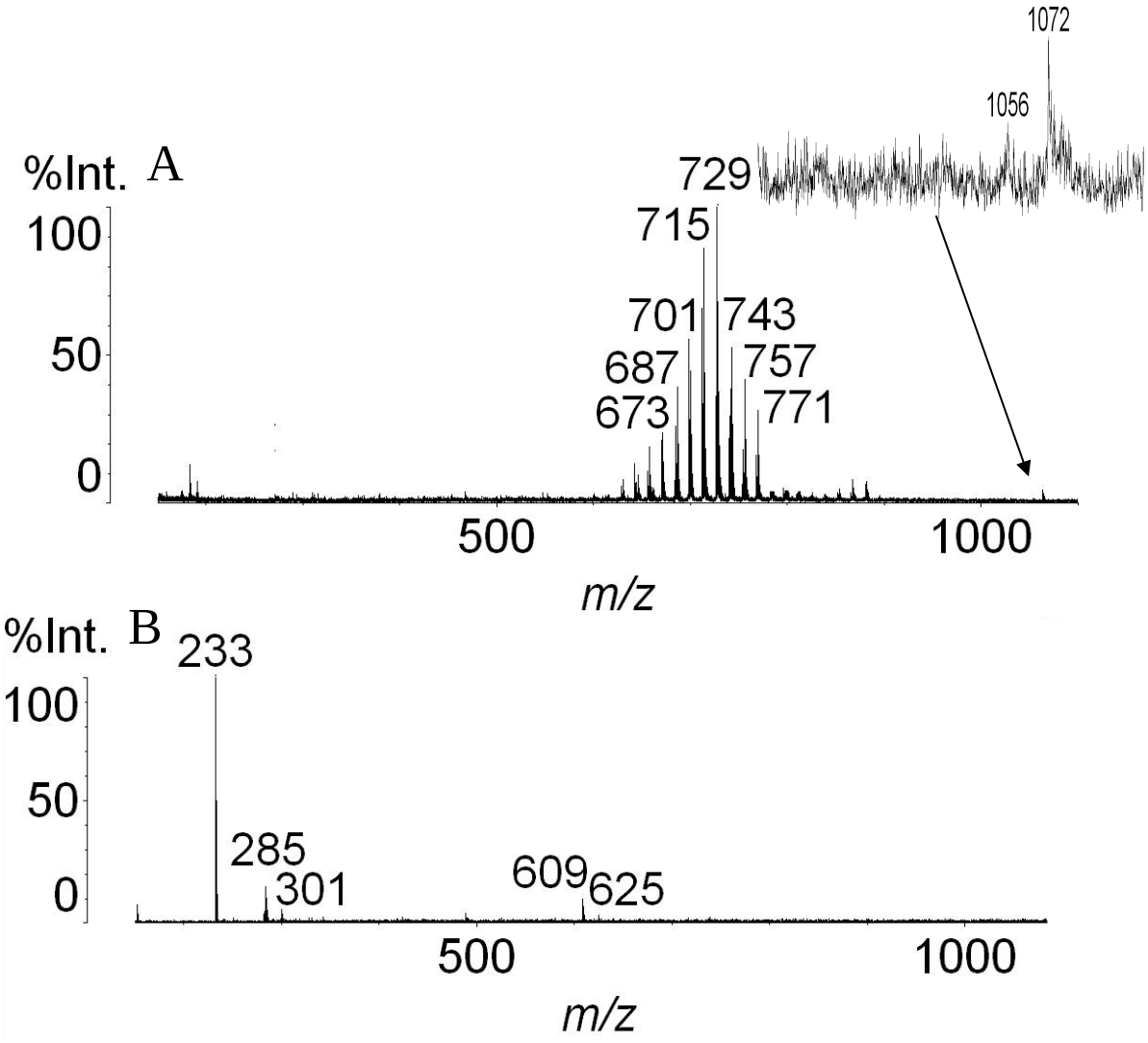

Figure III-5 Laser desorption ionization (LDI) mass spectra of trichome extracts from *S. habrochaites* LA1777 spotted on pencil lead-coated glass slides using (A) positive mode (B) negative mode. Post source decay (PSD) product ion spectra of (C) acylsugar S4:21 precursor=m/z 715 ($[M+Na]^+$) (D) mixed isomeric flavonoid glycosides rutin and kaempferol-O-diglucoside ($[M-H]^-$, m/z 609). Electrospray ionization in-source decay (ISD) mass spectra of (E) acylsugar S4:21 and (F) mixed flavonoid glycosides rutin and kaempferol-O-diglucoside $[M-H]^-$ acquired using TOF-MS and nonselective collision induced dissociation.

Figure III-5 (cont'd)

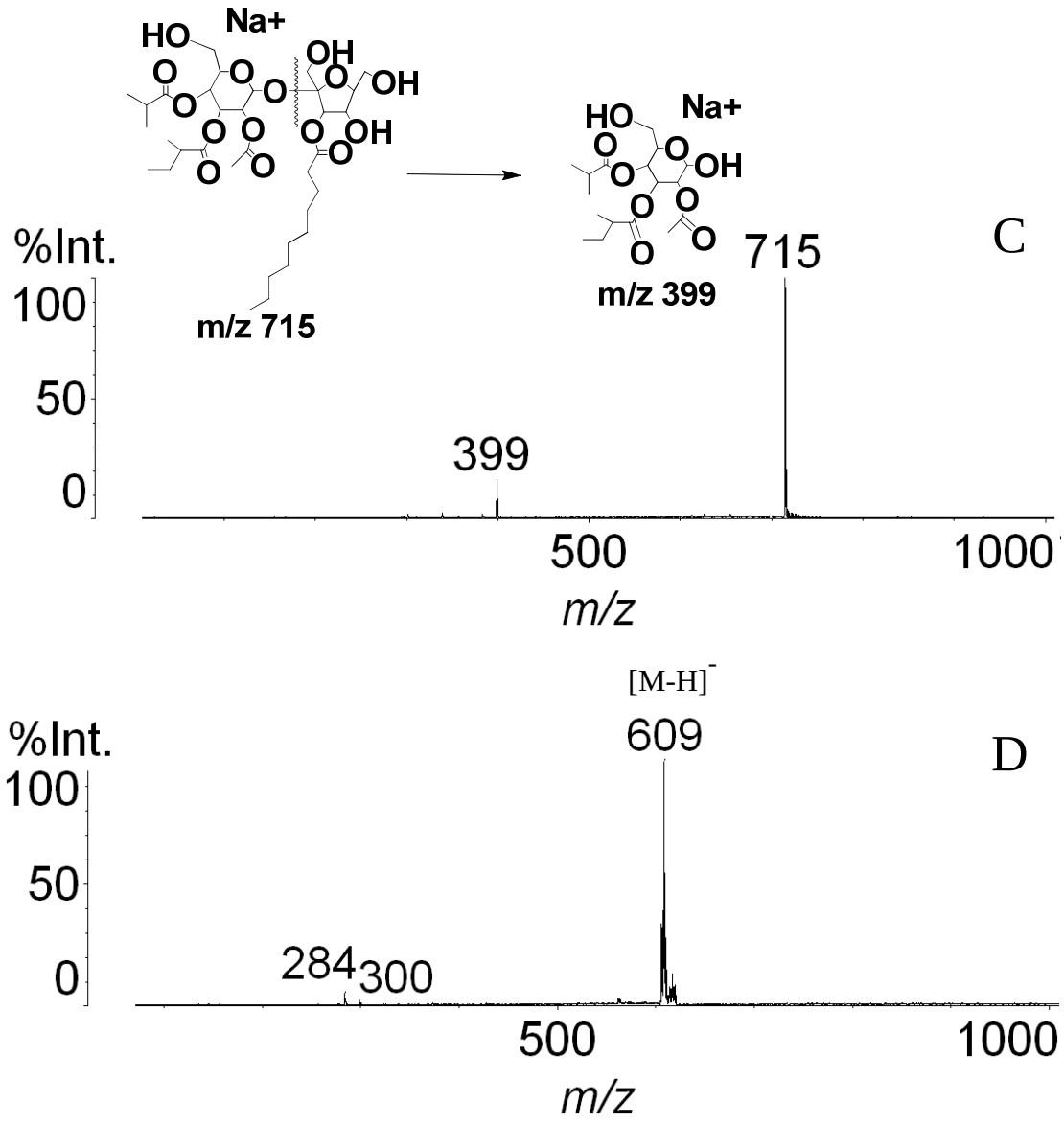

Figure III-5 (cont'd)

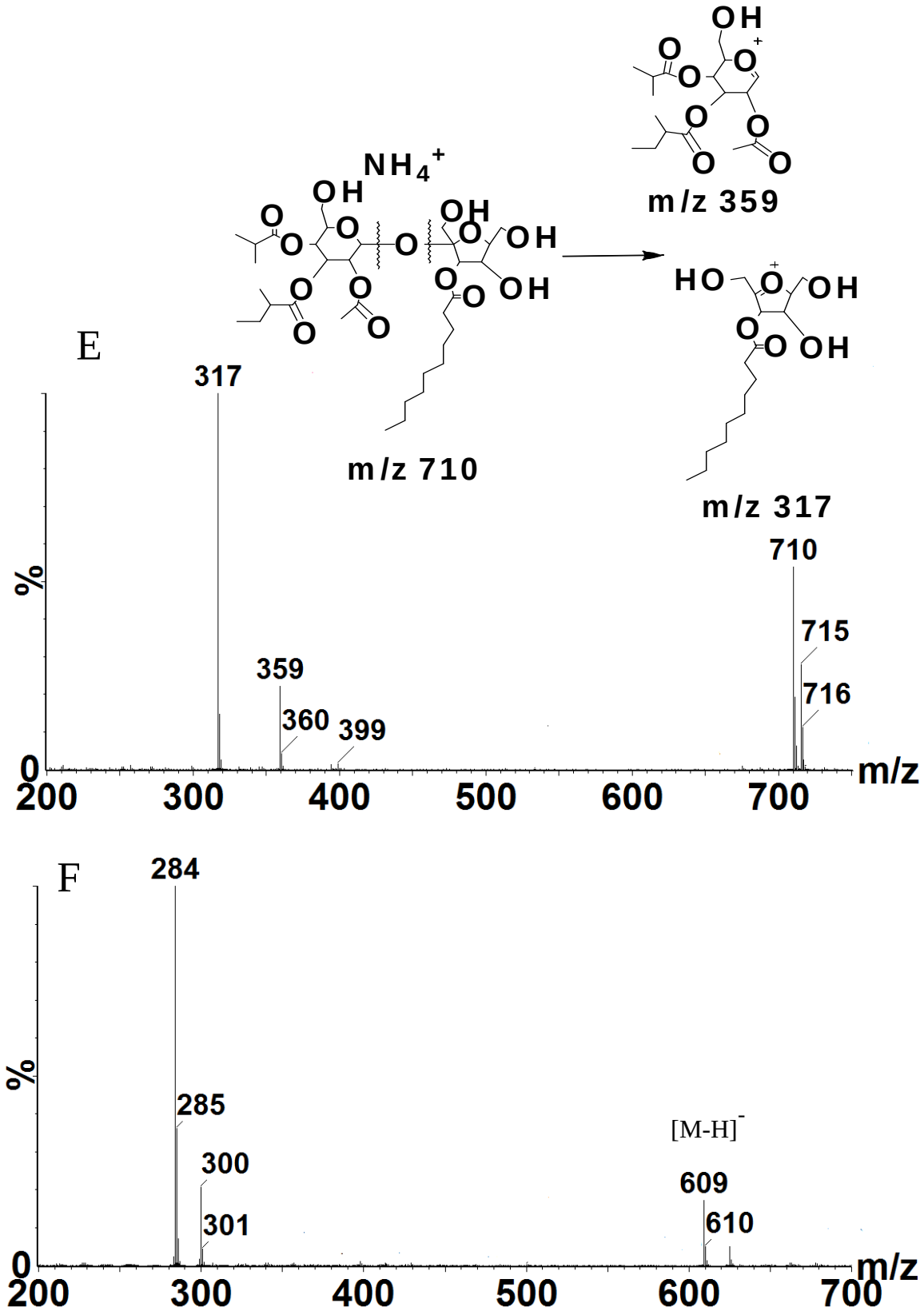

PSD mass spectra were generated in negative ion mode for the same *S. habrochaites* LA1777 trichome extract. The product ion (PSD) spectrum of m/z 609 showed two fragments at m/z 284 and 300 (Figure III-5D). These correspond to radical anion fragments for the flavonoid aglycones kaempferol and quercetin, respectively, and demonstrate resolution of two isomeric flavonoid glycosides in the trichome extract. This finding stands in contrast with the findings reported in Chapter II, in which all of the m/z 609 flavonoid glycosides were kaempferol derivatives. We attribute this difference to separate samplings of plants grown under different conditions (growth chamber vs. greenhouse).

One of the challenges that analysts face when performing MALDI imaging lies in the choice of a suitable matrix that can convert laser light into liftoff and ionization. It is common dogma that acidic matrices such as CHCA or DHB are effective for generating positive ions because they can donate protons to analytes, whereas 9-aminoacridine is preferred for negative mode because it is a proton scavenger. As a consequence, a single matrix may perform poorly when it is desirable, as is usually the case, to analyze materials in both positive and negative ion modes. Binary mixtures of matrices mixture have been used to generate information about metabolites in both positive and negative ion modes [201]. However, such an approach complicates further the matrix application process. By using a solid support such as carbon as the light-absorbing medium, LDI generates ions for a wide range of trichome metabolites in both positive and negative modes. An important consequence of this finding is that the laser can be rastered over the printed substrate to generate spectra for one polarity over the entire area, followed by a repeat analysis with the polarity inverted. The key issue that needed to be

addressed was the depletion of analyte with successive laser shots for a single pixel. Based on some preliminary data regarding signal depletion, experiments were performed using 20 laser shots per pixel in each mode.

Four classes of major metabolites were detected in both LC/MS of individual trichome types from *S. habrochaites* LA1777 and LDI analyses of trichome extracts and from tissue printing with imaging: acylsugars, flavonoids, alkaloids, and sesquiterpenoid acids (Table III-2). In LDI analyses, flavonoid and sesquiterpenoid acids could be readily detected as $[M-H]^-$ ions in negative mode, as they are weak acids. Acylsugar metabolites are not particularly basic or acidic, but since sodium and potassium are abundant ions in plant tissues, acylsugars are observed in positive ion mode mainly as $[M+Na]^+$ and $[M+K]^+$. Pseudomolecular ions of acylsugars were not observed in negative ion mode, and this finding highlights the need to perform analyses in both modes. In the lower m/z region of the negative ion spectra, a series of ions matching the masses of short fatty acid anions (e.g. m/z 87 for C4, m/z 101 for C5) was observed. Since acylsugars do not readily form $[M-H]^-$ ions and since the short chain fatty acids were not observed in LC/MS analyses, it is suspected that displacement or dissociation reactions in the plume are responsible for generation of the fatty acid anions from acylsugar metabolites. One surprising finding arose from the observed behavior of the glycoalkaloid tomatine. Tomatine has one basic nitrogen group, and was expected to be detected as $[M+H]^+$ in trichome extracts and printed glands. However, in spectra of trichome extracts, peaks at m/z 1056 and 1072 were observed, but signals corresponding to $[M+H]^+$ were not discernable (Figure III-5A). Two lines of reasoning may explain this phenomenon. First, both sodium and

potassium are abundant in plant tissues, and the large carbohydrate moiety is expected to have high affinity for these alkali metal cations. In addition, the high internal energies anticipated from LDI from carbon surfaces may lead to more extensive fragmentation of $[M+H]^+$ owing to proton mobility.

Table III-2 Major ions observed in laser desorption ionization (LDI) spectra of S. habrochaites LA1777 trichome extracts on pencil lead-coated glass slides.

	Polarity	*Major Ion*	*m/z*
S 4:14	*Positive*	$[M+Na]^+/[M+K]^+$	*617/633*
S 4:15	*Positive*	$[M+Na]^+/[M+K]^+$	*631/647*
S 4:16	*Positive*	$[M+Na]^+/[M+K]^+$	*645/661*
S 4:17	*Positive*	$[M+Na]^+/[M+K]^+$	*659/675*
S 4:18	*Positive*	$[M+Na]^+/[M+K]^+$	*673/689*
S 4:19	*Positive*	$[M+Na]^+/[M+K]^+$	*687/703*
S 4:20	*Positive*	$[M+Na]^+/[M+K]^+$	*701/717*
S 4:21	*Positive*	$[M+Na]^+/[M+K]^+$	*715/731*
S 4:22	*Positive*	$[M+Na]^+/[M+K]^+$	*729/745*
S 4:23	*Positive*	$[M+Na]^+/[M+K]^+$	*743/759*
S 4:24	*Positive*	$[M+Na]^+/[M+K]^+$	*757/773*
S 4:25	*Positive*	$[M+Na]^+/[M+K]^+$	*771/787*
tomatine	*Positive*	$[M+Na]^+$ $[M+K]^+$	*1056/1072*
Sesquiterpene acid	*Negative*	$[M-H]^-$	*233*
Rutin	*Negative*	$[M-H]^-$	*609*
Kaempferol-O-diglucoside	*Negative*	$[M-H]^-$	*609*
Quercetin-O-diglucoside	*Negative*	$[M-H]^-$	*625*

Imaging of printed trichomes from the upper surface of a leaflet from *S. habrochaites* LA1777 reveal distribution of some major metabolites throughout the leaf. Again, data were generated in both positive and negative ion modes for the same tissue. Data for Figure III-6A were generated using positive mode with 20 laser shots per pixel, and then the polarity was switched for negative mode acquisition, also with 20 laser shots per pixel. Figure III-6 shows the color-coded intensity map of pseudomolecular ion for one acylsugar (Figure III-6A), the aglycone fragment of a group of flavonoid glycosides (Figure III-6B), and a deprotonated sesquiterpene acid (Figure III-6C). For all three m/z images, the midvein area running up and down the center of the leaflet generates stronger signal than the rest of the tissue area. Visual inspection of the leaflet before printing showed higher trichome density around the midvein. Whether the strong signal intensities near the midvein largely reflect trichome densities or differences in composition of individual trichomes has yet to be established. It is not practical to sample individual trichomes around the midvein because the trichome density is so high as to preclude microsampling of individual glands. The images presented in Figure III-6 present a wide view of metabolite abundances across an entire leaflet. Based on findings reported in Chapter II, acylsugars predominantly accumulate in type I and IV glands, whereas flavonoid glycosides and sesquiterpene acids are abundant in type VI glands. The wide view does not distinguish contributions of individual trichomes to plant tissue chemistry, and highlight the need to probe individual gland chemistry. Such efforts are described below.

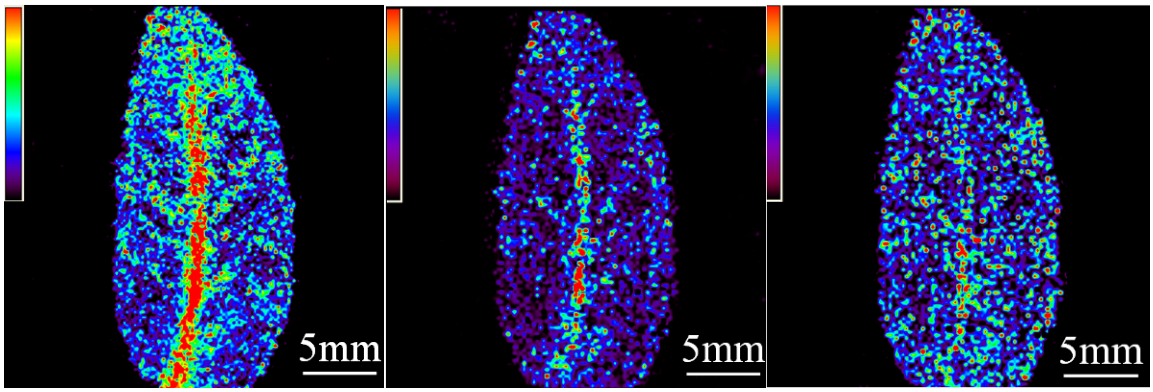

A B C

Figure III-6 LDI images of selected ions for contact printed trichomes from *S. habrochaites* LA1777 leaf on pencil lead-coated glass slides: (A) ion abundances of *m/z* 731 (acylsugar S4:21 $[M+K]^+$) using positive mode and laser power setting = 95, 125 µm stage step, and 20 laser shot per pixel. (B) *m/z* 301 in negative ion mode (aglycone fragment of quercetin glycosides), (C) *m/z 233* (sesquiterpene acid $[M-H]^-$ of various sesquiterpene acids) for the same leaf sample under negative mode with laser power setting of 105, and 20 laser shots per pixel. The key for color coding is presented at the left of each panel.

To assess how much metabolite was removed by laser ablation, 30 pixels selected to be representative of different regions of the leaflet were chosen. Initial data acquisition employed laser power = 95, which is the same condition used for imaging. Spectra were acquired into a single profile using 5 shots per pixel. Then 20 shots were fired on each spot to assess the ablation caused by typical imaging conditions. Afterwards, the spectrum profile was generated using another 5 shots at the same spot. This second sampling yielded 87±8% (N=30) signal intensity compared to the first 5-shot profile. The results suggest that the metabolites were slightly depleted by normal spectrum generation parameters. Changes in relative abundances of various metabolite ions were judged to be minimal following the 20-shot ablation.

For individual trichome analysis, the spatial resolution of imaging should resolve objects smaller than 50 µm (the approximate diameter of the type VI trichome and about the average distance between two trichomes). For the Axima cfr-plus instrument, details regarding the laser spot size were unknown when these experiments were conducted, but the spot diameter was estimated to be approximately 100 µm. The spatial resolution of the LDI imaging scheme was first tested by printing trichomes into transmission electron microscope (TEM) grids with different spacing between grid elements. The TEM grids were mounted on the top of the pencil scratched substrate. Plant leaves were pressed against it several times and trichomes were positioned into the space between the grids. LDI imaging was conducted after the grid was removed from the substrate because of concerns that the thickness of the TEM grid might interfere with illumination of the trichomes by the laser and with ion transmission from the surface to the mass analyzer. The diameter of the laser spot is estimated to be about 100 µm, which is larger than the smallest grid we tested (50 µm). To analyze the object which is smaller than the size of the laser spot, complete depletion [202] with a step size of 25 µm and laser power of 105 was employed. The resulting 100 µm grid can be clearly resolved, but the smaller spacing of the 50 µm grid hindered trichome transfer to the substrate surface. Nevertheless, the resulting image suggests that spatial resolution approaching 50 µm has been achieved (Figure III-7).

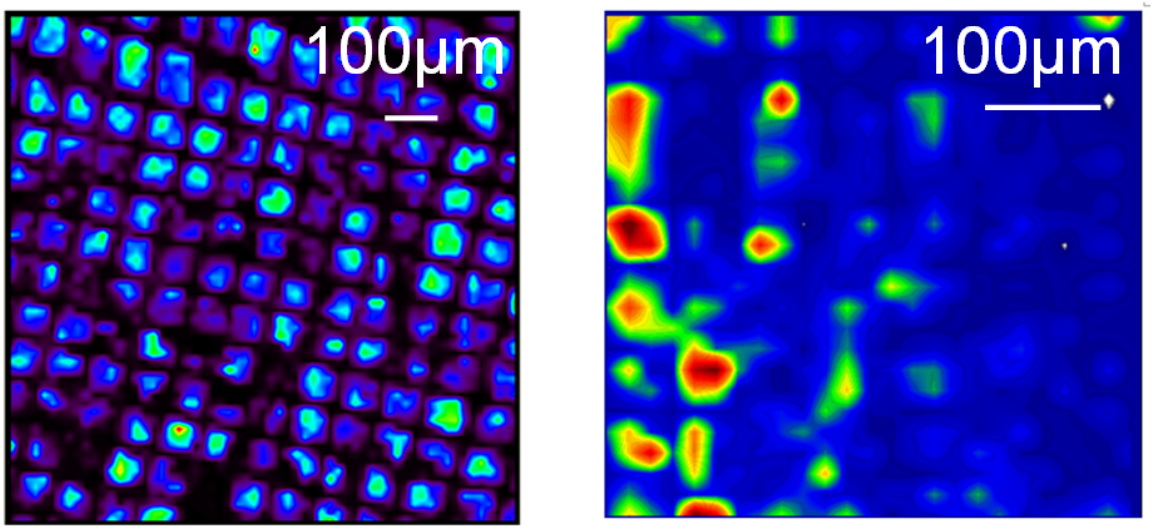

A B

Figure III-7 Imaging of metabolites from *S. habrochaites* LA1777 leaf trichomes transferred into the (A) 100 µm and (B) 50 µm TEM grids. Ion abundances are displayed for m/z 731 (acylsugar S4:21 $[M+K]^+$), using positive mode with laser power setting = 95, 25 µm stage step size, and 200 laser shot per pixel.

Pencil lead coating of substrate surfaces is a fast and simple sample preparation method for chemical imaging of leaf metabolites over a wide tissue area. However, when higher spatial resolution is needed for individual trichome imaging, small defects in the carbon coverage can compromise the analysis. A closer examination of the pencil lead-coated slide under the optical transmission microscope showed numerous spots of diameter less than 30 µm where no pencil lead had been deposited. For comparison, we evaluated deposition of the MALDI matrix CHCA using electrospray deposition. Again, the coating lacked uniform coverage unless a very thick layer (10-100 µm) of matrix was deposited. To minimize the effects of surface coating defects, several other substrates were explored for individual trichome imaging. First, a commercially available graphite plate (SPI supplies) was tested as a substrate. The porous

structure of the graphite plate gave high surface area which offers potential enhancement of the laser desorption/ionization efficiency [203]. However, in our test, the ion signal was less than for pencil lead coated glass slides. The extracts from *S. habrochaites* LA1777 yielded 50 mV signal for acylsugar ion m/z 731 (S4:21) using 90 laser power and 2B pencil lead coated glass slide. For the same extracts, a laser power setting of 135 was required to obtain the same signal using a graphite plate. As a second alternative, a thin layer of carbon paint (Ted Pella, Inc.) used for electron microscopy was painted on the back side of a stainless steel MALDI plate. The ingredients present in the carbon paint yielded more background ion signals at low mass range than rinsed pencil lead. To remedy this, the carbon paint coating was heated with a gas flame for 5-10 min to remove the impurities. Background was reduced after the heating except for one major background peak that has the same mass (m/z 233) in the negative mode as sesquiterpene acid metabolites present in trichomes. For this reason, this approach was not pursued further. Third, glassy carbon plate widely used for electrochemistry gave minimal background, and was judged to be a promising alternative. Glassy carbon was recently found to have structural features resembling fullerenes [204] and has been used for small molecule analysis by laser desorption ionization [205]. Fullerenes have also proven to be a successful matrix for laser desorption ionization [206, 207].

The surface of glassy carbon can be chemically etched or mechanically ground to increase the surface area, which should increase the ionization yield because the metabolites would be spread in a thinner film within the illuminated area. However, for transfer printing, the rough surface may decrease spatial resolution of LDI analyses because spreading of metabolites would

be more favorable. The choice of a solid laser-absorbing material is best considered as a trade off between ionization efficiency and spatial resolution. To illustrate this point, consider that each type VI gland contains about 100 pL of cell sap. The gland head is fragile and the sap can readily leak from the trichome upon application of mechanical force. For this reason, to achieve higher spatial resolution desired for single gland imaging, the glassy carbon surfaces described below were not subjected to any etching procedures.

Figure III-8 shows LDI images obtained in both positive and negative modes of trichomes transferred from a small (5 x 10 mm) leaflet of *S. habrochaites* LA1777 to a glassy carbon surface. The images document metabolite composition with spatial resolution of individual trichomes. Further examination of the mass spectra generated at different locations across the leaflet suggested a heterogeneous distribution of metabolites. In the positive mode spectra, an example spectrum selected from a bright spot on the m/z 731 image near the midvein shows a series of ions separated by 14 Da that correspond to potassium cationized acylsugars. The ion at m/z 731 corresponds to acylsucrose S4:21, and its abundance is suggestive of locations of type I and IV trichomes, which are responsible for acylsugar accumulation, as discussed in Chapter II. A different pixel farther away from the midvein also displays a strong m/z 731 signal, but shows abundance of S4:21 ions greater than those for other acylsugar homologs. Since the fatty acyl groups are believed to be derived from various amino acids, this finding suggests that metabolic conversion of amino acids to specialized metabolites has a significant dependence on trichome location within leaf tissue. Similar heterogeneity was observed in the negative ion image, which revealed a dominance of flavonoids, detected as m/z 301, the quercetin aglycone anion,

near the midvein, but greater prominence of sesquiterpene acids (m/z 233) in regions closer to the edge of the leaflet. Both of these metabolites are selectively accumulated in type VI trichomes [140], so this finding reflects biochemical differences, in a specific trichome type, at various locations across the tissue. Whether this reflects different access of trichomes to metabolite precursors in phloem near the midvein remains to be determined, and further investigation into the factors that control accumulation of metabolites in individual trichomes is recommended.

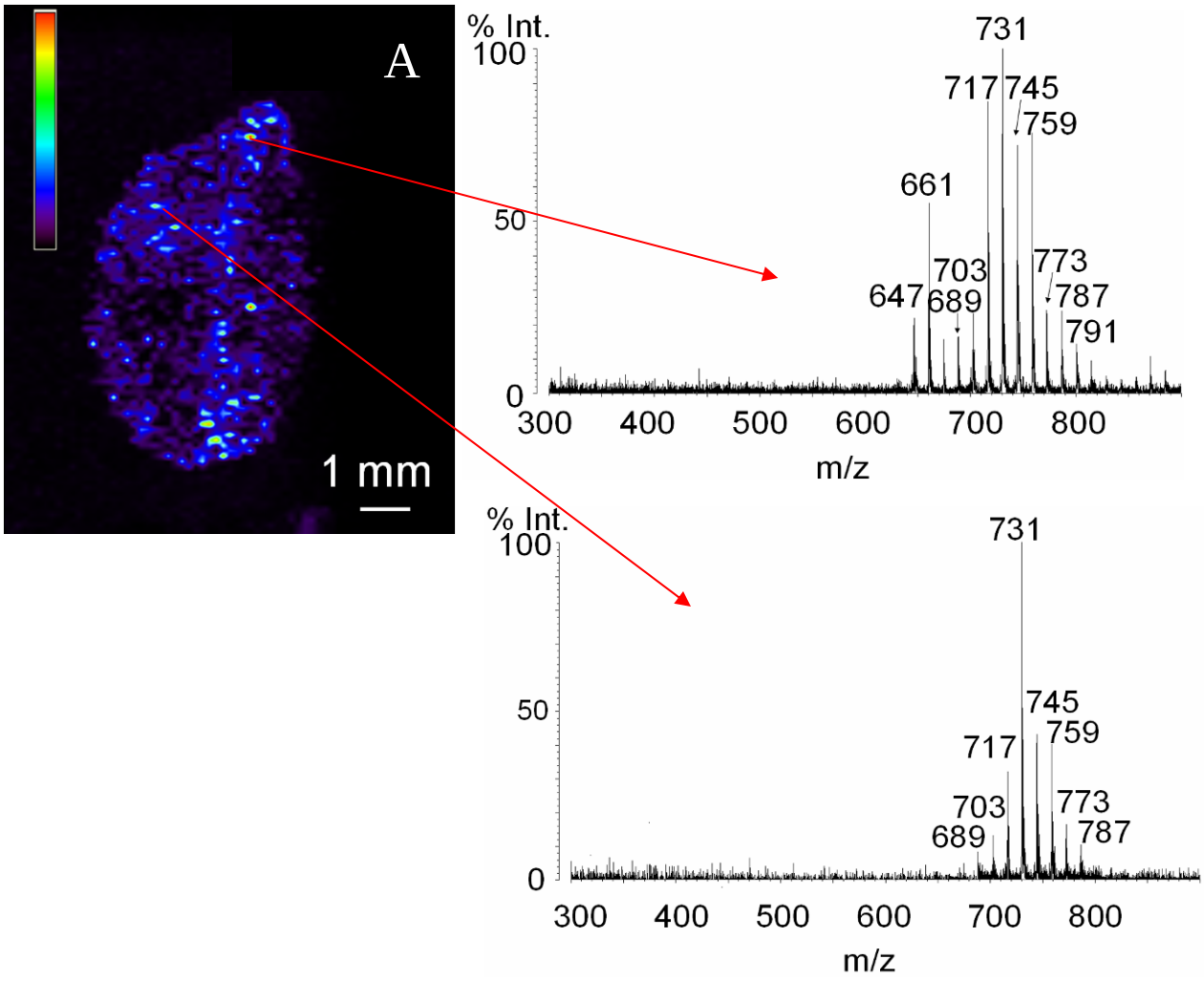

Figure III-8 Left: Mass spectrometry images of selected ions for *S. habrochaites* LA1777 trichomes transferred to glassy carbon. (A) m/z 731 in positive mode, corresponding to acylsugar S4:21 ($[M+K]^+$), using laser power setting of 105, 125 µm stage step, and 20 laser shots per pixel. (B) m/z 301 in negative mode (fragment ion of quercetin glycosides) for the same leaf sample using laser power setting of 115, 125 µm step size, and 20 laser shot per pixel. Right: (A) mass spectra for two individual pixels in positive mode (B) mass spectra for two pixels in negative mode.

Figure III-8 (cont'd)

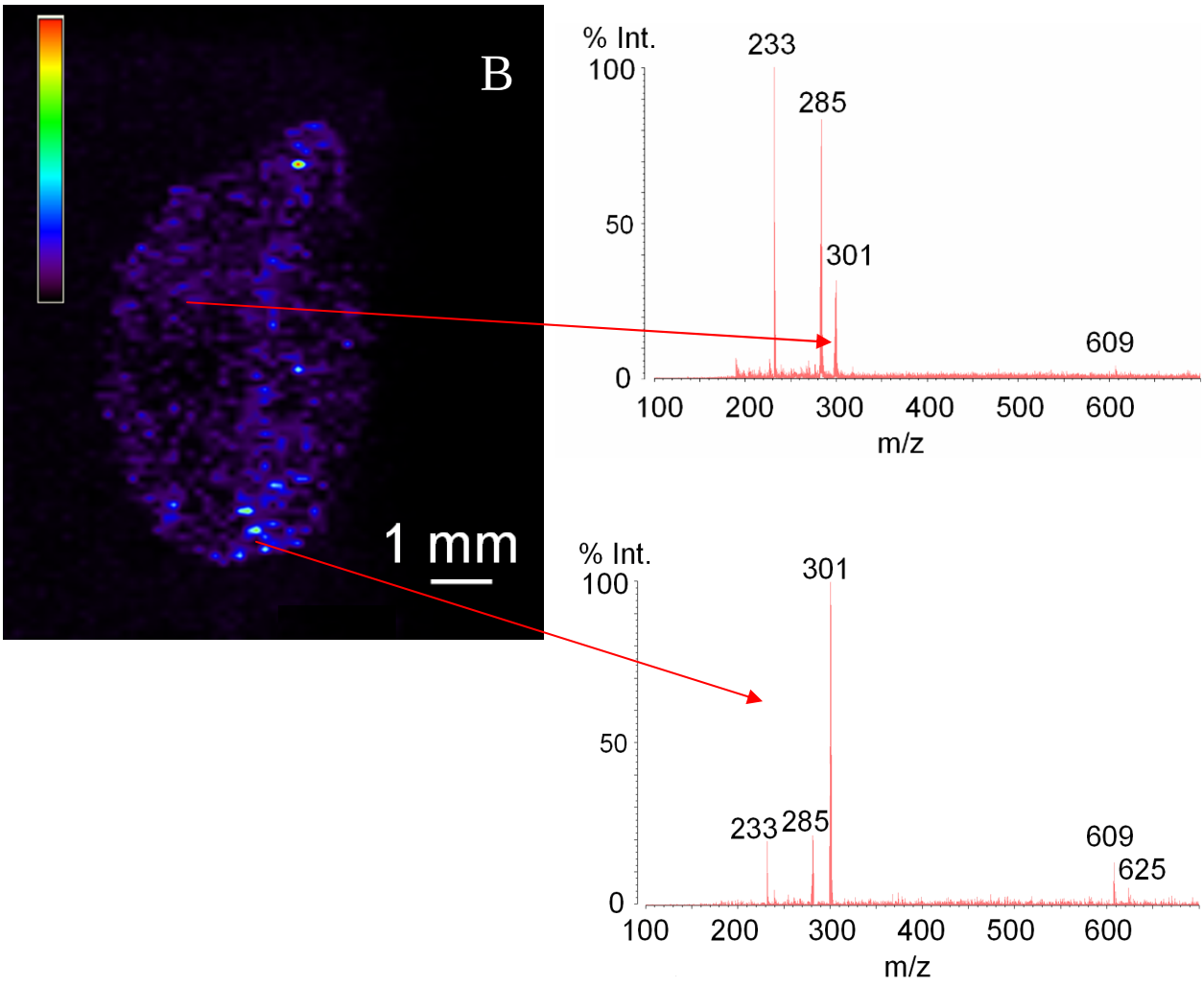

The differences in metabolic phenotypes between individual type VI trichomes is further illustrated in Figure III-9, which shows a reflected light microscope image of the transferred trichomes on a glassy carbon surface (Figure III-9A) and the corresponding LDI image of m/z 233 in negative mode. To address the challenges of aligning optical and mass spectrometry images, four position indicators were applied to the substrate using liquid paper, which is easily visualized using the camera in the MALDI instrument. These reference points lie outside the area shown in the images in Figure III-9. These images demonstrate that metabolite signals are

obtained with spatial resolution of individual trichomes. To further confirm the physical integrity of trichomes after the transfer printing process, a fluorescent microscope image was obtained (Figure III-9C), which shows fluorescence is confined to the interior of the type VI trichomes. To obtain this image, it was not feasible to use a carbon substrate. However, a thin film of carbon was deposited afterward using vacuum evaporation and deposition, in the same manner as is common in sample preparation for scanning electron microscopy (http://www.huck.psu.edu/facilities/electron-microscopy-up/faq/sample-preparation), which employs carbon thickness on the order of 10-50 nm. The LDI image (Figure III-9D) was obtained by transferring the carbon coated slide into the MALDI instrument. To obtain higher spatial resolution, complete ablation of each pixel was performed [202] using a laser power setting of 145. Due to the small stage step size and the relatively slow laser repetition rate (10 Hz), the imaging of an entire leaflet at single gland resolution would take about 15 days to complete, so the imaging was only conducted over a small area. As was the case with the glassy carbon substrate, substantial differences in the sesquiterpene acid signal at m/z 233 were observed for trichomes adjacent to one another on the leaf surface. This striking heterogeneity of trichome chemistry provides a compelling reason for performing chemical imaging of trichomes. If all trichomes on a leaf surface were chemically identical, the rationale for imaging them would fade.

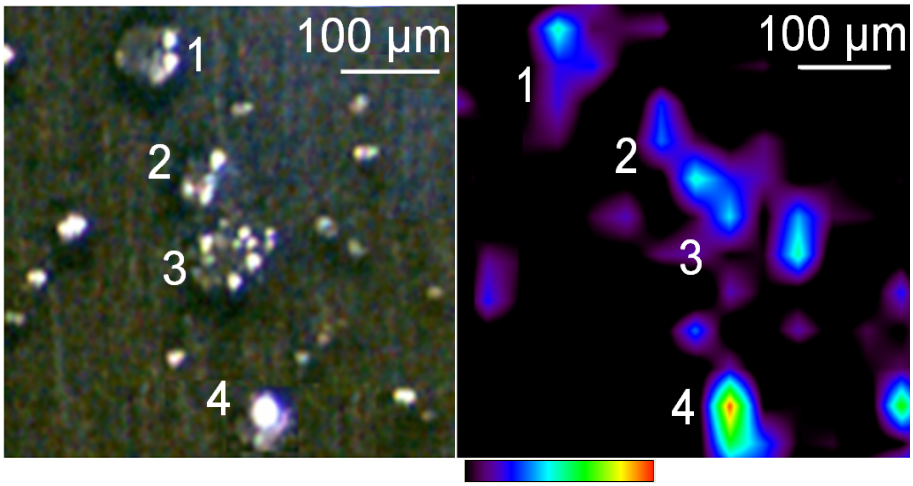

A B

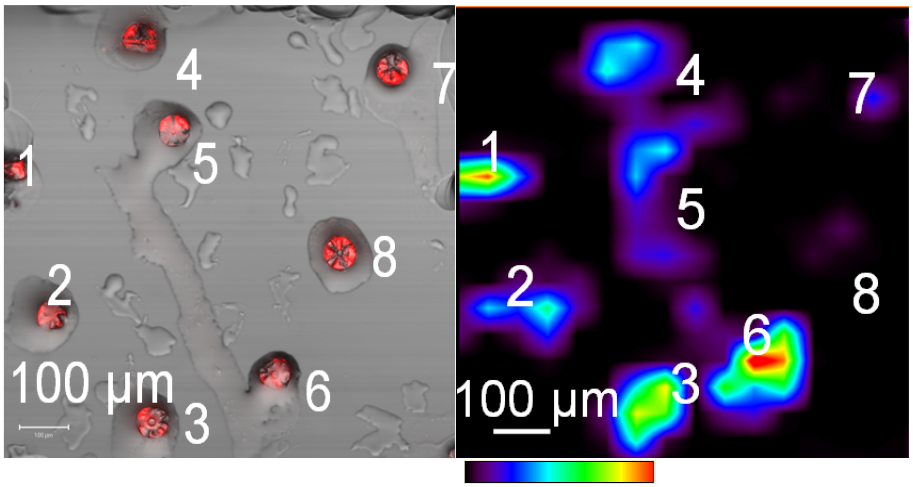

C D

Figure III-9 Images of *S. habrochaites* LA1777 trichomes printed on (A) glassy carbon surface, reflected light image (B) m/z 233 ion (sesquiterpene acids) in negative mode on the same glassy carbon area. Step size was 25 µm with 200 laser shots per pixel. (C) fluorescent image of *S. habrochaites* LA1777 trichomes printed on a glass slide using 543 nm excitation and 560 nm longpass emission. Slide was subjected to carbon coating afterward; (D) mass spectrometry image of the same glass slide as (C) after carbon coating, showing ion abundance map for m/z 233 in negative mode using 200 laser shots per pixel with 25 µm step size.

Despite the growing number of published reports using mass spectrometry imaging for protein and metabolite localization [208-211], validation of the performance of mass spectrometry imaging has been scarce. Several issues are relevant to validation of MS imaging, but most center around the effect of the cellular matrix on energy deposition and ionization efficiency. To explore matrix effects, a set of experiments examined LDI using the glassy carbon substrate using a mixtures of trichome extracts from two wild tomato species, *S. pennellii* LA0716 and *S. habrochaites* LA1777. The former was employed as a cellular matrix, and its amount was maintained in excess relative to the latter, and in constant quantity. The acylsugar profiles of these plants are easily distinguished by their molecular masses, as LA0716 accumulates acylglucoses, and LA1777 accumulates acylsucroses that are nearly 200 Da heavier. Varying amounts of LA1777 extract were diluted into the LA0716 extract, with the proportions normalized to the LC/MS extracted ion chromatogram peak areas for the most abundant acylsugar from each plant, and these were assumed to have equivalent response factors. Mixtures were prepared over the range of 0.01 to 1.0 for LA1777:LA0716, and an aliquot was deposited into 2 mm diameter wells cut into a parafilm mask using the tip of a Pasteur pipet. The amount of material deposited into each well is estimated to correspond to approximately 100 trichome equivalents per well. LDI mass spectra were generated from 200 laser shots by manually moving the stage to sample across the well. The signal intensity for LA1777 acylsugar S4:21 at m/z 731 was determined for triplicate wells for each mixture, and the relationship between signal and LA1777 concentration is presented in Figure III-10. The response approaches linearity over the 100-fold concentration range, suggesting that quantitative

comparisons in MS imaging should be reliable when experimental conditions are designed and executed properly.

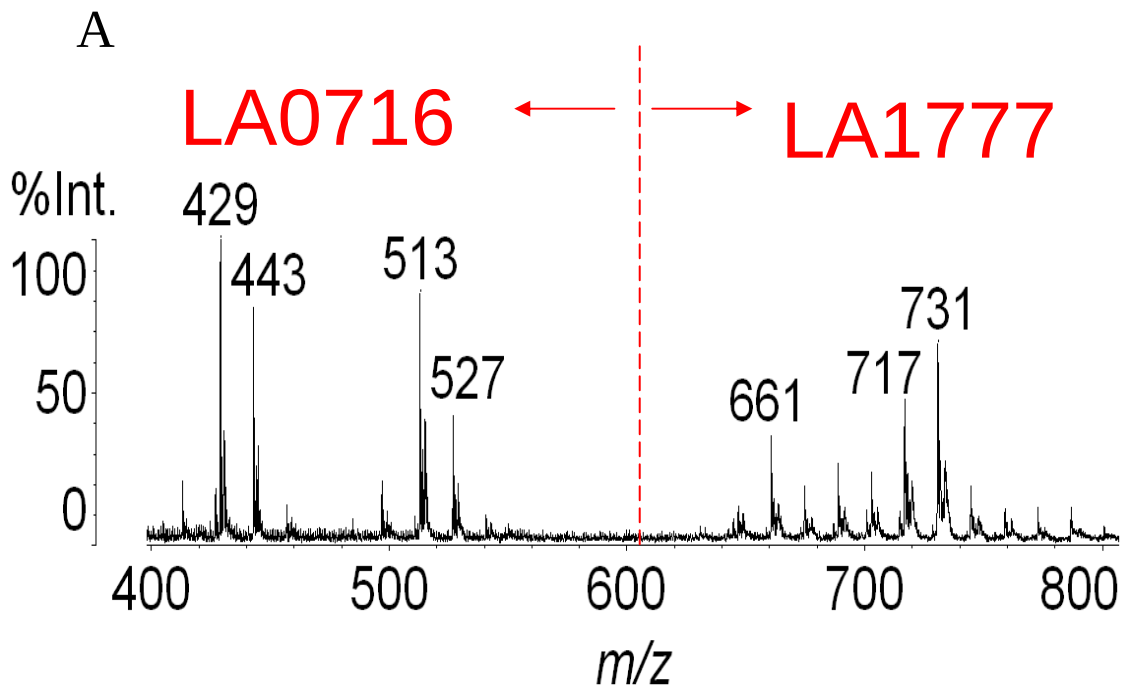

Figure III-10 (A) The LDI spectra of a mixture of *S. habrochaites* LA1777 and *S. pennellii* LA0716 extracts using positive linear mode. Using a laser power=145, spectra from 200 laser shots were averaged while rastering the laser across the spot. (B) Calibration curve showing ion abundance of m/z 731 (S4:21, $[M+K]^+$) relative to the least diluted LA1777 extract as a function of 1/dilution factor of LA1777 extract (n=3, ±SE). A constant amount of LA0716 extract was added to provide a matrix in which the LA1777 metabolites were diluted.

Figure III-10 (cont'd)

B

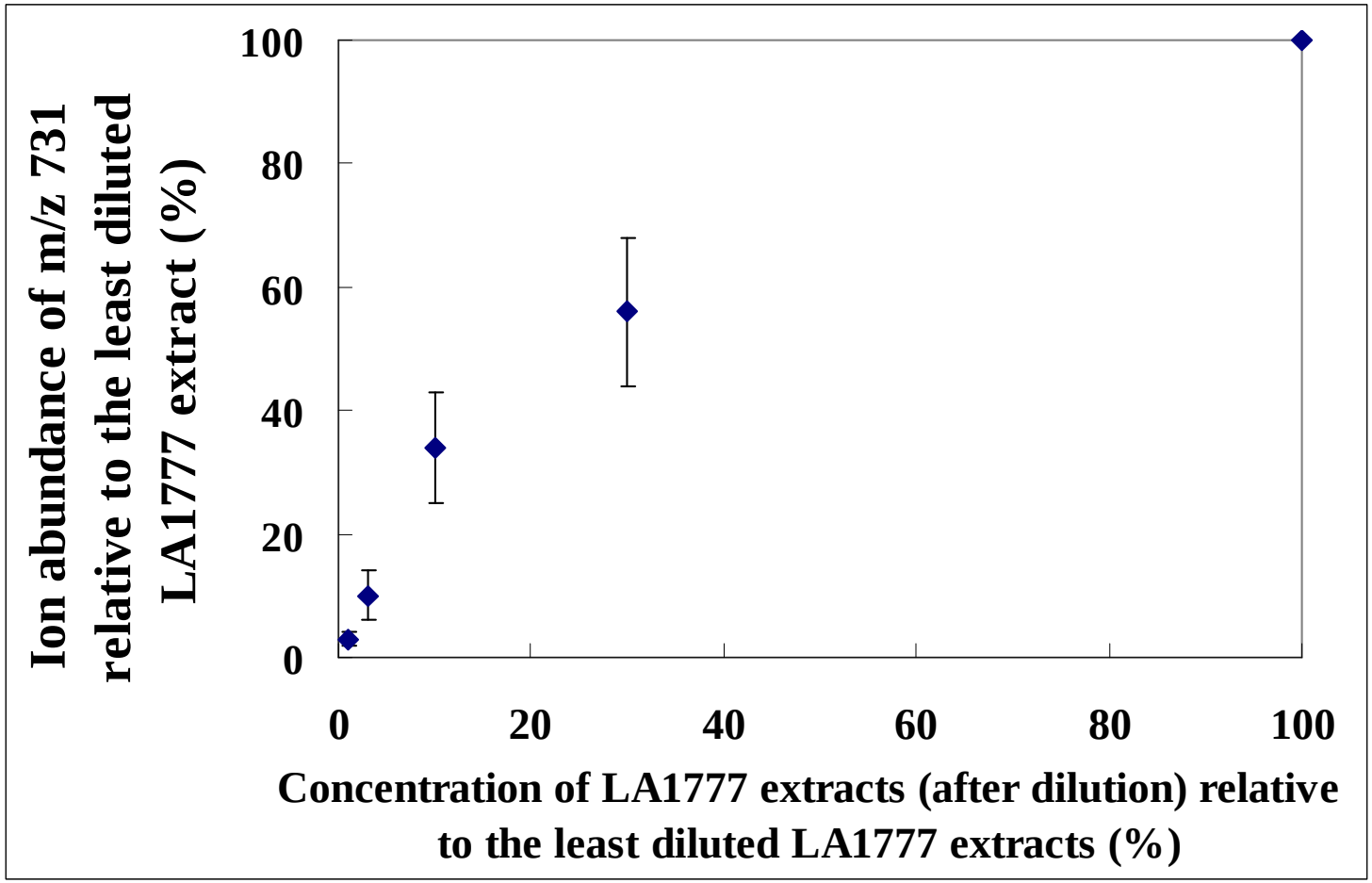

Another validation experiment involved comparing the LDI imaging signal of a metabolite per unit area around midvein to the same signal near the leaf edge. Two leaf samples of similar size from the same *S. habrochaites* LA1777 plant were collected. Glass Pasteur pipettes were used to sample a core in the leaf tissue from the midvein area and leaf edge area, with the removed tissue being contained within the pipette tip. Four spots near the midvein and four spots near the leaf edge were sampled for each leaf. After removing the plant tissues, pipette tips were broken off, and dropped into extraction solvent (acetonitrile:water:2-propanol 3:3:2) to extract metabolites using ultrasonication for each spot separately. One set of extracts was analyzed using LC/MS, and the peak areas were integrated for the extracted ion chromatogram for m/z 233. This signal corresponds to multiple isomers of sesquiterpene acids, which are type VI trichome specific metabolites. Choice of this signal avoids contributions from cells other than trichomes which are removed during the coring process. Corresponding cores from the second leaf were analyzed using LDI, employing the same 2 mm diameter wells described above. The spectra for each spot were averaged for 200 laser shots per well, and the signal for m/z 233 was tabulated. A comparison of the ratio of m/z 233 signal near the midvein relative to the signal near the leaf edge using the two analytical methods is presented in Figure III-11. Both methods confirm the greater abundance of sesquiterpene acids per unit tissue area near the midvein, and this finding supports the observation in the LDI imaging results (Figure III-6C).

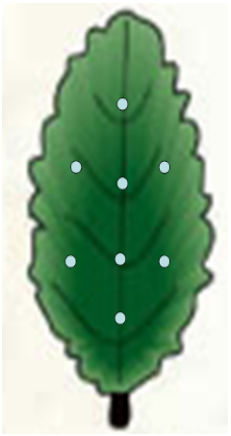

A

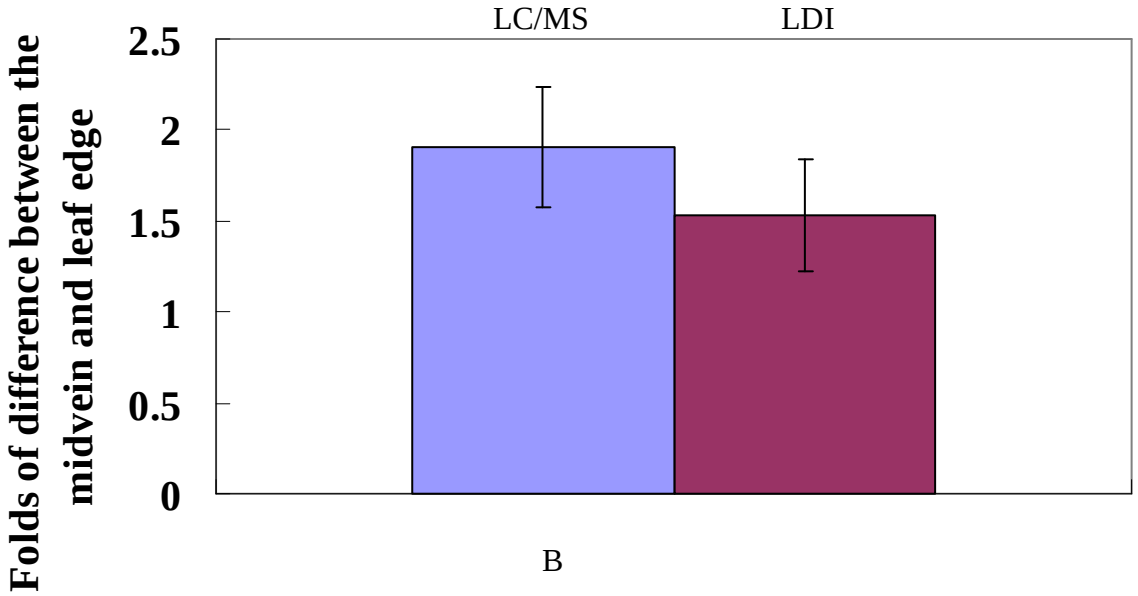

B

Figure III-11 (A) The schematic diagram showing the hole drilling experiment on the leaf surface for validation of LDI metabolite profiling using LC/MS. Four areas were collected around the leaf midvein and four areas were collected on the leaf edge. (B) The ratio of the sesquiterpene acid detected in the midvein (m/z 233) cut to the leaf edge was measured using two different analytical method; LC/MS and LDI. The experiment was conducted on two different leaves.

In some cases, optical imaging of printed trichomes showed liquid in areas outside the boundaries of individual trichomes. One question that needs to be answered is whether metabolites leaked from trichomes during the tissue printing process, or whether laser irradiation of trichomes leads to ejection of metabolites following rupturing of the trichome cell wall. In either case, the integrity of metabolite localization might be compromised. For individual trichome imaging, pre-checking of liquid leaking using a dissecting microscope can help select areas where leakage is minimal. After laser ablation, examination of the residual material on the substrate showed only tiny amounts of residue outside the trichome, but the gland structure appears intact (Figure III-12).

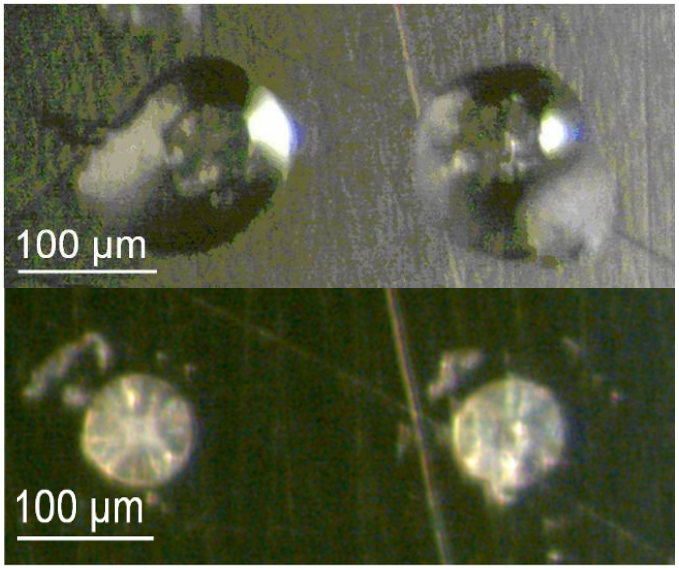

Figure III-12 The reflected light optical image of transferred *S. habrochaites* LA1777 trichomes on glassy carbon surface (A) taken right after the transfer. (B) after laser ablation with 200 laser shots per pixel and laser power =145.

One additional question to be addressed is whether LDI imaging can be performed on thick biological tissues. Typical dissected tissue in imaging experiment has been sectioned to around 10 µm thickness, or approximately the dimension of a eukaryotic cell. There are some previous reports about mass spectrometric imaging where tissue sections have been placed directly onto the substrate [152]. One attempt to extend the application of this experimental scheme involves determining whether a thin barrier between substrate and metabolite would still allow desorption and ionization of the metabolite to occur. To test this, a film of parafilm was stretched across the substrate to about 10 µm thickness which is close to the thickness of a typical tissue section for MALDI imaging. Another layer of parafilm cut with a "Spartan" logo was placed on the top the first parafilm and pressed against it to prevent leakage between the two layers of parafilm. A methanolic solution (100 µM) of the glycoalkaloid tomatine, which lacks a chromophore at the laser wavelength of 337 nm was pipetted into the recessed logo area, and LDI imaging was performed over the entire area. The imaging result is presented in Figure III-13. The results demonstrate that tomatine ions, predominantly the protonated aglycone fragment at m/z 416 can be ejected from the surface of the thin film even when a film provides a barrier to material transmission. No evidence was found to suggest that tomatine had leaked through to the substrate surface because no tomatine signals were detected after firing the laser at the glassy carbon substrate after the parafilm was removed. Control experiments were performed by placing another parafilm and tomatine film on a stainless steel MALDI target plate. No tomatine metabolite signals were detected, even using the highest laser power setting available for this instrument.

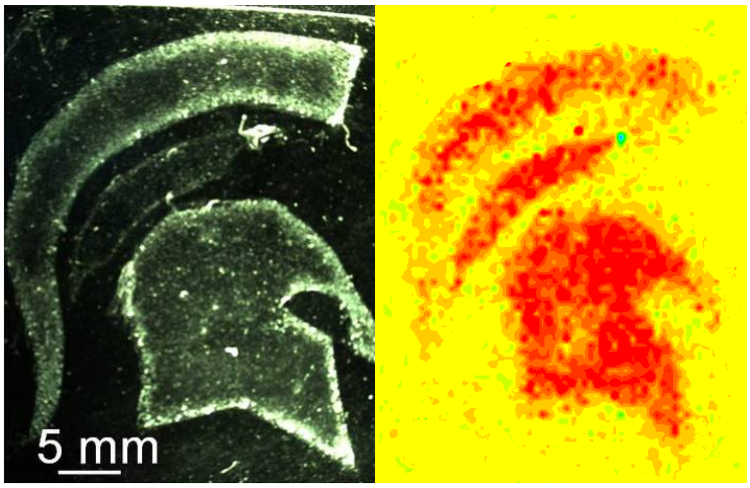

A B

Figure III-13 Imaging of "Spartan" logo constructed by tomatine deposited on the 10 µm of parafilm attached on the top of glassy carbon. (A) Optical image of the Spartan logo cut with a razor blade. (B) intensity map of tomatidine fragment ion (m/z 416) from tomatine. Spectra were acquired using linear positive mode using laser power of 155, and 20 laser shots per pixel.

3.4 Conclusions

The carbon based substrate coupled with contact printing sample preparation successfully addresses the challenges for imaging trichomes using mass spectrometry. For trichome imaging, the traditional imaging scheme that involves mounting tissue on a substrate, and coating with matrix, is not possible owing to the fragile trichomes and their incompatibility with fixation. The contact printing scheme possesses several layers of merit: 1) sophisticated sample preparation steps are not needed, 2) metabolite analysis does not suffer from interference from matrix or other additives, 3) the technique allows selective imaging of trichomes without

interference from other epidermal cell types. The approach provides spatial resolution of individual trichomes across much of the leaf surface for plants in the genus *Solanum*. The simplicity of sample preparation makes such experiments accessible to a broader range of researchers with limited technical expertise in sample preparation.

This printed transfer scheme offers other novel applications. By using the printed transfer method, two slides can be coated, and trichomes from both leaf surfaces can be transferred to separate substrate surfaces in a single step. This enables more complete analysis of a single leaf or other plant tissues. Another potential application is for fingerprint imaging. Fingerprint imaging using mass spectrometry has drawn attention recently in the areas of forensics or security [212]. The inexpensive carbon based substrate can be readily used to collect fingerprint for imaging mass spectrometry purposes. Last but not the least, this carbon based substrate imaging scheme is useful for remote sampling. Since the carbon substrate can be easily frozen, stored and shipped, it can be used to sample fresh sample in remote area and transfer spatially preserved chemical information to the laboratory for analysis. In summary, our work first time extended imaging mass spectrometry to specialized epidermal cells without using dissection or tissue fixation. The printed transfer method coupled with carbon based substrate provides a complementary sample preparation method for imaging mass spectrometry and provides potential novel applications.

CHAPTER FOUR

CHARACTERIZATION OF METHYLATED FLAVONOID REGIOISOMERS USING LC/MS/MS COUPLED WITH SEMISYNTHETIC ENZYMATIC METHYLATION

4.1 Introduction

Plants synthesize a diverse group of specialized metabolites that contribute to their survival and reproduction, with different plant species accumulating distinct sets of compounds [213]. Plants evolve to synthesize new compounds through the effects of mutations on functions of biosynthetic enzymes, and subtle mutations can modify enzyme functions in ways that are challenging to predict from DNA sequences alone. For this reason, there is renewed interest in determining functions of biosynthetic enzymes, and these efforts ultimately require a better understanding of plant chemistry.

One family of specialized metabolites that occurs widely across the plant kingdom is the flavonoids, of which more than 4000 different metabolites within this class are known. The diversity of flavonoid structures provides for a variety of physical, chemical, and biological properties [214] (Figure IV-1). Flavonoid metabolites such as anthocyanins are responsible for coloration in flowers, fruits, and other tissues, and have been proposed to confer protection from the damaging effects of ultraviolet radiation. In addition, flavonoids also play roles as regulators of transport of the plant hormone auxin [215], serve as signaling molecules in plant-symbiont interactions [216], control pollen tube growth and functionality which are

important in plant reproduction [217], and are precursors of antibiotic phytoalexins that strengthen plant defenses against pathogens [218, 219].

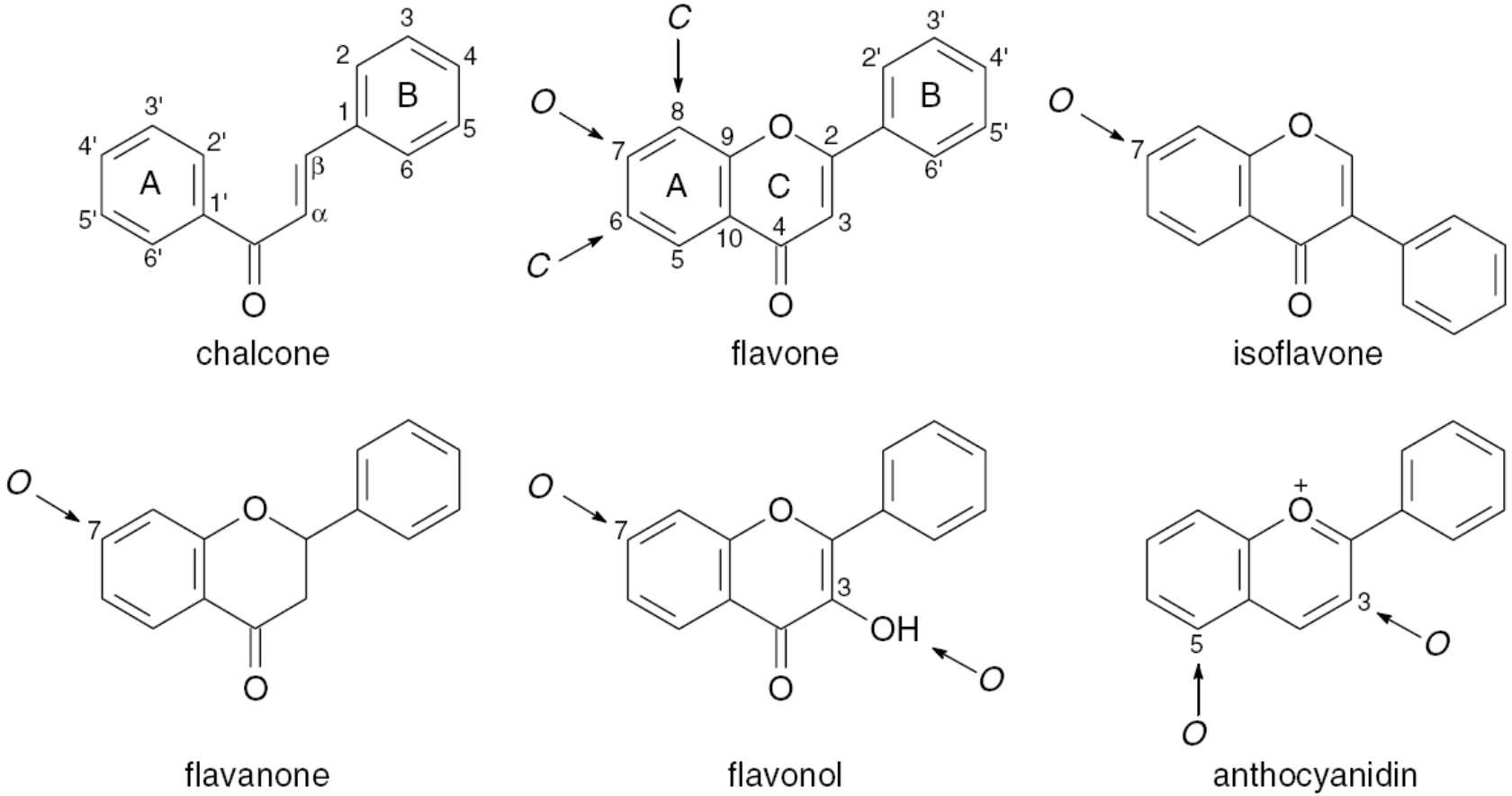

Figure IV-1 Basic structures of the main classes of flavonoids. Common O- and C-substitution positions are indicated with an arrow. Adapted from Reference [220].

Flavonoids have several hydroxyl groups that can be modified by reactions including methylation, acetylation, glycosylation, and sulfonation. Modification of the basic flavonoid structure serves an important role in determining where the different modified forms are found within the cell. For example, glycosylated flavonoids are water soluble and mostly present in the cytosol. *O*-methylation of flavonoids confers greater lipophilicity [221] and often precludes glycosylation. As a consequence of their physical properties, methylated forms of flavonoids are often secreted on leaf surfaces where they protect plant tissues from UV-B damage [222]. In addition, *O*-methylation enhances the antimicrobial activity of the flavonoid by increasing the lipophilicity and decreasing the reactivity of the phenolic hydroxyl groups toward oxidation, as flavonoid oxidation can generate intermediates that trigger reactions involved in mutagenicity [214].

Plants convert flavonoids to their methyl ethers through catalysis by O-methyltransferase enzymes, which use *S*-adenosylmethionine (SAM) as the methyl donor. Most plant genomes contain numerous methyltranferase genes, and they exhibit diverse substrate specificity. Their functions include modification of phenolic acids in the synthesis of lignin precursors, methylation of DNA and RNA, and methylation of numerous metabolites including the plant hormones salicylic acid and jasmonic acid. Although the methyl transfer reaction mechanism is the same for all phenolic hydroxyl groups, *O*-methyltransferase enzymes (OMTs) demonstrate significant substrate and stereochemical selectivity [223]. The study of OMT specificity and selectivity can help researchers better understand the functionality of methylation in plants. Besides that, regioselective OMTs have potential use for production of regiospecific methylated

compounds that are unavailable in nature, including precursors of novel drugs when chemical synthesis is not feasible [224-226].

The study of O-methyltransferase specificity requires first elucidating their products' structures. Although there are many reviews about flavonoid structure analysis [220, 227-232], techniques that can identify the position of methylation on flavonoids have been slow to develop. So far, most methylated flavonoid analysis relies on isolation of milligram quantities followed by NMR characterization [233-236]. *In planta*, methylated flavonoids usually exist at low levels and as mixtures of isomers, often making isolation from plant tissue impractical. A few reports have described use of chromatographic and spectroscopic techniques to characterize methyl flavonoids [237-240]. However, spectroscopic methods other than NMR are largely useful for pinpointing methylation at a specific position, e.g., using UV to pinpoint whether 5 position is methylated or not [241], but are inadequate when multiple methylations have occurred. To reliably distinguish and identify isomeric methylated flavonoids, comparisons to authentic standards are preferred, but the lack of authentic standards for most methylated flavonoids prevents detailed structure confirmation necessary to prove regioselectivity of methylation by OMTs. This has resulted in a significant gap in our knowledge about OMT functions and the biological importance of individual methylated flavonoids.

Mass spectrometry offers a sensitive and information-rich method for structure elucidation that is especially useful when only small amounts or impure substances are available. Mass spectra generated using electron ionization (EI) has been used to characterize methylated flavonoids [242-245], but still requires authentic standards or libraries derived from such

standards for comparison. Recently, several groups have investigated the fragmentation behavior of a few methylated flavonoid standards using soft ionization and tandem mass spectrometry [246-251]. Although some differences between the collision induced dissociation (CID) spectra have been observed for different isomers, the range of compounds has been somewhat limited, and the differences between isomers have been subtle. At the commencement of the research described below, comparisons to authentic standards were still needed for definitive identification of multiply-methylated flavonoids.

Several research teams have concluded that it is nearly impossible to identify positions of methylation on flavonoids from mass spectrometry alone [220, 227-232]. The basis for this conclusion is that in CID spectra of methylated flavonoids, loss of the O-methyl group, often as the neutral CH_3 radical, takes place with a lower threshold collision energy than other fragmentation pathways. Subsequent fragmentation of carbon-carbon bonds generate fragments specific to certain portions of the flavonoid ring system, but since such fragments may have already lost methyl groups, the resulting fragment ions whose masses are consistent with no methyl substituent do not provide reliable evidence that the methyl group is absent.

In many cases, definitive structure elucidation requires synthesis of the proposed compound because spectroscopic methods, including MS and NMR, often yield ambiguous results when authentic standards are not available. For many methylated flavonoids, the presence of numerous hydroxyl groups with similar reactivities makes such synthesis challenging, as selective introduction of methyl groups on a specific position requires position-selective chemical modification [252-261]. As an alternative, synthesis of methylated flavonoid

standards can be achieved by reaction of a flavonoid substrate with an O-methyltransferase enzyme of known function and regioselectivity. Unfortunately, the gaps in our understanding of OMT function and selectivity are large, but provide the rationale for much of the efforts at understanding biosynthetic enzyme functions that are at the heart of this dissertation.

As part of a collaborative effort with the laboratory of Professor Eran Pichersky at the University of Michigan, we recently identified two O-methyltransferases from the wild tomato relative *S. habrochaites* LA1777 [262]. Assignment of these enzymes as OMTs was initially based on DNA sequence similarity to other OMTs, but proof of function requires biochemical evaluation of OMT substrate selectivity and product identification. The characterization of the functions of these two enzymes was guided by the chemical characterization of their enzyme products *in vivo*, through LC/MS profiling of metabolites described in Chapter II, and *in vitro* using recombinant OMTs expressed in *E. coli.* These efforts were steered by the observation that metabolites from the trichomes of this plant had molecular masses consistent with polymethylated myricetin.

4.2 Experimental Methods

4.2.1 Material

4.2.1.1 Plant material

Seed stock of *S. habrochaites* LA1777 was obtained from the C.M. Rick Tomato Genetic Resource Center (TGRC, University of California Davis, USA). Seeds were germinated at room temperature on filter paper, and transferred to soil approximately 5 days after germination. Plants were maintained under controlled light conditions of 16 hours light and 8 hours dark. The temperature gradient was maintained between 24 °C and 18 °C (light:dark, respectively).

4.2.1.2 Chemicals

S-Adenosyl-*L*-methionine was purchased from Sigma-Aldrich (St. Louis, MO, USA) and d_3-labeled SAM was purchased from C/D/N isotopes (Quebec, Canada). Flavonoid and methylated flavonoid substrates included myricetin, laricitrin (3'-methylmyricetin), syringetin (3',5'-dimethylmyricetin), and 3',4',5'-trimethylmyricetin. Myricetin was purchased from Sigma-Aldrich and the remaining substrates were purchased from Extrasynthese (Benay, France). Methanol, 88% formic acid, and acetonitrile were purchased from VWR Scientific.

4.2.2 Enzyme cloning and expression

Recombinant ShMOMT1 and ShMOMT2 enzymes were cloned from cDNA made from *S. habrochaites* leaf RNA, expressed in *E.coli* BL21 Star (DE3) pLysS cells (Invitrogen), purified by anion exchange chromatography, and assayed by Adam Schmidt of the Pichersky laboratory at the University of Michigan. SDS-PAGE was used to establish the degree of purity of the active fractions.

4.2.3 O-methyltransferase assay

4.2.3.1 General methodology

Enzyme assays were performed by Adam Schmidt, using a Continuous Extraction Assay Method (CEAM) designed to optimize product accumulation for mass spectrometric analysis. Assays were performed in 1.5 mL glass vials (Supelco Analytical, 27080-U) in a final volume of 500 µL (aq). A layer of 500 µL 100% ethyl acetate was carefully applied over the aqueous assay volume to serve as a non-polar extraction phase. Briefly, the system provides an aqueous phase (where enzyme reaction takes place) and non-aqueous ethyl acetate phase, with an interface that promotes preferential partitioning of methylated products to the upper organic phase. As products are removed from the reaction mixture by diffusion into the non-polar phase, positive equilibrium is maintained and substrate turnover is enhanced. At the end of

each incubation, the upper organic phase was collected, evaporated to dryness using a SpeedVac, and redissolved in 50 µL of methanol:water 1:1 (v/v).

4.2.3.2 Individual enzyme assays

Assays for each enzyme contained approximately 23 µg (ShMOMT1) or 32 µg (ShMOMT2) of purified protein, 500 µM substrate (methyl group acceptor), 500 µM SAM or d_3-SAM (methyl group donor), and all were buffered with 50 mM Tris (pH 7.5).

4.2.3.3 Coupled enzyme assays

ShMOMT1 and ShMOMT2 were combined, 1:1 (v/v), in a final volume of 500 µL (aq). Each assay contained 500 µM substrate (methyl group acceptor), 500 µM SAM or d_3-SAM, and all were buffered with 50 mM Tris (pH 7.5).

4.2.4 LC/MS

Samples were analyzed on a QTRAP™ 3200 mass spectrometer from Applied Biosystems/MDS Sciex (Concord, Ontario, Canada) coupled to a Shimadzu LC-20AD binary pump and SIL-HTC autosampler. Separation was achieved by using Thermo BetaBasic C18 column (150 mm × 1.0 mm, 5 µm) at temperature of 30 °C. The mobile phase was A: 0.5%

formic acid and B: 0.5% formic acid in 60% methanol+ 40% acetonitrile. 0.5% formic acid was added to decrease the peak tailing [263, 264]. The mixture of methanol and acetonitrile is reported to provide superior chromatographic selectivity in separations of flavonoids [265]. A 15 min reverse phase gradient at flow rate of 0.100ml/min was used for separation. The liner gradient elution program was as follows: 10% B for 0.3 min, then an immediate step up to 40% B followed by a linear increase to 100% B from 0.31 to 8.5 min, followed by a hold at 100% B for 2.5 min. At 11 min, the solvent returned to 10% B, and the column was equilibrated for 4 min before the next injection. The mass spectrometer was operated in the positive ion mode with a TurboIonSpray source. Enhanced product ion scanning (EPI) with dynamic fill time was used to generate product ion MS/MS spectra using 40 V collision potential (parameter CE). Scan rate was set to 4000amu/sec. The other ionization parameters were as follows: curtain gas (CUR), 10; ion source gas 1 (GS1), 12; ion source gas 2 (GS2), 30; source temperature (TEM), 400 °C; entrance potential (EP), 10 V; CAD gas, HIGH; capillary potential 5500 V. The mass spectrometer and the HPLC system were controlled by Analyst 1.4.2 software from Applied Biosystems/MDS Sciex.

4.3 Results and Discussion

Kaempferol, quercetin, and myricetin derivatives are metabolites reported in tomato tissues [266]. However, reports of methylated forms of flavonoids in tissues of any tomato or its relatives are scarce [267], and are nonexistent for trichome profiling. Transcripts of two genes

were found expressed in the glandular trichomes of *Solanum habrochaites* LA1777, and were designated as methyltransferases ShMOMT1 and ShMOMT2 based on sequence homology to other methyltransferase genes. Six metabolites detected in extracts of isolated *S. habrochaites* LA1777 trichomes were initially assigned as putative methylated myricetin aglycones based upon their masses and retention times. In the cases of dimethyl- and trimethyl-derivatives, two putative isomers of each were observed. To annotate these methylated myricetin metabolites, commercial standards of methylated flavonol aglycones were incubated with recombinant methyltransferases to generate products of more extensive methylation. All these products are subjected to LC/MS/MS analysis.

Only three methylated myricetin derivatives were available from commercial suppliers: 3'-methylmyricetin, 3',5'-dimethylmyricetin, 3',4',5'-trimethylmyricetin. In light of the limited availability of standard reference compounds and the low levels of methylated myricetin metabolites in trichome extracts, alternative strategies needed to be developed to annotate methylated flavonoid metabolites. It was decided to exploit the expected selectivity of recombinant O-methyltransferase enzymes with tandem mass spectra to assign structures to methylated metabolites. Recombinant ShMOMT1 and ShMOMT2 enzyme were exploited to produce methylated products of myricetin and its methylated analogs. Products of these enzymatic reactions could then be compared to trichome metabolites to determine whether they would match retention times and product ion spectra. The first experiment involved incubation of myricetin substrate with each individual enzyme (ShMOMT1 or ShMOMT2) and separately with a mixture of both enzymes. Annotation of enzyme reaction products was accomplished

using a process of elimination, which starts from exhaustively considering all product structures consistent with observed pseudomolecular masses, and then various criteria were applied to eliminate candidate structures that were not consistent with retention time and mass spectrometric data.

The benefit of using enzyme-catalyzed reactions for metabolite semisynthesis arises from the regioselectivity of most enzymes. In many cases, addition of a single methyl group is the major reaction product, and this fact allows more straightforward assignment of methyl group position. The methylated positions in the precursors are preserved in the enzyme products, which reduces the number of the possible isomers that need to be considered. For example, a completely unknown trimethylmyricetin would have 20 possibilities based on random combinations of three methyl groups over six potential positions of methylation on myricetin hydroxyl groups. However, if a trimethyl myricetin compound is synthesized by reaction of a known dimethylmyricetin with a methyltransferase, only 4 isomers are possible. The success of this approach then depends on observations of isomer-specific MS/MS spectra that can discriminate among the four isomers, but might not distinguish all 20 isomers products by random methylation.

Another benefit of using enzymes for metabolite semisynthesis is that selective incorporation of CD_3 groups at selected positions can be achieved by using trideuterated co-substrate S-adenosylmethionine-d_3. The end products consist of specific substitutions of methyl and d_3-methyl groups at different positions. Such compounds are not available from natural sources and are also not readily synthesize, again, owing to the presence of multiple sites

for nonselective alkylation. These partially labeled methylated myricetins are valuable for distinguishing fragmentation behavior of specific methyl group using tandem mass spectrometry, and results from these investigations are described below.

Elimination of candidate metabolite structures is a progressive, and often iterative process. Any structures already identified from previous steps can be used as references to eliminate unsuitable candidates in the next step. Comparisons of retention times and MS/MS spectra of products from different enzymatic reactions were also used to facilitate candidate elimination or sometimes make conclusive annotation. Fragment ions observed in the MS/MS product ion spectra are annotated following previous proposed nomenclature [268] (Figure IV-2).

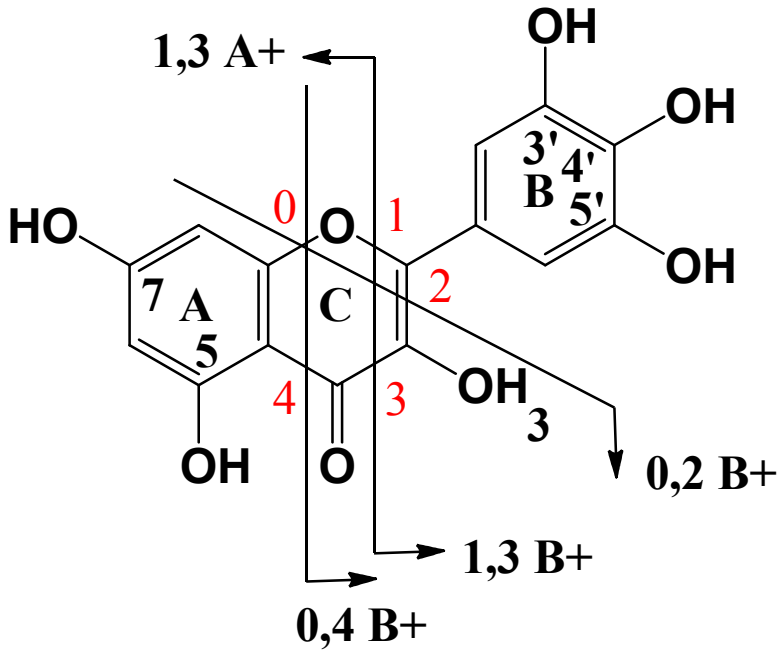

Figure IV-2 Structure of the flavonol aglycone myricetin. The ring was labeled as large letters in black. Positions of substitution by hydroxy or methoxy groups are numbered in black inside the myricetin structure. The bonds on the B ring that undergo cleavage during collision induced dissociation are numbered in red. Characteristic multiband fragmentations are labeled in black near the arrow heads, as proposed in Reference [220].

4.3.1 Retention time rules

Liquid chromatographic retention times are features that aid elimination of unsuitable candidate structures of metabolites, when compared with other isomers and authentic standards. Methylation converts phenolic groups from weak acids to neutral ethers, and increases the hydrophobicity of the molecule.

Methylation on different hydroxy groups exerts different degrees of increase of the molecule's hydrophobicity, largely because many phenolic groups on myricetin and other

flavonols can participate in intramolecular hydrogen bonding. Hydroxyl groups on the 3- and 5- positions can form hydrogen bonds with the C ring carbonyl group. Upon methylation at positions 3 or 5, the intramolecular hydrogen bond is removed, and this frees the electrons on the carbonyl oxygen to interact more with mobile phase and decreasing retention time. Methylation of hydroxyls involved in intramolecular hydrogen bonding may be expected to increase retention on reversed phase HPLC column by a lesser degree than methylation of other hydroxyl groups. It was observed in kaempferol and quercetin [238] that adding one extra methyl on 5 position almost has negligible effect on chromatographic retention times. Compared to methylation at the 5 position methylation, 3 position methylation increases retention time more than methylation at the 5 position [238-240]. Positions 3', 4' and 5' form even weaker intramolecular hydrogen bond with one another. Therefore, 3'; 4' or 5' methylation increases retention time more than 3 or 5 methylation. The 7 position phenolic group cannot form intramolecular hydrogen bonds based on molecular geometry. Therefore, methylation at position 7 increases the retention time more than for the other myricetin isomers. Also, it was reported before that 7 position has the highest gas phase acidity among the six hydroxyl groups [269], but this information is more relevant to mass spectrometric behavior than HPLC retention times.

Based on previous reports using reverse phase chromatography, the effect of individual methyl groups on retention of myricetin analogs are 7>3'(5') ≈4'>3>5 [238-240]. The principle of linear free energy relationships suggests that adding methyl groups will have consistent effects on the free energy of partitioning between mobile and stationary phases. However, this rule

assumes that all hydroxyl groups are equivalent. Instead, methylation of hydroxyl groups that have differential contributions to solute-solvent interactions are expected to have different retention time shifts upon methylation, and these shifts should be similar as long as the chemical properties of the group being modified are similar. Following this retention time rule (we name it rule #1 in our study), the retention times of isomers can be compared with any chemically similar standards, and this information can be combined with knowledge of chromatographic retention of already identified enzyme products to suggest methylation positions. However, retention time is only conservatively used as a tool to assist the elimination process but final assignments were mostly based on interpretation of MS/MS spectra. Comprehensive investigation of MS/MS product ion spectra provides additional information for metabolite annotation.

4.3.2 Characterization of enzymatic semisynthesis products

4.3.2.1 Myricetin as substrate

The LC/MS analysis of the products derived from incubating myricetin with ShMOMT1 showed one peak (RT: 8.15 min) in the extracted ion chromatogram (XIC) for monomethylated myricetin (m/z 333; Figure IV-3B). This compound elutes slightly later than the 3'-methylmyricetin standard (RT: 8.03 min; Figure IV-4A). The product ion spectrum (Figure IV-3E) is distinct from that of the 3'-methylmyricetin standard (Figure IV-4B) in that the

$[M+H]^+$, m/z 289, 259, 167, and 165 abundances are substantially lower than for 3'-methylmyricetin standard. Therefore, this monomethylmyricetin was assigned to not be 3'-methylmyricetin. Since 3- or 5- mono-O-methylmyricetins are expected to elute earlier than 3'-methylmyricetin, the remaining candidates could be 4'- or 7-monomethylmyricetins. Final annotation was made using further enzymatic processing of this metabolite as described below.

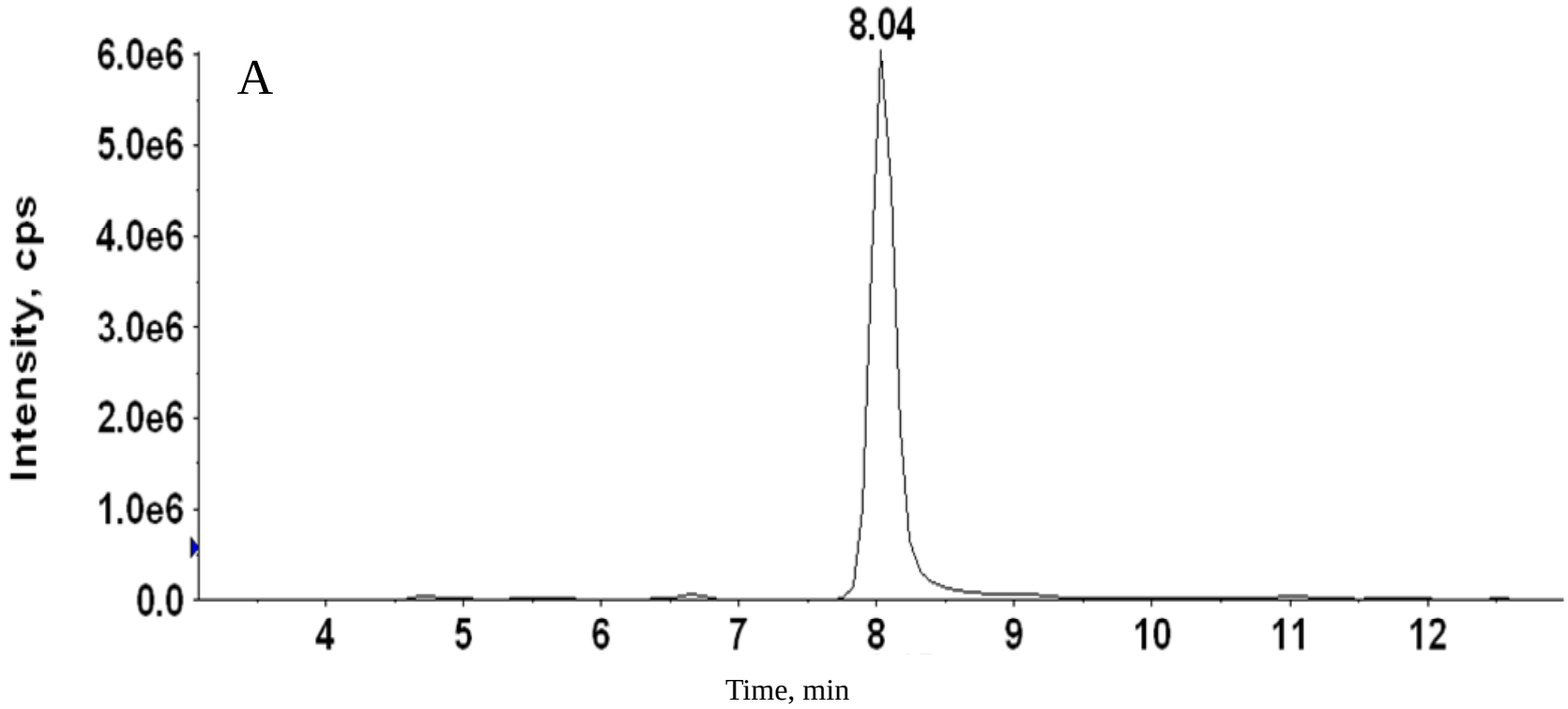

Figure IV-3 A) Extracted ion chromatogram (XIC) of m/z 333 for monomethyl product from incubation of ShMOMT2 with myricetin B) Extracted ion chromatogram (XIC) of m/z 333 for monomethyl product from incubation of ShMOMT1 with myricetin C) Extracted ion chromatogram (XIC) of m/z 333 for monomethyl product from incubation of both ShMOMT1 and ShMOMT2 with myricetin D） Enhanced product ion scan (EPI) spectra of monomethyl product from incubation of ShMOMT2 with myricetin, later annotated as 3’-methylmyricetin E）Enhanced product ion scan (EPI) spectra of monomethyl product from incubation of ShMOMT1 with myricetin, later annotated as 4’-,methylmyricetin. Data was acquired using Qtrap 3200 instrument using electrospray positive mode. EPI spectra were acquired under 40V collision energy.

Figure IV-3 (cont'd)

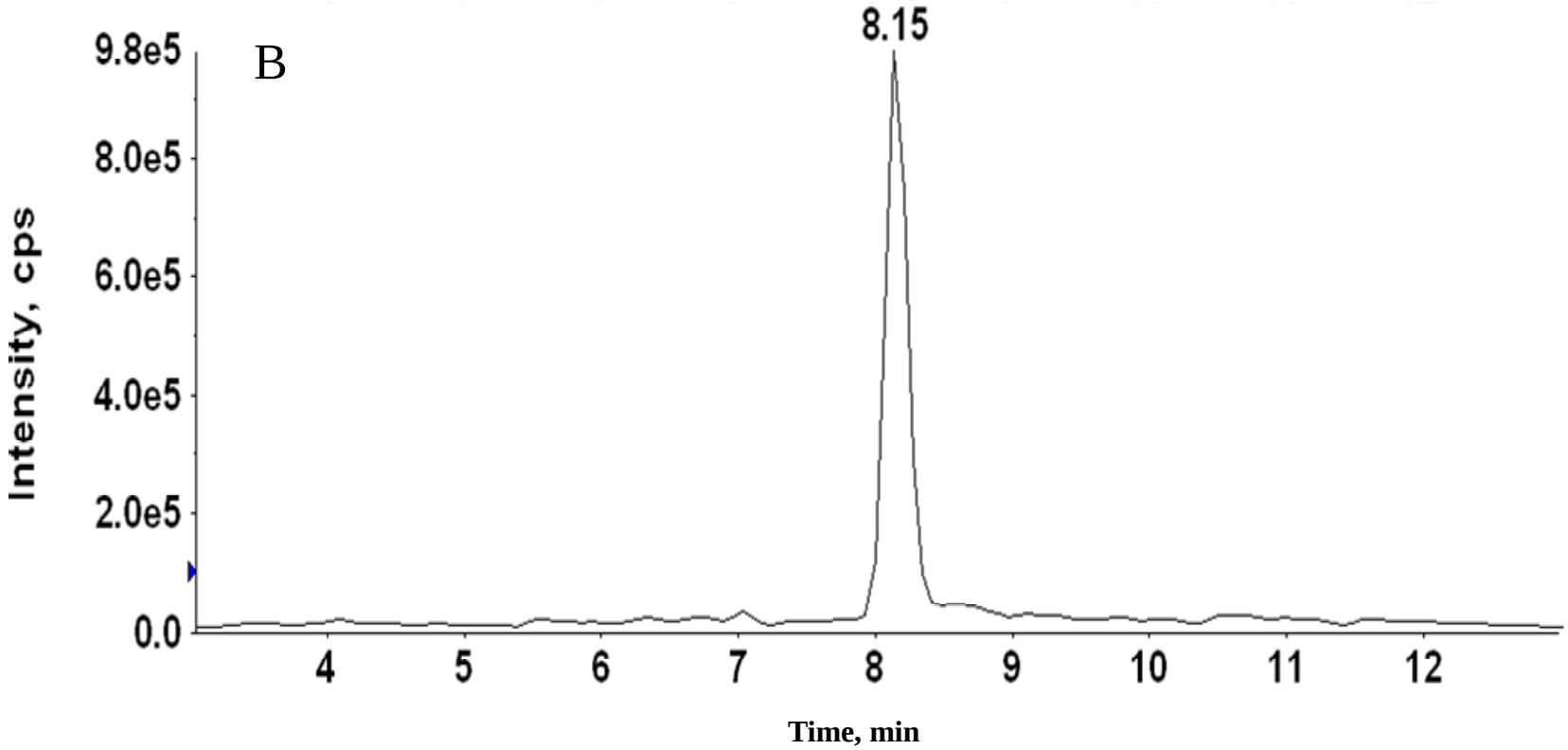

Figure IV-3 (cont'd)

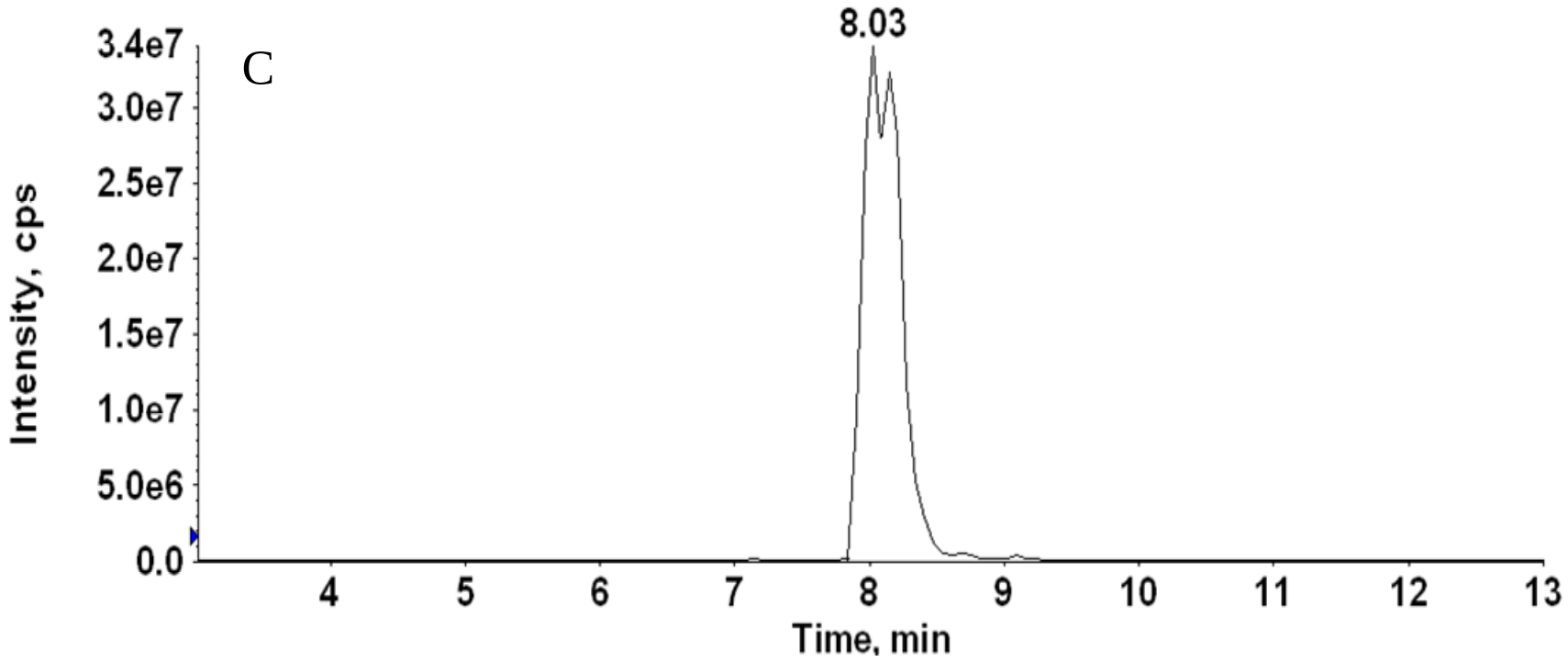

Figure IV-3 (cont'd)

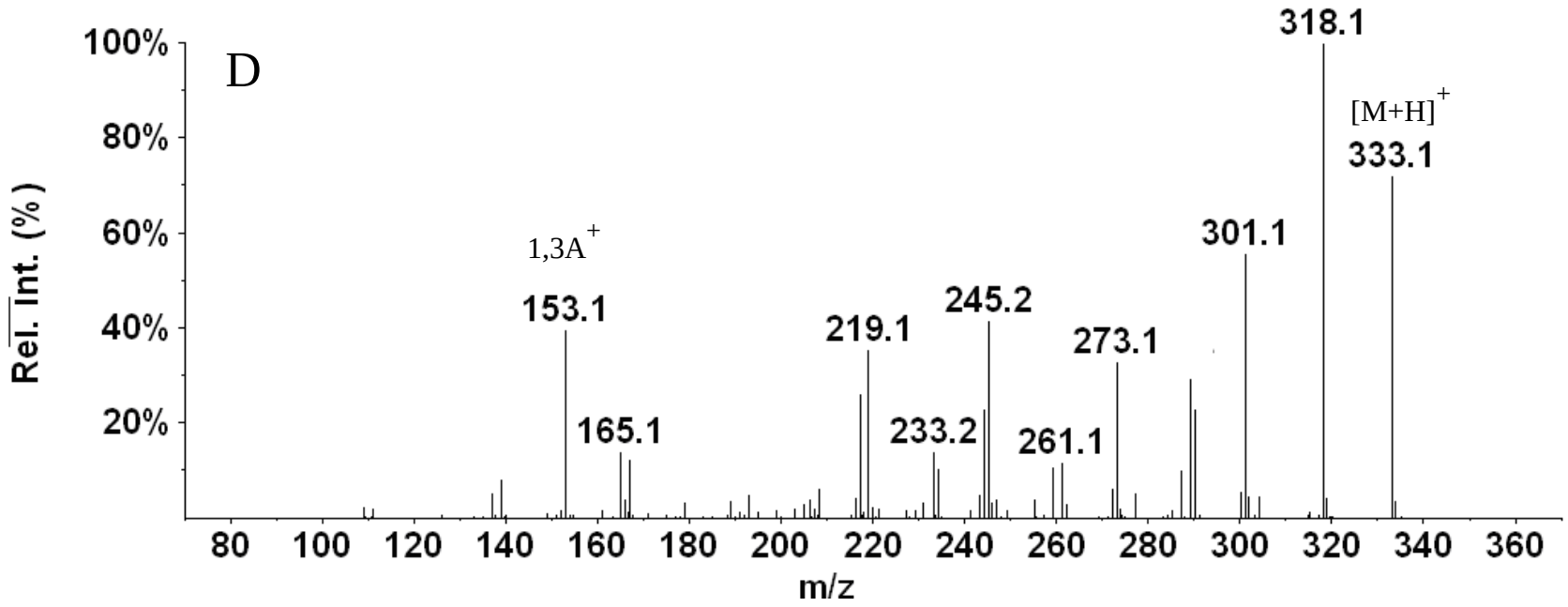

Figure IV-3 (cont'd)

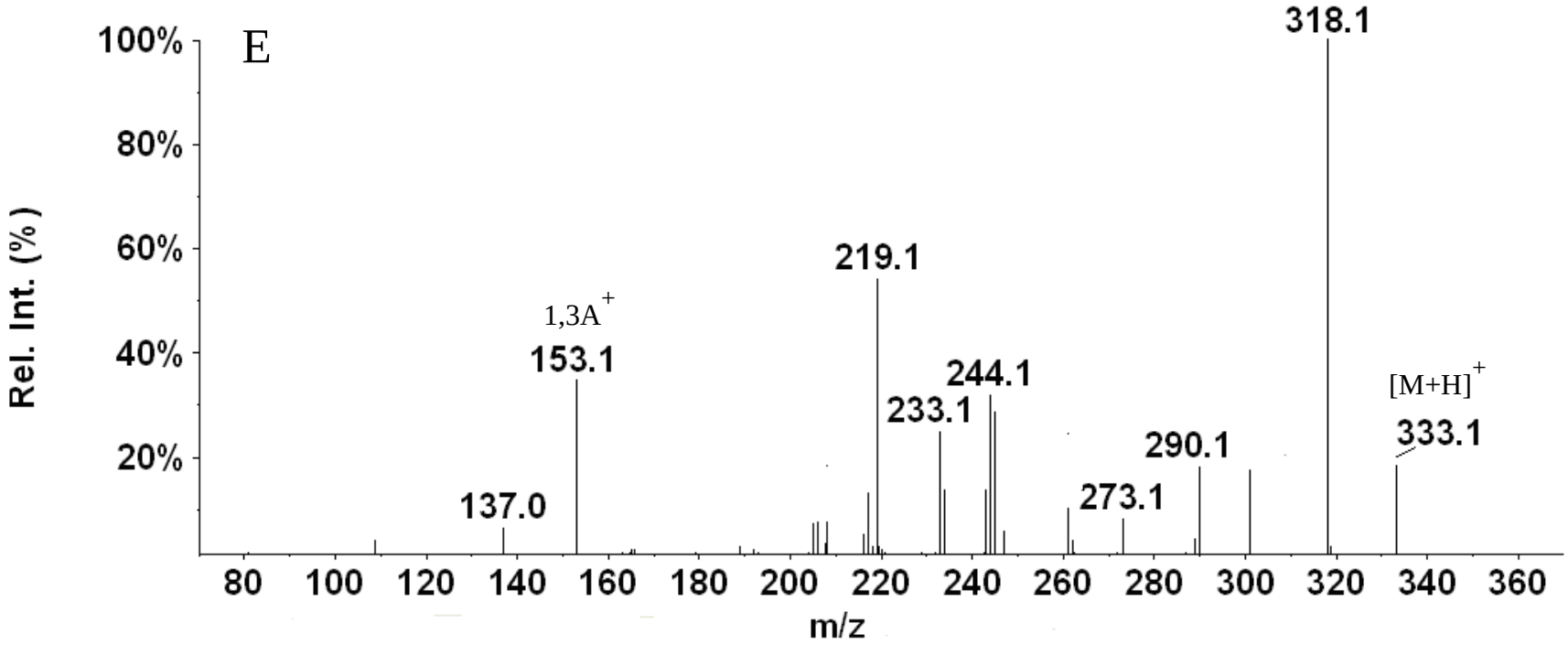

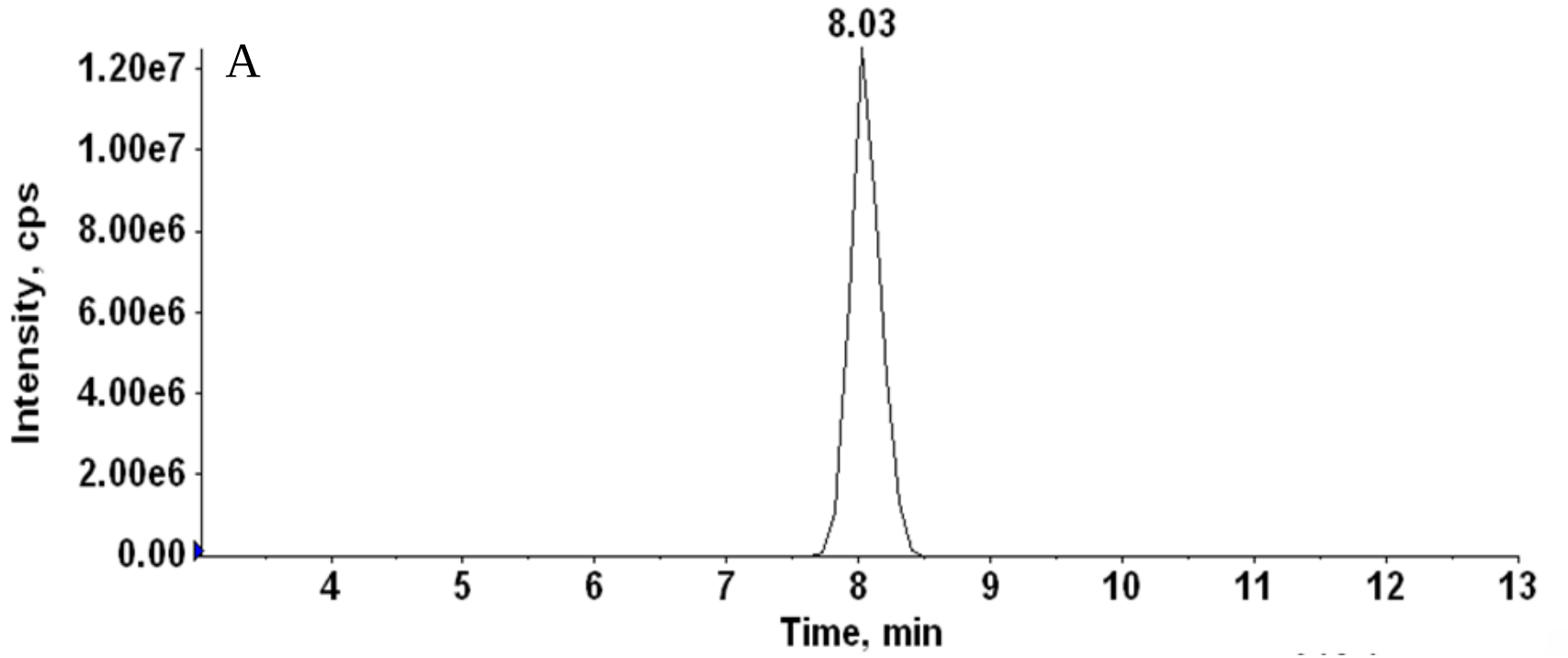

Figure IV-4 A) Extracted ion chromatogram (XIC) of m/z 333 for commercial standard 3'-methylmyricetin B) Enhanced product ion scan (EPI) spectrum for $[M+H]^+$ (m/z 333) of commercial standard 3'-methylmyricetin using 40 V collision potential. Data were acquired using a Qtrap 3200 mass spectrometer using electrospray ionization in positive mode.

Figure IV-4 (cont'd)

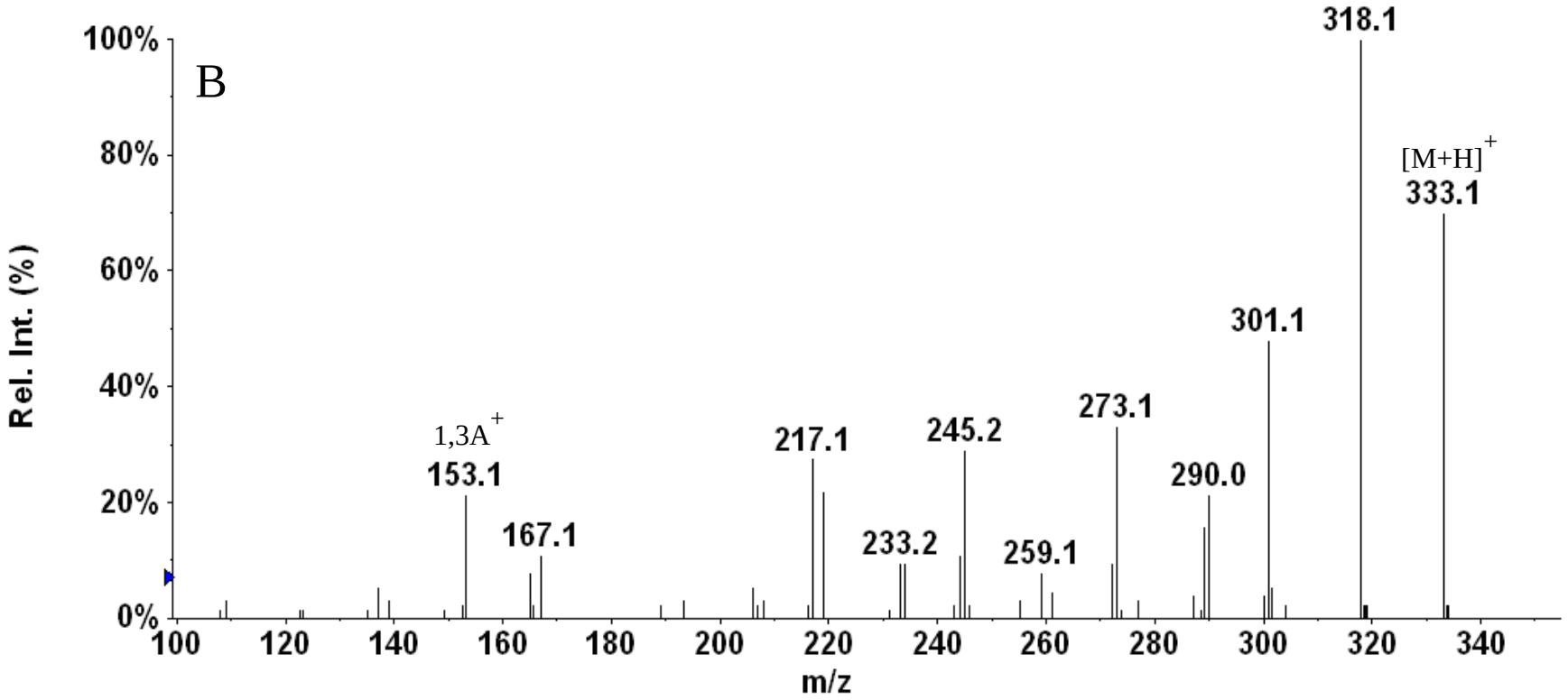

This monomethylmyricetin enzyme product can be methylated further by reaction catalyzed by ShMOMT1, and incubations gave one dimethylmyricetin product (RT 9.3 min) detected as m/z 347 (353 in the incubation using d_3-SAM as the cofactor; both as $[M+H]^+$). Enhanced product ion MS/MS spectra of m/z 347 yielded fragment ion m/z 167 using unlabeled SAM as substrate (Figure IV-5A), whereas incubations that employed d_3-SAM as substrate yielded a product heavier by 6 Da, consistent with two CD_3 groups. The EPI MS/MS spectrum of m/z 353 yields a fragment at m/z 170 which is 3 Da heavier than m/z 167 observed using unlabeled SAM, indicating that m/z 167 fragment ion has one methyl group (Figure IV-5). Among the higher mass product ions, we only observe one CH_3 loss (loss of 15 Da) from the protonated molecule. This finding suggests that one methyl group is far more labile than the other. The fragment at m/z 167 was reported to arise from a characteristic retro-Diels–Alder reaction (RDA) that is annotated as a $1,3A^+$ cleavage for flavonoids having A-ring methyl substitution [270](Figure IV-6). The m/z 167 fragment ion peak is the characteristic ion indicative of A ring methylation. (we name it as rule #2)

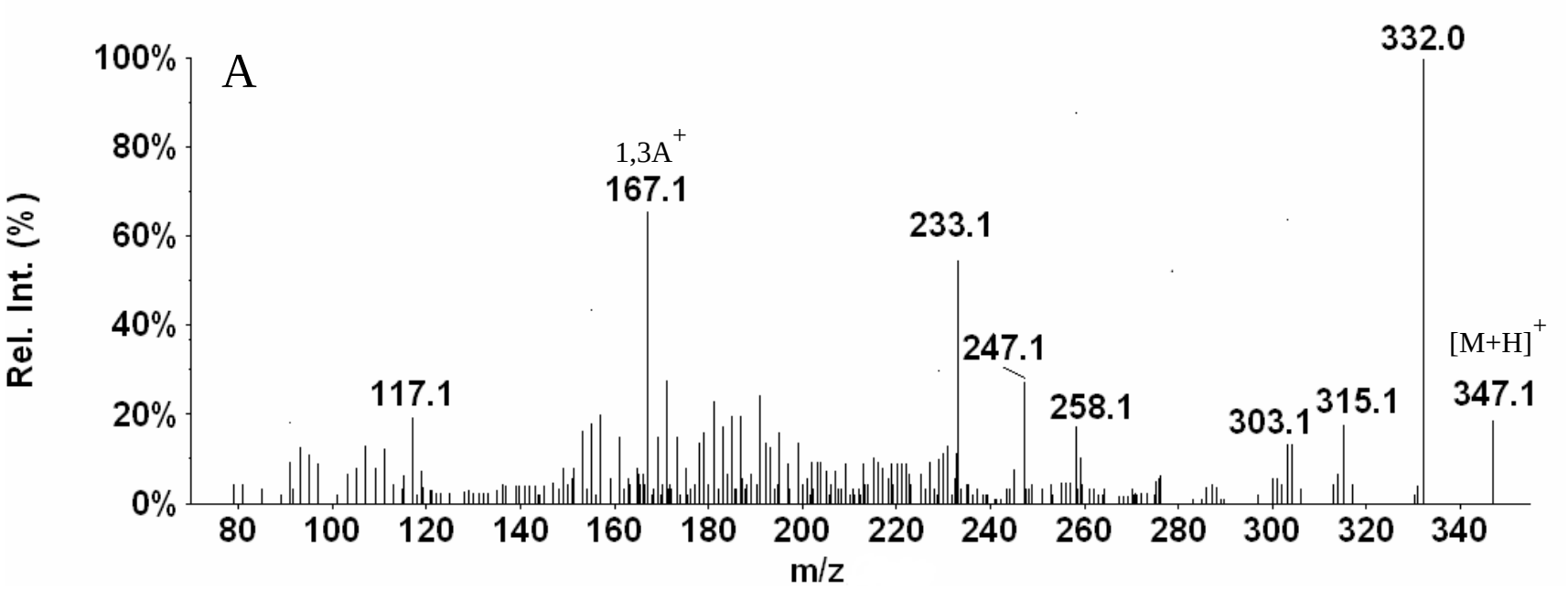

Figure IV-5 Enhanced product ion scan (EPI) spectra of protonated dimethylated product from A) incubation of myricetin with ShMOMT1 and SAM; later annotated as 4',7-dimethylmyricetin and B) incubation of myricetin with ShMOMT1 and d_3-SAM, later annotated as 4'(CD_3),7(CD_3)-dimethylmyricetin. Data were acquired using a Qtrap 3200 mass spectrometer using electrospray positive mode and 40 V collision potential.

Figure IV-5 (cont'd)

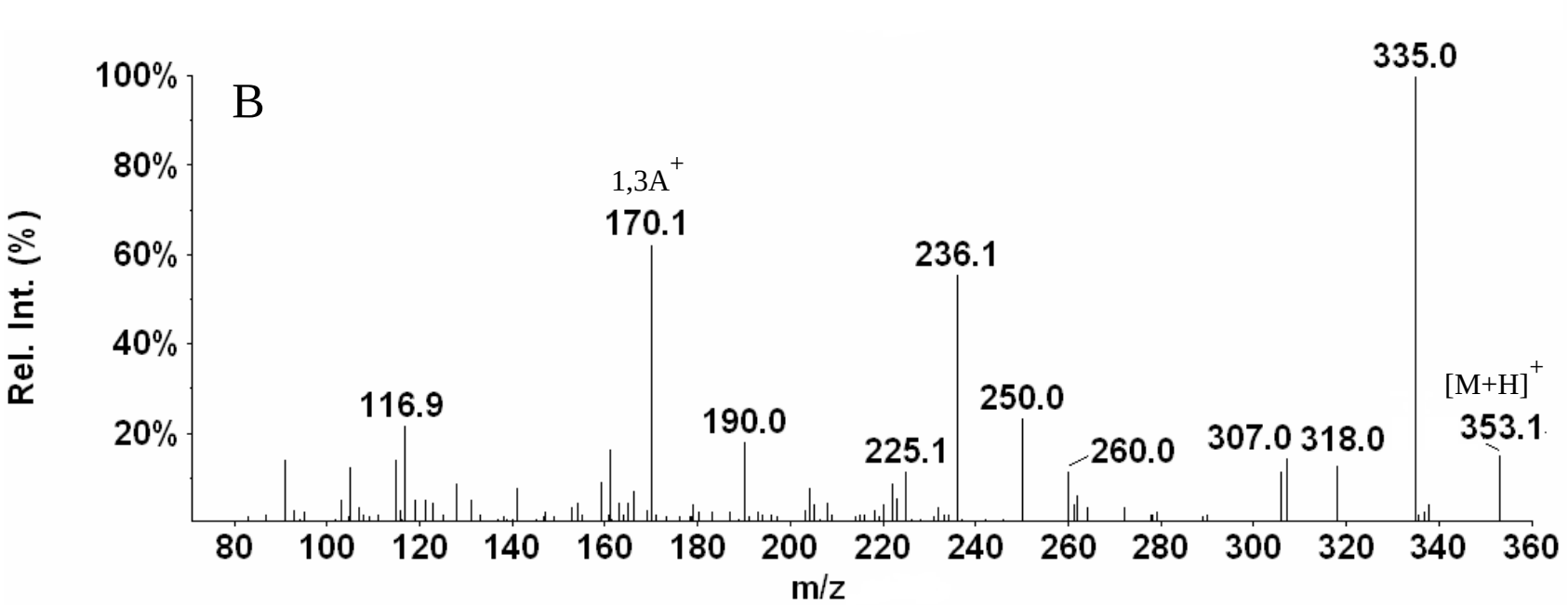

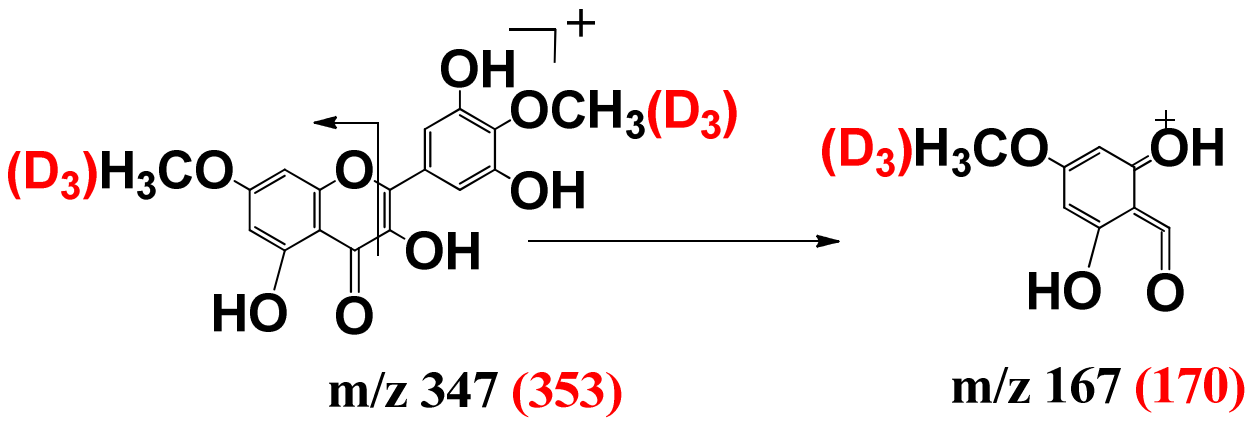

Figure IV-6 Fragments of m/z 167 derived from protonated 4',7-dimethylmyricetin that can distinguish sites of methylation through deuterium labeling. Pathway involves $1,3A^{+}$ cleavage with one methyl group remaining on A ring, retaining the deuterium label if labeled in the methyl on A ring.

There are two hydroxyl groups on the A-ring of myricetin, at the 5- and 7-positions, that could potentially undergo methylation. The appearance of the fragment at m/z 167 in the methylated myricetins suggests that one of these is methylated (Figure IV-5), and none of the enzyme incubations or plant extracts yielded product ions at m/z 181 that would point to methylation at both positions [271]. The mass spectra alone do not allow for definitive assignments as 5-methyl or 7-methyl substitutions. However, comparisons of the HPLC retention of the enzymatic (ShMOMT1) dimethylmyricetin product (RT 9.3 min) with 3',5'-dimethylmyricetin standard (RT 8.7 min), show later elution of the enzymatic product. The longer retention time is consistent with methylation at the 7-position because the 7-hydroxyl cannot participate in intramolecular hydrogen bonding, whereas methylation of the 5-hydroxy group would disrupt intramolecular hydrogen bonding, and would lead to a smaller increase in reversed phase retention upon methylation.

The monomethylated myricetin generated from ShMOMT1 showed a fragment at m/z 153 consistent with no methylation of the A-ring, and the dimethylmyricetin product was concluded to have undergone methylation at the 7-position. Based on the discussion of chromatographic retention of methylated myricetins described above, it was already concluded that the monomethylmyricetin product was not methylated at the 3- or 3'- positions. From this information, only one isomer is possible, specifically the 4',7-dimethylmyricetin. Since methyl group migrations during MOMT reactions have not been established (nor are they expected), the monomethylated product (RT 8.15 min) is assigned as 4'-monomethylmyricetin. One interesting aspect of the ShMOMT1 product mixture is that the enzyme is capable of adding a methyl group to the 7- position, but no 7-monomethylmyricetin was observed, which would have been evident from the m/z 167 indicator of A-ring methylation. From this information, it is concluded that ShMOMT1 catalyzed selective methylation of myricetin at the 4'-position, and the selective formation of 4',7-dimethylmyricetin suggests that 4'-monomethylmyricetin may be a better substrate for 7-position methylation than unmodified myricetin.

Using the second recombinant methyltransferase enzyme cloned from *S. habrochaites* LA1777 (ShMOMT2) for incubation with myricetin, only one chromatographic peak observed in the extracted ion chromatogram (XIC) for $[M+H]^+$ corresponding to monomethylmyricetin at m/z 333 is observed (RT 8.04 min; Figure IV-3A). Both retention time and enhanced product ion spectra are indistinguishable from 3'-methylmyricetin standard (Figure IV-3A and Figure IV-4). Therefore, the sole monomethylated product of ShMOMT2 is assigned as 3'-methylmyricetin. No incubations of ShMOMT2 with myricetin yielded detectable amounts

of products with more than one methyl group.

It is notable that one additional feature in the product ion spectra for $[M+H]^+$ of the 3'- and 4'- isomers of monomethylmyricetin distinguishes these isomers (Figure IV-3D and E). The residual abundance of protonated 4'-methylmyricetin in the product ion spectrum is nearly 4-fold lower than for 3'-methylmyricetin, when normalized to the base peak abundance. In both cases, the base peak arises from loss of methyl radical, and this distinguishing characteristic suggests that different methyl groups exhibit differential susceptibility to homolytic bond cleavage following collisional excitation. More detailed investigations into this phenomenon are described in Section 4.3.2.2.

Myricetin was incubated both with individual ShMOMT1 and ShMOMT2 enzymes separately, as well as in mixtures containing both enzymes, to generate as many products as possible to: (1) establish enzyme functions, and (2) elucidate characteristic fragment ions for different structures through a combinatorial synthetic approach. In incubations that employed both enzymes, a broader chromatographic peak for m/z 333 ($[M+H]^+$ for monomethylmyricetins) was observed, with a split peak top consistent with two or more overlapping isomers (Figure IV-3C). It was anticipated that the mixture of enzymes would form mixtures of methylated myricetins containing methyl groups at both the 3'- and 4'- positions based upon the activities of the individual enzymes, and LC/MS results confirmed that both were formed in comparable amounts. These two isomers could not be completely resolved using an assortment of HPLC columns and mobile phase compositions, and this is consistent with earlier observations that 3'- and 4'-methylated isomers of quercetin were the isomers most difficult to separate [238-240].

Incubations of myricetin with enzyme mixtures (ShMOMT1 and ShMOMT2) yielded four dimethylmyricetin isomers that were resolved using LC/MS, and enhanced product ion spectra for all four peaks are presented in Figure IV-7. Chromatographic peaks 3 (RT 9.34 min) and 4 (RT 9.50 min) both gave the m/z 167 fragment ions characteristic of a single methyl group on Ring A. Based on the earlier discussion, it is concluded that the A-ring substituent is on the 7-position oxygen. Since the two enzymes yield 3'- and 4'- monomethylmyricetins as initial products, and since ShMOMT1 exhibited catalytic activity toward further methylation at the 7-position, it is concluded that the two later eluting peaks are 3',7-dimethylmyricetin and 4',7-dimethylmyricetin. The direct annotation of peak 3 (RT 9.34 min) was made as 4',7-dimethylmyricetin because its retention time and MS/MS spectrum matched the product (4',7-dimethylmyricetin) generated from ShMOMT1 alone. Annotation of peak 4 was completed later through use of incubation of 3'-methylmyricetin with enzymes, and is discussed in greater detail in section 4.3.2.2. In summary, peak 4 was annotated as 3',7-dimethylmyricetin and peak 3 (RT 9.34 min) was annotated as 4',7-dimethylmyricetin.

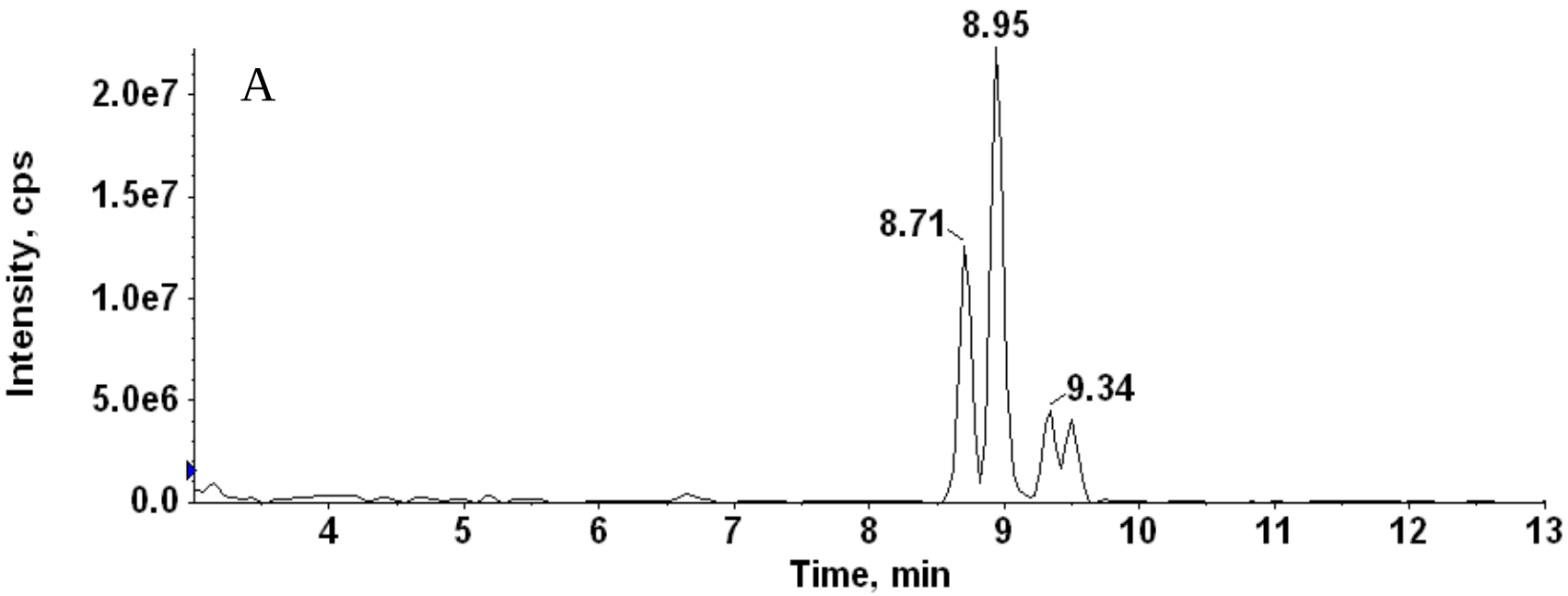

Figure IV-7 A) Extracted ion chromatogram (XIC) of m/z 347 for $[M+H]^+$ of dimethylated products from incubation of both ShMOMT1 and ShMOMT2 with myricetin; B) enhanced product ion scan (EPI) spectrum of dimethyl product (RT 8.71), annotated as 3',5'-dimethylmyricetin; C) enhanced product ion scan (EPI) spectrum of dimethylated product (RT 8.95), annotated as 3',4'-dimethylmyricetin; D) EPI spectrum of product (RT 9.34). annotated as 4',7-dimethylmyricetin; E) EPI spectrum of product (RT 9.50) annotated as 3',7-dimethylmyricetin. Data were acquired using a Qtrap 3200 mass spectrometer using electrospray positive mode and 40 V collision potential.

Figure IV-7 (cont'd)

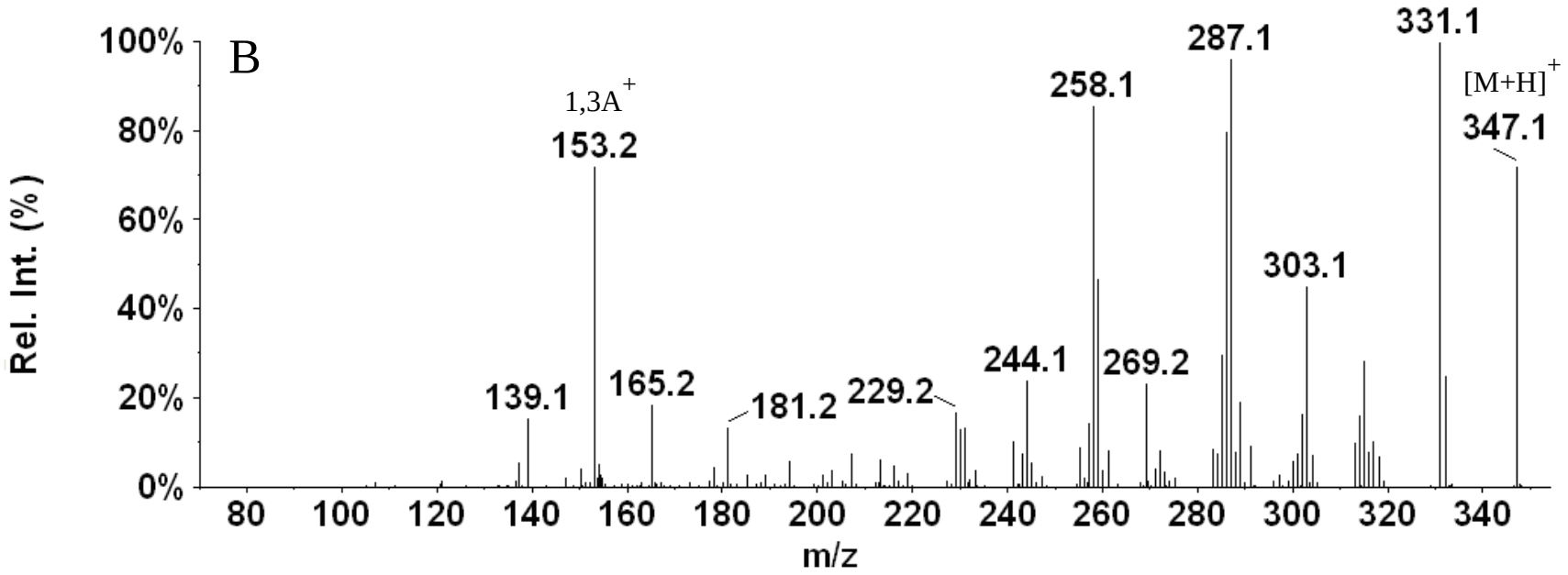

Figure IV-7 (cont'd)

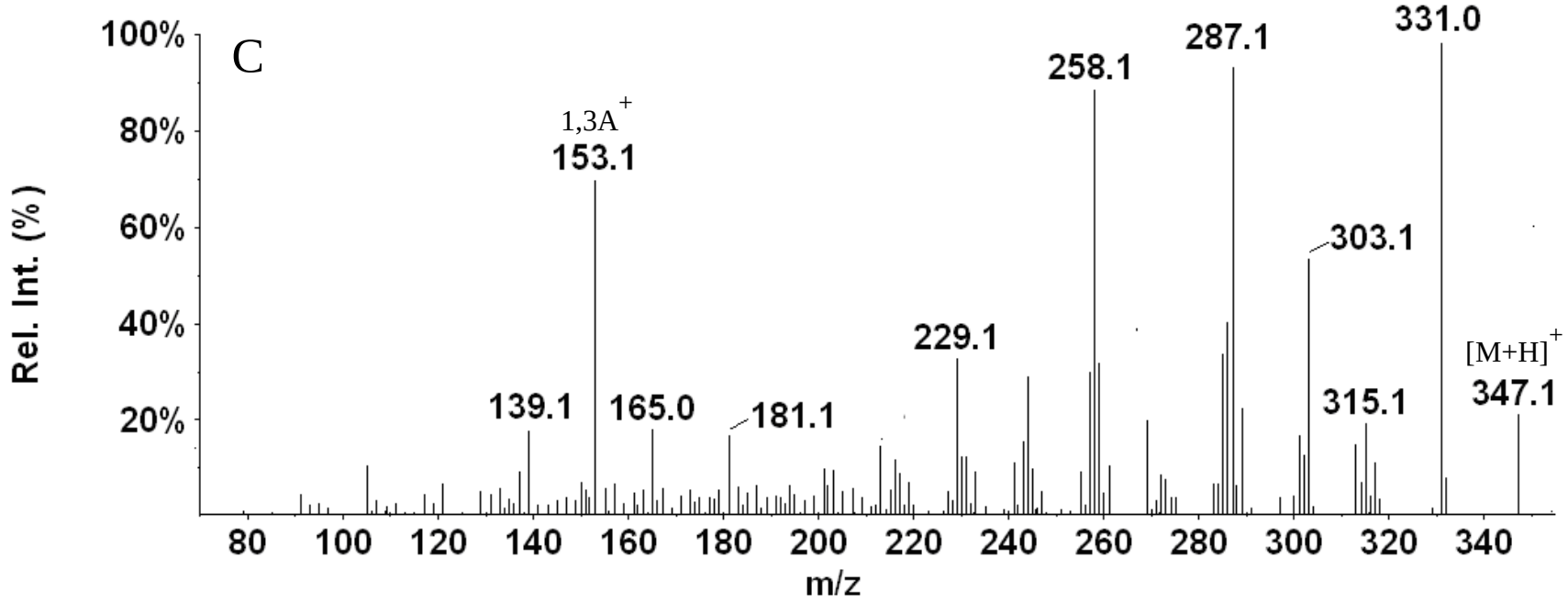

Figure IV-7 (cont'd)

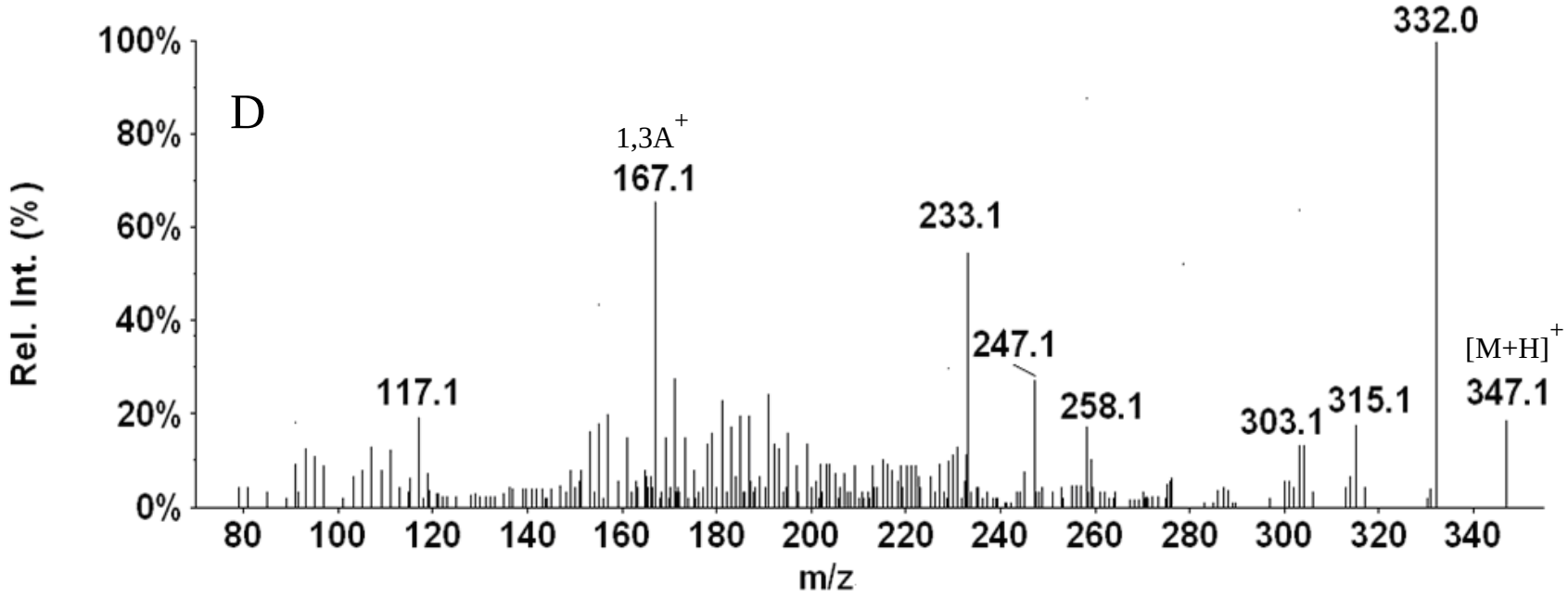

Figure IV-7 (cont'd)

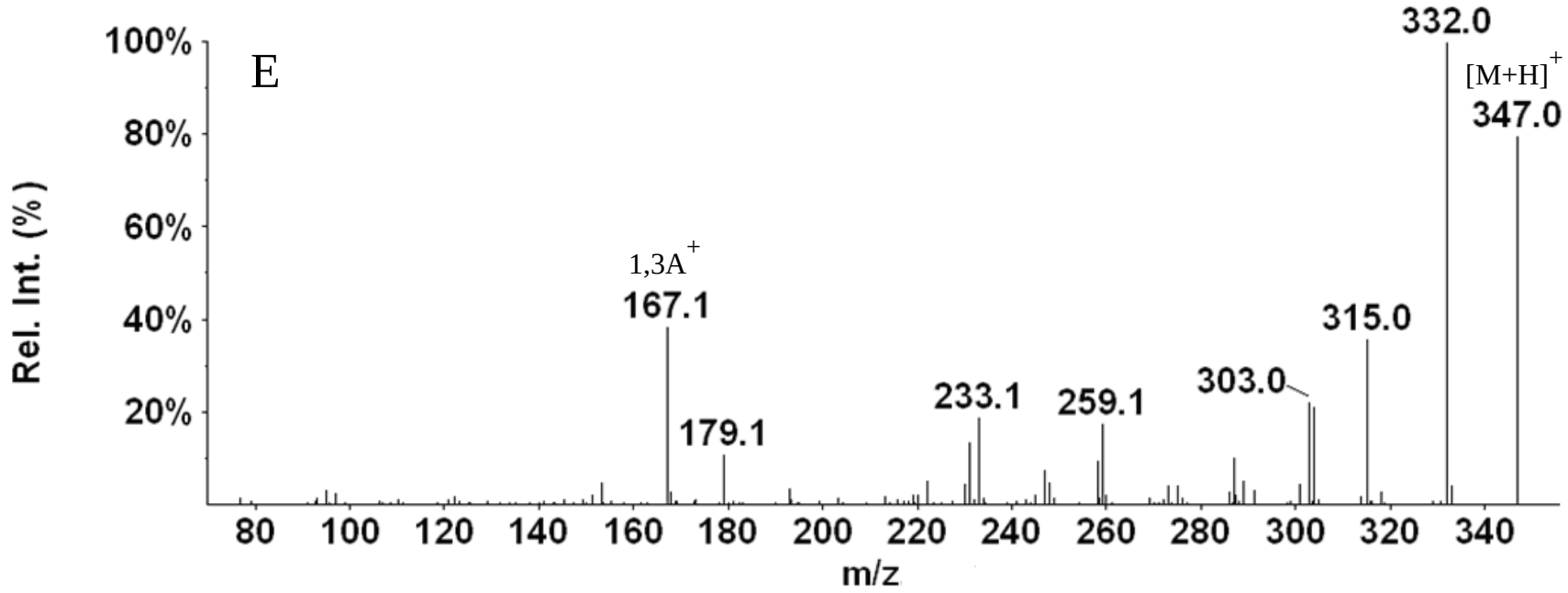

For the two early eluting dimethylmyricetin products generated from the mixed enzyme incubation (Figure IV-7A), the fragment of m/z 167 that is characteristic of A-ring methylation was not observed (Figure IV-7B and C), indicating no A-ring substitution.

Combining the information about the other metabolites, the following constraints are in place for both of the two early eluting dimethylmyricetin isomers derived from incubations with myricetin as substrate: 1) no methyl on A- ring; b) at least one or more methyl groups on the 3'- or 4'- positions; 3) 3' is equivalent to 5' owing to symmetry. Within these constraints, there are four possibilities for these two dimethylmyricetin isomers: (3',5'), (3',4'), (3,4') and (3,3'). The first peak (RT 8.71 min) matched retention time and fragmentation pattern of authentic 3',5'-dimethylmyricetin. Based on the chromatographic retention times, the best match of latter peak was 3',4'-dimethylmyricetin because it elutes about 0.2 min later (RT 8.95 min) than the 3',5'-isomer, and the 3,3'- and 3,4'-isomers would be expected to elute earlier owing to intramolecular hydrogen bonding. All of the four dimethylmyricetin products are consistent with the enzyme selectivity observed in the individual enzyme incubations that demonstrated methylations at 3'-, 4'-, and 7- positions of myricetin.

Several features in the MS/MS spectra of these two 3,3'- and 3,4'-isomers distinguish them from the 3',7- and 4'-7-dimethylmyricetins described above. The first, and most prominent feature, lies is the abundance of higher mass product ions. For both of 3,3'- and 3,4'-isomers, the most abundant product is m/z 331, which is 16 Da lower in mass than the precursor. In contrast, the dominant product ion for the later eluting isomers (3',7 and 4',7) was m/z 332, an odd-electron fragment corresponding to loss of methyl radical (15 Da). The loss of 16 Da in the

3,3'- and 3,4'-isomers can be explained either by successive losses of CH_3• and a hydrogen atom, or a concerted elimination of CH_4, which would require a hydrogen migration. A more complete and systematic exploration of the structural features responsible for these differences is presented in subsequent sections (Section 4.3.3) of this Chapter.

4.3.2.2 3'-methylmyricetin as methyltransferase substrate

The catalytic activity of ShMOMT2 yielded 3'-O-methylmyricetin as its only product. Because only one methylated product was formed, and since commercial sources of this product were available, more extensive investigations of ShMOMT1 functions could be explored. Incubations of ShMOMT1 with 3'-methylmyricetin and SAM yielded two peaks in extracted ion chromatograms corresponding to protonated dimethylmyricetins (m/z 347; Figure IV-8). The later eluting peak, (RT 9.47 min) gave the characteristic fragment ion at m/z 167 which indicates methylation at either the 5- or 7- positions. As discussed above, this was annotated as 3',7-dimethylmyricetin and not 3',5-dimethylmyricetin based on its late elution as compared to the 3',5'-dimethylmyricetin standard (RT 8.73 min). The retention time and product ion spectrum is indistinguishable from the fourth peak (RT 9.50 min) in the mixed enzyme incubation described in Section 4.3.2.1 (Figure IV-7E), and supports its assignment as 3',7-dimethylmyricetin also. The first chromatographic peak (RT 8.97 min; Figure IV-8) yielded fragment at m/z 153 but not m/z 167, which indicates no A-ring substitution. Considering the starting substrate is 3'-methylmyricetin, the remaining possibilities are (3',5'),

(3’,4’) or (3,3’) isomers. Comparison of the product ion spectra of this isomer with an authentic standard of 3’,5’-dimethylmyricetin led to its elimination as a candidate. Then only two possibilities are left which are (3’,4’) and (3,3’). Since its retention time and product ion spectra matched the second peak in the mixed enzyme incubation described in Section 4.3.2.1, it was identified as 3’,4’-dimethylmyricetin (Figure IV-7C).

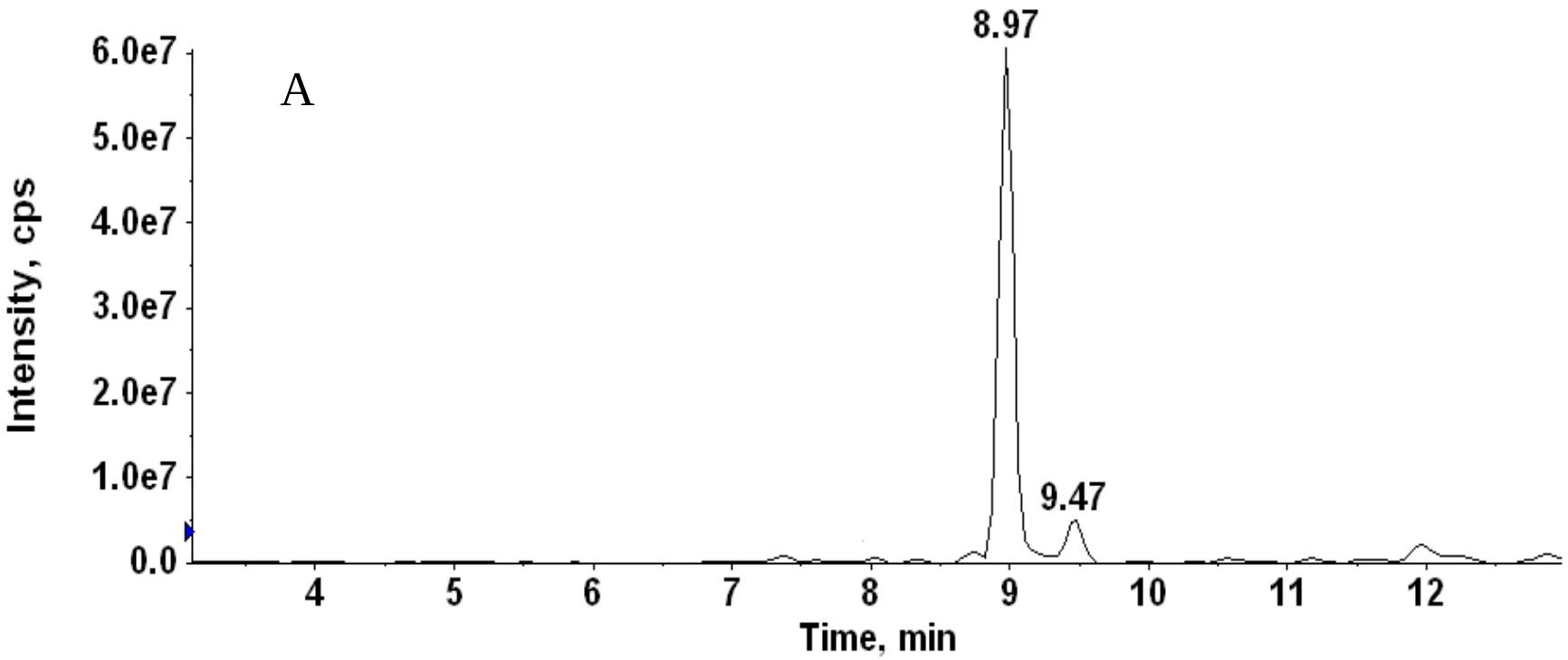

Figure IV-8 A) Extracted ion chromatogram (XIC) of m/z 347 ($[M+H]^+$) for dimethylmyricetin products from incubation of ShMOMT1 with 3'-monomethylmyricetin B) EPI spectrum of dimethylmyricetin product (RT 8.97), later annotated as 3',4'-dimethylmyricetin C) EPI spectrum of dimethyl product (RT 9.47), later annotated as 3',7-dimethylmyricetin. Data were acquired using a Qtrap 3200 mass spectrometer using electrospray positive mode and 40 V collision potential.

Figure IV-8 (cont'd)

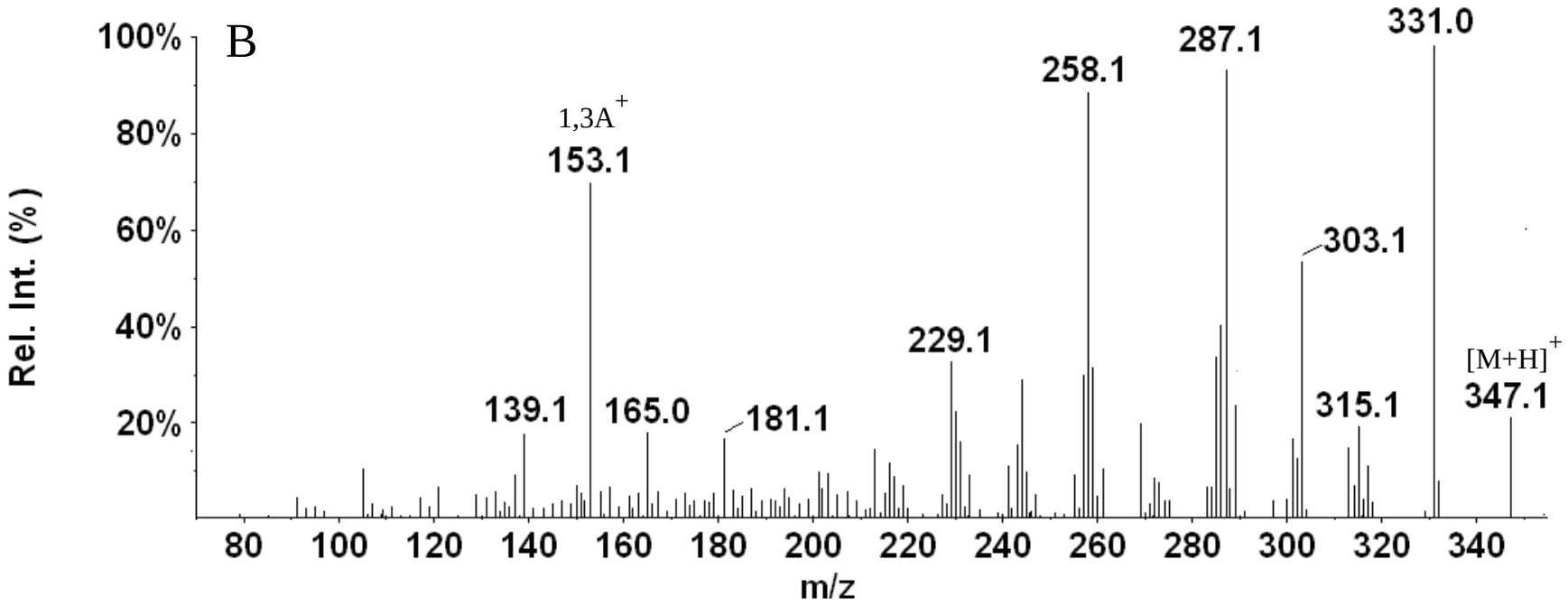

Figure IV-8 (cont'd)

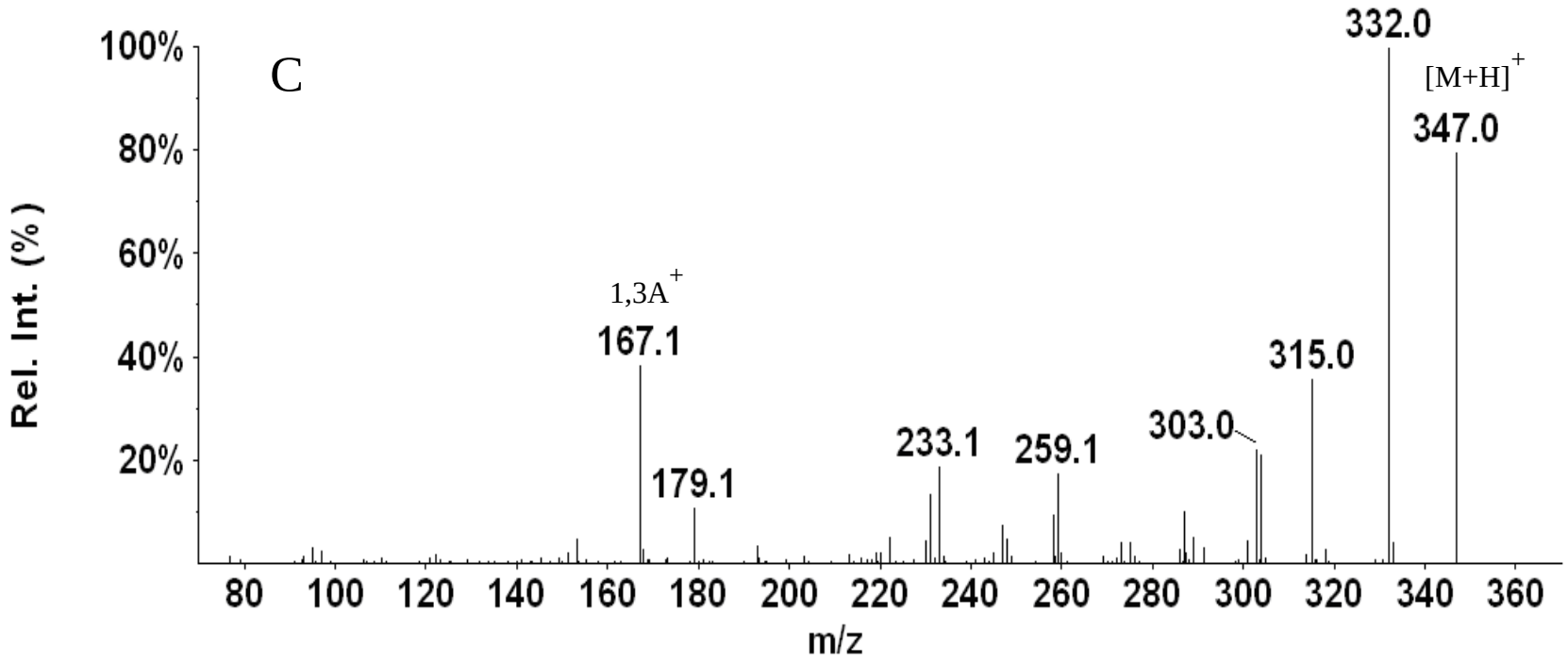

One trimethylmyricetin product was generated from incubations of 3'-methylmyricetin with ShMOMT1 (RT 10.22 min; Figure IV-9). The presence of m/z 167 in the product ion spectrum is indicative of A-ring methylation, which is consistent with methylation in both 4'- and 7-positions as these were formed independently. Furthermore, this isomer elutes later than 3',4',5'-trimethylmyricetin standard (RT: 9.70 min), which is consistent with its assignment as 3',4',7-trimethylmyricetin.

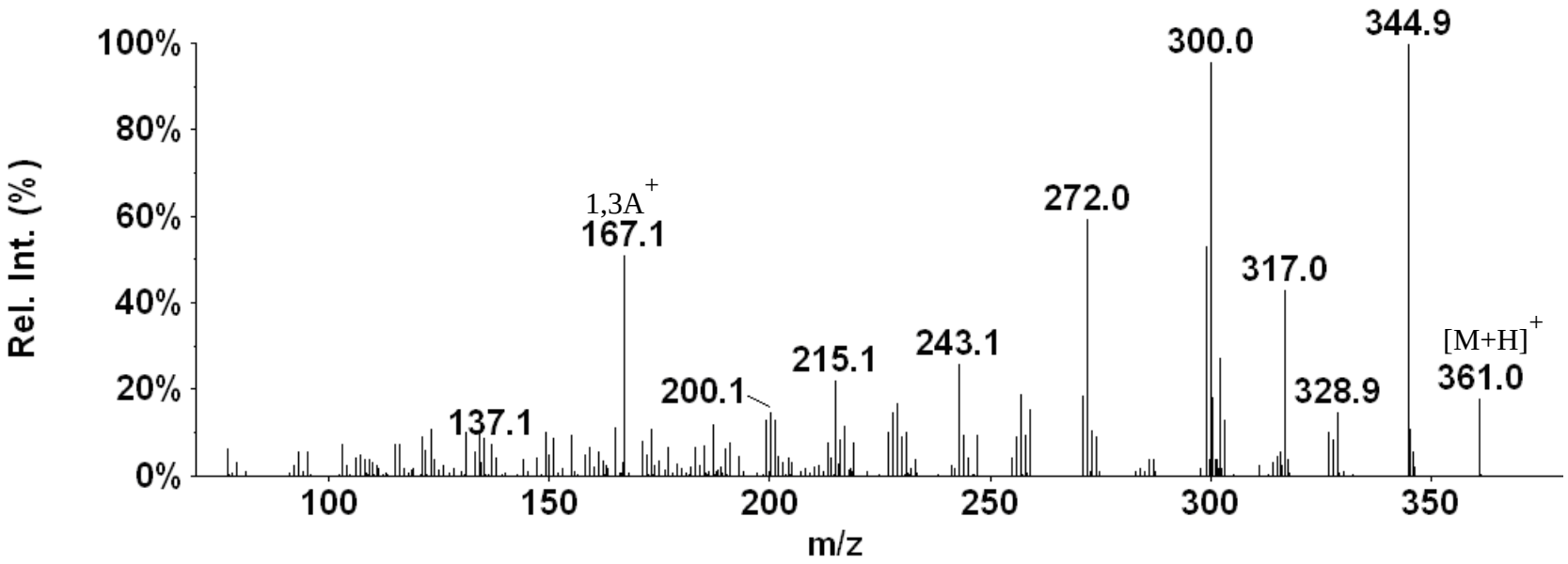

Figure IV-9 EPI spectrum of m/z 361 ($[M+H]^+$) for trimethylmyricetin product (RT 10.22 min) from incubation of ShMOMT1 with 3'-monomethylmyricetin, later annotated as 3', 4', 7-trimethylmyricetin. Data were acquired using a Qtrap 3200 mass spectrometer using electrospray positive mode and 40 V collision potential.

Incubations of 3’-methylmyricetin with ShMOMT2 or with mixtures of ShMOMT1 and ShMOMT2 yielded two chromatographic peaks in XIC (m/z 347) corresponding to dimethylmyricetins using ShMOMT2 incubation and four analogous chromatographic peaks in the products from the mixed enzyme incubations. Since the two dimethylmyricetins from ShMOMT2 incubation were also observed in the mixed enzyme incubation, coverage of the complete range of isomers is accomplished via analysis of the mixed enzyme products (Figure IV-10). Considering that 3’-methylmyricetin is the starting reagent, five dimethylmyricetin isomers are theoretically possible: (3’,4’), (3’,5’), (3,3’), (3’,5) and (3’,7). An exploration of the retention times and product ion spectra was undertaken to annotate the incubation products. The chromatographic retention of the (3’,7) isomer should be greatest, as discussed above, and this isomer would be expected to yield a fragment at m/z 167 that is characteristic of a monomethyl-subsituted A-ring. The latest eluting isomer (RT 9.50 min) did indeed show this fragment, and was therefore annotated as 3’,7-dimethylmyricetin. The second eluting isomer (RT 8.73 min) showed a strong match with retention and product ion spectra of the commercially available standard 3’,5’-dimethylmyricetin, and was annotated as such. The possibility that the third eluting isomer (Figure IV-10D) was 3’,5’-dimethylmyricetin was then excluded. Because the m/z 153 fragment indicates no A-ring methylation, and its late retention time (RT 8.98 min) argues against the 3,3’-substitution (which should elute earlier). The only remaining candidate is 3’,4’-dimethylmyricetin, and this finding is supported by of its match of retention time and MS/MS spectrum with the 3’,4’-dimethylmyricetin product formed by ShMOMT1 (which exhibits 4’- methyltransferase activity) methylation of 3’-methylmyricetin (Figure IV-8). The

remaining and earliest-eluting isomer (RT 8.34 min) is annotated from the remaining options, 3,3'- or 3',5-dimethylmyricetin. As discussed above, the 5-methyl isomer is expected to give the m/z 167 fragment peak through 1,3 A^+ cleavage. However, this isomer only shows a fragment at m/z 153, consistent with no A-ring methylation. Therefore, it is assigned as 3,3'-dimethylmyricetin.

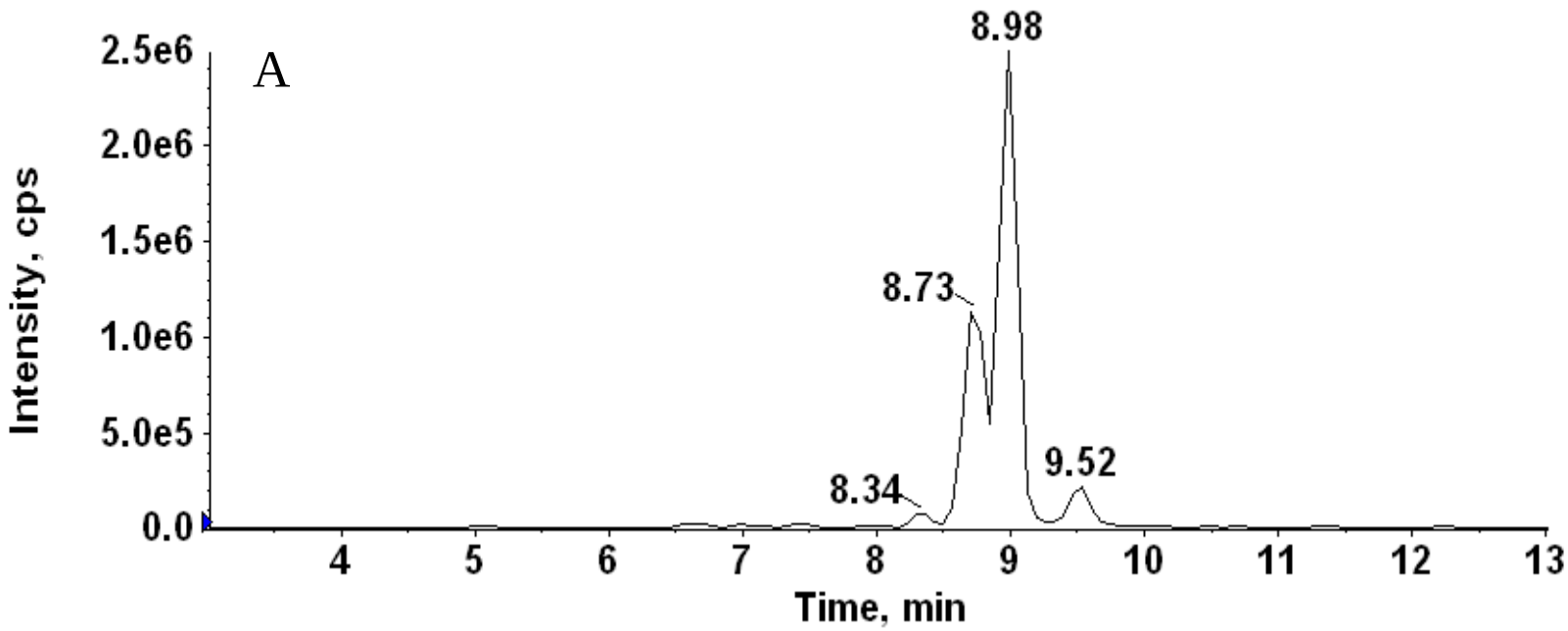

Figure IV-10 A) Extracted ion chromatogram (XIC) of m/z 347 ({M+H]$^+$) for dimethylmyricetin products from incubation of both ShMOMT1 and ShMOMT2 with 3'-monomethylmyricetin; B) EPI spectrum of product (RT 8.34 min), later annotated as 3,3'-dimethylmyricetin C) EPI spectrum of dimethyl product (RT 8.73 min), later annotated as 3',5'-dimethylmyricetin D) EPI spectrum of dimethyl product (RT 8.98min). later annotated as 3',4'-dimethylmyricetin E) EPI spectrum of dimethyl product (RT 9.52min). later annotated as 3',7-dimethylmyricetin. Data were acquired using a Qtrap 3200 mass spectrometer using electrospray positive mode and 40 V collision potential.

Figure IV-10 (cont'd)

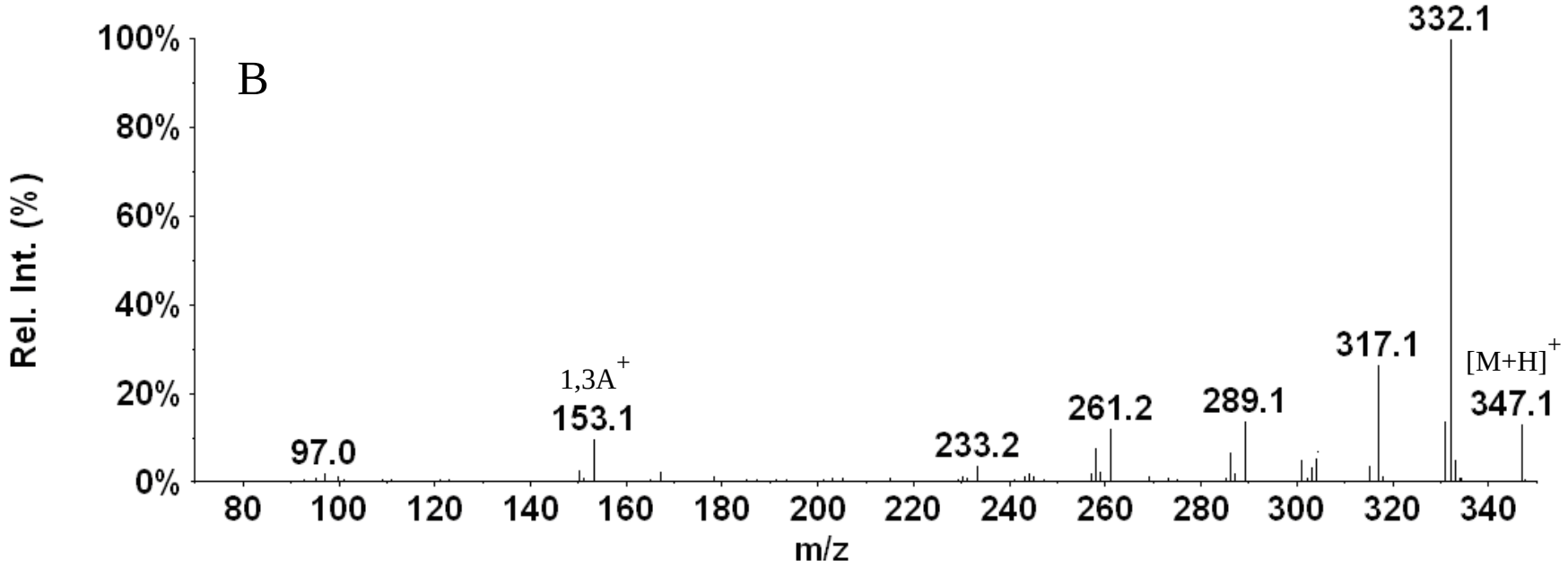

Figure IV-10 (cont'd)

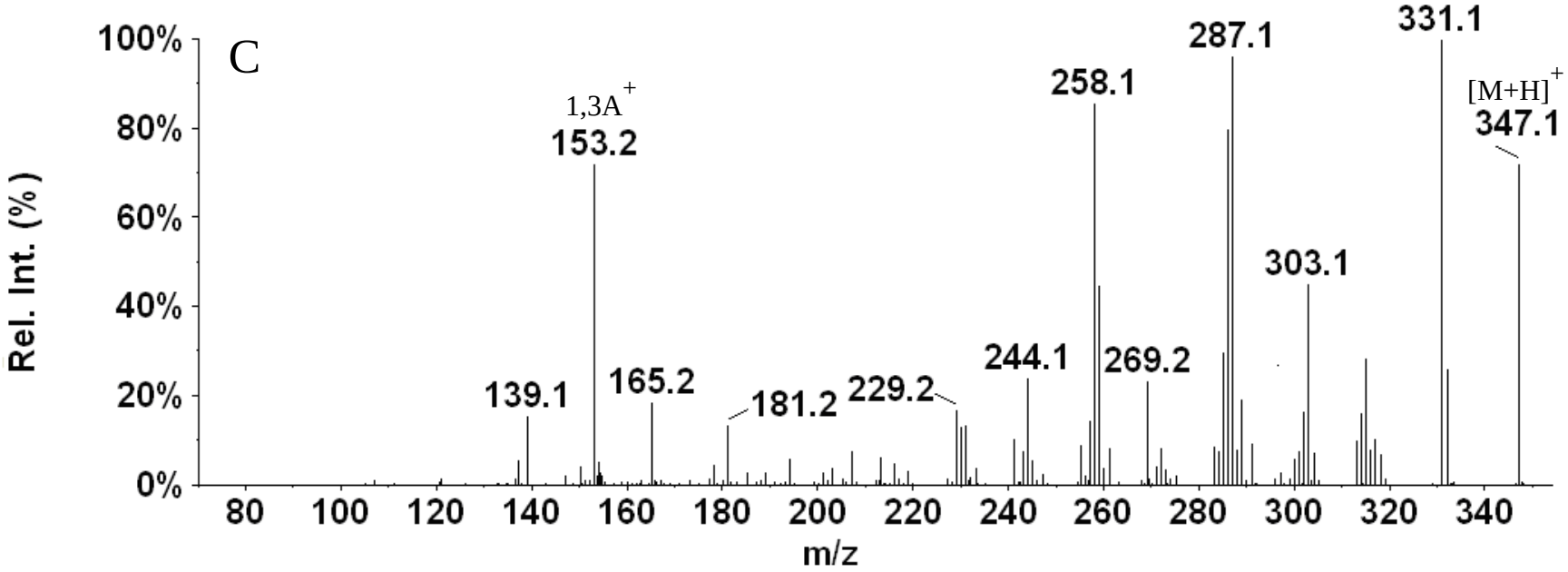

Figure IV-10 (cont'd)

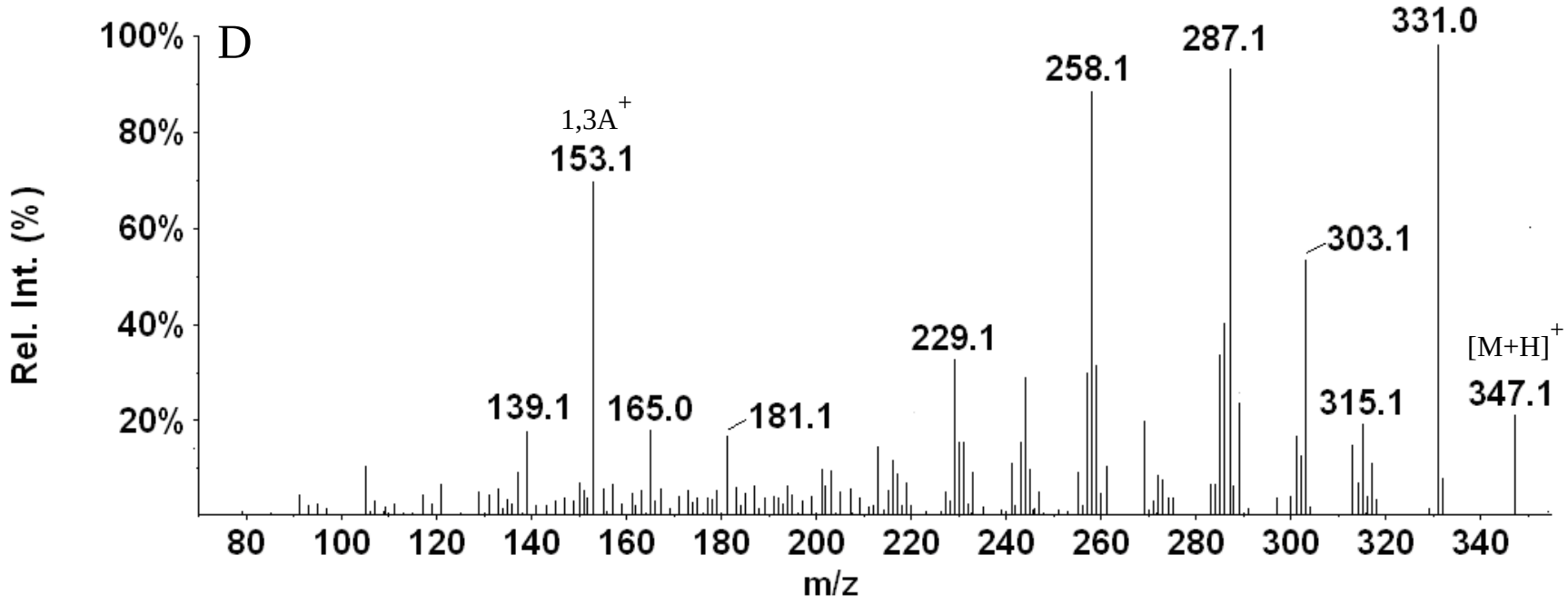

Figure IV-10 (cont'd)

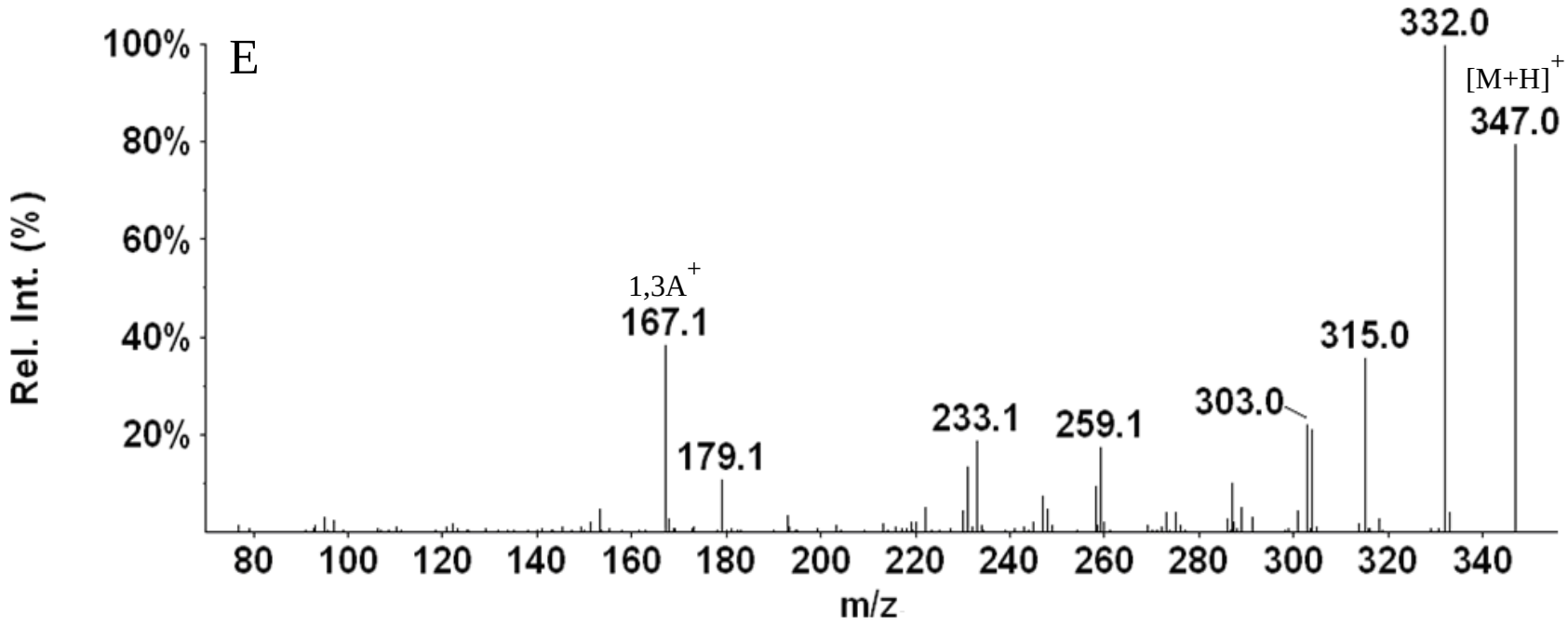

From these isomer annotations, it is also concluded that incubations of 3'-methylmyricetin with ShMOMT2 alone yield two isomers: 3,3'- and 3',5'-dimethylmyricetin, and this finding demonstrates that ShMOMT2 can methylate at the 3- and 5' (equivalent to 3')-positions. A summary of the enzymatic conversions of myricetin and the enzymatic monomethylmyricetins is presented in Scheme IV-1. One novel aspect of this discovery is the methylation at the 3-position by ShMOMT2, and this activity is considered rare among plant O-methyltransferases.

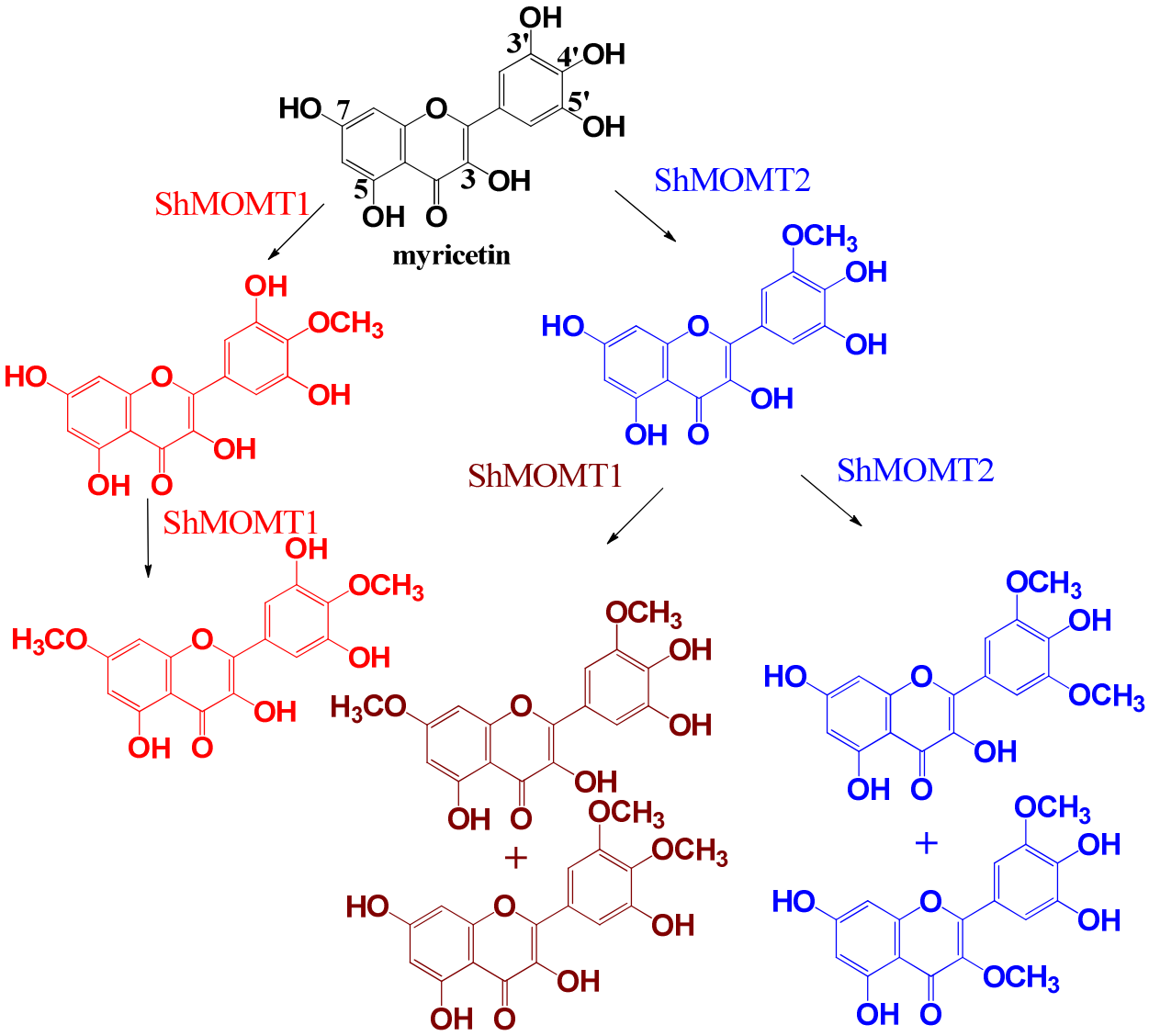

Scheme IV-1 Conversions of myricetin and monomethylmyricetins by ShMOMT1 and ShMOMT2 enzymes. Products of ShMOMT1 alone are colored red, of ShMOMT2 alone are colored blue, and products requiring both enzymes are colored brown.

As mentioned above in Section 4.3.2.1, product ion MS/MS spectra suggested that the fragmentation behavior of methyl groups varied based upon the position of the methyl group. However, to establish different methyl group behaviors in molecules containing multiple methyl groups, a tag or indicator of which methyl group is present in a product ion is needed. Selective

methylation of flavonoids using common chemical methylation reactions does not offer adequate selectivity to be useful for chemical synthesis without invoking complex schemes for protecting and deprotecting flavonoid functional groups. For this reason, enzymatic syntheses, which are usually more selective, were employed to introduce deuterated methyl groups in a limited range of positions on myricetin.

In incubations conducted using ShMOMT1 with 3'-methylmyricetin and deuterium labeled d_3-SAM, the 3'-methyl-4'-d_3-methylmyricetin contains one unlabeled and one labeled methyl group. The surprising finding in the product ion spectrum for $[M+H]^+$ is that it gives a barely detectable peak corresponds to loss of unlabeled methyl radical or CH_4 (m/z 335 or 334 respectively), as was observed for the unlabeled compound as described above. Instead, only loss of labeled methyl radical plus hydrogen atom (m/z 331, loss of 19 Da) was observed (Figure IV-11). Two explanations regarding this phenomenon are postulated. First, the initial fragment ion from loss of the 3'-O-methyl group may undergo more rapid conversion to other ionic products than occurs following 4'-O-methyl loss. However, loss of methyl radical or methane (CH_3•, -15 Da or CH_4, -16 Da) are the base peaks in product ion spectra from commercial standards of 3'-methylmyricetin and 3',5'-dimethylmyricetin, respectively, at the same collision potential (40 V). These findings argue against the unstable intermediate hypothesis. The second postulated option suggests that the rates of losses of methyl radical from the 3'- and 4'-positions are quite different, with loss of the 4'-position CD_3 group much faster than loss of the 3'- methyl radical when both are present in the same molecule. While kinetic isotope effects are anticipated, the magnitude of the kinetic differences would be difficult

to explain based on kinetic isotope effects alone.

As was the case for the 3'-methyl-4'-(d_3)-methyl isomer (Figure IV-11), the enhanced product ion spectra of 3(d_3)-methyl-3'-methylmyricetin show no CH_3 radical loss (m/z 335) but only CD_3 loss (m/z 332; Figure IV-12). As discussed above, this position-selective loss indicates the methyl group on the 3-position is more labile under these CID conditions relative to the 3' position.

The findings of this experiment demonstrate that differences in chemical behavior of methyl groups in methylated phenolic metabolites may provide a distinguishing feature useful for isomer discrimination. These kinds of isomers have been exceptionally difficult to resolve using mass spectrometry alone. Enzymatic synthesis of compounds having both labeled and unlabeled methyl groups are the key for this discovery because such compounds are not available in nature and also challenging to make by chemical synthesis. Understanding the reactivity of O-methyl groups and its dependence upon position of substitution provides a critical tool for metabolite structure identification, and its importance will be discussed more below.

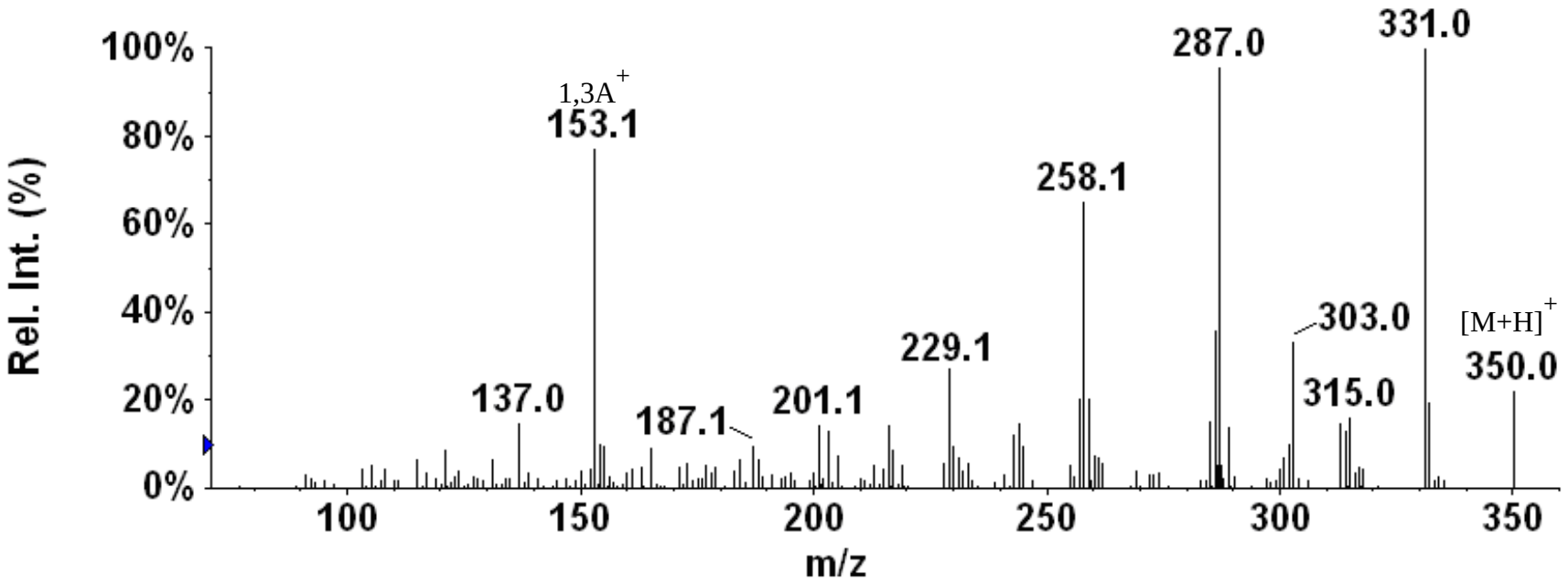

Figure IV-11 EPI spectrum of m/z 350 ($[M+H]^+$) for dimethylmyricetin product 3'-methyl-4'(d_3)-methylmyricetin from incubation of ShMOMT1 with 3'-monomethylmyricetin and d_3-SAM. Data were acquired using a Qtrap 3200 mass spectrometer using electrospray positive mode and 40 V collision potential.

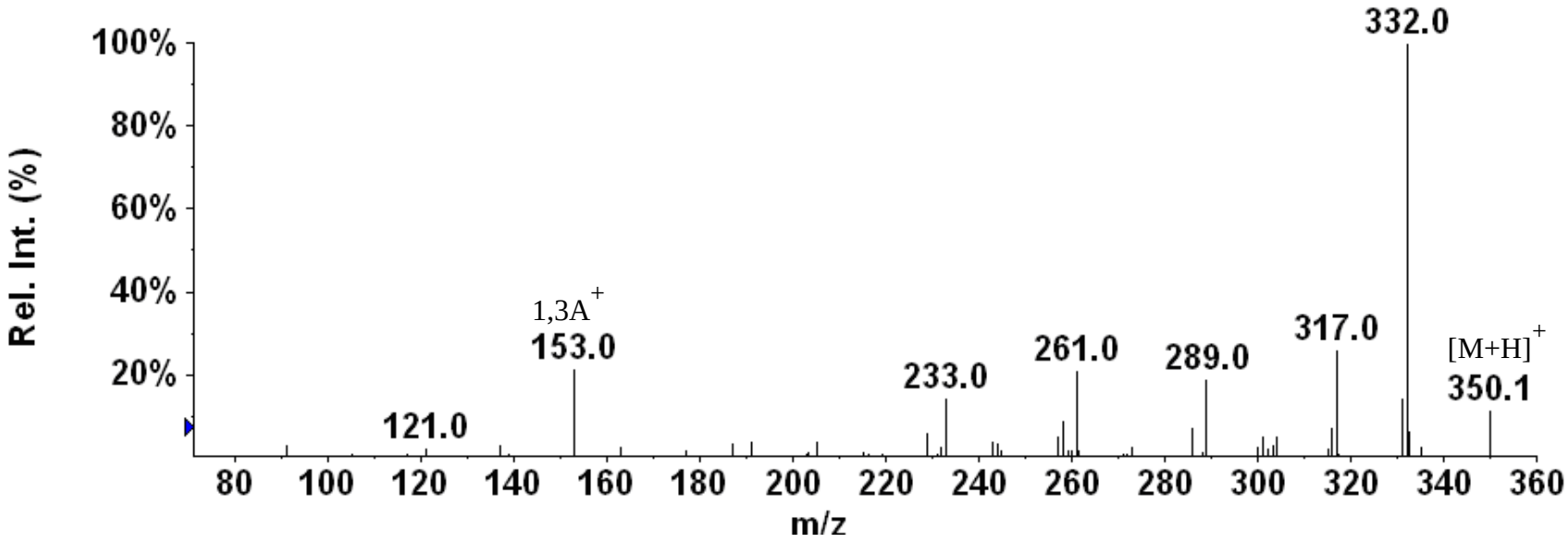

Figure IV-12 EPI spectrum of m/z 350 for dimethyl product 3(d_3)-methyl-3'-methylmyricetin from incubation of both ShMOMT1 and ShMOMT2 with 3'-monomethylmyricetin and d_3-SAM. Data were acquired using a Qtrap 3200 mass spectrometer using electrospray positive mode and 40 V collision potential.

4.3.2.3 3’, 5’-methylmyricetin as methyltransferase substrate

As described above, the catalytic activity of ShMOMT2 alone can convert myricetin to 3’-methyl- and 3’,5’-dimethylmyricetins. Since trichome extracts yielded an assortment of more extensively methylated myricetins, the possibility that these might form from actions of multiple methyltransferase enzymes was explored further. Incubation of 3’,5’-dimethylmyricetin with ShMOMT1 yielded two chromatographic peaks with masses (m/z 361; $[M+H]^+$) corresponding to trimethylmyricetin isomers. The first isomer (RT 9.70 min) matched retention time and product ion spectra with 3’,4’,5’-trimethylmyricetin, and was annotated as such. For the second isomer (RT 10.14 min), its product ion spectrum (Figure IV-13) gives the characteristic A-ring methylated product ion of m/z 167. Since its retention time is longer than 3’,4’,5’-trimethylmyricetin standard (RT 9.70 min) the only option is 3’,5’,7-trimethylmyricetin.

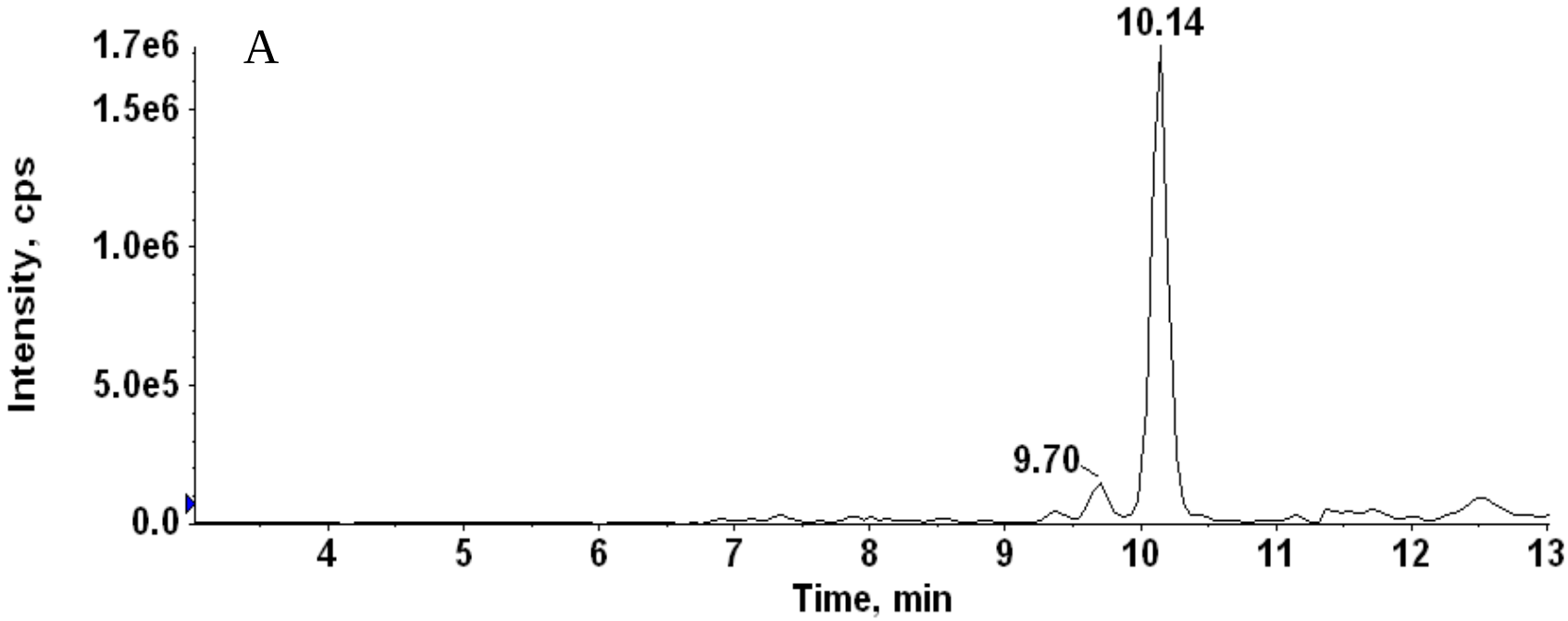

Figure IV-13 A) Extracted ion chromatogram (XIC) of m/z 361 ($[M+H]^+$) for trimethyl product from incubation of ShMOMT1 with 3',5'-dimethylmyricetin. B) EPI spectrum of m/z 361 for trimethyl product (RT 9.71min), later annotated as 3',4',5'-trimethylmyricetin C) EPI spectrum of m/z 361 for trimethyl product (RT 10.14 min), later annotated as 3',5',7-trimethylmyricetin. Data were acquired using a Qtrap 3200 mass spectrometer using electrospray positive mode and 40 V collision potential.

Figure IV-13 (cont'd)

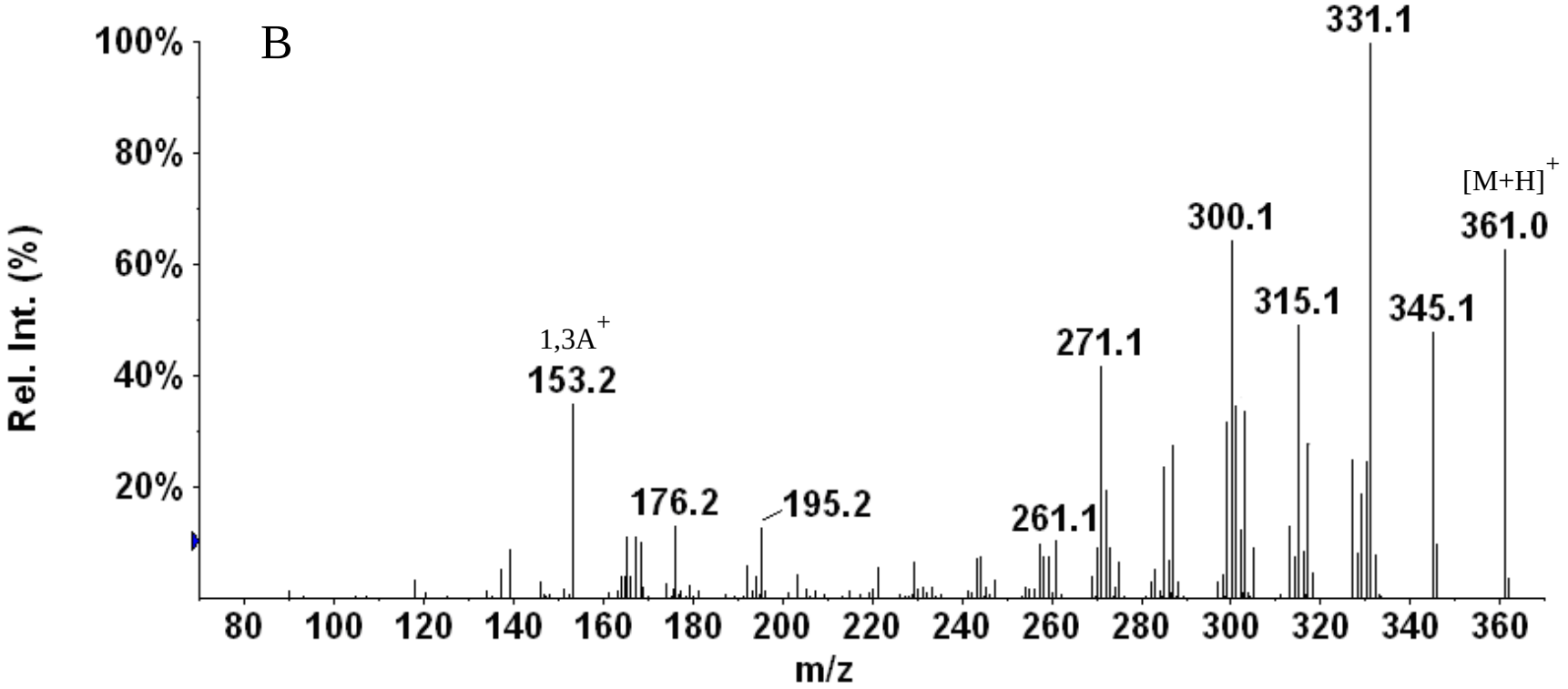

Figure IV-13 (cont'd)

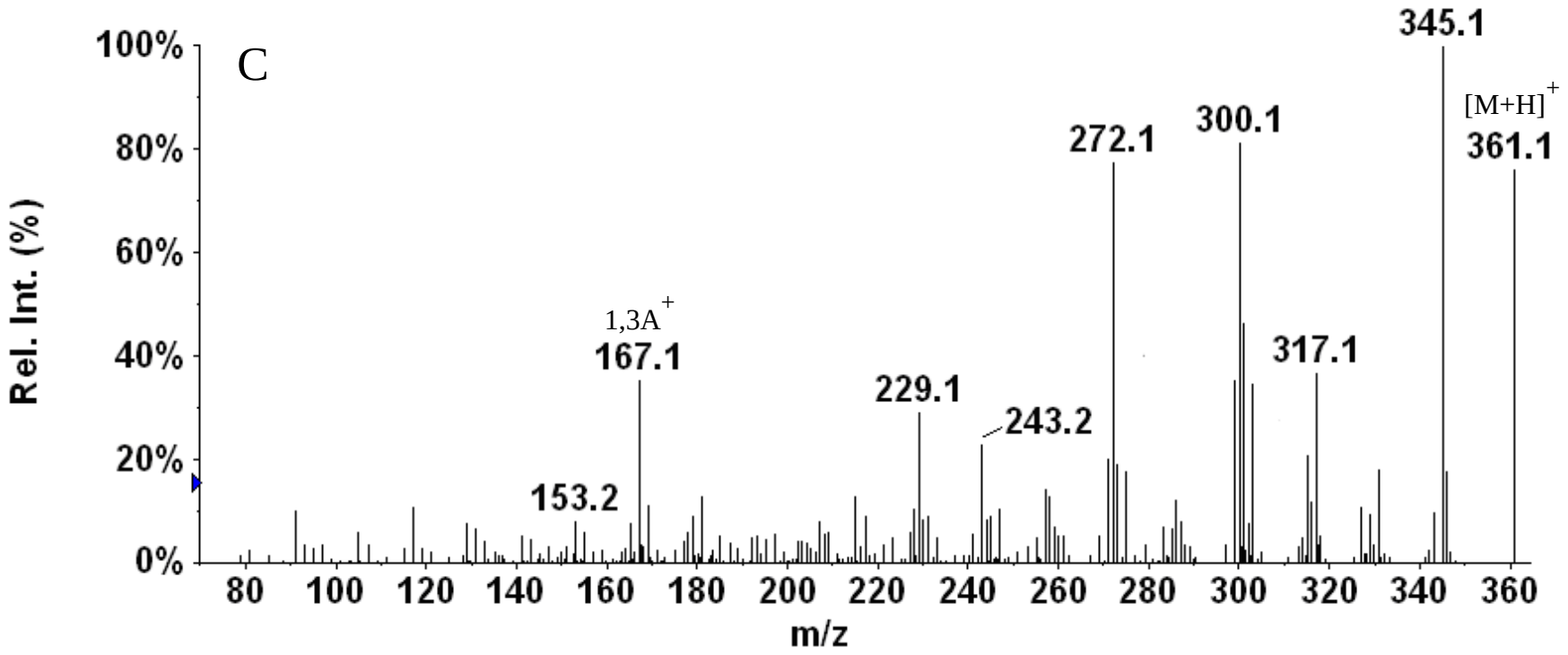

Incubations of 3',5'-dimethylmyricetin with ShMOMT2 yielded evidence of only a single trimethylmyricetin (RT 9.21 min) which eluted earlier than 3',4',5'-trimethylmyricetin standard (RT: 9.70 min). The product ion spectrum of this isomer yielded a peak at m/z 153 but not at m/z 167, pointing to no substitution on either the 5- or 7-positions. The only option consistent with these observations is 3,5',3'-trimethylmyricetin (Figure IV-14), and this structure provides evidence of a second ShMOMT2 substrate that is methylated at the 3-position. Product ion MS/MS spectra from $[M+H]^+$ of the trimethylmyricetin product generated from incubations using d_3-SAM showed a prominent neutral loss of 18 Da (CD_3 radical; m/z 346) but no peak corresponding to neutral loss of 15 Da (CH_3 radical; m/z 349) (Figure IV-14B). Again, this fragmentation is consistent with the finding described above that when 3- and 3'- (or 5'-) methyl groups are present on the same molecule, the direct methyl loss from the protonated molecule comes almost exclusively from the 3- methyl position.

To further understand the formation of more extensively methylated myricetins, 3',5'-dimethylmyricetin was incubated with a combination of ShMOMT1 and ShMOMT2. Unlike the incubation with ShMOMT2 alone, the mixture of enzymes generated two trimethylmyricetin isomers. These peaks are assigned as 3',5',7-trimethylmyricetin, which is presumed to be formed by the ShMOMT1 capacity to methylate at the 7-position, and 3,5',3'-trimethylmyricetin discussed above as a product of ShMOMT2 activity.

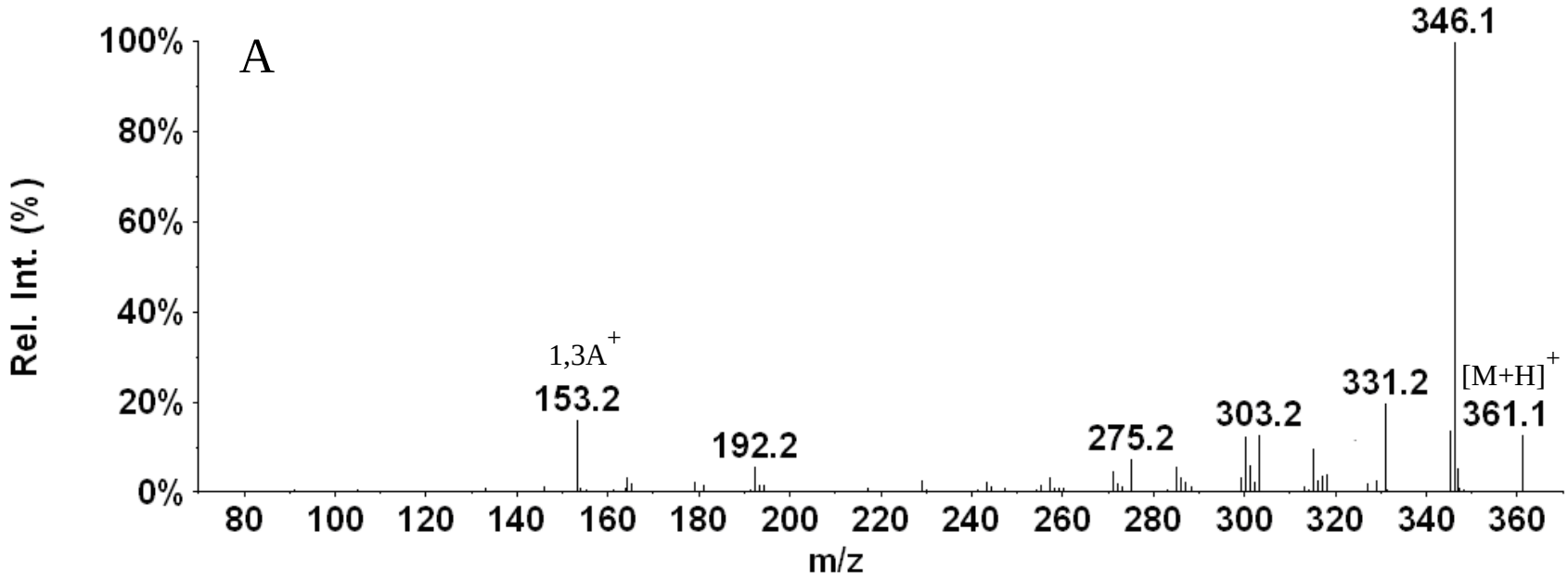

Figure IV-14 A) EPI spectra of m/z 361 ($[M+H]^+$) for trimethylmyricetin product from incubation of ShMOMT2 with 3',5'-dimethylmyricetin later annotated as 3, 3',5'-trimethylmyricetin; B) EPI spectrum of m/z 364 for trimethyl product from incubation of ShMOMT2 with 3',5'-dimethylmyricetin and d_3-SAM, later annotated as 3(d_3)-3',5' -trimethylmyricetin. Data were acquired using a Qtrap 3200 mass spectrometer using electrospray positive mode and 40 V collision potential.

Figure IV-14 (cont'd)

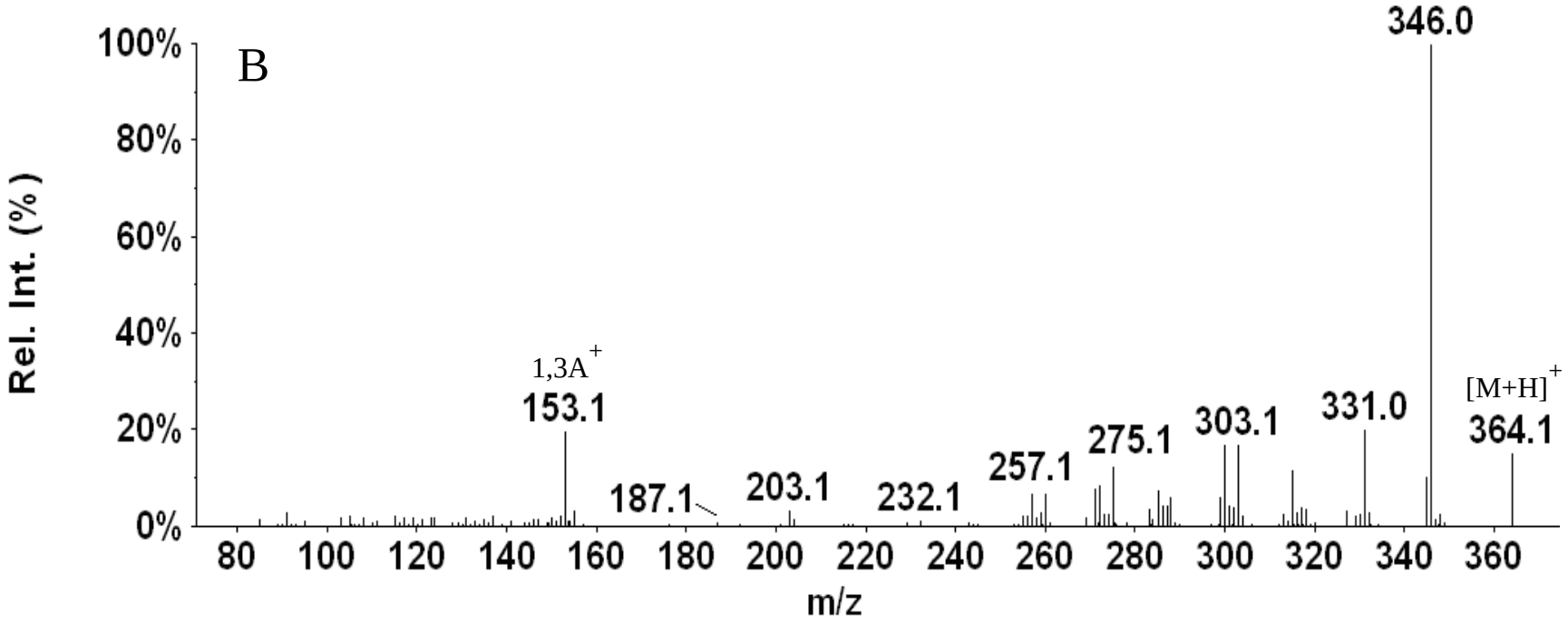

4.3.2.4 3',4',5',-trimethylmyricetin as methyltransferase substrate

The results described above demonstrated that ShMOMT1 can introduce methyl groups at the 4' position of myricetin, and ShMOMT2 can introduce methyls at the 3'- and 5'-positions. The combination of both enzymes can form 3',4',5'-trimethylmyricetin, and its further transformation was investigated, since authentic substrate was commercially available and this substrate has all three B-ring positions methylated. Incubation of 3',4',5'-trimethylmyricetin with ShMOMT2 yielded only one chromatographic peak with $[M+H]^+$ of m/z 375 (RT 9.81 min) consistent with a tetramethylmyricetin. The product ion MS/MS spectrum exhibited a strong m/z 153 fragment ion, which indicates no A-ring methylation (Figure IV-15). The only remaining possibility is 3,3',4',5'-tetramethylmyricetin, again demonstrating the capacity of ShMOMT2 to methylate the 3-position hydroxyl. In incubations using d_3-SAM as the co-substrate, the counterpart product of 3-d_3-methyl-3',4',5'-trimethylmyricetin gave a major neutral loss of 18 Da (CD_3; m/z 360) followed by a successive neutral loss of 15 Da (CH_3; m/z 345) but only a miniscule peak corresponding to loss of 16 Da (CH_3 plus H) from the protonated molecule. As observed for less methylated myricetins, when 3'- (or 5'-), 4'-, and 3- O-methyl groups are all present, the dominant methyl loss from the protonated molecule comes from the 3-position (Figure IV-15B). The minor peak that corresponds to neutral loss of 16 Da (CH_3+H; m/z 362) is believed to come from the 4'- position methyl radical loss plus an additional hydrogen atom, from sources yet to be discussed. Because we already observed when 4' and 3' (or 5') methyl groups are present, direct methyl loss from the protonated molecule mainly comes

from the 4’ position (Figure IV-11) unless a methyl group is also present at the 3-position oxygen. We conclude that the 3-O-methyl group is even more labile than 4’-O-methyl. Based on all of the trideuteromethyl analogs investigated for this project, we conclude when protonated polymethyl flavonoids undergo collisional activation, the rate of loss of methyl direct from the protonated molecule follow the ranking 3 > 4’ >> 3’(5’) >>7. The rate of loss of methyl groups provides a valuable tool that can differentiate isomers formed by methylation (Rule #3).

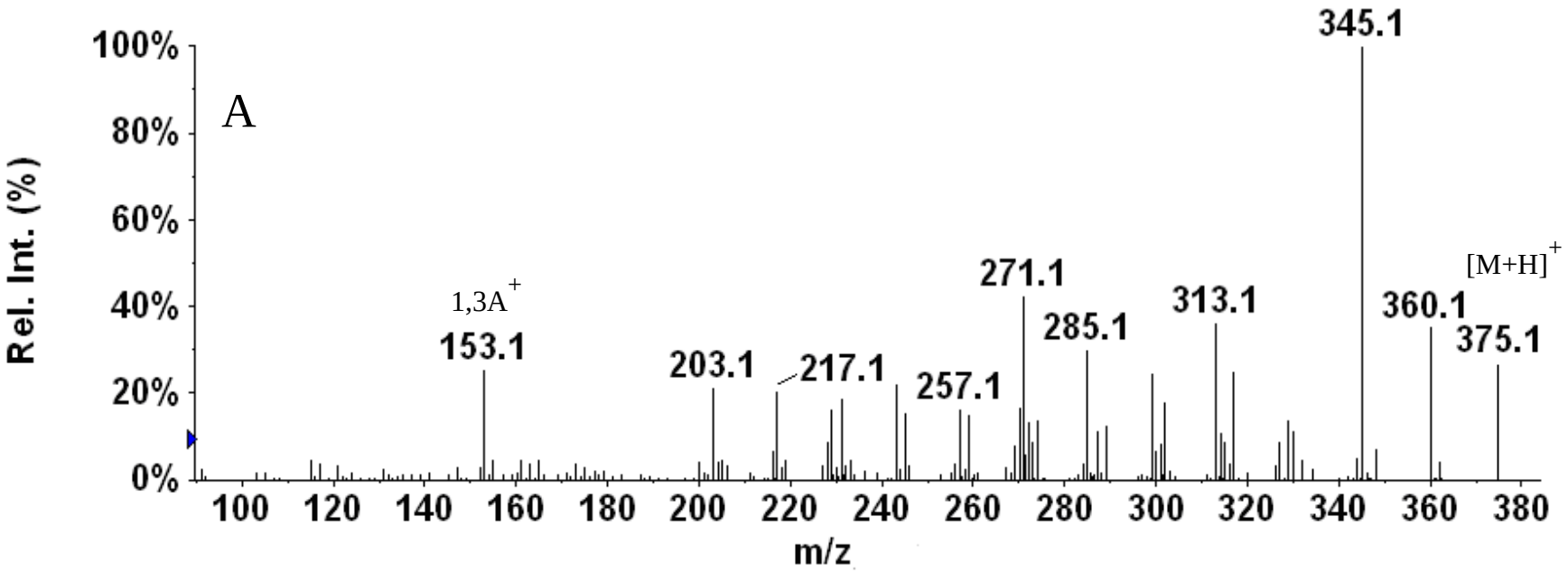

Figure IV-15 A) EPI spectrum of m/z 375 ($[M+H]^+$) for tetramethylmyricetin product (RT 9.81 min) from incubation of ShMOMT2 with 3',4',5'-trimethylmyricetin, later annotated as 3, 3', 4',5'-tetramethylmyricetin; B) EPI spectrum of m/z 378 ($[M+H]^+$) for tetramethylmyricetin product (RT 9.81 min) from incubation of ShMOMT2 with 3',4',5'-trimethylmyricetin and d_3-SAM, later annotated as 3(d_3) 3', 4',5'-tetramethylmyricetin. Data were acquired using a Qtrap 3200 mass spectrometer using electrospray positive mode and 40V collision potential.

Figure IV-15 (cont'd)

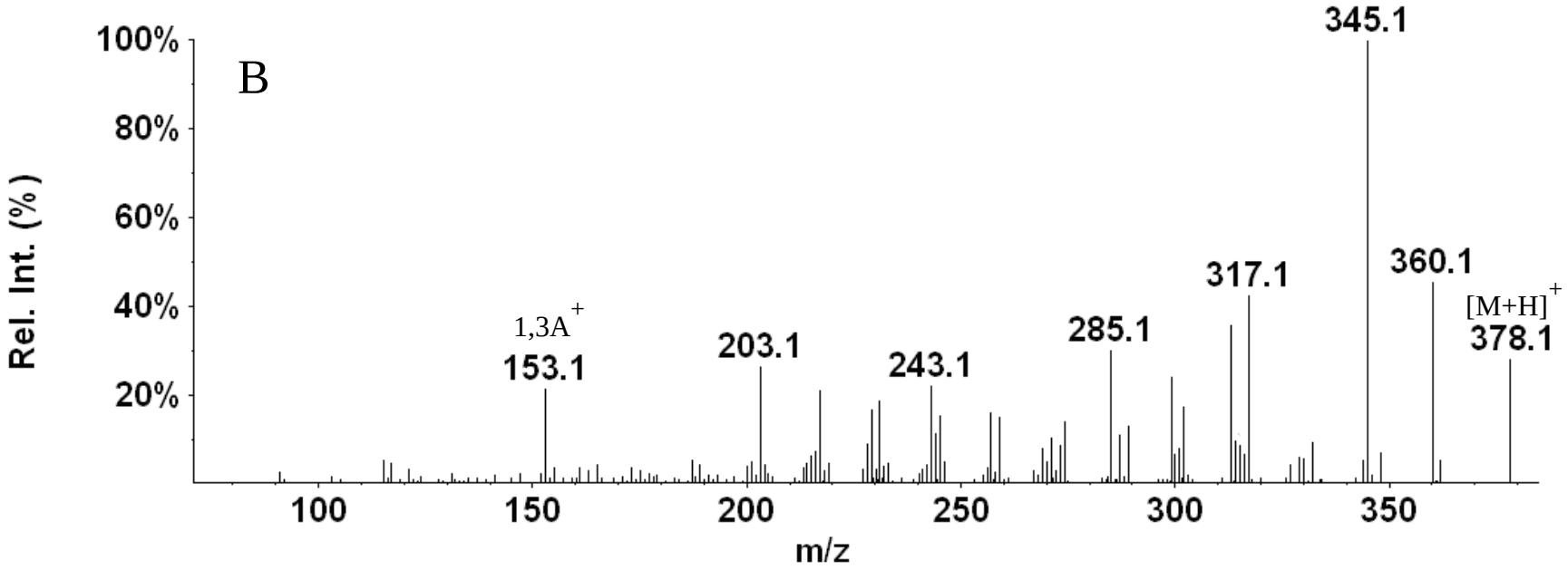

The 3',4',5'-trimethylmyricetin was also subjected to incubations with ShMOMT1, and only one chromatographic peak was observed to correspond to a tetramethylmyricetin, though in low yield. This single product, gives m/z 167 in the MS/MS product ion spectrum of $[M+H]^+$, an indication of a single methyl group on the A-ring (Figure IV-16). The two possibilities are 3',4',5,5'- or 3',4',5',7-tetramethylmyricetin. The enzymatic reaction product (RT 10.31 min) eluted later than 3, 3',4',5'-tetramethylmyricetin, (RT 9.81 min), and this is consistent with 3',4',5',7-tetramethylmyricetin. This finding is consistent with ShMOMT1-catalyzed methylation at the 7-position, as discussed above. Incubation of the 3',4',5'-trimethylmyricetin with the mixture of ShMOMT1 and ShMOMT2 yielded two tetramethylmyricetin products, which are the same as those generated by incubations with the individual enzymes.

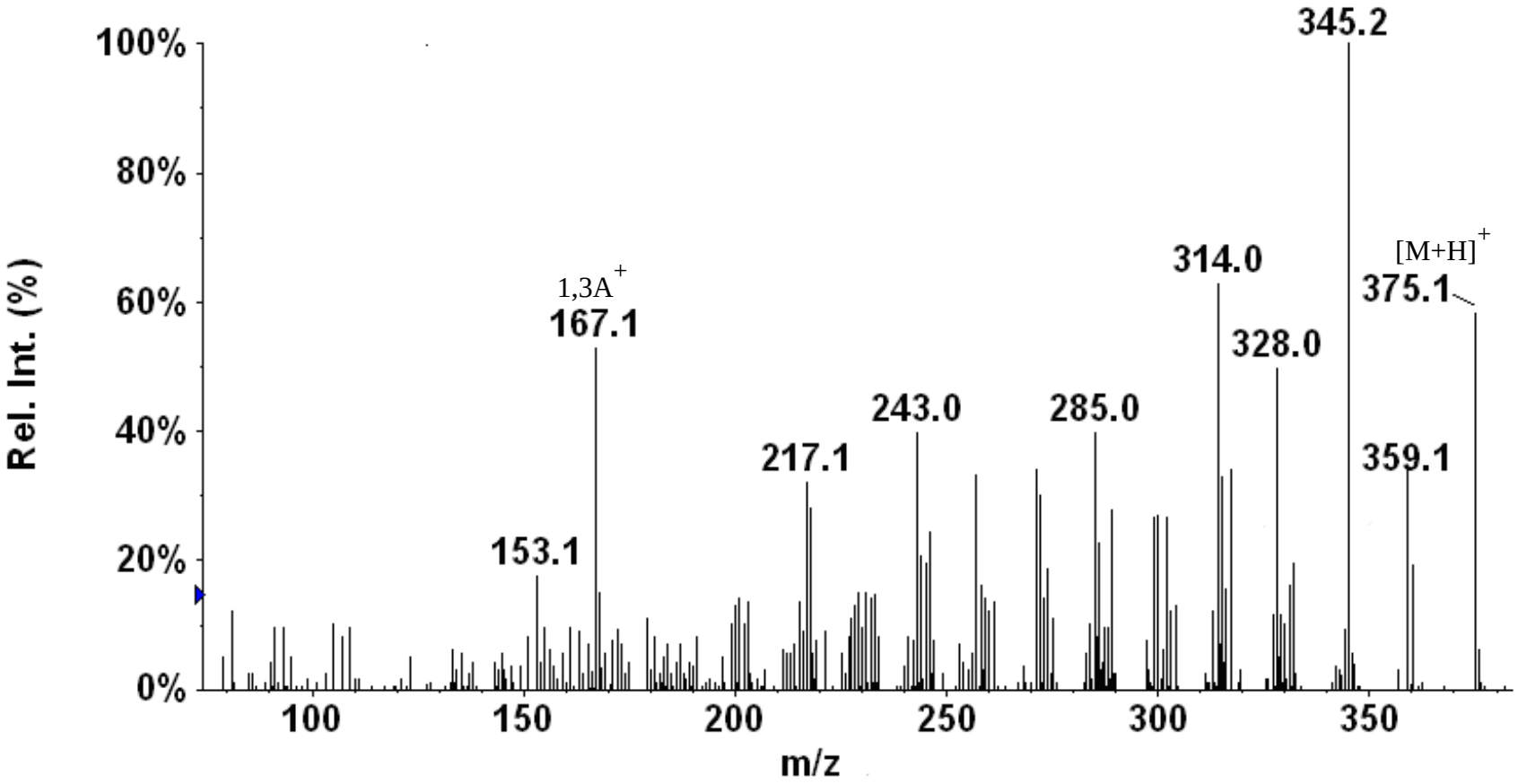

Figure IV-16 EPI spectrum of m/z 375 ($[M+H]^+$) for tetramethylmyricetin product (RT 10.31 min) from incubation of ShMOMT1 with 3',4',5'-trimethylmyricetin, later annotated as 3',4',5',7-tetramethylmyricetin. Data were acquired using a Qtrap 3200 mass spectrometer using electrospray positive mode and 40 V collision potential.

4.3.3 The origin of hydrogen radical loss from protonated O-methylflavonoids

In six authentic standards and products of enzymatic methylation of myricetin and its methylated analogs: 3',5'-dimethylmyricetin (Figure IV-7B), 3',4'-dimethylmyricetin (Figure IV-7C), 3',4',7-trimethylmyricetin (Figure IV-9), 3',4',5'-trimethylmyricetin (Figure IV-13B), 3',5',7-trimethylmyricetin (Figure IV-13C) and 3',4',5',7-tetramethylmyricetin (Figure IV-16), a major product ion corresponding to loss of methane (16 Dalton loss) from the protonated molecule is more abundant than loss of CH_3 (15 Dalton) using 40 V collision potential. This behavior stands in contrast to all other methylated myricetin derivatives studied, for which the product from loss of CH_3 was far more abundant than the 16 Da neutral loss. Interestingly, all six compounds that show a significant 16 Da neutral loss have two or more than two methyl substitutions on the B-ring, therefore it is concluded that that the apparent loss of methane is characteristic of compounds with two or more methyl groups on the B ring of myricetin. However, two methylated myricetins are exceptions to this rule: 3,3',5'-trimethylmyricetin (Fig IV-14A) and 3, 3',5',7 tetramethylmyricetin (Figure IV-21) , both of which have 3-position methyl groups which are more labile to loss of CH_3 than all B-ring methyl groups as discussed above. Therefore, it is suggested that a prominent loss of 16 Da from methylated myricetins is characteristic of two or more B-ring methyl groups and no substitution at the 3-position oxygen.

The mechanism that leads to loss of 16 Da from methylated myricetins with two B-ring methyl groups remains uncertain. Product ion spectra for the entire set of methylated

myricetins showed no evidence of loss of hydrogen radical from $[M+H]^+$ using CID potentials ranging from 25 to 80 V with 5 V increments. Subsequent MS^3 analysis of $[M+H]^+$—>$[M+H-15]^+$ —> product ions also failed to yield detectable fragments resulting from a hydrogen atom loss in the second dissociation. Based on these results, the possibility of a concerted loss of CH_4 cannot be discounted. If the elimination of CH_4 were concerted, the origin of the additional hydrogen must be within range of migrating to the carbon of the methyl group eliminated, such as: 1) the hydrogen involved in protonation, 2) a hydrogen atom from a hydroxyl group, most likely the 3- and 4' or 5' positions which are nearest; 3) carbon-bound hydrogen on the B-ring (e.g. 2' or 6' positions); 4) hydrogen from a nearby O-methyl group.

To address the source of the additional hydrogen in the 16 Da neutral loss from protonated methylated myricetins, product ion spectra were generated for the deuterated analogs described above. An analog with a single deuterated methyl group on the B-ring, 3'-methyl-5'(d_3)-methylmyricetin yielded neutral losses of 16 Da (-CH_4 or –CH_2D•, m/z 334), 17 Da (most likely -CH_3D, m/z 333), and 19 Da (-CD_3H, m/z 331) from the protonated molecule (Figure IV-17). In the corresponding unlabeled compound, the product from loss of CH_4 was more abundant than the product generated by loss of CH_3•. Both losses of 17 and 19 Da from the deuterated analog indicate that at least one deuterium from the 5'(d_3)-methyl group was lost in the neutral product. Similar results were also observed for other deuterated methylmyricetins including 3'(d_3),5'(d_3)-dimethylmyricetin which gave a prominent neutral loss of 20 Da (-CD_4, m/z 333) from the protonated molecule (Figure IV-18). These results provide compelling

evidence that methyl hydrogen are a source of hydrogen loss, either as a concerted loss of CH_4 or successive losses of CH_3• and H•. However, methyl hydrogens are not the only source of the lost hydrogen atom. For example, the 16 Da neutral loss product (m/z 334) from 3'-methyl-5'(d_3)-methylmyricetin corresponds to loss of CH_4, but no methyl hydrogens on the 5' position methyl group are available to donate a proton, as all are deuteriums. Therefore, this hydrogen must come from other sources. Since protonated 3',4',5'-trimethylmyricetin also yields a prominent product from loss of CH_4 (Figure IV-13B), a B-ring hydroxyl group is not a prerequisite for generating loss of CH_4. There is little evidence that B-ring free hydroxyl groups are the source of the final hydrogen, since no loss of 16 Da was observed for 3'-methyl- or 4'-methylmyricetin (Figure IV-3), both of which have two B-ring hydroxyls. Likewise, numerous methylmyricetins with hydroxyl groups on A- and C-rings did not yield loss of CH_4, suggesting that these are also not the hydrogen source. Using similar logic, all of these myricetin derivatives had protons at the 2'- and 6'-positions, and these therefore cannot show correlation with the occurrence of CH_4 loss. Having discounted the likelihood that the 2'- and 6'- hydrogens and hydroxyl hydrogens are important contributors in the neutral loss of CH_4 from 3'-methyl-5'(d_3)-methylmyricetin, attention should turn to the proton involved in ionization.

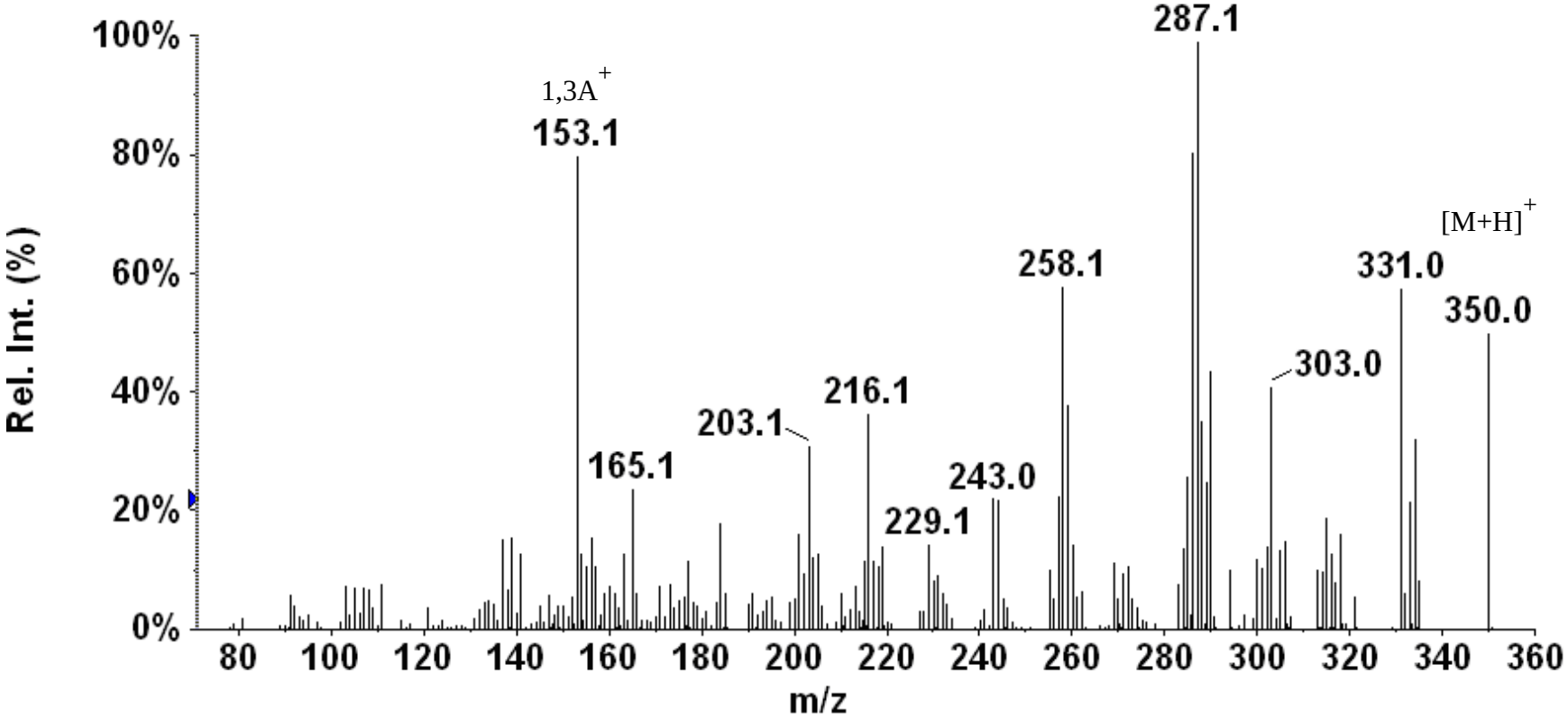

Figure IV-17 EPI spectrum of m/z 350 ($[M+H]^+$) for dimethylmyricetin products from incubation of ShMOMT2 with 3'-monomethylmyricetin and d_3-SAM, later annotated as 3'-methyl-5'(d_3)-methylmyricetin. Data were acquired using a Qtrap 3200 mass spectrometer using electrospray positive mode and 40 V collision potential.

Figure IV-17 (cont'd)

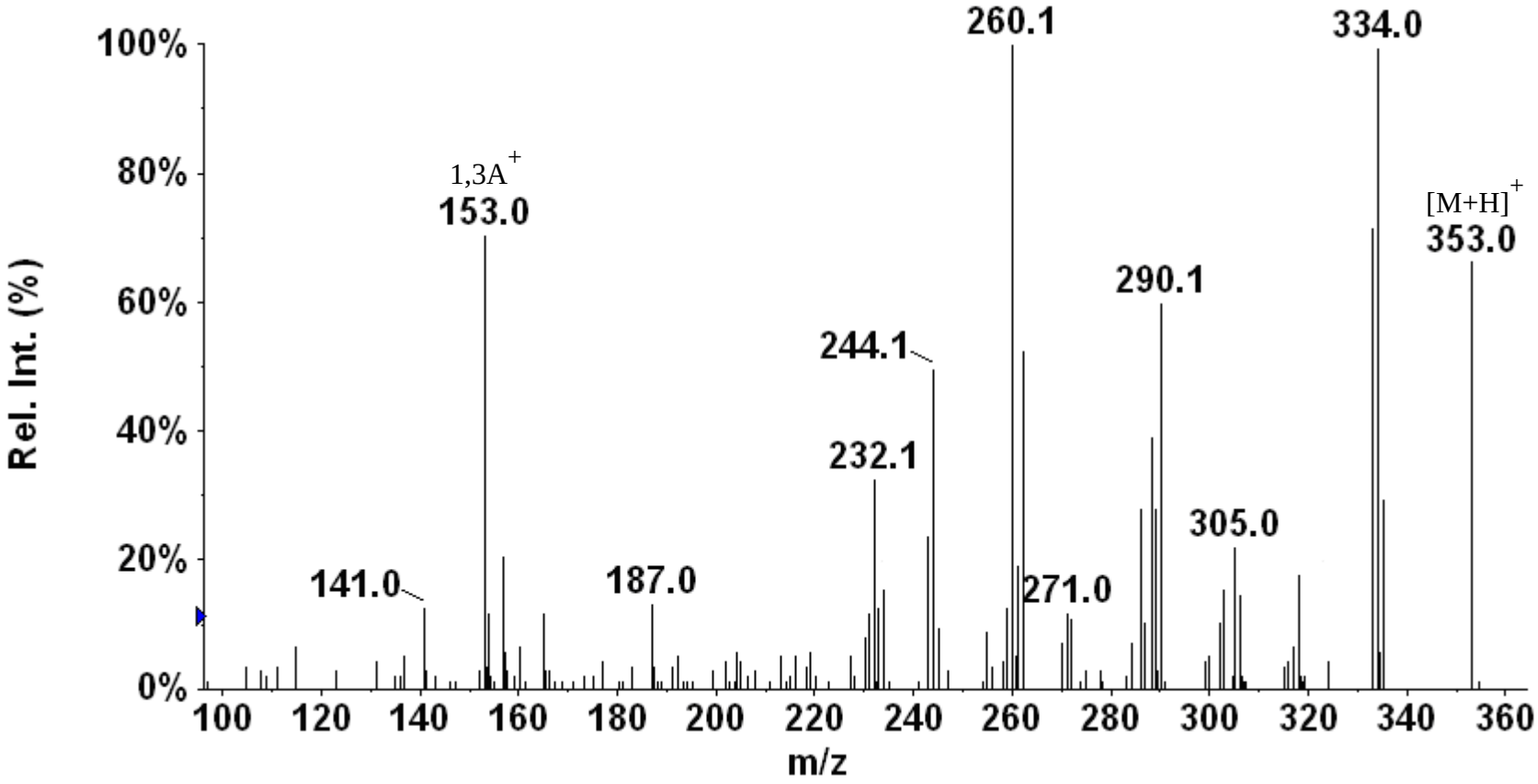

Figure IV-18 EPI spectrum of m/z 353 ($[M+H]^+$) for dimethylmyricetin product from incubation of both ShMOMT1 and ShMOMT2 with myricetin and d_3-SAM, later annotated as 3'(d_3),5'(d_3)-dimethylmyricetin. Data were acquired using a Qtrap 3200 mass spectrometer using electrospray positive mode and 40 V collision potential.

In summary, the product ion MS/MS spectra of an assortment of methylated myricetin derivatives demonstrated that neutral loss of CH4 is diagnostic for myricetin derivatives that have two or more B-ring O-methyl groups are present, provided that no methyl is situated on the 3-position (Rule #4). It is anticipated that structurally similar flavonoids such as quercetin derivatives may follow these rules of annotation owing to their similar chemical properties.

4.3.4 Application of annotation rules for identification of methylated myricetin metabolites in *S. habrochaites* LA1777 trichomes

In extracts of glandular trichomes from the wild tomato *S. habrochaites* LA1777, several compounds were detected using LC/MS profiling that exhibited molecular and fragment masses consistent with assorted methylated myricetins. The low levels of these compounds in trichome extracts precluded use of techniques such as NMR, therefore structure elucidation was performed using LC/MS/MS. For putative dimethylmyricetins, chromatographic peaks in the XIC (m/z 347) suggested two isomers of dimethylmyricetin. The more abundant of these (RT 9.51 min) matched the enzymatic product 3',7-dimethylmyricetin in both retention and fragmentation pattern (Figure IV-19). The earlier eluting but less abundant metabolite (RT 8.45 min) gave a product ion spectrum showing m/z 153 but not m/z 167, suggesting no methylation on the A-ring (5- or 7-positions). The absence of a neutral loss of 16 Da ($-CH_4$) argues against both methyl groups being on the B-ring (Rule #4). By comparison of chromatographic retention with products of enzymatic methylations, the 3,3'-dimethylmyricetin

was eliminated (Rule#1). Since this metabolite eluted later than the 3,3'- isomer (RT 8.34 min), the only remaining possibility is 3,4'-dimethylmyricetin. Here it is intriguing that a substantial difference in the pattern of methyl group losses was observed in comparisons of product ion MS/MS spectra of 3,4'-dimethylmyricetin and 3,3'-dimethylmyricetin generated using enzymatic synthesis (Figure IV-10B). For 3,3'-dimethylmyricetin, the dominant fragment ion arises from loss of a single CH_3• (m/z 332) with a substantially less abundant peak for losses of two CH_3 groups (m/z 317). In contrast, the 3,4'-dimethyl isomer yields m/z 317 (loss of two CH_3 groups) as the dominant fragment ion. Consistent with our proposed Rule # 3 (lability of methyl groups), the more facile loss of the second methyl argues for substitution at the 4' position rather than 3'.

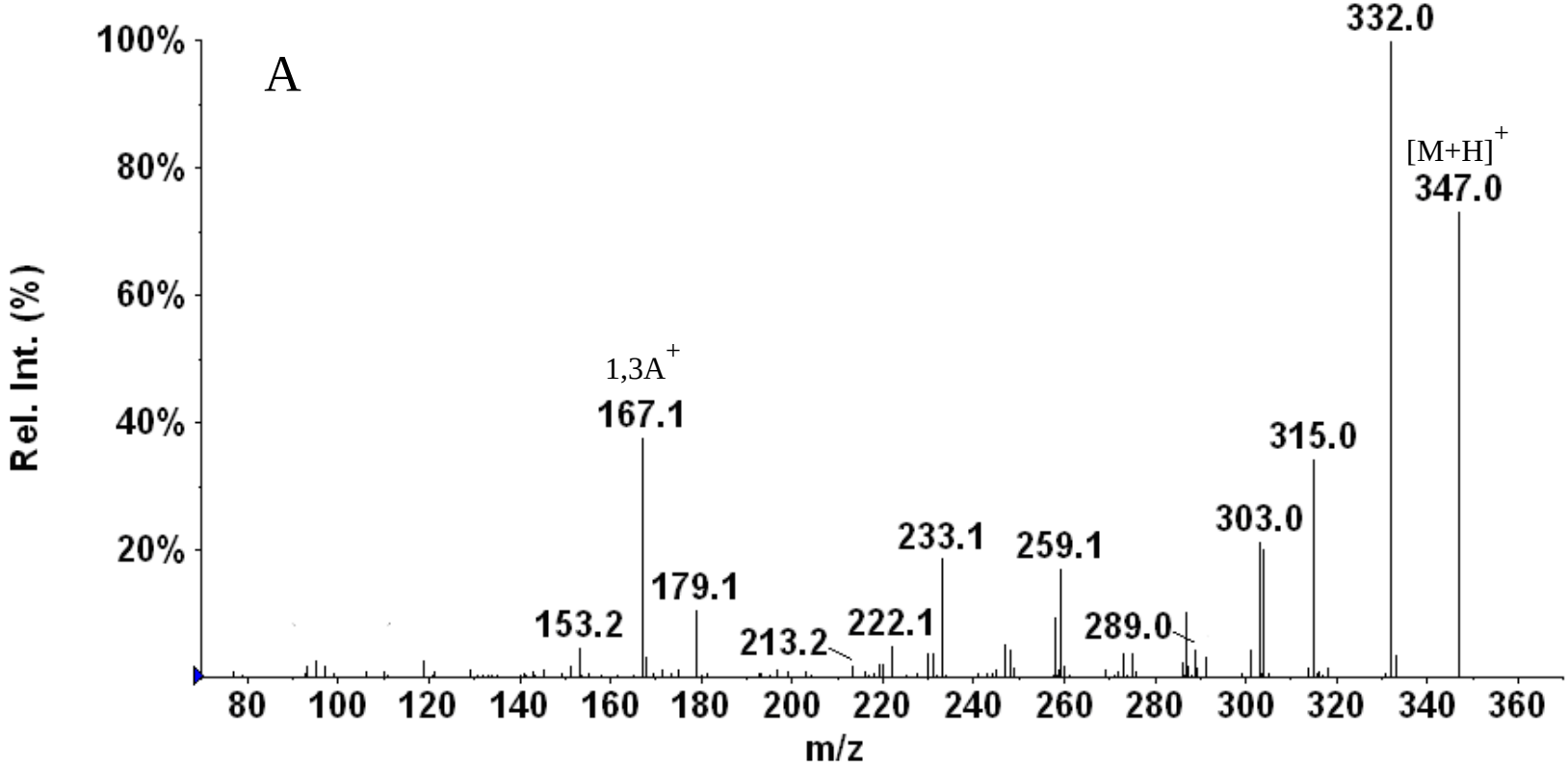

Figure IV-19 A) EPI spectrum of m/z 347 ($[M+H]^+$) for dimethylmyricetin metabolite in *S. habrochaites* LA1777 leaf dip extracts, later annotated as 3',7-dimethylmyricetin (RT 9.51 min); B) EPI spectrum of m/z 347 ($[M+H]^+$) for dimethylmyricetin metabolite in *S. habrochaites* LA1777 leaf dip extracts, later annotated as 3,4'-dimethylmyricetin (RT 8.45 min). Data were acquired using a Qtrap 3200 mass spectrometer using electrospray positive mode and 40 V collision potential.

Figure IV-19 (cont'd)

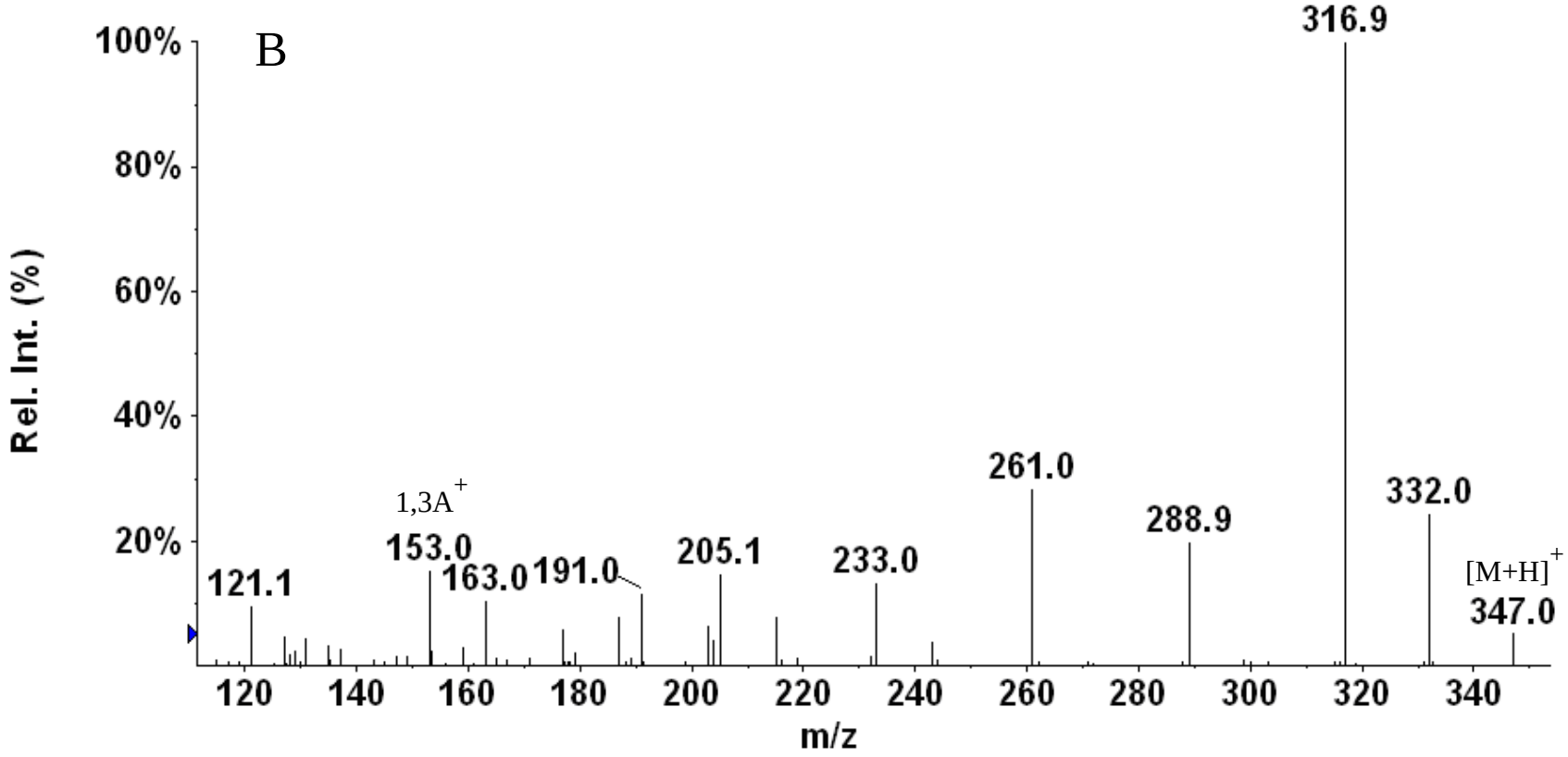

Trichome extracts of *S. habrochaites* LA1777 also yielded evidence for two trimethylmyricetin isomers (XIC of m/z 361; Figure IV-20). The later eluting chromatographic peak (RT 9.61 min) shows the m/z 167 fragment indicative of a single methyl substitution on an A-ring oxygen (Rule #2). The retention time for this peak lies between enzymatic synthesis products 3,3',5'-trimethylmyricetin (RT 9.21 min) and 3',4',7-trimethylmyricetin (RT 10.22 min). No authentic standard was available that matched this product. Based on the relatively long chromatographic retention time, we conclude the A-ring substituent is a methyl at the 7-position (Rule #1). The product ion MS/MS spectrum did not yield any major loss of CH_4 from the protonated molecule, indicating either a methyl at the 3-position or less than two methyls on the B-ring (Rule #4). From this information, two candidates remained: 3,3',7- or 3,4',7-trimethylmyricetin. As discussed above, the 4'-methyl group is more labile upon CID than the 3'- methyl. Relative abundances of the residual precursor ion to product ions attributed to losses of one and two CH_3 groups are useful diagnostics of the lability of the methyl substituents (Rule #3). For this more abundant trimethylmyricetin isomer, relative abundances match 3,3'-dimethylmyricetin (Figure IV-10B) better than 3,4'-dimethylmyricetin (Figure IV-19B), so it was annotated as 3,3',7-trimethylmyricetin. The less abundant isomer (RT 9.32 min) yielded m/z 153 rather than m/z 167 peaks indicating no A-ring substituent (Rule #2). It elutes earlier than the 3',4',5'- isomer (RT: 9.7 min) but slightly later than 3,3',5'-trimethylmyricetin (9.21 min). Excluding candidates with methylation at the 5- position (as these are expected to elute earlier) (Rule #1), and two standards, the commercial 3',4',5'- isomer and the enzyme product

3,3',5'-trimethylmyricetin which did not match retention time or fragmentation, the only remaining option was 3,3',4'-trimethylmyricetin. Although two methyl groups are situated on the B-ring, the methyl group on the 3- position is most labile and dominates the product ion spectrum, precluding the 16 Da loss that would occur in its absence.

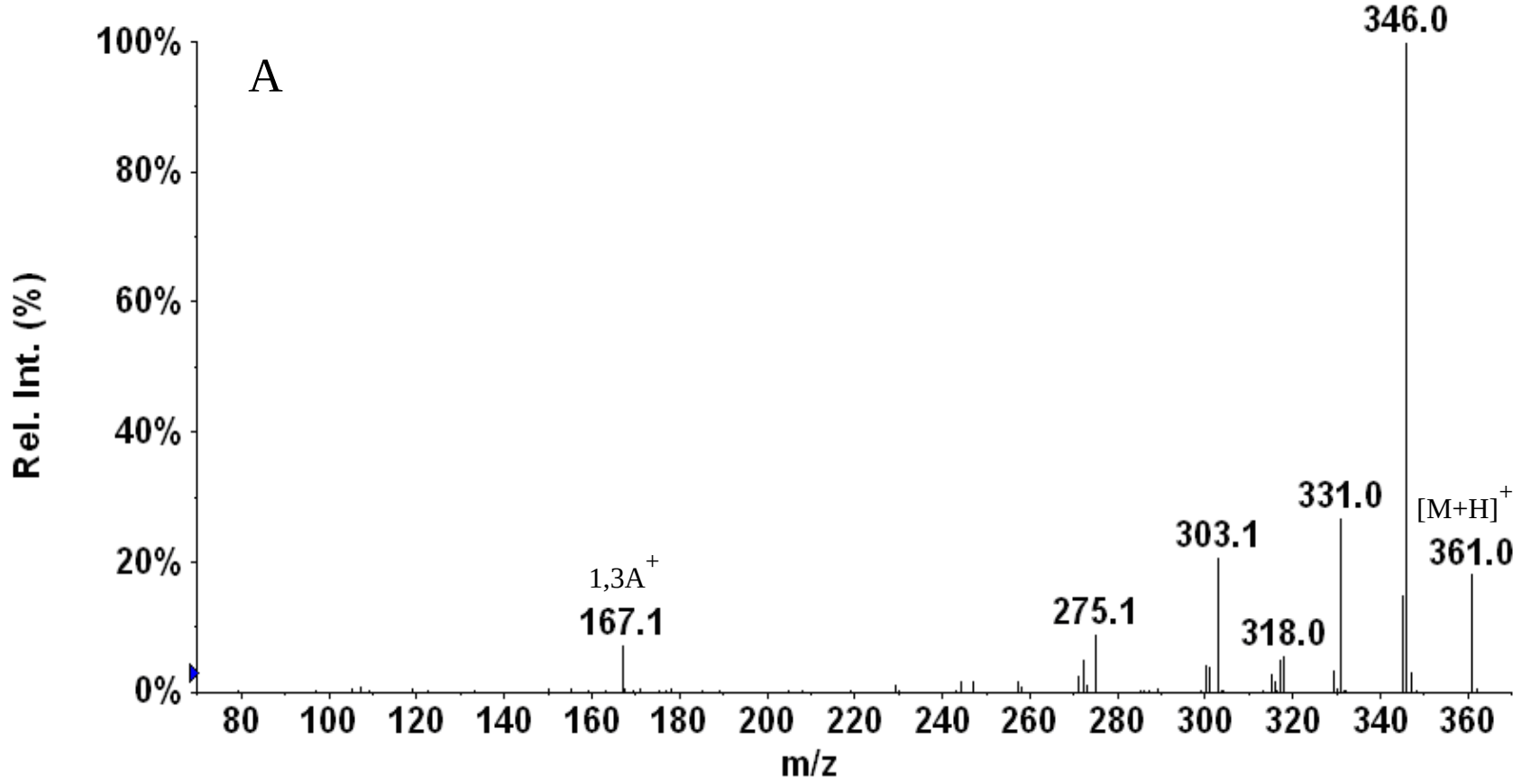

Figure IV-20 A) EPI spectrum of m/z 361 ($[M+H]^+$) for trimethylmyricetin metabolite in *S. habrochaites* LA1777 leaf dip extracts, later annotated as 3, 3',7-trimethylmyricetin, (RT 9.61 min); B) EPI spectrum of m/z 361 for trimethylmyricetin metabolites in *S. habrochaites* LA1777 leaf dip extracts, later annotated as 3,3',4'-trimethylmyricetin. (RT 9.32 min). Data were acquired using a Qtrap 3200 instrument using electrospray positive mode and 40 V collision potential.

Figure IV-20 (cont'd)

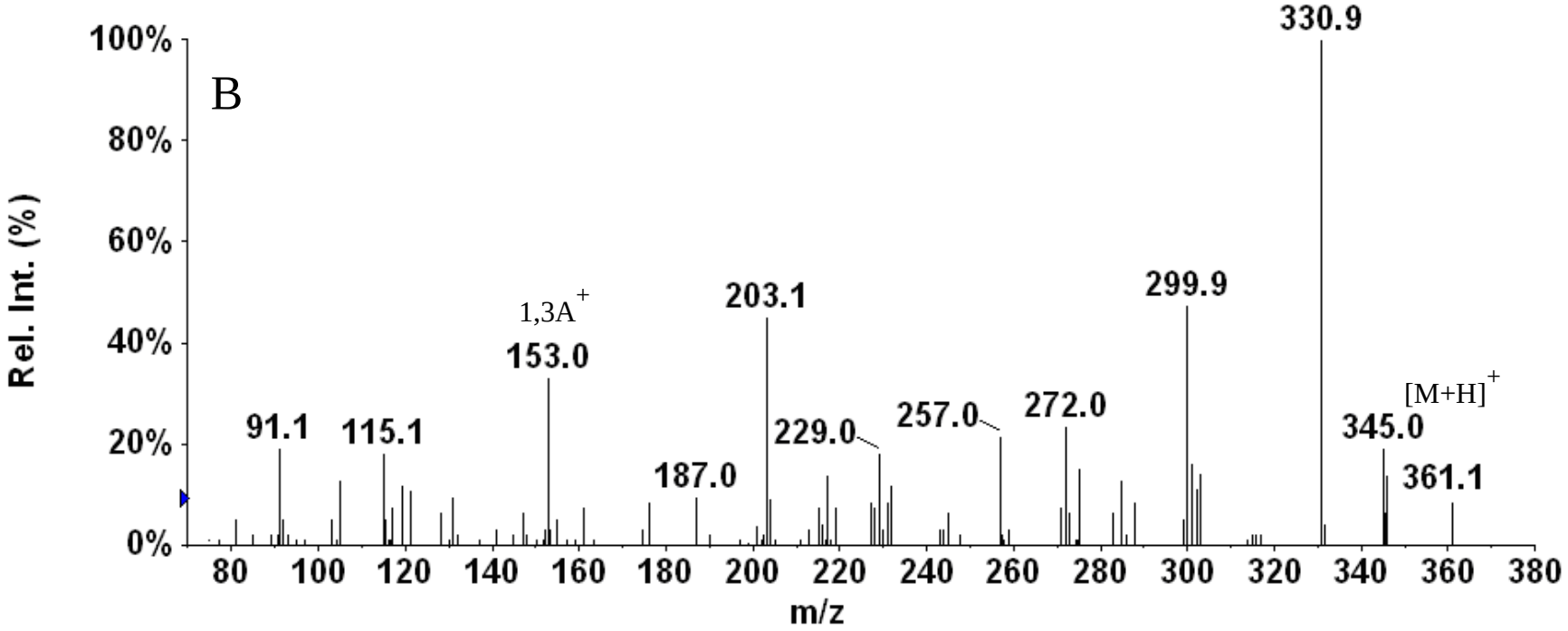

The trichome extract yielded a single chromatographic peak (RT 10.48 min) corresponding to a tetramethylmyricetin for which the product ion MS/MS spectrum was generated (Figure IV-21). The m/z 167 fragment ion indicates one methyl substituent on the A-ring (Rule #2). This metabolite eluted later than enzyme product 3,3',4',5'-tetramethylmyricetin (9.81 min), indicating that the A-ring methylation is on the 7- position (Rule #1). The absence of a fragment corresponding to loss of CH_4 eliminates the 3',4',5',7- isomer, and based on the relative abundances of the unfragmented precursor and successive methyl loss peaks, the best match was 3,3',5',7-tetramethylmyricetin (Rule #3, 4).

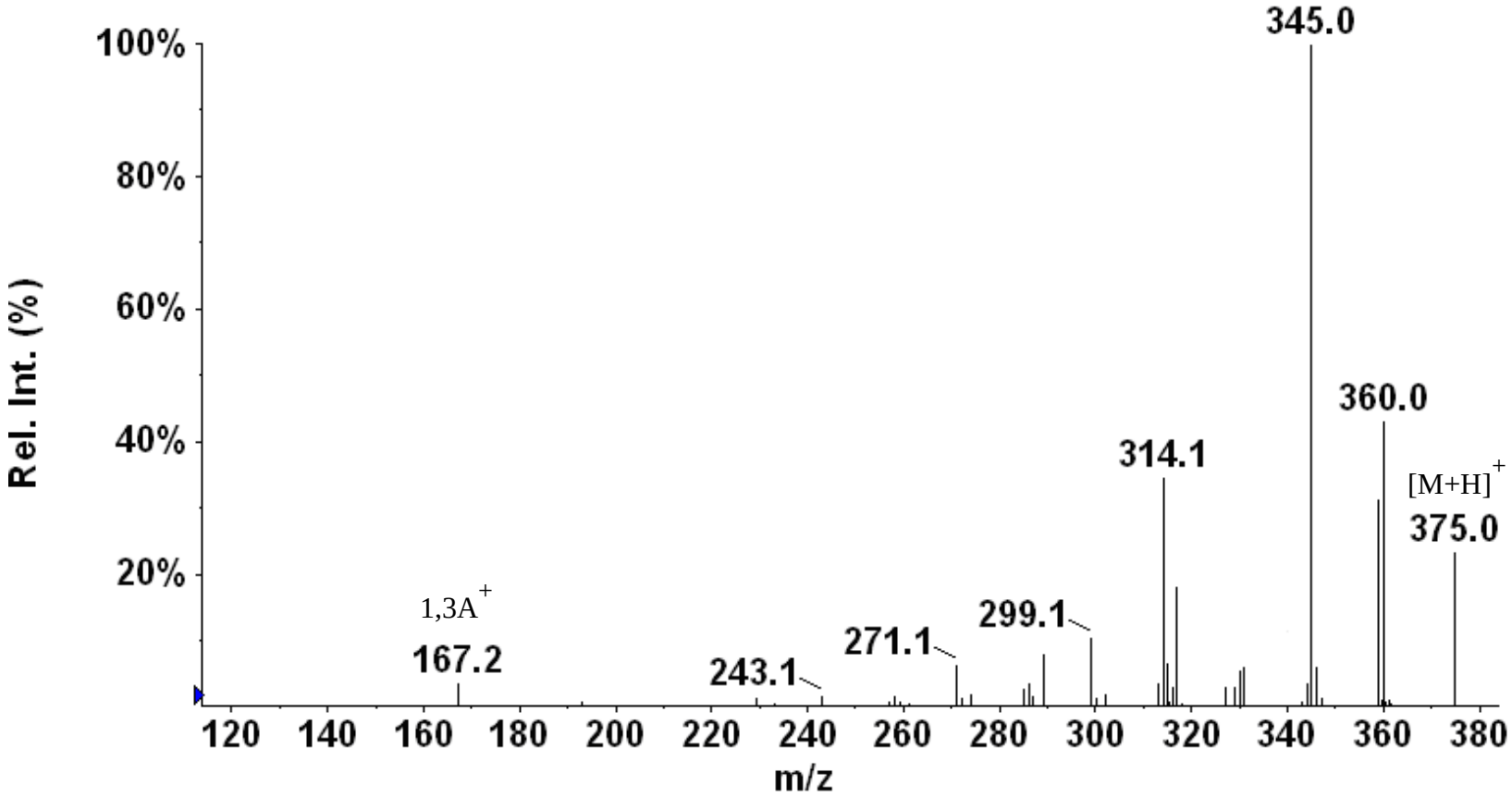

Figure IV-21 EPI spectrum of m/z 375 ($[M+H]^+$) for tetramethylmyricetin metabolite in *S. habrochaites* LA1777 leaf dip extracts, later annotated as 3,3',5',7-tetramethylmyricetin, (RT 10.48 min). Data were acquired using a Qtrap 3200 mass spectrometer using electrospray positive mode and 40 V collision potential.

The LC/MS analysis of the *S. habrochaites* LA1777 trichome extract also showed evidence of a single pentamethylmyricetin (RT: 11.18 min) for which the MS/MS product ion spectrum was obtained (Figure IV-22). Again, the fragment at m/z 167 indicates one methyl substituent on A-ring (Rule #2). Only one isomer is possible with this constraint -- 3,3',4',5',7-pentamethylmyricetin.

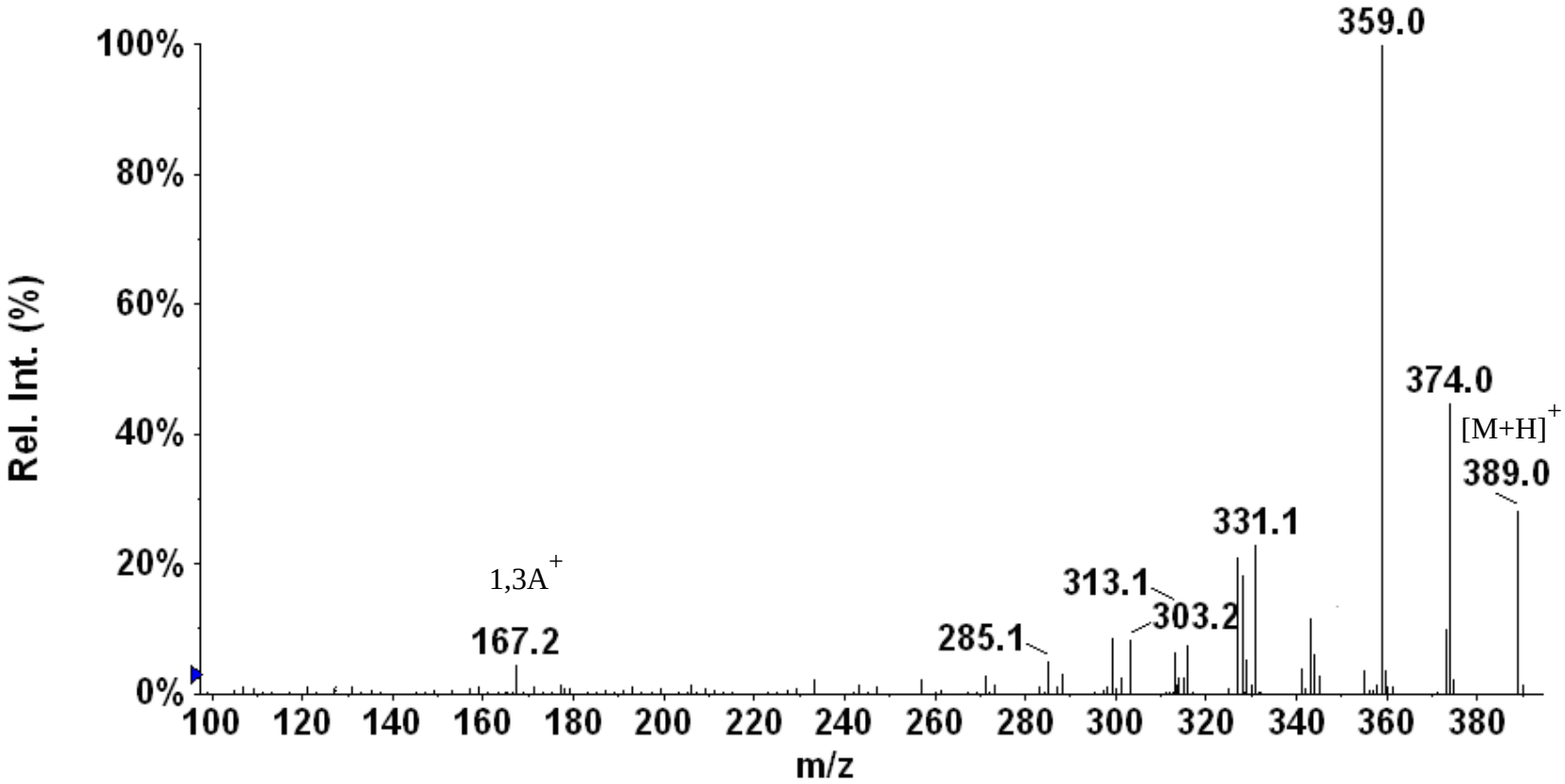

Figure IV-22 EPI spectrum of m/z 389 ($[M+H]^+$) for pentamethylmyricetin metabolite in *S. habrochaites* LA1777 leaf dip extracts, later annotated as 3,3',4',5',7-pentamethylmyricetin, (RT 11.18 min). Data were acquired using a Qtrap 3200 mass spectrometer using electrospray positive mode and 40 V collision potential.

4.4 Conclusions

Structure elucidation of methylated flavonoid regioisomers has long presented enormous technical challenges. In fact, a key 2004 review commented on this subject, "Although isomeric compounds show a different fragmentation behavior, the exact position of the methoxy group could not be defined without comparison with standards or NMR analysis." (Cuyckens 2004). Since levels of these metabolites are often too low for isolation of milligram quantities, improved strategies for mass spectrometric structure annotation have been necessary.

By combining the tools of selective enzymatic semisynthesis, HPLC, and tandem mass spectrometry, selective synthesis was achieved, including regioselective introduction of deuterated methyl groups onto the myricetin backbone. Combining these techniques allowed experiments to determine substrate selectivity of recombinant O-methyltransferase enzymes whose functions had not previously been established. In addition, MS/MS spectra of selectively labeled methylmyricetins allowed contributions of specific groups to observed fragmentation chemistry to be established.

A series of rules were presented for annotating methylated myricetins, which are:

Rule #1 [238-240]: Methylation increases chromatographic retention time differentially based on the position of the methyl group following the order 7>3'(5') ≈4'>3>5;

Rule #2: The number of methyl groups on the A-ring is evident from characteristic fragment ions (m/z 153 means 0; m/z 167 means 1; and m/z 181 means 2 methyl groups);

Rule #3: Methyl groups exhibit differential lability upon collisional activation, with the

rates of methyl loss following the order 3>4'>>3'(5')>>7;

Rule #4: Characteristic neutral loss of 16 Da (loss of CH_4) is diagnostic for two or more methyl substituents on the B-ring, and the absence of a methyl group at position 3.

Application of these rules does not require any derivatization which might introduce unanticipated artifacts or complicate analyses of other metabolites. This strategy of using LC/MS analysis coupled to recombinant enzyme assays may be applicable to other methylated flavonoids or even other enzyme catalyzed chemical isomers study.

CHAPTER FIVE

DETERMINATION OF BETAINE METABOLITES AND DIMETHYLSULFONIOPROPIONATE IN CORAL TISSUES USING LIQUID CHROMATOGRAPHY/TIME-OF-FLIGHT MASS SPECTROMETRY AND STABLE ISOTOPE-LABELED INTERNAL STANDARDS

5.1 Introduction

Corals are in decline worldwide [272, 273], and one of the most important causes of this decline is described as 'bleaching'—a reduction or loss of populations of zooxanthellae, which are algae that live in symbiotic relationships within coral tissues. Bleaching has been attributed to stresses of elevated water temperature and high light intensity acting in a synergistic manner [274-276]. Seawater temperatures only a few degrees Celsius above traditional norms have been suggested to be responsible for coral bleaching [272, 273, 277]. When corals experience bleaching, the primary insult is often to the complex of proteins known as photosystem II or to pathways of electron flow downstream from photosystem II in the coral algal symbionts [274-278]. Urgent attention deserves to be focused on factors the influence *in vivo* levels of metabolites with potential to protect photosystem II in corals against stresses of high temperature and high irradiance. In several organisms, a group of endogenous metabolites called betaines have been reported to stabilize photosystem II functions [279, 280].

Betaines of amino acids are quaternary ammonium metabolites derived from enzymatic methylation at the amino group nitrogen. The related analog dimethylsulfoniopropionate (DMSP) is a tertiary sulfonium metabolite produced by a wide range of higher plants and marine algae, and also found in (sometimes produced by) bacteria and animals [281-283]. Each of these metabolites possesses a functional group with a permanent positive charge and an acidic moiety such as a carboxylic acid that combine to confer zwitterion characteristics at physiological pH. The most firmly established function of betaines in animals is as osmolytes [284, 285], a role for which they are well poised because of their compatibility with normal structures and functions of macromolecules. In addition, in vascular plants and free-living algae, glycine betaine was found to play a key role in protecting photosystem II against a number of stresses, of which high temperature and high irradiance are noteworthy [286-290]. These effects are sufficiently established that multiple crops (or plants used as models in crop research) have been genetically engineered to increase betaine expression as a way of enhancing resistance to photosystem stress [291-296].

From preliminary investigations, accumulation of betaines to millimolar concentrations in coral tissues has been found. This finding suggests that corals synthesize high concentrations of betaines to resist the damaging effects of stressful environments, including those with elevated temperatures. In this context, Professor Richard Hill of the Michigan State University Zoology Department collected coral samples from a field location near Curacao to investigate whether betaine levels showed correlations with intensity of solar radiation, with depth in water serving

as an influence on light intensity. To achieve this goal, a reliable and accurate analytical method for quantification of betaines from coral tissues needed to be developed.

One of the challenging aspects of analysis of betaines and DMSP lies in their lack of useful chromophores, and their chemical structures have permanently charged groups that preclude gas chromatographic separation unless they are partially demethylated and converted to volatile derivatives. In the 1980s, analyses of betaines and DMSP relied on qualitative or semi-quantitative colorimetric tests that employed planar chromatography and Dragendorff's reagent [297, 298]. Because these methods are limited in their sensitivity, selectivity and quantitative accuracy, and ability to resolve multiple betaines, knowledge of the identities and absolute concentrations of betaines in biological tissues remained elusive. Pyrolytic dealkylation has allowed betaines and DMSP to be detected as their dealkylated forms using gas chromatography [299-307]. However these methods suffer from potential non-specificity, particularly if the dealkylated forms are also present in the native state. The reaction conditions used for dealkylation may convert other endogenous compounds to trimethylamine and dimethylsulfide after alkaline treatment. As a consequence, such methods may overestimate levels of tissue betaines and DMSP. For direct analysis of betaines or DMSP, chromophoric derivatives were developed for HPLC/UV detection [308-311]. However, during the use of this approach, the abundance of numerous other acidic metabolites compromises the selectivity of detection and analytical accuracy, and laborious extraction and sample preparation procedures are needed to remove matrix interferences. Similar derivatization schemes

were developed using capillary electrophoresis and UV detection, but are subject to similar complications [312-315].

The permanent cationic moieties of betaines and DMSP make mass spectrometry an attractive method for their detection, and the advent of soft ionization techniques provides a convenient means for determining their molecular masses and for efficient and mass-selective detection [316, 317]. Betaines in plant extracts were analyzed using electrospray ionization MS using off-line chromatographic clean-up [318], but the procedure employed strong basic conditions (6 M NH_3) that could cause artifacts in the measurement of metabolites such as DMSP and β-alanine betaine that are subject to base-induced decomposition. While a recent report described use of an ultraperformance liquid chromatography (UPLC)-MS method using a reversed phase column, and the procedure was applied to measure DMSP in marine algae [319], this approach relied on derivatization with a hydrophobic fluorescent tag to ensure adequate chromatographic retention on a reversed phase column and low level detection. Successful HPLC separations of betaines and DMSP have been reported using ion exchange (IC) chromatography [309, 320, 321]. However, coupling of IC with MS is complicated by mobile phase salts employed for IC separations owing to suppression of electrospray ionization by salts. These earlier achievements in the application of MS advanced the analysis of polar betaine metabolites and DMSP, but they highlight a need for improved separations of underivatized polar metabolites.

In recent years, numerous stationary phases have been developed for separations of polar metabolites [322-324]. In an earlier report from the Jones laboratory, the presence of cationic nitrogen-containing functional groups contributed to greater retention on a pentafluorophenylpropyl (PFPP) column using water-acetonitrile mixtures as mobile phase. Such retention of cationic analytes was more pronounced at high organic composition, and was attributed to simultaneous electrostatic interactions of analytes with silanol residues and hydrophobic or polar interactions of analytes with the pentafluorophenylpropyl group [325]. Mobile phase pH was found to be a critical parameter for selectivity of separation of basic compounds on PFPP column owing to pH-dependent shifts in ionization of silanol groups and analytes [325]. Such prior research offered prospects that betaines and DMSP might be separated using HPLC on PFPP columns and coupled to a mass spectrometer for metabolite identification and quantification.

In this chapter, describe a non-targeted quantitative method is described for measuring multiple betaines and DMSP in extracts of small biological samples without derivatization using HPLC-TOF-MS and a pentafluorophenylpropyl (PFPP) column for separation. This approach involves minimal sample processing, gentle processing conditions, and provides chromatographic resolution of isomeric and isobaric analytes with stable isotope-labeled internal standards for accurate quantification. In addition, this chapter presents an alternative synthetic scheme for preparation of deuterium-labeled DMSP for use as an internal quantification standard.

5.2 Materials and methods

5.2.1 Chemicals

Glycine betaine hydrochloride, β-alanine, γ-aminobutyric acid (GABA), iodomethane, iodomethane-d_3, 3-mercaptopropanoic acid, and 5-aminovaleric acid were purchased from Sigma-Aldrich (St. Louis, MO, U.S.A.). L-alanine and pivalic acid were obtained from Fluka. Proline was purchased from Applied Science. Glycine, ammonium acetate, methanol, 88% formic acid, and acetonitrile were purchased from VWR Scientific, and D_2O was purchased from Isotec, Inc. Unless otherwise stated, all other reagents were analytical or HPLC grade and were used without further purification.

5.2.2 Collection and extraction of coral tissue samples

Samples of whole corals were collected from Curaçao (Netherlands Antilles) and frozen as soon as possible in liquid nitrogen or dry ice. Coral samples were stored in dry ice during shipping and stored in a -80°C freezer afterward until sample extraction. Pieces of coral (~1-9 cm^2 surface area) were removed from the freezer, held at room temperature for 10-15 minutes, and transferred into a small polyethylene bag. Tissue was first blasted from the coral surface using a high-pressure stream of ice-cold distilled water from a Water-pik. The volume of the water with blasted tissue (collectively termed the *blastate*) was measured in a graduated cylinder.

Typical volume of blastate was about 50 mL. Then the blastate was immediately mixed 2:1 (v/v) with methanol and acidified to 3% formic acid. The treated blastate was vortexed to suspend any cellular debris. A 596-µL aliquot was promptly removed, and 4.0 µL of a stock solution containing a mixture of eight deuterated internal standards was added. Based on results from preliminary coral tissue extractions, the internal standard was added to yield 60 µM (36 nmol) for deuterated betaines of glycine and proline and 6.0 µM each (3.6 nmol) for the remaining six deuterated standards. Extraction was facilitated by sonicating the extracts in an ice bath for 10 min followed by centrifugation at 8000x*g* for 5 min and removal of the supernatant. The pellet was then resuspended in the same extraction solvent by vortexing, and centrifugation was repeated, to improve extraction efficiency. The supernatants were combined and evaporated to dryness using a SpeedVac. The dried residue was then redissolved in 600 µL of initial HPLC mobile phase (1% methanol/99% water, adjusted to pH 3.85 with formic acid) in preparation for LC-MS analysis.

5.2.3 Internal standard synthesis, characterization and quantification

Betaine standards that were not commercially available were synthesized following procedures described previously [326]. Betaine standards were synthesized by reaction of 1 mmol of amino acid and 16 mmol of CH_3I in 20 ml 1:1 (v:v) methanol/water mixture plus 1 g of $KHCO_3$. Reaction vessels were protected from light using aluminum foil, and reactions were allowed to proceed for 16 hours at 25 ˚C. Deuterium labeled betaine standards were

made by incubating the same amino acids with CD_3I using the same amounts of reagents and reaction conditions. The reaction solvent was then evaporated under a stream of N_2 gas and the residue was partitioned using 5 ml of chloroform with 5 ml of distilled water. The upper aqueous layer, which contains betaines, was collected. Labeled and unlabeled standards of dimethylsulfoniopropionate (DMSP) were synthesized by the reaction of CH_3I with 3-mercaptopropanoic acid in the same fashion but with 0.03 g of NaOH and 0.17 g of KH_2PO_4 as buffer. To stabilize the base-sensitive DMSP after solvent partitioning, the aqueous layer was promptly adjusted to pH~3 by addition of formic acid. All of the standards were stored at -20 ˚C until further use.

5.2.4 NMR characterization and quantification

Synthetic standards were characterized by ^{1}H-NMR spectroscopy using a Varian Inova 300 MHz spectrometer. For synthetic standard quantification, 1.0 mg of pivalic acid was added to 1.00 ml of synthetic standard solutions and co-dried in a drying oven at room temperature. Dried residue was redissolved in 99.9% D_2O. A ^{1}H water suppression pulse was employed to suppress the water resonance to aid accurate integration of methyl proton resonances. Peak areas of the methyl group proton resonance from pivalic acid and methyl group proton resonances from betaines were integrated, and used to calculate betaine concentrations. Concentrations of synthetic deuterium-labeled betaines were determined by LC-MS by comparisons to responses from unlabeled betaines. Quantification was performed

by comparing peak areas of extracted ion chromatograms of known concentrations of unlabeled betaine and DMSP standards with responses for deuterium-labeled betaine and DMSP solutions. After establishing concentrations of stock solutions of deuterium-labeled betaines and d_6-DMSP, known amounts, ranging from 1.6 to 34 nmol of deuterated betaines and d_6-DMSP, were added to each coral tissue extract, and isotope dilution was employed to quantify betaines and DMSP in these extracts.

5.2.5 LC-MS analyses of metabolites

Three Shimadzu LC-20AD HPLC pumps and SIL-5000 autosampler were fitted with a pentafluorophenylpropyl HPLC column (150 × 2.1 mm, 5 μm particles, Supelco Discovery-HS-F5) that was coupled to a Waters LCT Premier orthogonal acceleration time-of-flight mass spectrometer. The column temperature was maintained at 60 °C. Separations employed a ternary gradient based on solvents (A) water, adjusted to various pH values for method optimization ranging from 3.4 to 4.3 by addition of formic acid, (B) methanol, and (C) 0.15% aqueous formic acid containing 10 mM ammonium acetate. The total flow rate was 350 μL/min and the injected volume was 10 μL. Metabolite detection was conducted using electrospray ionization (ESI) in positive mode. Nebulization gas flow was 350 L/h at 350 ℃, and the source temperature was 100 °C. The capillary and the cone potentials were set to 3100 and 10 V, respectively. The mass spectrometer was operated in V optics mode, tuned to give mass resolution (FWHM) of 5000. Mass spectra were acquired at a rate of 1 s/spectrum using

dynamic range enhancement, and employed a 0.05 s interscan delay. Metabolite quantification was performed by calculating extracted ion chromatograms (XICs) for $[M+H]^+$ ions for each zwitterionic betaine and DMSP using a mass window of 0.2 Da.

5.2.6 Preparation of calibration and quality control standards

Since no coral tissues were found to be devoid of betaines, it was concluded that determining limits of detection by spiking a blank coral tissue extract with standard betaines at low levels was not feasible. Instead, extracts of field-collected coral tissues were subjected to addition of unlabeled betaine standards at different levels. To accomplish this, calibration standard solutions were prepared by adding NMR-standardized betaine and DMSP standards into pH 3.85 formic acid solution (the initial mobile phase used for LC separation) to give eight different concentrations ranging from 0.1-300 μM. Aliquots of stock solutions of deuterated internal standards (IS) were added to give concentrations of 60 μM each of glycine betaine-d_9 and proline betaine-d_6, and 6.0 μM for the remaining deuterated standards. Low-, medium- and high-level quality control (QC) spiked solutions were prepared separately to contain 0.3, 20, and 250 μM of unlabeled standards and the same concentrations of deuterated standards as described above. Triplicate *Madracis senaria* tissue extracts were spiked with unlabeled standards to reach 20 or 250 μM of unlabeled betaines and DMSP in the extracts to serve as QC extracts.

5.2.7 Evaluation of analytical method performance

Peak integration, generation of calibration curves, and calculations of analyte levels were performed using the QuanLynx routine within MassLynx v. 4.1 software (Waters). Calibration curves were based upon triplicate analyses and seven non-zero metabolite levels, and linear regression of ratios of XIC peak areas of unlabeled metabolites to XIC peak areas for deuterated internal standards (A_u/A_{IS}) against levels of the unlabeled metabolites.

Limits of detection (LOD) were defined as signal-to-RMS noise of 3 for each XIC, and low limit of quantification (LLOQ) was defined as the lowest concentration that yielded signal meeting all of the following criteria: S/N $\geq$ 5, accuracy between 80-120% of the true value, and relative standard deviation $\leq$15%. Two different measures of LOD were calculated. Instrumental LODs were determined by adding standards to pH 3.85 aqueous formic acid and measuring S/N for different metabolite concentrations, and extrapolating to calculate the concentration for which S/N = 3. LODs for coral tissue extracts were determined by spiking extracts with deuterated internal standards, quantifying betaines and DMSP, measuring S/N ratios for each metabolite peak, and extrapolating to the metabolite concentration corresponding to S/N = 3.

Effects of the coral extract matrix on method accuracy and precision were evaluated by preparing and analyzing QC samples consisting of a coral tissue (*M. senaria*) extract with a cocktail of metabolites (20 or 250 µM) added both pre- and post-processing and three QC metabolite cocktail solutions (0.3, 20, and 250 µM for each metabolite) prepared in pH 3.85

aqueous solution. Five technical replicate analyses were performed each day for all QC solutions over a 3-day period.

To evaluate metabolite recoveries, coral tissue blastate was homogenized by vortexing and divided into three 500-µL aliquots. The same amount of unlabeled betaine cocktail (either 20 or 250 µM) was added to one aliquot before the processing steps of extraction, centrifugation, solvent evaporation, and redissolution. The same amount of betaine cocktail was added to a second aliquot after processing, and the third aliquot did not receive any unlabeled betaines. The cocktail of deuterated internal standards was added to each after processing. Recovery (R) was calculated for each metabolite using the following equation:

$$R = 1 - \frac{A_{post} / A_{IS-post} - A_{pre} / A_{IS-pre}}{A_{post} / A_{IS-post} - A_{endog} / A_{IS-endog}}$$

where A_{post} is the analyte peak area for unlabeled betaine introduced after sample processing, A_{pre} is analyte peak area spiked before sample processing, A_{endog} is peak area of endogenous analyte (no spike), and $A_{IS\text{-}post}$, $A_{IS\text{-}pre}$, and $A_{IS\text{-}endog}$ are peak areas of deuterated internal standard for the corresponding solutions. Four technical replicates were analyzed by LC/MS for each solution.

5.3 Results and Discussion

5.3.1 Standard synthesis, characterization and quantification

Before this report, the standard method employed for synthesis of dimethylsulfoniopropionate (DMSP) has involved reaction of dimethylsulfide with acrylic acid [327]. A drawback of this synthetic approach is posed by the volatility and odor of dimethylsulfide. Here, a new synthetic method is described that avoids using dimethylsulfide, and allows for synthesis of deuterated DMSP using the same labeled reagent (CD_3I) as was used for synthesis of deuterated betaines. Synthesis of DMSP was achieved in this case by methylation of 3-mercaptopropanoic acid using an excess of methyl iodide. The synthesis was carried out by mixing an aqueous solution of 3-mercaptopropanoic acid in pH 7.0 phosphate buffer with an equal volume of methanol, followed by addition of CH_3I. Reaction conditions avoid exposing DMSP to alkaline conditions, which promote its rapid dealkylation to dimethylsulfide and acrylate [328].

The carboxylic group on DMSP or betaines offers a secondary potential site of reaction with iodomethane to form methyl esters. To ensure that such undesirable methyl ester formation had not occurred to a significant extent, characterization of all synthetic products was performed using both LC-MS and NMR. A single peak in the extracted ion chromatogram for the protonated zwitterion was observed for each synthetic standard. NMR spectra of all synthetic standards matched expected spectra without showing detectable singlet proton resonances around

3.7 ppm corresponding to -OCH_3, confirming that methyl esterified products were below limits of detection (<< 1% of total), even in the case of the DMSP synthesis.

Separation of betaines and DMSP was achieved on the PFPP column using a ternary gradient based on water and methanol, with the aqueous pH adjusted to exploit differences in pKa values for the carboxylic groups of the various metabolites. The more hydrophobic betaines such as 5-aminovaleric acid betaine required both a higher organic concentration and addition of 10 mM ammonium acetate to the mobile phase, owing to the strong retention of hydrophobic cationic analytes at high proportions of methanol. Using 100% methanol, 30 minutes of isocratic elution failed to elute 5-aminovaleric acid betaine from the column. Such retention behavior is consistent with contributions of ion-exchange mechanisms at high organic contents as observed in an earlier study [325]. Incorporation of ammonium acetate in the initial mobile phase decreased retention and resolution of early-eluting betaines, therefore this additive was added later in the gradient.

5.3.2 Extraction of Metabolites from Coral

Several extraction methods were tested on corals before selecting the method described above. Overnight extractions of pieces of coral skeleton with tissue were judged to extract metabolites from deep in the coral skeleton, and thus were presumed to sample residues left from dead tissues. Repeated extractions of whole coral pieces with water/methanol mixtures suggested a slow and persistent release of betaines from the coral skeleton or dead tissues within

the skeleton, with levels in the third extraction declining to about 25% of betaine relative to the first extraction. To focus analyses on tissues alive at the time of coral harvesting, an approach was used employing a Water-pik, commonly used in coral studies, for selective removal of coral tissues from the skeleton surface to minimize contributions from the bulk coral skeleton and to generate information about betaine levels in tissues alive at the time of sample collection [329]. Various mixtures of methanol and water were tested as potential blasting solutions, with methanol proving to be incompatible with the Water-pik construction. Cold water blastate was immediately mixed with methanol and acidified with formic acid to quench metabolism and minimize metabolite degradation because although most betaines are stable during extraction, DMSP and β-alanine betaine are susceptible to decomposition to acrylate under basic conditions [328, 330].

The recoveries for all target betaines and DMSP from coral tissue extracts are summarized in Table V-1. Since most betaines exhibit chemical stability and high aqueous solubility, the double extraction gives high recovery for analytes from 82 -104% . The minor losses of DMSP (82-92% recovery) during sample processing do not present problems for quantitative analysis, but highlight the value of using isotope-labeled DMSP as an internal standard.

Table V-1 Mean recoveries of betaines and DMSP in spiked coral tissue extracts (n=4).

Compound	Recovery (%)	
	Low Spike (20 μM)	High Spike (250 μM)
Glycine betaine	95	95
Alanine betaine	90	88
β-Alanine betaine	104	91
DMSP	82	92
GABA betaine	98	91
Proline betaine	90	94
Hydroxyproline betaine	88	87
Aminovaleric acid betaine	102	94

5.3.3 LC-MS analyses of betaines and DMSP

Initial efforts to analyze betaines using an assortment of reversed phase HPLC columns (C4 and C18) and mobile phases provided unsatisfactory results owing to limited retention using all conditions. While addition of perfluoroheptanoic acid as an ion pairing agent afforded acceptable retention, it was decided to pursue separations that would not risk long-term instrument contamination by ion pairing reagents.

As an alternative, both ion-exchange and hydrophobic retention mechanisms offered by the PFPP stationary phase were exploited, and metabolite separations capitalized on subtle differences in pKa of the carboxylic acid moiety to achieve separation of metabolite isomers and isobaric analytes. By adjusting the pH of mobile phase, analytes including internal standards were resolved, allowing separation of multiple betaines and DMSP

metabolites (Figure V-1) in coral samples, their detection using LC-MS, and quantification by stable isotope dilution. Betaines and DMSP have groups with a permanent positive charge that confer increased water solubility and yield poor retention using reversed phase LC separations. Though retention of such metabolites can often be achieved using anionic ion-pairing reagents, such reagents often suppress ionization in mass spectrometry. Pentafluorophenylpropyl (PFPP) columns offer enhanced retention of cationic analytes using water-organic mobile phases. Unlike alkyl silica phases that minimize ionic mechanisms of retention [331], PFPP columns exploit a combination of ionic and hydrophobic retention mechanisms that provide suitable retention of betaines and DMSP.

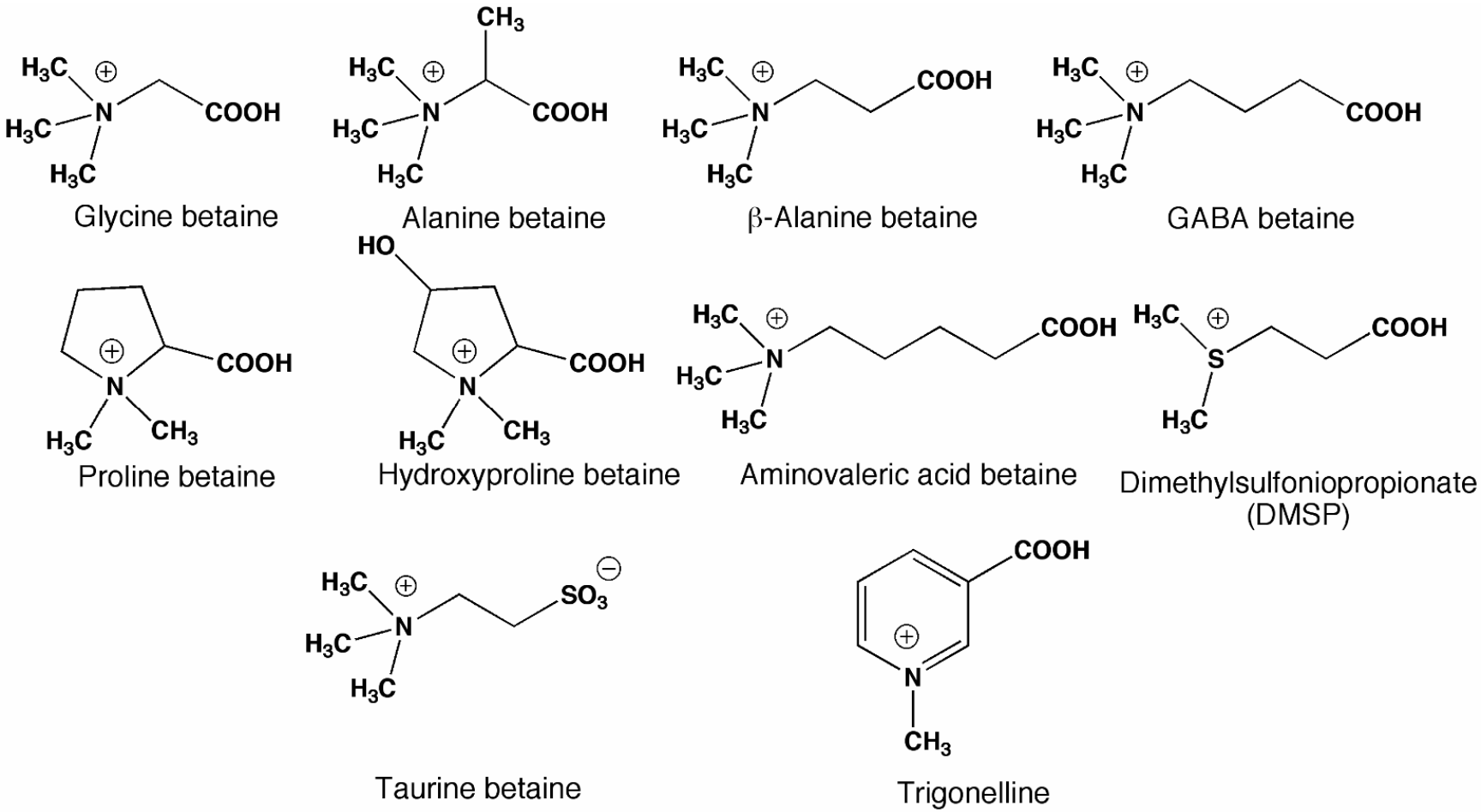

Figure V-1 Structures of betaines and DMSP detected in extracts of coral tissues.

All tested analytes yielded abundant $[M+H]^+$ ions (based on M corresponding to the neutral zwitterionic form), but several analytes are isomers or isobaric and require chromatographic separation. In addition to the two isomers of alanine betaine, three deuterium-labeled standards all give signals at a common nominal mass: namely, alanine betaine-d_9, β-alanine betaine-d_9, DMSP-d_6 are all detected as $[M+H]^+$ at *m/z* 141. Subtle differences in charge and solubility were exploited to resolve these compounds (Figure V-2). Both alanine betaine and β-alanine betaine eluted in mobile phases containing < 50% methanol, which corresponds to "reverse phase"-like conditions using PFPP columns [325]. Systematic adjustment of the aqueous solvent pH to a point near the reported pKa values, yielded chromatographic resolution that could not be achieved through hydrophobic interactions alone [331]. It is anticipated that the greater distance between the carboxylic group and the electron-withdrawing positive charge in β-alanine betaine and DMSP would make their carboxylic acid groups less acidic than betaines of alpha amino acids, and therefore have a higher proportion in neutral form within specific pH conditions. Adjusting pH of the aqueous mobile phase component to lie between estimated carboxylic acid pKa values of alanine betaine, β-alanine betaine, and DMSP enhanced retention differences. Since reference pKa values for all three compounds were not found, the optimal pH for resolving these metabolites was determined empirically. Retention of alanine betaine was unchanged from pH 3.4 to 4.3 (Figure V-2). Carboxylic acid pKa values were estimated to be ~2 for betaines of α-amino acids, so the specified retention behavior of alanine betaine is consistent with the carboxylic acid group being largely in anionic form at pH 3.4-4.3. For DMSP and β-alanine betaine, the greater distances between the cation and carboxylic acid groups

are expected to result in less acidic carboxylic acid groups. As mobile phase pH increases, an increase in retention of both β-alanine betaine and DMSP is observed, but retention decreases upon further pH increase (Figure V-2). The increased retention is attributed to an increase in ionization of surface silanol groups, followed by a decrease in retention as the carboxylic group becomes ionized at pH>4. The optimized retention is consistent with a hydrophobically assisted ion-exchange mechanism [332, 333], in which both ion-ion interaction and hydrophobic interaction are important for the retention. Mobile phase pH should be regarded as the critical parameter that can be adjusted to optimize separation of these three compounds. Optimal separation of these three metabolites was achieved at pH 3.85 for the aqueous component of the mobile phase. DMSP, alanine betaine and β-alanine betaine were well resolved using this solvent composition (Figure V-3). Adjusting column temperatures over the range of 30-60 °C had negligible effect on resolution of these three analytes.

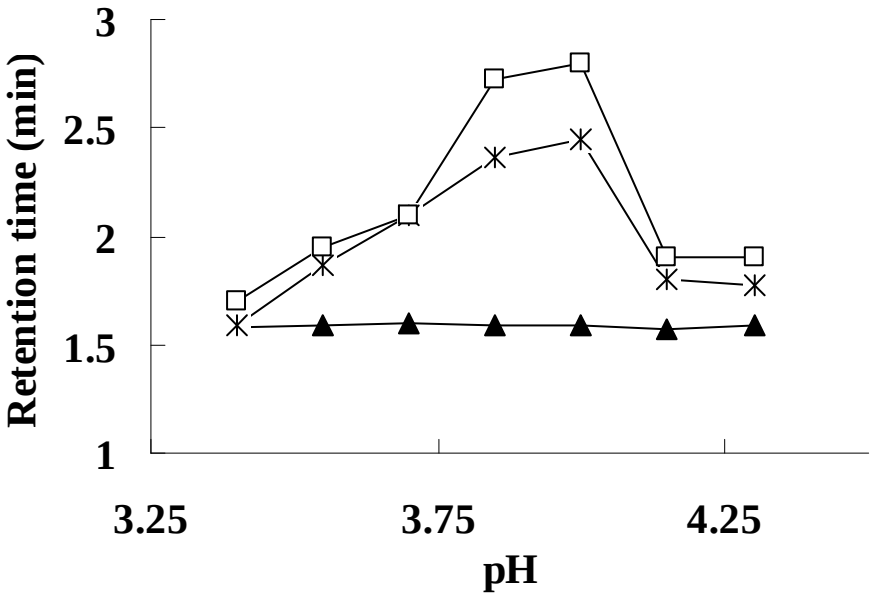

Figure V-2 Retention times of alanine betaine (□), DMSP (✳) and β-alanine betaine (▲) on a pentafluoropropyl HPLC column over pH 3.4 to 4.3 in the aqueous mobile phase component.

Binary gradients based on aqueous formic acid (pH 3.85) and methanol failed to elute aminovaleric acid betaine, which is more hydrophobic than the other detected metabolites. Such behavior is attributed to the greater hydrophobicity and the cation-exchange retention, which is more pronounced at high organic mobile phase content. To elute this metabolite without compromising the separation described above, a ternary gradient was implemented to elute long-chain and short-chain betaines in a single HPLC separation (Table V-2). This gradient was based on incorporation of a second aqueous component, after elution of the more hydrophilic betaines, that incorporated 10 mM ammonium acetate added to water, with subsequent adjustment to pH 3.85 with formic acid. The ammonium acetate provides a mechanism for displacement of the ionic retention of aminovaleric acid betaine by ammonium

cation. This gradient allowed for elution and resolution of all of the betaine analytes using a 15-min gradient.

Detection of betaines and other metabolites employed time-of-flight mass spectrometry with high mass accuracy and high mass resolution. Narrow mass-window (*m/z* 0.1) extracted ion chromatograms filtered out signal from ions with the same nominal mass, and yielded clean chromatograms for coral extracts that were useful for metabolite quantification. This approach aided nontargeted metabolite profiling for corals and other marine organisms, providing accurate mass measurements for metabolite discovery with simultaneous quantification of targeted metabolites using stable isotope dilution. In addition to the anticipated betaines and DMSP metabolites described above, additional metabolites (Figure V-1) taurine betaine (observed *m/z* 168.0727, theoretical *m/z* 168.0689) and trigonelline (observed *m/z* 138.0555, theoretical *m/z* 138.0584) were observed in coral extracts and confirmed based on accurate mass measurements and separate offline MS/MS analyses.

Figure V-3 Extracted ion chromatograms showing betaines and DMSP extracted from the tissue covering about 0.05 mm^2 area of skeleton in a specimen of the coral species *Madracis mirabilis* collected in the Netherlands Antilles. (A): Peak #1, glycine betaine (*m/z* 118, t_R 1.41 min); peak #2: alanine betaine (*m/z* 132, t_R 1.60 min); peak #3: β-alanine betaine (*m/z* 132. t_R 2.71 min); peak #4: DMSP (*m/z* 135, t_R 2.36 min); peak #5: proline betaine (*m/z* 144, t_R 1.67 min); peak #6: GABA betaine (*m/z* 146, t_R 6.68 min); peak #7: hydroxyproline betaine (*m/z* 160, t_R 1.28 min) and peak #8: aminovaleric acid betaine (*m/z* 160, t_R 8.57 min); (B): Extracted ion chromatogram for *m/z* 141, which shows peaks corresponding to chromatographically resolved internal standards alanine betaine-d_9 (peak a) DMSP-d_6 (peak b) and β-alanine betaine-d_9 (peak c).

Figure V-3 (cont'd)

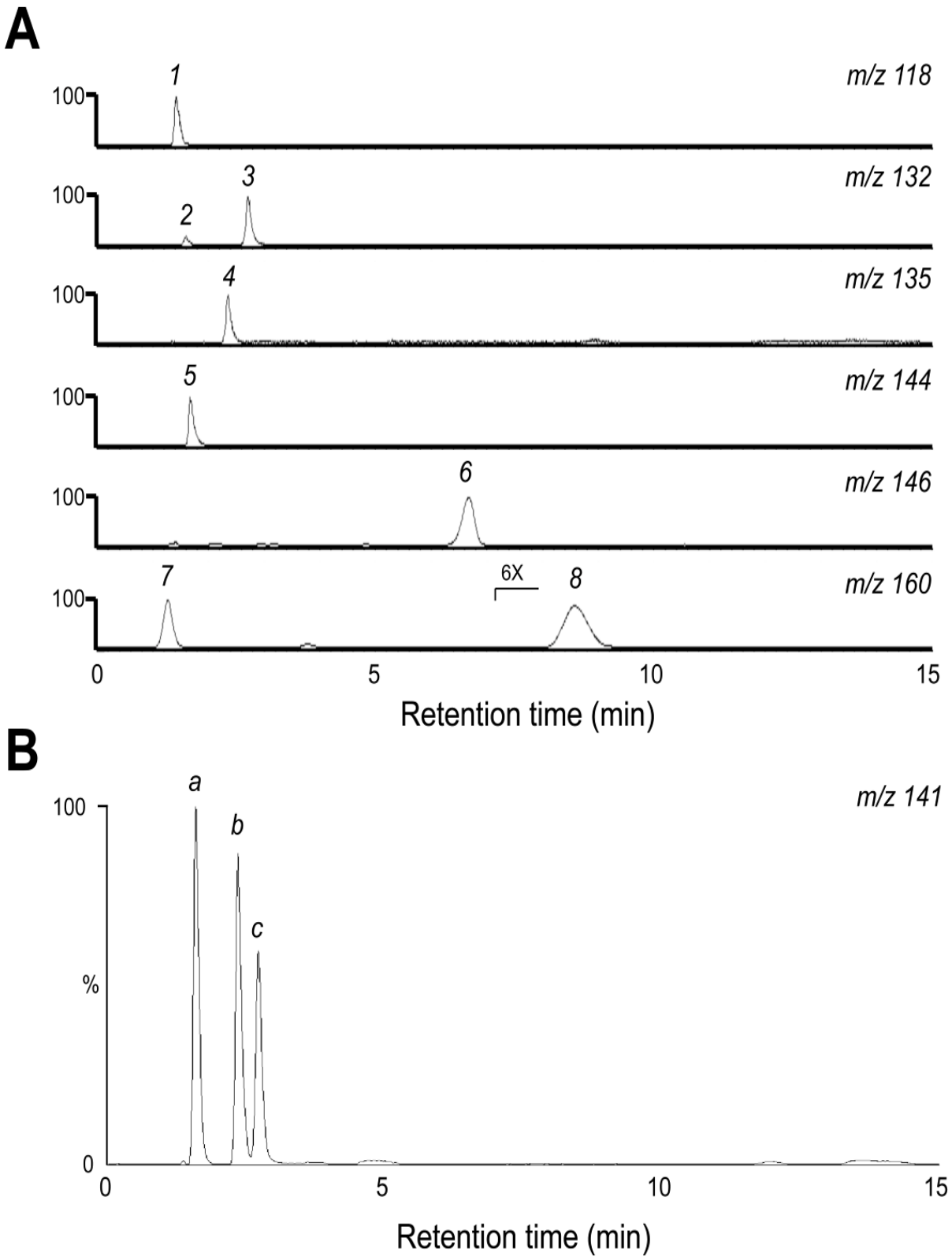

Table V-2 Solvent composition used in the ternary gradient for elution of long-chain and short-chain betaines on the pentafluorophenylpropyl silica column. Solvent A: water adjusted to pH 3.85 with formic acid, solvent B : methanol, solvent C: 0.15% aqueous formic acid + 10 mM ammonium acetate.

Time (min.)	A%	B%	C%
1.00	99	1	0
3.00	99	1	0
3.01	75	25	0
6.50	50	50	0
7.50	50	50	0
7.51	0	50	50
11.00	0	50	50
11.01	99	1	0
15.00	99	1	0

5.3.4 Method Performance and Validation

Although there are clear and comprehensive guidelines for validating quantitative methods in the context of administration of exogenous xenobiotics, there are far more questions than answers regarding how to validate methods for endogenous metabolites, especially for materials other than human plasma samples [334]. These challenges are particularly acute for studies of field-collected marine invertebrates because tissue availability is limited by the remoteness of sampling locations. Furthermore, the evidence from this study suggests that endogenous betaine levels are high in all coral samples collected, and no blank matrix was available that is free of betaines that could be used for spiking experiments to determine limits of detection.

To address a desire to evaluate method performance, calibration curves were constructed using 7 different concentrations for each betaine and DMSP in aqueous solution instead of sample matrices. Linear responses ($r^2 \geq 0.99$) were obtained over metabolite concentrations ranging from 100 nM to 300 µM. These curves were used to estimate analytical limits of detection (LOD) for standards prepared in aqueous formic acid (pH 3.85) and using spiked coral tissue extracts (Table V-3). Based on this approach, it is estimated that LODs for all tested betaines and DMSP ranged from 6-50 nM in redissolved extracts of coral tissue, which corresponds to endogenous metabolite concentrations measured in <0.05 mm^2 of sample tissue using the current protocol.

Table V-3 Limits of detection (LODs) of betaines and DMSP determined in aqueous formic acid and in coral tissue extract matrix.

Compound	LOD (nM) (in aqueous solvent)	LOD (nM) (coral tissue extract)
Glycine betaine	30	20
Alanine betaine	30	30
β-Alanine betaine	50	40
DMSP	8	15
GABA betaine	6	12
Proline betaine	30	30
Hydroxyproline betaine	8	6
Aminovaleric acid betaine	6	11

Method intra-day and inter-day accuracy and precision are summarized in Table V-4. All of the quality control analyses met the criteria that accuracy between 80-120% of the true value,

and relative standard deviation ≤15%, demonstrating that the method is robust and reproducible. The data from the two quality controls made in coral extracts suggests that using the aqueous calibration curve with stable isotopic labeled standards can accurately and precisely quantify the sample in coral matrix.

All coral tissue extracts contained one or more abundant betaines, and blank field-collected coral tissues were not available for evaluating method performance using procedures normally employed for exogenous xenobiotics, as commonly practiced in a pharmaceutical analysis context. To address effects of the coral tissue extract matrix on instrument response and quantitative performance of the method, the matrix effect (ME) was calculated as

$$ME = \frac{A_{post} - A_{endog}}{A_{sspike}}$$

where A_{post} is metabolite peak area for post-process standard addition, A_{endog} is the peak area of endogenous metabolite without spike, and A_{sspike} is metabolite peak area for spiked aqueous solvent without tissue extract. After addition of a betaine cocktail to a coral tissue extract at two different metabolite levels (20 and 250 μM), the processed extracts were analyzed and the effect of matrix on analyte signal was calculated (Table V-5). The decrease in analyte signal caused by the matrix was never greater than 11% for any of the metabolites. This surprisingly small matrix effect is attributed to the high betaine concentrations found in corals relative to other cellular constituents, which allowed blasting of tissue quantities of a few milligrams or less into a blastate volume of about 50 mL. This extensive dilution reduces concentrations of matrix constituents, including betaines and DMSP, by 2-3 orders of magnitude. Substances that might

suppress ionization are also diluted, and have minimal effects on ionization of betaines and DMSP.

Table V-4 Accuracy and precision of quality control samples with addition of multiple betaine metabolites and DMSP.

Compound	Nominal concentration (μM)	Intra-day (n=5)		Inter-day (n=3)	
		Accuracy (%)	CV (%)	Accuracy (%)	CV (%)
Glycine betaine	0.3	89	6	92	5
	20	93	4	91	5
	250	95	4	96	7
	20 (coral matrix)	106	6	103	6
	250 (coral matrix)	103	2	106	3
Alanine betaine	0.3	91	5	95	4
	20	106	6	106	3
	250	98	4	95	5
	20	91	6	94	5
	250	94	9	97	6
β-Alanine betaine	0.3	116	8	112	8
	20	98	5	95	8
	250	97	5	96	5
	20 (coral matrix)	93	3	92	2
	250 (coral matrix)	109	13	106	12
DMSP	0.3	84	3	90	6
	20	89	6	93	7
	250	95	4	96	6
	20 (coral matrix)	95	5	92	5
	250 (coral matrix)	97	5	97	7
GABA betaine	0.3	94	5	91	7
	20	106	7	112	4
	250	102	5	108	5
	20 (coral matrix)	97	7	95	10
	250 (coral matrix)	93	10	91	12
Proline betaine	0.3	91	7	93	7
	20	94	5	93	4
	250	97	4	99	6
	20 (coral matrix)	108	8	107	3
	250 (coral matrix)	108	4	105	6

Table V-4 (cont'd)

Hydroxyproline betaine	0.3	90	4	91	6
	20	96	4	93	4
	250	106	7	108	8
	20 (coral matrix)	98	3	94	4
	250 (coral matrix)	103	6	99	6
Aminovaleric acid betaine	0.3	108	9	109	11
	20	96	7	95	6
	250	96	4	94	6
	20 (coral matrix)	92	9	93	10
	250 (coral matrix)	102	4	94	5

Table V-5 Experimental determination of matrix effect on determination of individual betaines and DMSP in coral tissue extracts (n=3).

Compound	QC sample (20 μM)		QC sample (250 μM)	
	Matrix Effect (%)	CV (%)	Matrix Effect (%)	CV (%)
Glycine betaine	89	6	90	8
Alanine betaine	90	4	92	6
β-Alanine betaine	93	3	92	7
DMSP	93	7	94	8
GABA betaine	95	5	94	7
Proline betaine	93	4	93	7
Hydroxyproline betaine	93	5	94	5
Aminovaleric acid betaine	97	5	96	6

Since subtle changes in mobile phase pH have critical effects on chromatographic resolution of the two alanine betaine isomers and DMSP, the stability of freshly prepared mobile phase solvent was also tested. Three replicate 250 ml volumes of solvent A were prepared at pH 3.85 and stored in sealed glass bottles at room temperature. The bottles were opened to the air every 12 h, and the solution pH was measured using a calibrated pH meter. The rate of pH drift was

calculated to be 0.02±0.01 pH units/24 h, and reached pH 3.97±0.03 after 7 days storage. Since baseline chromatographic resolution of DMSP and the two alanine betaine isomers was achieved over the pH range of 3.8-4, it is recommend that fresh mobile phase solution A be prepared at least once a week.

5.4 Betaine in coral reef samples

Betaines were the most abundant metabolites detected within the 50–1,500 Dalton range of molecular masses from coral extracts. Tissue molar concentrations of betaines were estimated by assuming a model tissue thickness of 1 mm. Taking this approach, 10% of the tissue shows molar concentration of a individual betaine in mmol per liter of tissue volume and summed tissue molar concentrations of all betaines estimated in this way were 12 to 204 (mean = 75) mmol per liter of tissue volume in 110 coral samples. Studies of other photosynthetic organisms indicate that tissue molar concentrations of this magnitude are sufficient for stabilization of protein and membrane functions by betaines [293-296]. Operative subcellular betaine concentrations in Curacao coral tissues are probably substantially higher than those estimated here because the estimation assumes a homogenous subcellular distribution, whereas betaines are probably, in fact, more concentrated in some subcellular regions than others.

Although the biological function of betaine in coral is yet to determined, this study shows strong evidence that corals substantially modulate tissue concentrations of betaines in response to environmental conditions.

For study of patterns of variation in betaine concentrations in field populations of corals, *Madracis mirabilis* was the focal species because its is common at a wide range of depths, where it grows almost always in fully exposed (unshaded) locations [335], so that (on a given reef) the depth of a colony is an excellent proxy for the irradiance the colony experiences. The concentrations of several betaines: glycine betaine (GlyB), alanine betaine (AlaB), proline betaine (ProB), and hydroxyproline betaine (HproB) varied inversely with depth (Table V-6). The second species *Madracis pharensis* occurs in both exposed and highly shaded locations at most depths shows concentrations of several betaines averaged significantly higher in exposed than shaded colonies (Table V-7). Furthermore, *Madracis senaria*, which is the most exposed colonies available at three depths (5, 10, and 20 m) at two times (morning and afternoon) shows GlyB, AlaB, and HProB were more concentrated in afternoon (15:30-17:00 local time) - than morning (09:30-11:00 local time) -collected specimens (Table V-8).

The metabolite profiling of betaine shows the correlation of betaine level with irradiance level, which calls for focused consideration of the full range of roles that betaines play. The deeper understanding of betaine function may give opportunities to prevent the decline of coral worldwide.

Table V-6 Concentrations (mean ± SE) in *Madracis mirabilis* collected from exposed (unshaded) locations. Values for specific depths are listed only for compounds that showed statistically significant differences in concentration as a function of depth. AlaB = alanine betaine, βAlaB = β-alanine betaine, DMSP = dimethylsulfoniopropionate, GlyB = glycine betaine, HProB = hydroxyproline betaine, ProB = proline betaine, TauB = taurine betaine, Trig = trigonelline. n = 24, 8, 8, and 8 for the four columns.

	concentration ($100 \times \mu mol\ cm^{-2}$)			
compound	all colonies sampled	colonies at 5 m	colonies at 10 m	colonies at 20 m
DMSP	6.01 ± 0.23			
GlyB	39.8 ± 2.6	52.6 ± 3.2	37.2 ± 1.9	29.5 ± 3.4
AlaB	3.55 ± 0.18	4.05 ± 0.32	3.64 ± 0.27	2.96 ± 0.24
βAlaB	2.23 ± 0.45			
ProB	1430 ± 71	1640 ± 112	1520 ± 94	1140 ± 92
HProB	2.73 ± 0.31	3.32 ± 0.46	3.16 ± 0.65	1.71 ± 0.28
TauB	23.7 ± 2.7			
Trig	4.58 ± 0.39	5.90 ± 0.51	4.04 ± 0.34	3.79 ± 0.88

Table V-7 Concentrations (mean ± SE) in *Madracis pharensis* at 10 m. Values for exposed and shaded colonies are listed only for compounds that showed statistically significant differences in concentration as a function of exposure. n = 19, 10, and 9 for the three columns.

	concentration ($100 \times \mu mol\ cm^{-2}$)		
compound	all colonies sampled	exposed colonies	shaded colonies
DMSP	7.05 ± 0.82		
GlyB	38.7 ± 3.2	43.7 ± 5.0	33.2 ± 3.2
AlaB	2.99 ± 0.25	3.36 ± 0.32	2.58 ± 0.37
βAlaB	5.96 ± 1.9		
ProB	1020 ± 87	1190 ± 127	829 ± 84
HProB	4.56 ± 2.5		
TauB	16.4 ± 2.1		
Trig	2.70 ± 0.33		

Table V-8 Concentrations (mean ± SE) in *Madracis senaria* collected from exposed locations. Values for colonies collected in morning (09:30-11:00) and afternoon (15:30-17:00) are listed only for compounds that showed statistically significant differences in concentration between the times. n = 25, 7, and 18 for the three columns. Pheophytin and protein are in units of $100 \times \text{mg cm}^{-2}$.

	concentration ($100 \times \mu\text{mol cm}^{-2}$)		
compound	all colonies sampled	morning-collected colonies	afternoon-collected colonies
DMSP	8.84 ± 0.67		
GlyB	55.1 ± 4.1	35.9 ± 6.1	62.6 ± 4.0
AlaB	2.27 ± 0.20	1.63 ± 0.26	2.51 ± 0.23
βAlaB	0.601 ± 0.21		
ProB	27.2 ± 3.4		
HProB	0.861 ± 0.083	0.546 ± 0.072	0.983 ± 0.099
TauB	24.0 ± 2.4	14.4 ± 1.3	27.8 ± 2.9
Trig	11.2 ± 0.94	8.50 ± 0.82	12.3 ± 1.2

In summary, the pentafluorophenylpropyl HPLC separation provides fast and effective analyses of betaines and DMSP with high accuracy typical of isotope dilution quantitative methods. This method avoids analyte derivatization and employs an approach that is simple, rapid, and easy to conduct. This is beneficial for analysis of unstable metabolites such as DMSP, and is suitable for analysis of field-collected tissues that are frozen upon collection. The metabolite profiling of betaine metabolite by LC/MS shows the most comprehensive coverage of betaine metabolites in coral reef samples so far. A question aroused from this study is the subcellular distribution of betaines and the mechanisms that regulate betaine accumulation. In an animal–alga symbiosis, the subcellular sites of metabolite accumulation (animal or algal)

can differ from sites of metabolite biosynthesis. To fully understand the betaine function and mechanism, the localization of betaine relative to the photosynthesis protein need to be studies therefore subcellular analysis is necessary. Based on the analyses of coral extracts, this LC/MS method routinely detected multiple betaines at levels corresponding to extraction of as little as 0.05 mm^2 area of tissue. The detection limits achievable (below 100 nM in extracts) highlight the potential for using this method to perform spatially resolved profiling analyses of betaine metabolites in coral tissue if suitable microsampling methods can be developed.

CHAPTER SIX

CONCLUDING REMARKS

Compared to the more established approaches typical of modern genomics, transcriptomics, and proteomics, metabolomics is currently practiced by fewer research teams, but its application is growing at a rapid pace. Much of the appeal of metabolomics derives from the close relationship between cellular metabolite composition and phenotypes. One important aspect that one learns when doing metabolomics is an awareness of the variability between individual samples and between individual portions within a single tissue. This variation can probably be attributed to localized variation in environment, as the availability of nutrients and other regulatory molecules need not be uniform across a tissue. As an important consequence of this variability, it follows that metabolome analyses need to be performed on large numbers of tissues, using organisms grown under various environmental conditions and treatments, and by collecting subsamples from different cell populations within a tissue or organism. These factors drive an emerging principle of metabolite profiling – specificially that such analyses must be performed faster, ought to cover the metabolome more deeply, and must profile metabolites in smaller local domains within a tissue.

Identification of novel metabolites remains one of the great bottlenecks in metabolome analysis, and this limitation is particularly acute when sample sizes are small or when metabolite levels are low. Chapter II of this dissertation presented the application of a new technology called multiplexed collision induced dissociation, which generates mass spectra using several

collision energies, to profile and identify metabolites from glandular trichomes of single gland types. This technology has several layers of merit. The TOF mass spectrometry platform is inexpensive compared to other instruments that provide high mass resolution and accuracy, and the multiplexed CID approach yields such information for both molecular and fragment ions which are important for identification of novel metabolites. Multiplexed CID yields nonselective activation and fragmentation of all ions, and does not require pre-knowledge of metabolites, nor does it involve data-dependent acquisition, which can compromise comparison between samples. This approach also eliminates compound optimization steps, and can extend the dynamic range for quantifying high level metabolites [117]. With this methodology, information about thousands of metabolites was captured in a single analysis. By using this approach, metabolite profiles were used to make intra- and interspecies comparisons for trichome metabolites in specific cell types. Metabolite profiles revealed the differences in abundances of bioactive compounds in trichomes including acylsugars, glycoalkaloids, flavonoids, and several novel terpenoid related metabolites. When combined with transcript data for trichomes collected from the same tissues, the resulting database has helped identify candidate genes that may be responsible for regulating biosynthesis of specific metabolites. Research to confirm these gene functions is continuing in the laboratories of collaborators Robert Last and Cornelius Barry at Michigan State University, and Eran Pichersky at the University of Michigan. One important discovery from metabolite profiles of isolated trichomes is the recognition that discrepancies between transcript and metabolite data point to the need to investigate the dynamic behavior of both the transcriptome and metabolome.

Since metabolites may be synthesized at confined locations in a tissue such as a single cell or organelle, bulk analysis of large tissue samples often fails to differentiate biochemical behavior of cell types. As a result, metabolite profiles from whole tissues represent multiple cell types, and the behavior of individual cell types may be lost in the noise from the tissue metabolome. In Chapters II and V, sampling methods were described to collect metabolites in individual trichomes and also from epidermal tissues from field-collected corals. The resulting metabolite profiles, generated using mass spectrometric methods, provide some of the first evidence for the abundance of certain metabolites in specific tissues and cell types, and this information is expected to serve as the foundation for engineering more productive biological production of valuable chemicals and as the basis for understanding coral responses to environmental stresses.

The need for rapid and localized metabolite profiling was addressed in Chapter III, which presented a scheme capable of high throughput profiling of individual trichomes using contact printing and laser desorption ionization mass spectrometry from carbon substrates. These advances have provided some of the clearest details regarding how individual cells from a single tissue vary in chemical composition. The observation that individual glands differ substantially in composition provides a powerful reason to propel further development of metabolome imaging mass spectrometry, or 'micrometabolomics'. At the outset of this project, nearly all imaging mass spectrometry reports focused on analyses of animal tissues which were usually sectioned to yield a flat layer of tissue. Such an approach was not appropriate for imaging trichomes on plant tissue surfaces owing to their fragility and scarcity on a single sectioned plane.

The contact printing method addresses several technical challenges for mass spectrometric imaging of trichome metabolites. By rastering the laser across the printed cells, trichome chemical imaging is performed across the whole leaf tissue, while preserving spatial information about metabolite location. This approach avoids the tissue deformation encountered when fresh tissues are placed in vacuum, and also eliminates the interfering signals coming from cells below the trichomes. The graphite substrate employed for tissue printing gives a clean background spectrum using laser desorption ionization, and the cleaner spectra simplifies interpretation of metabolite mass spectra. The simple sample preparation method avoids damaging the integrity of metabolite localization which is often encountered when applying matrix to cells. The images generated in this research reached 50 µm resolution, which is suitable for single gland analysis. Chemical images of trichomes showed heterogeneous metabolite distribution across the surface of *Solanum* leaflet tissues. The factors driving this phenomenon remain unclear, but these findings may indicate that different glands were at different developmental stages at the time of sampling.

Some of the challenges encountered in distinguishing isomeric metabolites were addressed in Chapter IV, which focused on identification of isomeric methylated flavonoids. By combining enzymatic semi-synthesis using recombinant enzymes, selective incorporation of deuterium labels using enzymatic synthesis, and retention times and detection of isomer-selective fragment ions using MS/MS, an entire suite of methylated flavonoid isomers were distinguished. The success of this approach illustrates the power of combining multiple instrumental and biochemical tools to accelerate solutions to the problems of metabolite identification.

Due to the diversified physicochemical properties of metabolites, comprehensive metabolome coverage often requires nontraditional column separations, particularly for polar hydrophilic metabolites. In Chapter V, a novel separation scheme was developed for separating an assortment of betaine metabolites extracted from reef corals collected from marine field locations. The separation of several hydrophilic isobaric and isomeric metabolites was achieved through combination of judicious choice of mobile phase pH and an unusual stationary phase chemistry. Accurate profiling of betaines and the related metabolite DMSP, a precursor of atmospheric dimethylsulfide, was achieved using stable isotope dilution methodology. One important finding of this work has been that tissue levels of betaines correlate with light levels across multiple coral species, and may represent a metabolic adaptation of corals to high light stress.

Although metabolomics technologies and applications have advanced rapidly over the past decade, numerous substantial challenges remain. One major challenge is the lack of reference compounds to support structure identification, and this remains one of the great bottlenecks for metabolomics research. Second, analytical instruments and protocols now generate chemical information at remarkably fast rates. For example, between the Michigan State University Mass Spectrometry Core and the Jones laboratory, approximately 20,000 metabolite profiles are generated each year, with hundreds to thousands of compounds measured per profile. The primary goal of metabolome analysis is to answer biological questions, but this can rarely be accomplished from metabolite profiles alone. Combining metabolome data with modern tools of genetics, bioinformatics, and molecular biology promises to pose even greater interpretation

and analysis challenges, and building interdisciplinary teams that attack these issues from multiple directions should be pursued to accelerate biological discoveries. Although we remain far away from a holistic understanding of plant metabolism, the technology-driven progress made in a short time has enlightened the path towards this ultimate goal.

REFERENCES

REFERENCES

1. Eisenstein, E., Gilliland, G.L., Herzberg, O., Moult, J., Orban, J., Poljak, R.J., Banerjei, L., Richardson, D., and Howard, A.J. (2000). Biological function made crystal clear - annotation of hypothetical proteins via structural genomics. Current Opinion in Biotechnology *11*, 25-30.

2. Blattner, F.R., Plunkett, G., Bloch, C.A., Perna, N.T., Burland, V., Riley, M., ColladoVides, J., Glasner, J.D., Rode, C.K., Mayhew, G.F., et al. (1997). The complete genome sequence of Escherichia coli K-12. Science *277*, 1453-1462.

3. Goffeau, A., Barrell, B.G., Bussey, H., Davis, R.W., Dujon, B., Feldmann, H., Galibert, F., Hoheisel, J.D., Jacq, C., Johnston, M., et al. (1996). Life with 6000 genes. Science *274*, 563-567.

4. Kaul, S., Koo, H.L., Jenkins, J., Rizzo, M., Rooney, T., Tallon, L.J., Feldblyum, T., Nierman, W., Benito, M.I., Lin, X.Y., et al. (2000). Analysis of the genome sequence of the flowering plant Arabidopsis thaliana. Nature *408*, 796-815.

5. Yu, J., Hu, S.N., Wang, J., Wong, G.K.S., Li, S.G., Liu, B., Deng, Y.J., Dai, L., Zhou, Y., Zhang, X.Q., et al. (2002). A draft sequence of the rice genome (Oryza sativa L. ssp indica). Science *296*, 79-92.

6. Austin, C.P. (2003). The completed human genome: Implications for chemical biology. Current Opinion in Chemical Biology 7, 511-515.

7. Wang, Z., Gerstein, M., and Snyder, M. (2009). RNA-Seq: A revolutionary tool for transcriptomics. Nature Reviews Genetics *10*, 57-63.

8. Gygi, S.P., Rochon, Y., Franza, B.R., and Aebersold, R. (1999). Correlation between protein and mRNA abundance in yeast. Molecular and Cellular Biology *19*, 1720-1730.

9. Anderson, L., and Seilhamer, J. (1997). A comparison of selected mRNA and protein abundances in human liver. Electrophoresis *18*, 533-537.

10. Ross, J. (1995). Messenger-rna stability in mammalian-cells. Microbiological Reviews *59*, 423-450.

11. Guhaniyogi, J., and Brewer, G. (2001). Regulation of mRNA stability in mammalian cells. Gene *265*, 11-23.

12. Sumner, L.W., Mendes, P., and Dixon, R.A. (2003). Plant metabolomics: Large-scale phytochemistry in the functional genomics era. Phytochemistry *62*, 817-836.

13. Schmidt, C.W. (2004). Metabolomics: What's happening downstream of DNA. Environmental Health Perspectives *112*, A410-A415.

14. Feist, A.M., Herrgard, M.J., Thiele, I., Reed, J.L., and Palsson, B.O. (2009). Reconstruction of biochemical networks in microorganisms. Nature Reviews Microbiology *7*, 129-143.

15. Libourel, I.G.L., and Shachar-Hill, Y. (2008). Metabolic flux analysis in plants: From intelligent design to rational engineering. Annual Review of Plant Biology *59*, 625-650.

16. Fiehn, O., and Spranger, J. (2003). Use of metabolomics to discover metabolic patterns associated with human diseases. In Metabolic Profiling: Its Role in Biomarker Discovery and Gene Function Analysis (Springer), pp. 199-215.

17. Hall, R.D. (2006). Plant metabolomics: From holistic hope, to hype, to hot topic. New Phytologist *169*, 453-468.

18. Dixon, R.A., and Strack, D. (2003). Phytochemistry meets genome analysis, and beyond. Phytochemistry *62*, 815-816.

19. D'Auria, J.C., and Gershenzon, J. (2005). The secondary metabolism of Arabidopsis thaliana: Growing like a weed. Current Opinion in Plant Biology *8*, 308-316.

20. Matsumoto, T., Wu, J.Z., Kanamori, H., Katayose, Y., Fujisawa, M., Namiki, N., Mizuno, H., Yamamoto, K., Antonio, B.A., Baba, T., et al. (2005). The map-based sequence of the rice genome. Nature *436*, 793-800.

21. Beale, M.H., and Sussman, M.R. (2011). Metabolomics of *Arabidopsis thaliana*. In Biology of Plant Metabolomics (Wiley-Blackwell), pp. 157-180.

22. Gibon, Y., Blaesing, O.E., Hannemann, J., Carillo, P., Hohne, M., Hendriks, J.H.M., Palacios, N., Cross, J., Selbig, J., and Stitt, M. (2004). A robot-based

platform to measure multiple enzyme activities in Arabidopsis using a set of cycling assays: Comparison of changes of enzyme activities and transcript levels during diurnal cycles and in prolonged darkness. Plant Cell *16*, 3304-3325.

23. Stewart, D. (2011). Crops and tasty, nutritious food – How can metabolomics help? In Biology of Plant Metabolomics (Wiley-Blackwell), pp. 181-218.

24. Giovinazzo, G., D'Amico, L., Paradiso, A., Bollini, R., Sparvoli, F., and DeGara, L. (2005). Antioxidant metabolite profiles in tomato fruit constitutively expressing the grapevine stilbene synthase gene. Plant Biotechnology Journal *3*, 57-69.

25. Bino, R.J., de Vos, C.H.R., Lieberman, M., Hall, R.D., Bovy, A., Jonker, H.H., Tikunov, Y., Lommen, A., Moco, S., and Levin, I. (2005). The light-hyperresponsive high pigment-2(dg) mutation of tomato: Alterations in the fruit metabolome. New Phytologist *166*, 427-438.

26. Davuluri, G.R., van Tuinen, A., Fraser, P.D., Manfredonia, A., Newman, R., Burgess, D., Brummell, D.A., King, S.R., Palys, J., Uhlig, J., et al. (2005). Fruit-specific RNAi-mediated suppression of DET1 enhances carotenoid and flavonoid content in tomatoes. Nature Biotechnology *23*, 890-895.

27. Broeckling, C.D., Huhman, D.V., Farag, M.A., Smith, J.T., May, G.D., Mendes, P., Dixon, R.A., and Sumner, L.W. (2005). Metabolic profiling of Medicago truncatula cell cultures reveals the effects of biotic and abiotic elicitors on metabolism. Journal of Experimental Botany *56*, 323-336.

28. Dunn, W.B., and Ellis, D.I. (2005). Metabolomics: Current analytical platforms and methodologies. Trac-Trends in Analytical Chemistry *24*, 285-294.

29. Lindon, J.C., Holmes, E., and Nicholson, J.K. (2003). So what's the deal with metabonomics? Metabonomics measures the fingerprint of biochemical perturbations caused by disease, drugs, and toxins. Analytical Chemistry *75*, 384A-391A.

30. Plumb, R.S., Stumpf, C.L., Gorenstein, M.V., Castro-Perez, J.M., Dear, G.J., Anthony, M., Sweatman, B.C., Connor, S.C., and Haselden, J.N. (2002). Metabonomics: The use of electrospray mass spectrometry coupled to reversed-phase liquid chromatography shows potential for the screening of rat urine in drug development. Rapid Communications in Mass Spectrometry *16*, 1991-1996.

31. Want, E.J., Cravatt, B.F., and Siuzdak, G. (2005). The expanding role of mass spectrometry in metabolite profiling and characterization. Chembiochem *6*, 1941-1951.

32. Defernez, M., Gunning, Y.M., Parr, A.J., Shepherd, L.V.T., Davies, H.V., and Colquhoun, I.J. (2004). NMR and HPLC-UV profiling of potatoes with genetic modifications to metabolic pathways. Journal of Agricultural and Food Chemistry *52*, 6075-6085.

33. Desbrosses, G.G., Kopka, J., and Udvardi, M.K. (2005). Lotus japonicus metabolic profiling. Development of gas chromatography-mass spectrometry resources for the study of plant-microbe interactions. Plant Physiology *137*, 1302-1318.

34. Lenz, E.M., and Wilson, I.D. (2007). Analytical strategies in metabonomics. Journal of Proteome Research *6*, 443-458.

35. MacNair, J.E., Patel, K.D., and Jorgenson, J.W. (1999). Ultrahigh pressure reversed-phase capillary liquid chromatography: Isocratic and gradient elution using columns packed with 1.0-μm particles. Analytical Chemistry *71*, 700-708.

36. Verhoeven H.A., Ricde Vos C.H., Bino R.J., Hall R.D. (2006). Plant Metabolomics (Heidelberg, Germany: Springer Verlag), pp. 33-48.

37. Hill, D.W., Kertesz, T.M., Fontaine, D., Friedman, R., and Grant, D.F. (2008). Mass spectral metabonomics beyond elemental formula: Chemical database querying by matching experimental with computational fragmentation spectra. Analytical Chemistry *80*, 5574-5582.

38. Liao, W.T., Draper, W.M., and Perera, S.K. (2008). Identification of unknowns in atmospheric pressure ionization mass spectrometry using a mass to structure search engine. Analytical Chemistry *80*, 7765-7777.

39. Bocker, S., and Rasche, F. (2008). Towards de novo identification of metabolites by analyzing tandem mass spectra. Bioinformatics *24*, I49-I55.

40. Benton, H.P., Wong, D.M., Trauger, S.A., and Siuzdak, G. (2008). XCMS2: Processing tandem mass spectrometry data for metabolite identification and structural characterization. Analytical Chemistry *80*, 6382-6389.

41. Giavalisco, P., Kohl, K., Hummel, J., Seiwert, B., and Willmitzer, L. (2009). C_{13} isotope-labeled metabolomes allowing for improved compound annotation and relative quantification in liquid chromatography-mass spectrometry-based metabolomic research. Analytical Chemistry *81*, 6546-6551.

42. Martin, C., Bhatt, K., and Baumann, K. (2001). Shaping in plant cells. Current Opinion in Plant Biology *4*, 540-549.

43. Kehr, J. (2003). Single cell technology. Current Opinion in Plant Biology *6*, 617-621.

44. Kehr, J. (2001). High resolution spatial analysis of plant systems. Current Opinion in Plant Biology *4*, 197-201.

45. Moco, S., Capanoglu, E., Tikunov, Y., Bino, R.J., Boyacioglu, D., Hall, R.D., Vervoort, J., and De Vos, R.C.H. (2007). Tissue specialization at the metabolite level is perceived during the development of tomato fruit. Journal of Experimental Botany *58*, 4131-4146.

46. Fait, A., Hanhineva, K., Beleggia, R., Dai, N., Rogachev, I., Nikiforova, V.J., Fernie, A.R., and Aharoni, A. (2008). Reconfiguration of the achene and receptacle metabolic networks during strawberry fruit development. Plant Physiology *148*, 730-750.

47. Li, S.H., Schneider, B., and Gershenzon, J. (2007). Microchemical analysis of laser-microdissected stone cells of Norway spruce by cryogenic nuclear magnetic resonance spectroscopy. Planta *225*, 771-779.

48. Schneider, B., and Holscher, D. (2007). Laser microdissection and cryogenic nuclear magnetic resonance spectroscopy: An alliance for cell type-specific metabolite profiling. Planta *225*, 763-770.

49. Nelson, T., Gandotra, N., and Tausta, S.L. (2008). Plant cell types: Reporting and sampling with new technologies. Current Opinion in Plant Biology *11*, 567-573.

50. Brandt, S.P. (2005). Microgenomics: Gene expression analysis at the tissue-specific and single-cell levels. Journal of Experimental Botany *56*, 495-505.

51. Tomos, A.D., and Sharrock, R.A. (2001). Cell sampling and analysis (SiCSA):

Metabolites measured at single cell resolution. Journal of Experimental Botany *52*, 623-630.

52. Verscht, J., Tomos, D., and Komor, E. (2006). Sugar concentrations along and across the Ricinus communis L. hypocotyl measured by single cell sampling analysis. Planta *224*, 1303-1314.

53. Xu, B.J. (2010). Combining laser capture microdissection and proteomics: Methodologies and clinical applications. Proteomics Clinical Applications *4*, 116-123.

54. Balestrini, R., and Bonfante, P. (2008). Laser Microdissection (LM): Applications to plant materials. Plant Biosystems *142*, 331-336.

55. Schutze, K., Niyaz, Y., Stich, M., and Buchstaller, A. (2007). Noncontact laser microdissection and catapulting for pure sample capture. In Laser Manipulation of Cells and Tissues (San Diego: Elsevier Academic Press Inc), pp. 649-673.

56. Angeles, G., Berrio-Sierra, J., Joseleau, J.P., Lorimier, P., Lefebvre, A., and Ruel, K. (2006). Preparative laser capture microdissection and single-pot cell wall material preparation: A novel method for tissue-specific analysis. Planta *224*, 228-232.

57. An, G.H., Suh, O.S., Kwon, H.C., Kim, K., and Johnson, E.A. (2000). Quantification of carotenoids in cells of Phaffia rhodozyma by autofluorescence. Biotechnology Letters *22*, 1031-1034.

58. Berg, J., Hung, Y.P., and Yellen, G. (2009). A genetically encoded fluorescent reporter of ATP:ADP ratio. Nature Methods *6*, 161-166.

59. Chang, H.T., and Yeung, E.S. (1995). Determination of catecholamines in single adrenal-medullary cells by capillary electrophoresis and laser-induced native fluorescence. Analytical Chemistry *67*, 1079-1083.

60. Fehr, M., Frommer, W.B., and Lalonde, S. (2002). Visualization of maltose uptake in living yeast cells by fluorescent nanosensors. Proceedings of the National Academy of Sciences *99*, 9846-9851.

61. Fuller, R.R., Moroz, L.L., Gillette, R., and Sweedler, J.V. (1998). Single neuron analysis by capillary electrophoresis with fluorescence spectroscopy. Neuron *20*, 173-181.

62. Lan, H., and Kennedy, R.T. (1995). Exploring single-cell dynamics using chemically-modified microelectrodes. Trac-Trends in Analytical Chemistry *14*, 158-164.

63. Cannon, D.M., Winograd, N., and Ewing, A.G. (2000). Quantitative chemical analysis of single cells. Annual Review of Biophysics and Biomolecular Structure *29*, 239-263.

64. Kozminski, K.D., Gutman, D.A., Davila, V., Sulzer, D., and Ewing, A.G. (1998). Voltammetric and pharmacological characterization of dopamine release from single exocytotic events at rat pheochromocytoma (PC12) cells. Analytical Chemistry *70*, 3123-3130.

65. Zhang, B., Adams, K.L., Luber, S.J., Eves, D.J., Heien, M.L., and Ewing, A.G. (2008). Spatially and temporally resolved single-cell exocytosis utilizing individually addressable carbon microelectrode arrays. Analytical Chemistry *80*, 1394-1400.

66. Rubakhin, S.S., Greenough, W.T., and Sweedler, J.V. (2003). Spatial profiling with MALDI MS: Distribution of neuropeptides within single neurons. Analytical Chemistry *75*, 5374-5380.

67. Page, J.S., Rubakhin, S.S., and Sweedler, J.V. (2000). Direct cellular assays using off-line capillary electrophoresis with matrix-assisted laser desorption/ionization time-of-flight mass spectrometry. Analyst *125*, 555-561.

68. Zimmerman, T.A., Rubakhin, S.S., Romanova, E.V., Tucker, K.R., and Sweedler, J.V. (2009). MALDI mass spectrometric imaging using the stretched sample method to reveal neuropeptide distributions in Aplysia nervous tissue. Analytical Chemistry *81*, 9402-9409.

69. Holscher, D., Shroff, R., Knop, K., Gottschaldt, M., Crecelius, A., Schneider, B., Heckel, D.G., Schubert, U.S., and Svatos, A. (2009). Matrix-free UV-laser desorption/ionization (LDI) mass spectrometric imaging at the single-cell level: Distribution of secondary metabolites of Arabidopsis thaliana and Hypericum species. Plant Journal *60*, 907-918.

70. Jun, J.H., Song, Z.H., Liu, Z.J., Nikolau, B.J., Yeung, E.S., and Lee, Y.J. (2010). High-spatial and high-mass resolution imaging of surface metabolites of Arabidopsis thaliana by laser desorption-ionization mass spectrometry using colloidal silver. Analytical Chemistry *82*, 3255-3265.

71. Northen, T.R., Yanes, O., Northen, M.T., Marrinucci, D., Uritboonthai, W., Apon, J., Golledge, S.L., Nordstrom, A., and Siuzdak, G. (2007). Clathrate nanostructures for mass spectrometry. Nature *449*, 1033-U1033.

72. Shimizu, M., Ojima, N., Ohnishi, H., Shingaki, T., Hirakawa, Y., and Masujima, T. (2003). Development of the single-cell MALDI-TOF (matrix-assisted laser desorption/ionization time-of-flight) mass-spectroscopic assay. Analytical Sciences *19*, 49-53.

73. Mizuno, H., Tsuyama, N., Harada, T., and Masujima, T. (2008). Live single-cell video-mass spectrometry for cellular and subcellular molecular detection and cell classification. Journal of Mass Spectrometry *43*, 1692-1700.

74. Shrestha, B., and Vertes, A. (2009). In situ metabolic profiling of single cells by laser ablation electrospray ionization mass spectrometry. Analytical Chemistry *81*, 8265-8271.

75. Lapainis, T., Rubakhin, S.S., and Sweedler, J.V. (2009). Capillary electrophoresis with electrospray ionization mass spectrometric detection for single-cell metabolomics. Analytical Chemistry *81*, 5858-5864.

76. Ostrowski, S.G., Kurczy, M.E., Roddy, T.P., Winograd, N., and Ewing, A.G. (2007). Secondary ion MS imaging to relatively quantify cholesterol in the membranes of individual cells from differentially treated populations. Analytical Chemistry *79*, 3554-3560.

77. Piehowski, P.D., Davey, A.M., Kurczy, M.E., Sheets, E.D., Winograd, N., Ewing, A.G., and Heien, M.L. (2009). Time-of-flight secondary ion mass spectrometry imaging of subcellular lipid heterogeneity: Poisson counting and spatial resolution. Analytical Chemistry *81*, 5593-5602.

78. Tobias, H.J., Pitesky, M.E., Fergenson, D.P., Steele, P.T., Horn, J., Frank, M., and Gard, E.E. (2006). Following the biochemical and morphological changes of Bacillus atrophaeus cells during the sporulation process using bioaerosol mass spectrometry. Journal of Microbiological Methods *67*, 56-63.

79. Koek, M.M., Bakels, F., Engel, W., van den Maagdenberg, A., Ferrari, M.D., Coulier, L., and Hankemeier, T. (2009). Metabolic profiling of ultrasmall sample volumes with GC/MS: From microliter to nanoliter samples. Analytical Chemistry *82*, 156-162.

80. Mizuno, H., Tsuyama, N., Date, S., Harada, T., and Masujima, T. (2008). Live single-cell metabolomics of tryptophan and hHistidine mMetabolites in a rat basophil leukemia cell. Analytical Sciences *24*, 1525-1527.

81. Fung, E.N., and Yeung, E.S. (1998). Direct analysis of single rat peritoneal mast cells with laser vaporization ionization mass spectrometry. Analytical Chemistry *70*, 3206-3212.

82. Shimizu, M., Levi-Schaffer, F., Ojima, N., Shingaki, T., and Masujima, T. (2002). A single-cell matrix-assisted laser desorption/ionization time-of-flight mass-spectroscopic assay of the cell-maturation process. Analytical Sciences *18*, 107-108.

83. Gholipour, Y., Nonami, H., and Erra-Balsells, R. (2008). Application of pressure probe and UV-MALDI-TOF MS for direct analysis of plant underivatized carbohydrates in subpicoliter single-cell cytoplasm extract. Journal of the American Society for Mass Spectrometry *19*, 1841-1848.

84. Rubakhin, S.S., and Sweedler, J.V. (2008). Quantitative measurements of cell-cell signaling peptides with single-cell MALDI MS. Analytical Chemistry *80*, 7128-7136.

85. Fletcher, J.S., Rabbani, S., Henderson, A., Blenkinsopp, P., Thompson, S.P., Lockyer, N.P., and Vickerman, J.C. (2008). A new dynamic in mass spectral imaging of single biological cells. Analytical Chemistry *80*, 9058-9064.

86. Berman, E.S.F., Fortson, S.L., Checchi, K.D., Wu, L., Felton, J.S., Wu, K.J.J., and Kulp, K.S. (2008). Preparation of single cells for imaging/profiling mass spectrometry. Journal of the American Society for Mass Spectrometry *19*, 1230-1236.

87. Amantonico, A., Urban, P.L., and Zenobi, R. (2009). Facile analysis of metabolites by capillary electrophoresis coupled to matrix-assisted laser desorption/ionization mass spectrometry using target plates with polysilazane nanocoating and grooves. Analyst *134*, 1536-1540.

88. Amantonico, A., Urban, P.L., Oh, J.Y., and Zenobi, R. (2009). Interfacing microfluidics and laser desorption/ionization mass spectrometry by continuous deposition for application in single cell analysis. Chimia *63*, 185-188.

89. Mellors, J.S., Jorabchi, K., Smith, L.M., and Ramsey, J.M. (2010). Integrated

microfluidic device for automated single cell analysis using electrophoretic separation and electrospray ionization mass spectrometry. Analytical Chemistry *82*, 967-973.

90. Mellors, J.S., Gorbounov, V., Ramsey, R.S., and Ramsey, J.M. (2008). Fully integrated glass microfluidic device for performing high-efficiency capillary electrophoresis and electrospray ionization mass spectrometry. Analytical Chemistry *80*, 6881-6887.

91. Urban, P.L., Jefimovs, K., Amantonico, A., Fagerer, S.R., Schmid, T., Madler, S., Puigmarti-Luis, J., Goedecke, N., and Zenobi, R. High-density micro-arrays for mass spectrometry. (2010). Lab on a Chip *10*, 3206-3209.

92. Chughtai, K., and Heeren, R.M.A. (2010). Mass spectrometric imaging for biomedical tissue analysis. Chemical Reviews *110*, 3237-3277.

93. Fletcher, J.S. (2009). Cellular imaging with secondary ion mass spectrometry. Analyst *134*, 2204-2215.

94. Rubakhin, S.S., and Sweedler, J.V. (2007). Characterizing peptides in individual mammalian cells using mass spectrometry. Nature Protocols *2*, 1987-1997.

95. Coello, Y., Jones, A.D., Gunaratne, T.C., and Dantus, M. (2010). Atmospheric pressure femtosecond laser imaging mass spectrometry. Analytical Chemistry *82*, 2753-2758.

96. Larkin, J.C., Brown, M.L., and Schiefelbein, J. (2003). How do cells know what they want to be when they grow up? Lessons from epidermal patterning in Arabidopsis. Annual Review of Plant Biology *54*, 403-430.

97. Chen, F., D'Auria, J.C., Tholl, D., Ross, J.R., Gershenzon, J., Noel, J.P., and Pichersky, E. (2003). An Arabidopsis thaliana gene for methylsalicylate biosynthesis, identified by a biochemical genomics approach, has a role in defense. Plant Journal *36*, 577-588.

98. Laue, G., Preston, C.A., and Baldwin, I.T. (2000). Fast track to the trichome: Induction of N-acyl nornicotines precedes nicotine induction in Nicotiana repanda. Planta *210*, 510-514.

99. Fordyce, J.A., and Agrawal, A.A. (2001). The role of plant trichomes and caterpillar group size on growth and defence of the pipevine swallowtail Battus

philenor. Journal of Animal Ecology *70*, 997-1005.

100. Zvereva, E.L., Kozlov, M.V., and Niemela, P. (1998). Effects of leaf pubescence in Salix borealis on host-plant choice and feeding behaviour of the leaf beetle, Melasoma lapponica. Entomologia Experimentalis et Applicata *89*, 297-303.

101. Mauricio, R., and Rausher, M.D. (1997). Experimental manipulation of putative selective agents provides evidence for the role of natural enemies in the evolution of plant defense. Evolution *51*, 1435-1444.

102. Klich, M.G. (2000). Leaf variations in Elaeagnus angustifolia related to environmental heterogeneity. Environmental and Experimental Botany *44*, 171-183.

103. Schreuder, M.D.J., Brewer, C.A., and Heine, C. (2001). Modelled influences of non-exchanging trichomes on leaf boundary layers and gas exchange. Journal of Theoretical Biology *210*, 23-32.

104. Luckwill, L. (1943). The genus *Locopersicon*, an historical, biolgical, and taxonomic survey of the wild and cultivated tomatoes (Aberdeen: The University Press), pp. 1-44.

105. Rodriguez, A.E., Tingey, W.M., and Mutschler, M.A. (1993). Acylsugars of lycopersicon-pennellii deter settling and feeding of the green peach aphid (homoptera, aphididae). Journal of Economic Entomology *86*, 34-39.

106. Oghiakhe, S. (1997). Trichomes and resistance to major insect pests in cowpea, Vigna unguiculata (L.) Walp.: A review. Discovery and Innovation *9*, 173-178.

107. Medeiros, A.H., and Tingey, W.M. (2006). Glandular trichomes of Solanum berthaultii and its hybrids with Solanum tuberosum affect nymphal emergence, development, and survival of Empoasca fabae (Homoptera : Cicadellidae). Journal of Economic Entomology *99*, 1483-1489.

108. Zhang, X.M., Thacker, R.R., and Snyder, J.C. (2008). Occurrence of 2,3-dihydrofarnesoic acid, a spidermite repellent, in trichome secretions of Lycopersicon esculentum x L-hirsutum hybrids. Euphytica *162*, 1-9.

109. Besser, K., Harper, A., Welsby, N., Schauvinhold, I., Slocombe, S., Li, Y., Dixon, R.A., and Broun, P. (2009). Divergent regulation of terpenoid metabolism in the trichomes of wild and cultivated tomato species. Plant Physiology *149*, 499-514.

110. Puterka, G.J., Farone, W., Palmer, T., and Barrington, A. (2003). Structure-function relationships affecting the insecticidal and miticidal activity of sugar esters. Journal of Economic Entomology *96*, 636-644.

111. Chao, W.S., Serpe, M.D., Anderson, J.V., Gesch, R.W., and Horvath, D.P. (2006). Sugars, hormones, and environment affect the dormancy status in underground adventitious buds of leafy spurge (Euphorbia esula). Weed Science *54*, 59-68.

112. Nonomura, T., Xu, L., Wada, M., Kawamura, S., Miyajima, T., Nishitomi, A., Kakutani, K., Takikawa, Y., Matsuda, Y., and Toyoda, H. (2009). Trichome exudates of Lycopersicon pennellii form a chemical barrier to suppress leaf-surface germination of Oidium neolycopersici conidia. Plant Science *176*, 31-37.

113. Schilmiller, A.L., Schauvinhold, I., Larson, M., Xu, R., Charbonneau, A.L., Schmidt, A., Wilkerson, C., Last, R.L., and Pichersky, E. (2009). Monoterpenes in the glandular trichomes of tomato are synthesized from a neryl diphosphate precursor rather than geranyl diphosphate. Proceedings of the National Academy of Sciences *106*, 10865-10870.

114. Kang, J.H., Shi, F., Jones, A.D., Marks, M.D., and Howe, G.A. (2009). Distortion of trichome morphology by the hairless mutation of tomato affects leaf surface chemistry. Journal of Experimental Botany *61*, 1053-1064.

115. Gang, D.R., Wang, J.H., Dudareva, N., Nam, K.H., Simon, J.E., Lewinsohn, E., and Pichersky, E. (2001). An investigation of the storage and biosynthesis of phenylpropenes in sweet basil. Plant Physiology *125*, 539-555.

116. Fridman, E., Wang, J.H., Iijima, Y., Froehlich, J.E., Gang, D.R., Ohlrogge, J., and Pichersky, E. (2005). Metabolic, genomic, and biochemical analyses of glandular trichomes from the wild tomato species Lycopersicon hirsutum identify a key enzyme in the biosynthesis of methylketones. Plant Cell *17*, 1252-1267.

117. Shi, F. (2009). Profiling of specialized metabolites in glandular trichomes of the genus solanum using liquid chromatography and mass spectrometry. In Department of Chemistry, Michigan State University, Doctoral Thesis (East Lansing).

118. Stewart, A.J., Bozonnet, S., Mullen, W., Jenkins, G.I., Lean, M.E.J., and Crozier, A. (2000). Occurrence of flavonols in tomatoes and tomato-based products. Journal of Agricultural and Food Chemistry *48*, 2663-2669.

119. Tokusoglu, O., Unal, M.K., and Yildirim, Z. (2003). HPLC-UV and GC-MS characterization of the flavonol aglycons quercetin, kaempferol, and myricetin in tomato pastes and other tomato-based products. Acta Chromatographica. *13*, 196-207.

120. Le Gall, G., DuPont, M.S., Mellon, F.A., Davis, A.L., Collins, G.J., Verhoeyen, M.E., and Colquhoun, I.J. (2003). Characterization and content of flavonoid glycosides in genetically modified tomato (*Lycopersicon esculentum*) fruits. Journal of Agricultural and Food Chemistry *51*, 2438-2446.

121. Le Gall, G., Colquhoun, I.J., Davis, A.L., Collins, G.J., and Verhoeyen, M.E. (2003). Metabolite profiling of tomato (Lycopersicon esculentum) using H-1 NMR spectroscopy as a tool to detect potential unintended effects following a genetic modification. Journal of Agricultural and Food Chemistry *51*, 2447-2456.

122. Ferreres, F., Taveira, M., Pereira, D.M., Valentao, P., and Andrade, P.B. Tomato (*Lycopersicon esculentum*) seeds: New flavonols and cytotoxic effect. Journal of Agricultural and Food Chemistry *58*, 2854-2861.

123. Li, J.Y., Oulee, T.M., Raba, R., Amundson, R.G., and Last, R.L. (1993). Arabidopsis flavonoid mutants are hypersensitive to uv-b irradiation. Plant Cell *5*, 171-179.

124. Dixon, R.A., and Paiva, N.L. (1995). Stress-induced phenylpropanoid metabolism. Plant Cell *7*, 1085-1097.

125. Fobes, J.F., Mudd, J.B., and Marsden, M.P.F. (1985). Epicuticular lipid-accumulation on the leaves of lycopersicon-pennellii (corr) darcy and lycopersicon-esculentum mill. Plant Physiology *77*, 567-570.

126. Bonierbale, M.W., Plaisted, R.L., Pineda, O., and Tanksley, S.D. (1994). QTL analysis of trichome-mediated insect resistance in potato. TAG Theoretical and Applied Genetics *87*, 973-987.

127. Chortyk, O.T., Kays, S.J., and Teng, Q. (1997). Characterization of insecticidal sugar esters of Petunia. Journal of Agricultural and Food Chemistry *45*, 270-275.

128. Lawson, D.M., Lunde, C.F., and Mutschler, M.A. (1997). Marker-assisted transfer of acylsugar-mediated pest resistance from the wild tomato, *Lycopersicon pennellii*, to the cultivated tomato, *Lycopersicon esculentum*. Molecular Breeding *3*, 307-317.

129. McKenzie, C.L., Weathersbee, A.A., and Puterka, G.J. (2005). Toxicity of sucrose octanoate to egg, nymphal, and adult Bemisia tabaci (Hemiptera : Aleyrodidae) using a novel plant-based bioassay. Journal of Economic Entomology *98*, 1242-1247.

130. Hill, K., and Rhode, O. (1999). Sugar-based surfactants for consumer products and technical applications. Fett-Lipid *101*, 25-33.

131. Chortyk, O.T., Severson, R.F., Cutler, H.C., and Sisson, V.A. (1993). Antibiotic activities of sugar esters isolated from selected nicotiana species. Bioscience, Biotechnology, and Biochemistry *57*, 1355-1356.

132. Coates, R.M., Denissen, J.F., Juvik, J.A., and Babka, B.A. (1988). Identification of alpha-santalenoic and endo-beta-bergamotenoic acids as moth oviposition stimulants from wild tomato leaves. Journal of Organic Chemistry *53*, 2186-2192.

133. Frelichowski, J.E., and Juvik, J.A. (2001). Sesquiterpene carboxylic acids from a wild tomato species affect larval feeding behavior and survival of Helicoverpa zea and Spodoptera exigua (Lepidoptera:Noctuidae). Journal of Economic Entomology *94*, 1249-1259.

134. Li, L., Zhao, Y.F., McCaig, B.C., Wingerd, B.A., Wang, J.H., Whalon, M.E., Pichersky, E., and Howe, G.A. (2004). The tomato homolog of Coronatine-insensitive1 is required for the maternal control of seed maturation, jasmonate-signaled defense responses, and glandular trichome development. Plant Cell *16*, 783-783.

135. Stagliano, M.C., DeKeyser, J.G., Omiecinski, C.J., and Jones, A.D. Bioassay-directed fractionation for discovery of bioactive neutral lipids guided by relative mass defect filtering and multiplexed collision-induced dissociation. Rapid Communications in Mass Spectrometry *24*, 3578-3584.

136. Peralta, I.E., and Spooner, D.M. (2001). Granule-bound starch synthase (GBSSI) gene phylogeny of wild tomatoes (Solanum L. section Lycopersicon [Mill.] Wettst. subsection Lycopersicon). American Journal of Botany *88*, 1888-1902.

137. Kumar, N.K.K., Ullman, D.E., and Cho, J.J. (1995). Frankliniella-occidentalis (thysanoptera, thripidae) landing and resistance to tomato spotted wilt tospovirus among *lycopersicon* accessions with additional comments on thrips tabaci (thysanoptera, thripidae) and trialeurodes-vaporariorum (homoptera, aleyrodidae). Environmental Entomology *24*, 513-520.

138. Pico, B., Diez, M., and Nuez, F. (1998). Evaluation of whitefly-mediated inoculation techniques to screen Lycopersicon esculentum and wild relatives for resistance to tomato yellow leaf curl virus. Euphytica *101*, 259-271.

139. Martins Santana, F., Ribeiro, S.D., Moita, A.W., Moreira, D.J., and Giordano, L.D. (2001). Sources of resistance in *Lycopersicon* spp. to a bipartite whitefly-transmitted geminivirus from Brazil. Euphytica *122*, 45-51.

140. McDowell, E.T., Kapteyn, J., Schmidt, A., Li, C., Kang, J.H., Descour, A., Shi, F., Larson, M., Schilmiller, A., An, L.L., et al. (2011). Comparative functional genomic analysis of solanum glandular trichome types. Plant Physiology *155*, 524-539.

141. Fiehn, O. (2002). Metabolomics - the link between genotypes and phenotypes. Plant Molecular Biology *48*, 155-171.

142. Buchholz, A., Hurlebaus, J., Wandrey, C., and Takors, R. (2002). Metabolomics: Quantification of intracellular metabolite dynamics. Biomolecular Engineering *19*, 5-15.

143. Nicholson, J.K., Lindon, J.C., and Holmes, E. (1999). 'Metabonomics': Understanding the metabolic responses of living systems to pathophysiological stimuli via multivariate statistical analysis of biological NMR spectroscopic data. Xenobiotica *29*, 1181-1189.

144. Bahar, R., Hartmann, C.H., Rodriguez, K.A., Denny, A.D., Busuttil, R.A., Dolle, M.E.T., Calder, R.B., Chisholm, G.B., Pollock, B.H., Klein, C.A., et al. (2006). Increased cell-to-cell variation in gene expression in ageing mouse heart. Nature *441*, 1011-1014.

145. Levsky, J.M., and Singer, R.H. (2003). Gene expression and the myth of the average cell. Trends in Cell Biology *13*, 4-6.

146. Kaern, M., Elston, T.C., Blake, W.J., and Collins, J.J. (2005). Stochasticity in gene expression: From theories to phenotypes. Nature Reviews Genetics *6*, 451-464.

147. Karrer, E.E., Lincoln, J.E., Hogenhout, S., Bennett, A.B., Bostock, R.M., Martineau, B., Lucas, W.J., Gilchrist, D.G., and Alexander, D. (1995). In-situ isolation of messenger-rna from individual plant-cells - creation of cell-specific cdna libraries. Proceedings of the National Academy of Sciences of the United

States of America *92*, 3814-3818.

148. Brandt, S., Kloska, S., Altmann, T., and Kehr, J. (2002). Using array hybridization to monitor gene expression at the single cell level. Journal of Experimental Botany *53*, 2315-2323.

149. EmmertBuck, M.R., Bonner, R.F., Smith, P.D., Chuaqui, R.F., Zhuang, Z.P., Goldstein, S.R., Weiss, R.A., and Liotta, L.A. (1996). Laser capture microdissection. Science *274*, 998-1001.

150. Katsuragi, T., and Tani, Y. (2001). Single-cell sorting of microorganisms by flow or slide-based (including laser scanning) cytometry. Acta Biotechnologica *21*, 99-115.

151. Chao, T.C., and Ros, A. (2008). Microfluidic single-cell analysis of intracellular compounds. Journal of the Royal Society Interface *5*, S139-S150.

152. Nelson, A.R., Allbritton, N.L., and Sims, C.E. (2007). Rapid sampling for single-cell analysis by capillary electrophoresis. In Laser Manipulation of Cells and Tissues (San Diego: Elsevier Academic Press Inc), pp. 709-722.

153. Schulte, A., and Schuhmann, W. (2007). Single-cell microelectrochemistry. Angewandte Chemie-International Edition *46*, 8760-8777.

154. Yang, Q., Zhang, X.L., Bao, X.H., Lu, H.J., Zhang, W.J., Wu, W.H., Miao, H.N., and Jiao, B.H. (2008). Single cell determination of nitric oxide release using capillary electrophoresis with laser-induced fluorescence detection. Journal of Chromatography A *1201*, 120-127.

155. Li, L.J., Garden, R.W., and Sweedler, J.V. (2000). Single-cell MALDI: A new tool for direct peptide profiling. Trends in Biotechnology *18*, 151-160.

156. Amantonico, A., Oh, J.Y., Sobek, J., Heinemann, M., and Zenobi, R. (2008). Mass spectrometric method for analyzing metabolites in yeast with single cell sensitivity. Angewandte Chemie-International Edition *47*, 5382-5385.

157. Simmons, T.L., Coates, R.C., Clark, B.R., Engene, N., Gonzalez, D., Esquenazi, E., Dorrestein, P.C., and Gerwick, W.H. (2008). Biosynthetic origin of natural products isolated from marine microorganism-invertebrate assemblages. Proceedings of the National Academy of Sciences of the United States of America *105*, 4587-4594.

158. Yang, Y.L., Xu, Y.Q., Straight, P., and Dorrestein, P.C. (2009). Translating metabolic exchange with imaging mass spectrometry. Nature Chemical Biology *5*, 885-887.

159. Shroff, R., Vergara, F., Muck, A., Svatos, A., and Gershenzon, J. (2008). Nonuniform distribution of glucosinolates in *Arabidopsis thaliana* leaves has important consequences for plant defense. Proceedings of the National Academy of Sciences *105*, 6196-6201.

160. Knochenmuss, R. (2006). Ion formation mechanisms in UV-MALDI. Analyst *131*, 966-986.

161. Vertes, A., Irinyi, G., and Gijbels, R. (1993). Hydrodynamic model of matrix-assisted laser-desorption mass-spectrometry. Analytical Chemistry *65*, 2389-2393.

162. Zhigilei, L.V., Leveugle, E., Garrison, B.J., Yingling, Y.G., and Zeifman, M.I. (2003). Computer simulations of laser ablation of molecular substrates. Chemical Reviews *103*, 321-347.

163. Ehring, H., Karas, M., and Hillenkamp, F. (1992). Role of photoionization and photochemistry in ionization processes of organic-molecules and relevance for matrix-assisted laser desorption ionization mass-spectrometry. Organic Mass Spectrometry *27*, 472-480.

164. Land, C.M., and Kinsel, G.R. (2001). The mechanism of matrix to analyte proton transfer in clusters of 2,5-dihydroxybenzoic acid and the tripeptide VPL. Journal of The American Society for Mass Spectrometry *12*, 726-731.

165. Ludemann, H.C., Redmond, R.W., and Hillenkamp, F. (2002). Singlet-singlet annihilation in ultraviolet matrix-assisted laser desorption/ionization studied by fluorescence spectroscopy. Rapid Communications in Mass Spectrometry *16*, 1287-1294.

166. Wang, B.H., Dreisewerd, K., Bahr, U., Karas, M., and Hillenkamp, F. (1993). Gas-phase cationization and protonation of neutrals generated by matrix-assisted laser desorption. Journal of The American Society for Mass Spectrometry *4*, 393-398.

167. Karas, M., Gluckmann, M., and Schafer, J. (2000). Ionization in matrix-assisted laser desorption/ionization: singly charged molecular ions are the lucky survivors.

Journal of Mass Spectrometry *35*, 1-12.

168. Kruse, R.A., Li, X.L., Bohn, P.W., and Sweedler, J.V. (2001). Experimental factors controlling analyte ion generation in laser desorption/ionization mass spectrometry on porous silicon. Analytical Chemistry *73*, 3639-3645.

169. Nordstrom, A., Apon, J.V., Uritboonthal, W., Go, E.P., and Siuzdak, G. (2006). Surfactant-enhanced desorption/ionization on silicon mass spectrometry. Analytical Chemistry *78*, 272-278.

170. Luo, G.H., Chen, Y., Siuzdak, G., and Vertes, A. (2005). Surface modification and laser pulse length effects on internal energy transfer in DIOS. The Journal of Physical Chemistry B *109*, 24450-24456.

171. Law, K.P. Laser desorption/ionization mass spectrometry on nanostructured semiconductor substrates: DIOS (TM) and QuickMass (TM). International Journal of Mass Spectrometry *290*, 72-84.

172. Law, K.P. Surface-assisted laser desorption/ionization mass spectrometry on nanostructured silicon substrates prepared by iodine-assisted etching. International Journal of Mass Spectrometry *290*, 47-59.

173. Alimpiev, S., Grechnikov, A., Sunner, J., Karavanskii, V., Simanovsky, Y., Zhabin, S., and Nikiforov, S. (2008). On the role of defects and surface chemistry for surface-assisted laser desorption ionization from silicon. The Journal of Chemical Physics *128*, 19.

174. Nemes, P., and Vertes, A. (2010). Atmospheric-pressure molecular imaging of biological tissues and biofilms by laesi mass spectrometry. Journal of Visualized Experiments, e2097.

175. Vertes, A., and Shrestha, B. (2010). Direct analysis of single cells by mass spectrometry at atmospheric pressure. Journal of Visualized Experiments, e2144.

176. Takats, Z., Wiseman, J.M., Gologan, B., and Cooks, R.G. (2004). Mass spectrometry sampling under ambient conditions with desorption electrospray ionization. Science *306*, 471-473.

177. Kertesz, V., and Van Berkel, G.J. (2008). Improved imaging resolution in desorption electrospray ionization mass spectrometry. Rapid Communications in

Mass Spectrometry *22*, 2639-2644.

178. Costa, A.B., and Cooks, R.G. (2008). Simulated splashes: Elucidating the mechanism of desorption electrospray ionization mass spectrometry. Chemical Physics Letters *464*, 1-8.

179. Chandra, S., and Morrison, G.H. (1995). Imaging ion and molecular-transport at subcellular resolution by secondary-ion mass-spectrometry. International Journal of Mass Spectrometry and Ion Processes *143*, 161-176.

180. Strick, R., Strissel, P.L., Gavrilov, K., and Levi-Setti, R. (2001). Cation-chromatin binding as shown by ion microscopy is essential for the structural integrity of chromosomes. Journal of Cell Biology *155*, 899-910.

181. Marks, M.D., Wenger, J.P., Gilding, E., Jilk, R., and Dixon, R.A. (2009). Transcriptome analysis of arabidopsis wild-type and gl3-sst sim trichomes identifies four additional genes required for trichome development. Molecular Plant *2*, 803-822.

182. Breuer, C., Kawamura, A., Ichikawa, T., Tominaga-Wada, R., Wada, T., Kondou, Y., Muto, S., Matsui, M., and Sugimoto, K. (2009). The trihelix transcription factor gtl1 regulates ploidy-dependent cell growth in the arabidopsis trichome. Plant Cell *21*, 2307-2322.

183. Wagner, G.J., Wang, E., and Shepherd, R.W. (2004). New approaches for studying and exploiting an old protuberance, the plant trichome. Annals of Botany *93*, 3-11.

184. Simmons, A.T., and Gurr, G.M. (2005). Trichomes of Lycopersicon species and their hybrids: Effects on pests and natural enemies. Agricultural and Forest Entomology *7*, 265-276.

185. Yerger, E.H., Grazzini, R.A., Hesk, D., Coxfoster, D.L., Craig, R., and Mumma, R.O. (1992). A rapid method for isolating glandular trichomes. Plant Physiology *99*, 1-7.

186. Wienkoop, S., Zoeller, D., Ebert, B., Simon-Rosin, U., Fisahn, J., Glinski, M., and Weckwerth, W. (2004). Cell-specific protein profiling in Arabidopsis thaliana trichomes: Identification of trichome-located proteins involved in sulfur metabolism and detoxification. Phytochemistry *65*, 1641-1649.

187. Zhang, X.G., and Oppenheimer, D.G. (2004). A simple and efficient method for isolating trichomes for downstream analyses. Plant and Cell Physiology *45*, 221-224.

188. Kaletas, B.K., van der Wiel, I.M., Stauber, J., Dekker, L.J., Guzel, C., Kros, J.M., Luider, T.M., and Heeren, R.M.A. (2009). Sample preparation issues for tissue imaging by imaging MS. Proteomics *9*, 2622-2633.

189. Chaurand, P., Norris, J.L., Cornett, D.S., Mobley, J.A., and Caprioli, R.M. (2006). New developments in profiling and imaging of proteins from tissue sections by MALDI mass spectrometry. Journal of Proteome Research *5*, 2889-2900.

190. Murphy, R.C., Hankin, J.A., and Barkley, R.M. (2009). Imaging of lipid species by MALDI mass spectrometry. Journal of Lipid Research *50*, S317-S322.

191. Varner, J.E., and Ye, Z.H. (1994). Tissue printing. Faseb Journal *8*, 378-384.

192. Jacobsen, J.V., and Knox, R.B. (1973). Cytochemical localization and antigenicity of alpha-amylase in barley aleurone tissue. Planta *112*, 213-224.

193. Kotecha, S.A., Eley, D.W., and Turner, R.W. (1997). Tissue printed cells from teleost electrosensory and cerebellar structures. Journal of Comparative Neurology *386*, 277-292.

194. Gaston, S.M., Soares, M.A., Siddiqui, M.M., Vu, D., Lee, J.M., Goldner, D.L., Brice, M.J., Shih, J.C., Upton, M.P., Perides, G., et al. (2005). Tissue-print and print-phoresis as platform technologies for the molecular analysis of human surgical specimens: Mapping tumor invasion of the prostate capsule. Nature Medicine *11*, 95-101.

195. Todd, P.J., Schaaff, T.G., Chaurand, P., and Caprioli, R.M. (2001). Organic ion imaging of biological tissue with secondary ion mass spectrometry and matrix-assisted laser desorption/ionization. Journal of Mass Spectrometry *36*, 355-369.

196. Caprioli, R.M., Farmer, T.B., and Gile, J. (1997). Molecular imaging of biological samples: Localization of peptides and proteins using MALDI-TOF MS. Analytical Chemistry *69*, 4751-4760.

197. Sjovall, P., Lausmaa, J., Nygren, H., Carlsson, L., and Malmberg, P. (2003). Imaging of membrane lipids in single cells by imprint-imaging time-of-flight

secondary ion mass spectrometry. Analytical Chemistry *75*, 3429-3434.

198. Mullen, A.K., Clench, M.R., Crosland, S., and Sharples, K.R. (2005). Determination of agrochemical compounds in soya plants by imaging matrix-assisted laser desorption/ionisation mass spectrometry. Rapid Communications in Mass Spectrometry *19*, 2507-2516.

199. Prideaux, B., Atkinson, S.J., Carolan, V.A., Morton, J., and Clench, M.R. (2007). Sample preparation and data interpretation procedures for the examination of xenobiotic compounds in skin by indirect imaging MALDI-MS. International Journal of Mass Spectrometry *260*, 243-251.

200. Vidova, V., Novak, P., Strohalm, M., Pol, J., Havlicek, V., and Volny, M. (2010). Laser desorption-ionization of lipid transfers: Tissue mass spectrometry imaging without MALDI matrix. Analytical Chemistry *82*, 4994-4997.

201. Zhong, G., and Lin, H. (2007). A binary matrix for background suppression in MALDI-MS of small molecules. Analytical and Bioanalytical Chemistry *387*, 1939-1944.

202. Jurchen, J.C., Rubakhin, S.S., and Sweedler, J.V. (2005). MALDI-MS imaging of features smaller than the size of the laser beam. Journal of the American Society for Mass Spectrometry *16*, 1654-1659.

203. Chen, Y.F., Chen, H.Y., Aleksandrov, A., and Orlando, T.M. (2008). Roles of water, acidity, and surface morphology in surface-assisted laser desorption/ionization of amino acids. Journal of Physical Chemistry C *112*, 6953-6960.

204. Harris, P.J.F. (2004). Fullerene-related structure of commercial glassy carbons. Philosophical Magazine *84*, 3159-3167.

205. Huang, J.P., Yuan, C.H., Shiea, J., and Chen, Y.C. (1999). Rapid screening for diuretic doping agents in urine by C60-assisted laser-desorption-ionization-time-of-flight mass spectrometry. Journal of Analytical Toxicology *23*, 337-342.

206. Michalak, L., Fisher, K.J., Alderdice, D.S., Jardine, D.R., and Willett, G.D. (1994). C60-assisted laser desorption-ionization mass-spectrometry. Organic Mass Spectrometry *29*, 512-515.

207. Hopwood, F.G., Michalak, L., Alderdice, D.S., Fisher, K.J., and Willett, G.D. (1994). C60-assisted laser desorption/ionization mass-spectrometry in the analysis of phosphotungstic acid. Rapid Communications in Mass Spectrometry *8*, 881-885.

208. Seeley, E.H., and Caprioli, R.M. (2011). MALDI imaging mass spectrometry of human tissue: Method challenges and clinical perspectives. Trends in Biotechnology *29*, 136-143.

209. Rauser, S., Deininger, S.O., Suckau, D., Hofler, H., and Walch, A. Approaching MALDI molecular imaging for clinical proteomic research: Current state and fields of application. Expert Review of Proteomics *7*, 927-941.

210. Fernandez, J.A., Ochoa, B., Fresnedo, O., Giralt, M.T., and Rodriguez-Puertas, R. (2011). Matrix-assisted laser desorption ionization imaging mass spectrometry in lipidomics. Analytical and Bioanalytical Chemistry *401*, 29-51.

211. Shanta, S.R., Kim, Y., Kim, Y.H., and Kim, K.P. (2011). Application of MALDI tissue imaging of drugs and metabolites: A new frontier for molecular histology. Biomolecules & Therapeutics *19*, 149-154.

212. Ifa, D.R., Manicke, N.E., Dill, A.L., and Cooks, G. (2008). Latent fingerprint chemical imaging by mass spectrometry. Science *321*, 805-805.

213. Pichersky, E., and Lewinsohn, E. (2011). Convergent evolution in plant specialized metabolism. Annual Review of Plant Biology *62*, 549-566.

214. Middleton, E., and Kandaswami, C. (1993). The impact of plant flavonoids on mammalian biology: Implications for immunity, inflammation and cancer. In The Flavonoids: Advances in Research Since 1986 (London: Chapman and Hall), pp 619-652.

215. Jacobs, M., and Rubery, P.H. (1988). Naturally-occurring auxin transport regulators. Science *241*, 346-349.

216. Long, S.R. (1989). Rhizobium-legume nodulation - life together in the underground. Cell *56*, 203-214.

217. Ylstra, B., Touraev, A., Moreno, R.M.B., Stoger, E., Vantunen, A.J., Vicente, O., Mol, J.N.M., and Heberlebors, E. (1992). Flavonols stimulate development, germination, and tube growth of tobacco pollen. Plant Physiology *100*, 902-907.

218. Dixon, R.A., Dey, P.M., and Lamb, C.J. (1983). Phytoalexins - enzymology and molecular-biology. In Advances in Enzymology and Related Areas of Molecular Biology (John Wiley & Sons, Inc), pp 1-136.

219. Dakora, F.D., and Phillips, D.A. (1996). Diverse functions of isoflavonoids in legumes transcend anti-microbial definitions of phytoalexins. Physiological and Molecular Plant Pathology *49*, 1-20.

220. Cuyckens, F., and Claeys, M. (2004). Mass spectrometry in the structural analysis of flavonoids. Journal of Mass Spectrometry *39*, 1-15.

221. Ibrahim, R.K., Deluca, V., Khouri, H., Latchinian, L., Brisson, L., and Charest, P.M. (1987). Enzymology and compartmentation of polymethylated flavonol glucosides in chrysosplenium-americanum. Phytochemistry *26*, 1237-1245.

222. Cuadra, P., and Harborne, J.B. (1996). Changes in epicuticular flavonoids and photosynthetic pigments as a plant response to UV-B radiation. Zeitschrift Fur Naturforschung C-a Journal of Biosciences *51*, 671-680.

223. Kim, B.G., Jung, B.R., Lee, Y., Hur, H.G., Lim, Y., and Ahn, J.H. (2006). Regiospecific flavonoid 7-0-methylation with Streptomyces avermitilis O-methyltransferase expressed in Escherichia coli. Journal of Agricultural and Food Chemistry *54*, 823-828.

224. Kim, B.G., Shin, K.H., Lee, Y., Hur, H.G., Lim, Y., and Ahn, J.H. (2005). Multiple regiospecific methylations of a flavonoid by plant O-methyltransferases expressed in E-coli. Biotechnology Letters *27*, 1861-1864.

225. Frick, S., Ounaroon, A., and Kutchan, T.M. (2001). Combinatorial biochemistry in plants: The case of O-methyltransferases. Phytochemistry *56*, 1-4.

226. Walle, T. (2007). Methoxylated flavones, a superior cancer chemopreventive flavonoid subclass? Seminars in Cancer Biology *17*, 354-362.

227. de Rijke, E., Out, P., Niessen, W.M.A., Ariese, F., Gooijer, C., and Brinkman, U.A.T. (2006). Analytical separation and detection methods for flavonoids. Journal of Chromatography A *1112*, 31-63.

228. Bloor, S.J. (2001). Overview of methods for analysis and identification of flavonoids. In Flavonoids and Other Polyphenols (San Diego: Academic Press Inc), pp. 3-14.

229. Stobiecki, M. (2000). Application of mass spectrometry for identification and structural studies of flavonoid glycosides. Phytochemistry *54*, 237-256.

230. Merken, H.M., and Beecher, G.R. (2000). Measurement of food flavonoids by high-performance liquid chromatography: A review. Journal of Agricultural and Food Chemistry *48*, 577-599.

231. Robards, K., and Antolovich, M. (1997). Analytical chemistry of fruit bioflavonoids - A review. Analyst *122*, R11-R34.

232. March, R., and Brodbelt, J. (2008). Analysis of flavonoids: Tandem mass spectrometry, computational methods, and NMR. Journal of Mass Spectrometry *43*, 1581-1617.

233. Kim, H., Moon, B.H., Ahn, J.H., and Lim, Y. (2006). Complete NMR signal assignments of flavonol derivatives. Magnetic Resonance in Chemistry *44*, 188-190.

234. Lambert, M., Staerk, D., Hansen, S.H., Sairafianpour, M., and Jaroszewski, J.W. (2005). Rapid extract dereplication using HPLC-SPE-NMR: Analysis of isoflavonoids from Smirnowia iranica. Journal of Natural Products *68*, 1500-1509.

235. Park, Y., Moon, B.H., Lee, E., Hong, S., Lee, S., and Lim, Y. (2008). The H-1 and C-13 NMR data of 19 methoxyflavonol derivatives. Bulletin of the Korean Chemical Society *29*, 81-84.

236. Lee, S., Park, Y., Moon, B.H., Lee, E., Hong, S., and Lim, Y. (2008). Substitution effect of hydroxyl groups on the H-1 and C-13 chemical shifts in hydroxyflavonols. Bulletin of the Korean Chemical Society *29*, 1597-1600.

237. Markham, K.R. (1989). A reassessment of the data supporting the structures of blumea-malcolmii flavonols. Phytochemistry *28*, 243-244.

238. Greenham, J., Williams, C., and Harborne, J.B. (1995). Identification of lipophilic flavonols by a combination of chromatographic and spectral techniques. Phytochemical Analysis *6*, 211-217.

239. Greenham, J., Harborne, J.B., and Williams, C.A. (2003). Identification of lipophilic flavones and flavonols by comparative HPLC, TLC and UV spectral analysis. Phytochemical Analysis *14*, 100-118.

240. Stefova, M., Stafilov, T., Kulevanova, S., Stefkov, G., and Bankova, V.S. (2007). QSRR of flavones: Evaluation of substituent contributions to RP HPLC retention. Journal of Liquid Chromatography & Related Technologies *30*, 1035-1049.

241. Mabry, T.J., Markham, K.R., and Thomas, M.B. (1970). The Systematic Identification of Flavonoids (New York: Springer).

242. Kingston, D.G. (1971). Mass spectrometry of organic compounds .6. electron-impact spectra of flavonoid compounds. Tetrahedron *27*, 2691-2700.

243. Berahia, T., Gaydou, E.M., Cerrati, C., and Wallet, J.C. (1994). Mass-spectrometry of polymethoxylated flavones. Journal of Agricultural and Food Chemistry *42*, 1697-1700.

244. Guidugli, F.H., Ardanaz, C.E., Kavka, J., Garibay, M.E., and Josephnathan, P. (1986). Further mass-spectral studies of flavones. Organic Mass Spectrometry *21*, 117-124.

245. Hedin, P.A., and Phillips, V.A. (1992). Electron-impact mass-spectral analysis of flavonoids. Journal of Agricultural and Food Chemistry *40*, 607-611.

246. Justesen, U. (2001). Collision-induced fragmentation of deprotonated methoxylated flavonoids, obtained by electrospray ionization mass spectrometry. Journal of Mass Spectrometry *36*, 169-178.

247. Cren-Olive, C., Deprez, S., Lebrun, S., Coddeville, B., and Rolando, C. (2000). Characterization of methylation site of monomethylflavan-3-ols by liquid chromatography/electrospray ionization tandem mass spectrometry. Rapid Communications in Mass Spectrometry *14*, 2312-2319.

248. Ma, Y.L., Van den Heuvel, H., and Claeys, M. (1999). Characterization of 3-methoxyflavones using fast-atom bombardment and collision-induced dissociation tandem mass spectrometry. Rapid Communications in Mass Spectrometry *13*, 1932-1942.

249. Wang, K.W., and Zhang, H. (2009). Positive electrospray ionization tandem mass spectrometry of polymethoxylated flavones. Rapid Communications in Mass Spectrometry *23*, 2107-2111.

250. Zhou, D.Y., Chen, D.L., Xu, Q., Xue, X.Y., Zhang, F.F., and Liang, X.M. (2007). Characterization of polymethoxylated flavones in Fructus aurantii by liquid

chromatography with atmospheric pressure chemical ionization combined with tandem mass spectrometry. Journal of Pharmaceutical and Biomedical Analysis *43*, 1692-1699.

251. Wang, D.D., Wang, J., Huang, X.H., Tu, Y., and Ni, K.Y. (2007). Identification of polymethoxylated flavones from green tangerine peel (Pericarpium Citri Reticulatae Viride) by chromatographic and spectroscopic techniques. Journal of Pharmaceutical and Biomedical Analysis *44*, 63-69.

252. Bouktaib, M., Lebrun, S., Atmani, A., and Rolando, C. (2002). Hemisynthesis of all the O-monomethylated analogues of quercetin including the major metabolites, through selective protection of phenolic functions. Tetrahedron *58*, 10001-10009.

253. Boers, F., Deng, B.L., Lemiere, G., Lepoivre, J., DeGroot, A., Dommisse, R., and Vlietinck, A.J. (1997). An improved synthesis of the anti-picornavirus flavone 3-O-methylquercetin. Archiv Der Pharmazie *330*, 313-316.

254. Cren-Olive, C., Lebrun, S., and Rolando, C. (2002). An efficient synthesis of the four mono methylated isomers of (+)-catechin including the major metabolites and of some dimethylated and trimethylated analogues through selective protection of the catechol ring. Journal of the Chemical Society-Perkin Transactions *1*, 821-830.

255. Jurd, L. (1958). Plant polyphenols. V. selective alkylation of the 7-hydroxyl group in polyhydroxyflavones. Journal of the American Chemical Society *80*, 5531-5536.

256. Jurd, L. (1962). Selective alkylation of polyphenols .1. use of diphenylmethylene as a protective grouping for o-dihydroxyflavones. Journal of Organic Chemistry *27*, 872-875.

257. Jurd, L. (1962). Selective alkylation of polyphenols .2. methylation of 7-, 4'-, and 3'-hydroxyl groups in flavonols. Journal of Organic Chemistry *27*, 1294-1297.

258. Picq, M., Prigent, A.F., Chabannes, B., and Pacheco, H. (1984). O-alkylation of quercetin and the synthesis of 3,7,3',4'-tetra-o-ethyl-5-[h-3]-o-ethylquercetin. Tetrahedron Letters *25*, 2227-2230.

259. Yoo, H., Kim, S.H., Lee, J., Kim, H.J., Seo, S.H., Chung, B.Y., Jin, C., and Lee, Y.S. (2005). Synthesis and antioxidant activity of 3-methoxyflavones. Bulletin of the Korean Chemical Society *26*, 2057-2060.

260. Li, H.J., Luan, X.H., and Zhao, Y.M. (2004). Facile synthesis of 3-O-methylquercetin. Chinese Journal of Organic Chemistry *24*, 1619-1621.

261. Kim, J., Park, K.S., Lee, C., and Chong, Y. (2007). Synthesis of a complete series of O-methyl analogues of naringenin and apigenin. Bulletin of the Korean Chemical Society *28*, 2527-2530.

262. Schmidt, A., Li, C., Shi, F., Jones, A.D., and Pichersky, E. Polymethylated myricetin in trichomes of the wild tomato species *solanum habrochaites* and characterization of trichome-specific 3'/5'- and 7/4'-myricetin o-methyltransferases. Plant Physiology *155*, 1999-2009.

263. Crozier, A., Jensen, E., Lean, M.E.J., and McDonald, M.S. (1997). Quantitative analysis of flavonoids by reversed-phase high-performance liquid chromatography. Journal of Chromatography A *761*, 315-321.

264. Merken, H.M., and Beecher, G.R. (2000). Liquid chromatographic method for the separation and quantification of prominent flavonoid aglycones. Journal of Chromatography A *897*, 177-184.

265. Geng, H.M., Zhang, D.Q., Zha, J.P., and Qi, J.L. (2007). Simultaneous HPLC determination of five flavonoids in *Flos Inulae*. Chromatographia *66*, 271-275.

266. Moco, S., Bino, R.J., Vorst, O., Verhoeven, H.A., de Groot, J., van Beek, T.A., Vervoort, J., and de Vos, C.H.R. (2006). A liquid chromatography-mass spectrometry-based metabolome database for tomato. Plant Physiology *141*, 1205-1218.

267. Ferreres, F., Taveira, M., Pereira, D.M., Valentao, P., and Andrade, P.B. (2010). Tomato (Lycopersicon esculentum) seeds: New flavonols and cytotoxic effect. Journal of Agricultural and Food Chemistry *58*, 2854-2861.

268. Ma, Y.L., Li, Q.M., VandenHeuvel, H., and Claeys, M. (1997). Characterization of flavone and flavonol aglycones by collision-induced dissociation tandem mass spectrometry. Rapid Communications in Mass Spectrometry. *11*, 1357-1364.

269. Musialik, M., Kuzmicz, R., Pawlowski, T.S., and Litwinienko, G. (2009). Acidity of hydroxyl groups: An overlooked influence on antiradical properties of flavonoids. Journal of Organic Chemistry *74*, 2699-2709.

270. Stevens, J.F., Wollenweber, E., Ivancic, M., Hsu, V.L., Sundberg, S., and Deinzer,

M.L. (1999). Leaf surface flavonoids of Chrysothamnus. Phytochemistry *51*, 771-780.

271. Reddy, N.P., Reddy, B.A.K., Gunasekar, D., Blond, A., Bodo, B., and Murthy, M.M. (2007). Flavonoids from Limnophila indica. Phytochemistry *68*, 636-639.

272. Carpenter, K.E., Abrar, M., Aeby, G., Aronson, R.B., Banks, S., Bruckner, A., Chiriboga, A., Cortes, J., Delbeek, J.C., DeVantier, L., et al. (2008). One-third of reef-building corals face elevated extinction risk from climate change and local impacts. Science *321*, 560-563.

273. Hoegh-Guldberg, O., Mumby, P.J., Hooten, A.J., Steneck, R.S., Greenfield, P., Gomez, E., Harvell, C.D., Sale, P.F., Edwards, A.J., Caldeira, K., et al. (2007). Coral reefs under rapid climate change and ocean acidification. Science *318*, 1737-1742.

274. Warner, M.E., Fitt, W.K., and Schmidt, G.W. (1999). Damage to photosystem II in symbiotic dinoflagellates: A determinant of coral bleaching. Proceedings of the National Academy of Sciences *96*, 8007-8012.

275. Fitt, W.K., Brown, B.E., Warner, M.E., and Dunne, R.P. (2001). Coral bleaching: Interpretation of thermal tolerance limits and thermal thresholds in tropical corals. Coral Reefs *20*, 51-65.

276. Lesser, M.P., and Farrell, J.H. (2004). Exposure to solar radiation increases damage to both host tissues and algal symbionts of corals during thermal stress. Coral Reefs *23*, 367-377.

277. Hill, R., Larkum, A.W.D., Frankart, C., Kuhl, M., and Ralph, P.J. (2004). Loss of functional Photosystem II reaction centres in zooxanthellae of corals exposed to bleaching conditions: Using fluorescence rise kinetics. Photosynthesis Research *82*, 59-72.

278. Jones, R.J., and Hoegh-Guldberg, O. (2001). Diurnal changes in the photochemical efficiency of the symbiotic dinoflagellates (Dinophyceae) of corals: Photoprotection, photoinactivation and the relationship to coral bleaching. Plant, Cell and Environment *24*, 89-99.

279. Papageorgiou, G.C., and Murata, N. (1995). The unusually strong stabilizing effects of glycine betaine on the structure and function of the oxygen-evolving photosystem-ii complex. Photosynthesis Research *44*, 243-252.

280. Schiller, H., and Dau, H. (2000). Preparation protocols for high-activity Photosystem II membrane particles of green algae and higher plants, pH dependence of oxygen evolution and comparison of the S-2-state multiline signal by X-band EPR spectroscopy. Journal of Photochemistry and Photobiology B: Biology *55*, 138-144.

281. Blunden, G., and Gordon, S.M. (1986). Betaines and their sulphonio analogues in marine algae. Progress in Phycological Research *4*, 39-80.

282. Csonka, L.N., and Hanson, A.D. (1991). Prokaryotic osmoregulation - genetics and physiology. Annual Review of Microbiology *45*, 569-606.

283. Rhodes, D., and Hanson, A.D. (1993). Quaternary ammonium and tertiary sulfonium compounds in higher-plants. Annual Review of Plant Physiology and Plant Molecular Biology *44*, 357-384.

284. Anthoni, U., Christophersen, C., Hougaard, L., and Nielsen, P.H. (1991). Quaternary ammonium-compounds in the biosphere - an example of a versatile adaptive strategy. Comparative Biochemistry and Physiology - Part B: Biochemistry & Molecular Biology *99*, 1-18.

285. Yancey, P.H. (2005). Organic osmolytes as compatible, metabolic and counteracting cytoprotectants in high osmolarity and other stresses. Journal of Experimental Biology *208*, 2819-2830.

286. Yang, G.P., Rhodes, D., and Joly, R.J. (1996). Effects of high temperature on membrane stability and chlorophyll fluorescence in glycinebetaine-deficient and glycinebetaine-containing maize lines. Australian Journal of Plant Physiology *23*, 437-443.

287. Allakhverdiev, S.I., Hayashi, H., Nishiyama, Y., Ivanov, A.G., Aliev, J.A., Klimov, V.V., Murata, N., and Carpentier, R. (2003). Glycinebetaine protects the D1/D2/Cytb559 complex of photosystem II against photo-induced and heat-induced inactivation. Journal of Plant Physiology *160*, 41-49.

288. Allakhverdiev, S.I., Kreslavski, V.D., Klimov, V.V., Los, D.A., Carpentier, R., and Mohanty, P. (2008). Heat stress: An overview of molecular responses in photosynthesis. Photosynthesis Research *98*, 541-550.

289. Klimov, V.V., Allakhverdiev, S.I., Nishiyama, Y., Khorobrykh, A.A., and Murata, N. (2003). Stabilization of the oxygen-evolving complex of photosystem II by

bicarbonate and glycinebetaine in thylakoid and subthylakoid preparations. Functional Plant Biology *30*, 797-803.

290. Hema, R., Senthil-Kumar, M., Shivakumar, S., Reddy, P.C., and Udayakumar, M. (2007). Chlamydomonas reinhardtii, a model system for functional validation of abiotic stress responsive genes. Planta *226*, 655-670.

291. McNeil, S.D., Nuccio, M.L., and Hanson, A.D. (1999). Betaines and related osmoprotectants. Targets for metabolic engineering of stress resistance. Plant Physiology *120*, 945-949.

292. Sakamoto, A., and Murata, N. (2002). The role of glycine betaine in the protection of plants from stress: Clues from transgenic plants. Plant, Cell and Environment *25*, 163-171.

293. Prasad, K., and Saradhi, P.P. (2004). Enhanced tolerance to photoinhibition in transgenic plants through targeting of glycinebetaine biosynthesis into the chloroplasts. Plant Science *166*, 1197-1212.

294. Shirasawa, K., Takabe, T., and Kishitani, S. (2006). Accumulation of glycinebetaine in rice plants that overexpress choline monooxygenase from spinach and evaluation of their tolerance to abiotic stress. Annals of Botany *98*, 565-571.

295. Yang, X.H., Wen, X.G., Gong, H.M., Lu, Q.T., Yang, Z.P., Tang, Y.L., Liang, Z., and Lu, C.M. (2007). Genetic engineering of the biosynthesis of glycinebetaine enhances thermotolerance of photosystem II in tobacco plants. Planta *225*, 719-733.

296. Chen, T.H.H., and Murata, N. (2008). Glycinebetaine: An effective protectant against abiotic stress in plants. Trends in Plant Science *13*, 499-505.

297. Blunden, G., Elbarouni, M.M., Gordon, S.M., McLean, W.F.H., and Rogers, D.J. (1981). Extraction, purification and characterization of dragendorff-positive compounds from some british marine-algae. Botanica Marina *24*, 451-456.

298. Grieve, C.M., and Grattan, S.R. (1983). Rapid assay for determination of water-soluble quaternary ammonium-compounds. Plant and Soil *70*, 303-307.

299. Hitz, W.D., and Hanson, A.D. (1980). Determination of glycine betaine by pyrolysis-gas chromatography in cereals and grasses. Phytochemistry *19*,

2371-2374.

300. Howard, A.G., Freeman, C.E., Russell, D.W., Arbab-Zavar, M.H., and Chamberlain, P. (1998). Flow injection system with flame photometric detection for the measurement of the dimethylsulphide precursor beta-dimethylsulphoniopropionate. Analytica Chimica Acta *377*, 95-101.

301. Karsten, U., Wiencke, C., and Kirst, G.O. (1990). The beta-dimethylsulphoniopropionate (DMSP) content of macroalgae from antarctica and southern Chile. Botanica Marina *33*, 143-146.

302. Kiene, R.P., and Slezak, D. (2006). Low dissolved DMSP concentrations in seawater revealed by small-volume gravity filtration and dialysis sampling. Limnology and Oceanography-Methods *4*, 80-95.

303. Niki, T., Fujinaga, T., Watanabe, M.F., and Kinoshita, J. (2004). Simple determination of dimethylsulfide (DMS) and dimethylsulfoniopropionate (DMSP) using solid-phase microextraction and gas chromatography-mass spectrometry. Journal of Oceanography *60*, 913-917.

304. Reed, R.H. (1983). Measurement and osmotic significance of beta-dimethylsulphoniopropionate in marine macrolagae. Marine Biology Letters *4*, 173-181.

305. Smith, G.C., Clark, T., Knutsen, L., and Barrett, E. (1999). Methodology for analyzing dimethyl sulfide and dimethyl sulfoniopropionate in seawater using deuterated internal standards. Analytical Chemistry *71*, 5563-5568.

306. Visscher, P.T., Kiene, R.P., and Taylor, B.F. (1994). Demethylation and cleavage of dimethylsulfoniopropionate in marine intertidal sediments. Fems Microbiology Ecology *14*, 179-189.

307. Yang, G.P., Levasseur, M., Michaud, S., and Scarratt, M. (2005). Biogeochemistry of dimethylsulfide (DMS) and dimethylsulfoniopropionate (DMSP) in the surface microlayer and subsurface water of the western North Atlantic during Spring. Marine Chemistry *96*, 315-329.

308. Gorham, J. (1984). Separation of plant betaines and their sulfur analogs by cation-exchange high-performance liquid-chromatography. Journal of Chromatography *287*, 345-351.

309. Gorham, J. (1986). Separation and quantitative estimation of betaine esters by high-performance liquid-chromatography. Journal of Chromatography *361*, 301-310.

310. Gorham, J., and McDonnell, E. (1985). High-performance liquid-chromatographic method for the separation and estimation of choline, glycinebetaine aldehyde and related-compounds. Journal of Chromatography *350*, 245-254.

311. Rajakyla, E., and Paloposki, M. (1983). Determination of sugars (and betaine) in molasses by high-performance liquid-chromatography - comparison of the results with those obtained by the classical lane eynon method. Journal of Chromatography *282*, 595-602.

312. Nishimura, N., Zhang, J.H., Abo, M., Okubo, A., and Yamazaki, S. (2001). Application of capillary electrophoresis to the simultaneous determination of betaines in plants. Analytical Sciences *17*, 103-106.

313. Zhang, J.H., Nagahama, T., Abo, M., Okubo, A., and Yamazaki, S. (2005). Capillary electrophoretic analysis of dimethylsulfoniopropionate in sugarcane and marine algal extracts. Talanta *66*, 244-248.

314. Zhang, J.H., Nishimura, N., Abo, M., Okubo, A., and Yamazaki, S. (2001). Determination of 3-dimethylsulfoniopropionate in marine algae by low-pH capillary electrophoresis. Bunseki Kagaku *50*, 819-824.

315. Zhang, J.H., Nishimura, N., Okubo, A., and Yamazaki, S. (2002). Development of an analytical method for the determination of betaines in higher plants by capillary electrophoresis at low pH. Phytochemical Analysis *13*, 189-194.

316. Rhodes, D., Rich, P.J., Myers, A.C., Reuter, C.C., and Jamieson, G.C. (1987). Determination of betaines by fast-atom-bombardment mass-spectrometry - identification of glycine betaine deficient genotypes of zea-mays. Plant Physiology *84*, 781-788.

317. Bonham, C.C., Wood, K.V., Yang, W.J., Nadolskaorczyk, A., Samaras, Y., Gage, D.A., Poupart, J., Burnet, M., Hanson, A.D., and Rhodes, D. (1995). Identification of quaternary ammonium and tertiary sulfonium compounds by plasma desorption mass-spectrometry. Journal of Mass Spectrometry *30*, 1187-1194.

318. Wood, K.V., Bonham, C.C., Miles, D., Rothwell, A.P., Peel, G., Wood, B.C., and

Rhodes, D. (2002). Characterization of betaines using electrospray MS/MS. Phytochemistry *59*, 759-765.

319. Wiesemeier, T., and Pohnert, G. (2007). Direct quantification of dimethylsulfoniopropionate (DMSP) in marine micro- and macroalgae using HPLC or UPLC/MS. Journal of Chromatography B-Analytical Technologies in the Biomedical and Life Sciences *850*, 493-498.

320. Colmer, T.D., Corradini, F., Cawthray, G.R., and Otte, M.L. (2000). Analysis of dimethylsulphoniopropionate (DMSP), betaines and other organic solutes in plant tissue extracts using HPLC. Phytochemical Analysis *11*, 163-168.

321. Zhang, J.J., and Zhu, Y. (2007). Determination of betaine, choline and trimethylamine in feed additive by ion-exchange liquid chromatography/non-suppressed conductivity detection. Journal of Chromatography A *1170*, 114-117.

322. Needham, S.R., and Brown, P.R. (2000). The high performance liquid chromatography electrospray ionization mass spectrometry analysis of diverse basic pharmaceuticals on cyanopropyl and pentafluorophenylpropyl stationary phases. Journal of Pharmaceutical and Biomedical Analysis *23*, 597-605.

323. Needham, S.R., Brown, P.R., Duff, K., and Bell, D. (2000). Optimized stationary phases for the high-performance liquid chromatography-electrospray ionization mass spectrometric analysis of basic pharmaceuticals. Journal of Chromatography A *869*, 159-170.

324. Needham, S.R., Jeanville, P.M., Brown, P.R., and Estape, E.S. (2000). Performance of a pentafluorophenylpropyl stationary phase for the electrospray ionization high-performance liquid chromatography-mass spectrometry-mass spectrometry assay of cocaine and its metabolite ecgonine methyl ester in human urine. Journal of Chromatography B *748*, 77-87.

325. Bell, D.S., and Jones, A.D. (2005). Solute attributes and molecular interactions contributing to "U-shape" retention on a fluorinated high-performance liquid chromatography stationary phase. Journal of Chromatography A *1073*, 99-109.

326. Chen, F.C.M., and Benoiton, N.L. (1976). New method of quaternizing amines and its use in amino-acid and peptide chemistry. Canadian Journal of Chemistry/Revue Canadiene de Chimie *54*, 3310-3311.

327. Chambers, S.T., Kunin, C.M., Miller, D., and Hamada, A. (1987). Dimethylthetin can substitute for glycine betaine as an osmoprotectant molecule for Escherichia-Coli. Journal of Bacteriology *169*, 4845-4847.

328. Dacey, J.W.H., and Blough, N.V. (1987). Hydroxide decomposition of dimethylsulfoniopropionate to form dimethylsulfide. Geophysical Research Letters *14*, 1246-1249.

329. Johannes, R.E., and Wiebe, W.J. (1970). Method for determination of coral tissue biomass and composition. Limnology and Oceanography *15*, 822-824.

330. Bouchereau, A., Duhaze, C., Martin-Tanguy, J., Guegan, J.P., and Larher, F. (1999). Improved analytical methods for determination of nitrogenous stress metabolites occurring in Limonium species. Journal of Chromatography A *836*, 209-221.

331. Yamamoto, F.M., and Rokushika, S. (2000). Retention properties of the fluorinated bonded phase on liquid chromatography of aromatic hydrocarbons. Journal of Chromatography A *898*, 141-151.

332. Neue, U.D., Phoebe, C.H., Tran, K., Cheng, Y.F., and Lu, Z.L. (2001). Dependence of reversed-phase retention of ionizable analytes on pH, concentration of organic solvent and silanol activity. Journal of Chromatography A *925*, 49-67.

333. Yang, X.Q., Dai, J., and Carr, P.W. (2003). Analysis and critical comparison of the reversed-phase and ion-exchange contributions to retention on polybutadiene coated zirconia and octadecyl silane bonded silica phases. Journal of Chromatography A *996*, 13-31.

334. Houghton, R., Horro, P.C., Ward, I., and Macarthur, R. (2009). Generic approach to validation of small-molecule LC–MS/MS biomarker assays. Bioanalysis *1*, 1365-1374.

335. Vermeij, M.J.A., and Bak, R.P.M. (2002). How are coral populations structured by light? Marine light regimes and the distribution of Madracis. Marine Ecology Progress Series *233*, 105-116.